AD 655384

INVESTIGATION OF THE EFFECT OF SURFACE CONDITIONS ON THE RADIANT PROPERTIES OF METALS

Part II, Measurements on Roughened Platinum and Oxidized Stainless Steel

R. E. Rolling
A. I. Funai
Lockheed Missiles & Space Company

TECHNICAL REPORT NO. AFML-TR-64-363, Part II

April 1967

Air Force Materials Laboratory
Directorate of Laboratories
Air Force Systems Command
Wright-Patterson Air Force Base, Ohio

RECEIVED

AUG 3 1967

C 11

DDC

JUL 2 7 1967

B

INVESTIGATION OF THE EFFECT OF SURFACE CONDITIONS ON THE RADIANT PROPERTIES OF METALS

Part II, Measurements on Roughened Platinum and Oxidized Stainless Steel

R. E. Rolling
A. I. Funai

FOREWORD

This report has been reviewed and is approved.

HYMAN MARCUS, Acting Chief
Thermo & Chemical Physics Branch
Materials Physics Division
Air Force Materials Laboratory

ABSTRACT

Experimental results are presented to show the effect of surface roughness and of surface oxidation on the radiant properties of platinum and of 304 stainless steel. The radiant properties investigated include total and spectral normal, hemispherical, and directional emittance as a function of emission angle, polarization, temperature, and surface roughness or oxide film thickness.

Emittance data are presented for five platinum samples with surface roughness values between 0.20 and 2.50 μ, rms, at five temperatures between 865 and 1645 K, and at selected wavelengths between 1 and 12 μ. Similar data are presented for nine stainless steel samples with surface oxide film-thickness values between 0 and 1.5 μ, at five temperatures between 535 and 1090 K. Variations in the radiant properties of each material are explained in terms of the differences in surface characteristics of the samples, or of changes in their surface characteristics as the result of annealing, recrystallization, and oxidation during the high temperature emittance tests.

Methods used to evaluate the physical, chemical, and geometrical characteristics of the sample surface include: profilometry, optical and electron microscopy, x-ray and electron diffraction, and arc spectroscopy. The advantages and short-comings of these methods are discussed and typical results are presented.

Distribution of this abstract is unlimited.

TABLE OF CONTENTS

LIST OF ILLUSTRATIONS

LIST OF TABLES

Table		Page

LIST OF ABBREVIATIONS AND SYMBOLS

The definitions and symbols used in this report for the thermal radiation properties of materials and surfaces are the same as described in (1). Words ending in _ivity_ are used to describe intrinsic properties of a bulk material; words ending in _ance_ denote properties of a specimen surface; and words ending in _ion_ describe processes. Thus, emissivity is an intrinsic property of the pure, bulk material; emittance is a property of the emitting surface measured relative to the same property for a blackbody; and emission is the process by which thermal energy is emitted by a surface or body by virtue of its temperature. The symbols used in this report are defined in the following list:

NOMENCLATURE

A	area
a	correlation distance for rough surface
b_2	constant defined in Eq. (7)
b_3	constant defined in Eq. (7)
c	speed of light in vacua
c_1	first radiation constant
c_2	second radiation constant
c_3	constant defined in Eq. (7)
d	oxide film thickness
E	emissive power
e	electron charge
$\overline{H}$	average ratio of hemispherical-to-normal emittance
$\hbar$	Planck constant
i	$\sqrt{-1}$
I	current

K	constant, characteristic of a metal, Eq. (8)
$\bar{K}$	absorption coefficient
K_R	radiation conductivity
k	imaginary part of $\bar{n}$ (absorption index)
k_o	Boltzmann constant
M	atomic weight
m	mass of carrier
N	carrier density
n	real part of $\bar{n}$
$\bar{n}$	complex index of refraction
n_o	index of refraction of surrounding medium
P_L	power loss term in Eq. (25)
S	average spacing between shields
$\bar{S}$	backscatter coefficient
T	absolute temperature
V	voltage
ϵ	emittance
ξ	surface plane
Θ'	characteristic temperature of a metal
Θ'_o	constant defined in Eq. (9)
θ	angle of emission
θ'	angle of incidence
λ	wavelength
λ_1	characteristic wavelength defined in Eq. (2)

λ_2	characteristic wavelength defined in Eq. (2)
μ	micron, 10^{-4} cm
μin.	microinch, 10^{-6} in.
ρ	reflectance
σ	electrical conductivity
σ_0	Stefan-Boltzmann constant
σ_m	rms roughness
$\bar{\sigma}$	$\sqrt{\bar{K}(\bar{K}+2\bar{S})}$
τ	transmittance
τ_0	relaxation time
ϕ	complex angle of refraction
ϕ'	angle of internal reflection
χ	plane of emission

Subscripts

a	ambient
b	property of the blackbody
m	property of the mirror
N	direction normal to the surface
s	property of the sample
w	property of the window
$\parallel$	electric vector vibrating in plane of emission
$\perp$	electric vector vibrating perpendicular to plane of emission

Parentheses

(θ, λ, T) spectral directional

(θ_N, λ, T) spectral normal

(λ, T) spectral hemispherical

(θ, T) total directional

(θ_N, T) total normal

(T) total hemispherical

$\dfrac{(\theta, \lambda, T)}{(\theta_N, \lambda, T)}$ relative spectral directional

$\dfrac{(\theta, T)}{(\theta_N, T)}$ relative total directional

(θ_{max}) angle at which relative directional ϵ is a maximum

$\epsilon(\theta)_{max}$ maximum relative directional emittance

Section I

INTRODUCTION

The research described in this report is a continuation of that reported in AFML-TR-64-363, Investigation of the Effect of Surface Condition on the Radiant Properties of Metals (1). The purpose of these studies was to experimentally and analytically investigate the effects of surface condition (e.g., roughness and oxidation) on the emittance properties of metals. During the first year, experimental techniques were developed for preparation of pure metal specimens with varying degrees of surface roughness and for measurement of their absolute and relative directional emittance properties. Results were presented for carefully prepared specimens of copper, tungsten, and platinum. Analytical methods were used to obtain the optical constants for each metal from the relative spectral directional emittance data for each of the smooth-surface specimens. Theories for the reflection of electromagnetic energy from a randomly rough surface were examined to determine their applicability for prediction of roughness effects on the directional distribution of emitted thermal energy.

This report describes effort in the second year during which additional studies were completed on the effect of surface roughness on the emittance properties of platinum, and an investigation was made of the effects of surface oxidation and roughness on the emittance properties of stainless steel.

The physical condition and geometric features of the roughened platinum surfaces were evaluated using profilometric and photomicrographic methods similar to those described in (1). Several new techniques, principally involving the use of electron microscopy, were investigated for evaluation of the thickness, morphology, and composition of the oxide films that were obtained on the stainless steel specimens. These methods are described in Section III and the results are discussed in Section V.

Emittance results are presented for five platinum specimens and nine stainless steel specimens and include the total normal, total hemispherical, spectral normal, relative total directional, and relative spectral directional emittance. These properties were determined at temperatures between 535° and 1645°K and at wavelengths between 1 and 12 μ. The relative spectral directional emittance determinations were made for both the parallel and the perpendicular components of polarized radiation from the specimens. Complete sets of emittance data were obtained at each test temperature as permitted by available energy levels. The results are presented in the same format as was used for (1), with complete sets of data for each test specimen presented in a separate section (Section VII) to facilitate detailed study by other investigators.

1

Section II

RADIANT PROPERTIES OF SURFACES

1. INTRODUCTION

Although the thermal emission of radiant energy by a material is usually thought of as a surface phenomenon, the emitted energy actually originates from within the body of the material. The energy is generated by thermal excitation of atomic and molecular oscillators (i.e., free and bound electrons and/or lattice bonds) that are characteristic of the chemical composition of the material and its physical state. At a given temperature, each collection of oscillators generates a unique spectrum of electromagnetic frequencies (or wavelengths) characteristic of the material lattice. The amount of energy that reaches the surface depends upon the frequency of the radiation, the distance between the oscillator and the surface, the optical constants of the material, i.e., index of refraction and absorption coefficient, and the scattering characteristics of the material.

For the wavelengths commonly associated with optical and thermal energy (i.e., 0.25 to 40 μ), the depth of penetration of an incident electromagnetic field can range from very small to very large values depending on the absorption and scattering properties of the material. Since the extinction (absorption) coefficients for metals are large in this spectral region, the radiant energy cannot travel farther than a few hundred angstroms before total absorption occurs. Similarly, the internally generated radiant energy reaching the surface of a metal originates from oscillators in a very thin surface layer, from 0 to perhaps 1000 $\overset{\circ}{A}$ deep. As the extinction coefficient decreases, there is a corresponding increase in the effective depth of the surface layer. If the material is a metal oxide, the depth of penetration may be one or two orders of magnitude larger than for metals. However, since few data are available on the optical constants of metal oxides commonly encountered in engineering practice, a definite statement of depth cannot be made. If the oxide is thick enough to be opaque then all the energy reaching the surface will have been generated within the oxide layer. As the thickness decreases below opacity, an increasing percentage of the energy reaching the emitting surface will originate from the metal substrate.

Regardless of its origin, a portion of the energy reaching the surface is emitted by transmission and refraction into a new medium, e.g., air, vacuum, or a thin film with different optical constants, and the remainder is internally reflected back into the original material. The relative proportions of emitted and reflected energy at the surface depend upon the wavelength of the radiation, its angle of incidence on the surface, and the relative index of refraction of the two media.

2

When all of the parameters are known or specified, it is possible to calculate the emittance properties of the surface [e.g., see (2, 3, 4)]. However, even for smooth surfaces the calculations are tedious except for the case of normal incidence. For off-normal angles of incidence, the reflected (and refracted) energy is a function of polarization and phase-change phenomena as well as wavelength and temperature. Therefore, computer techniques are usually employed to obtain solutions of the equations.

The solutions obtained generally apply for ideal conditions of uniform surface coatings on smooth metallic substrates. Application of the equations to those surfaces created by oxidation of common materials is extremely difficult due to the tremendous variety of surface layer structures that exist on practical engineering materials used for optical and heat-transfer applications. Geometrical variations in surface profile, various preferred orientations of crystal lattice, strains and/or defects in the lattice structure, porosity or chemical inhomogeneities in the surface layer, and thin contaminant films are commonly found on engineering materials. These physical, chemical, and geometrical variations of the surface layer produce conditions far from the ideal state. Therefore, laboratory measurements are presently the only source of reliable values for the radiant properties of a given complex surface. Hopefully, as methods and techniques are developed for complete surface characterization, and as experimental data on the radiant properties of carefully characterized surfaces are accumulated, then a more thorough assessment of the effects of surface condition on radiant properties will be possible.

2. SMOOTH SURFACES

The optical behavior of smooth, pure, metal surfaces has received the attention of a large number of investigators for many years. As a result, a vast amount of literature is available describing experimental and theoretical results which apply to pure, polished surfaces. The proceedings of a recent colloquium (5) provide an excellent indication of the progress being made in this area of study.

The pure, polished surface is of interest since its behavior is closely linked with properties of the bulk material. These are altered by nonideal surface conditions. Therefore, the properties of smooth samples were experimentally determined to establish the required reference values. The nomenclature used to describe reflection and emission from a surface was presented previously in (1) and is repeated herein for convenience of the reader.

In Figure 1 the surface plane of an emitting material is represented by ξ, $\bar{n}$ is the complex index of refraction of the material, and n_0 is the index of refraction of the surrounding medium. Internally generated thermal radiation incident on the surface at angle ϕ to the surface normal is either reflected at angle ϕ' or is transmitted and refracted into the surrounding medium at angle θ. Similarly for the reflectance case, external energy incident on the surface at angle θ' is either reflected at angle θ or is refracted into the material at angle ϕ'. Except for the case of normal

3
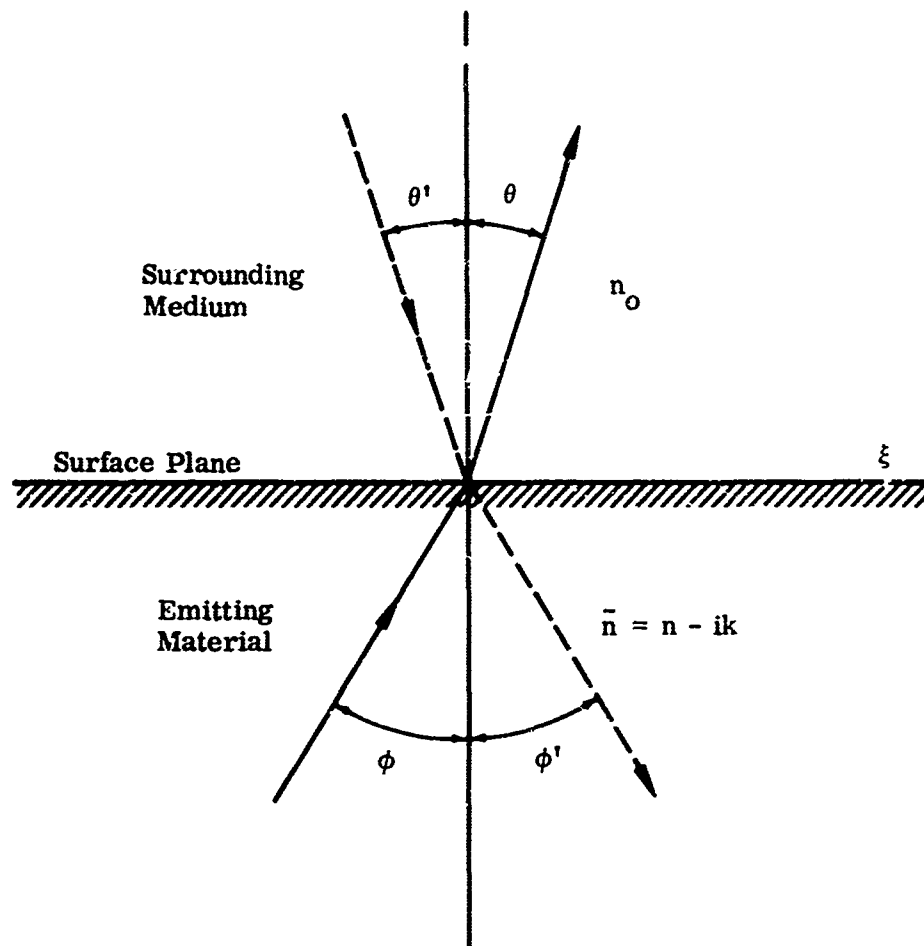
Figure 1. Reflection and Refraction Angles at a Surface

4

incidence, both the direction of propagation and the direction of polarization of the radiation must be considered to calculate either the reflectance or the emittance of the surface.

In Figure 2 the plane of emission, χ, is defined as a horizontal plane perpendicular to the surface plane ξ. The angle of emission, θ, gives the direction of propagation in the plane of emission, measured from the normal to the sample plane. The direction of polarization is specified for the electric vector of the wave where the parallel ($\parallel$) component is that which vibrates in the plane of emission and the perpendicular ($\perp$) component is that which vibrates normal to the plane of emission.

Using the nomenclature defined by Figures 1 and 2, expressions for the spectral normal and spectral directional emittance of a material in vacuum, in terms of the optical constants of the material, were developed from the Fresnel equations in (1). Such expressions are readily available in open literature and will not be repeated here. It is important to note that the complex index of refraction is a function of temperature and wavelength which requires separate solution of the equations for each condition of interest. Unfortunately, very few optical constant data are available for metals over the ranges of wavelength and temperature commonly used in heat-transfer computations. Also, it is rare that metallic surfaces used in construction satisfy the conditions assumed in the formulation. That is, only special laboratory samples are optically smooth and free of surface strain and oxidation. For these reasons, direct application of results obtained from the Fresnel equations is limited to special circumstances or is at best an approximation of actual conditions.

In spite of the departure of most practical surfaces from ideal conditions, it will often be found that the effects of surface roughness, oxidation, and surface strain are sufficiently minor to permit the assumption of ideal conditions for the purposes of heat-transfer computations. This approach would be satisfactory for the roughened platinum and nonoxidized stainless steel samples examined during this program. The results presented in Section V show that roughness up to 2μ rms increases the absolute total emittance by approximately 7% for a roughened, annealed, clean specimen. Additionally, the ratio of hemispherical to normal emittance is increased only slightly (approximately 7%) by roughening in this range. These minor departures from ideal conditions have little influence on the accuracy of heat-transfer computations that use emittance properties obtained from smooth, polished specimens.

The temperature and wavelength dependence of spectral emittance was observed during this program to be a greater influence on the total emittance properties of platinum than was the influence of surface roughening. Therefore, an analytical study was completed for the purpose of establishing straightforward relationships from which the emittance of pure metals could be computed from the fundamental optical properties. Once the emittance properties are established, it is possible to perform heat-transfer computations without the assumption of gray surfaces or complete reliance on experimental results.

5
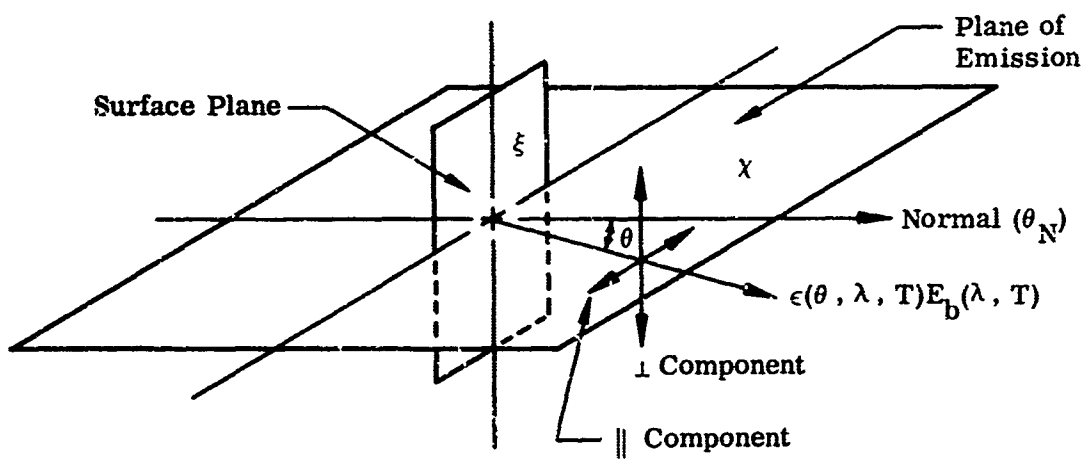
Figure 2. Propagation and Polarization Directions for Emitted Radiation

ϵ.

A number of approaches to the computation of energy transfer between nongray surfaces have been suggested by recent investigators. These generally require semigray approximations (6, 7), experimental spectral emittance data (8, 9), or idealized multiband models (10, 11). All of these approaches require detailed numerical computations and fail to reveal a general functional dependence between optical properties of the materials and the radiant heat exchange. The numerical work reported by Branstetter (8) provides interesting results in that the net energy exchange between metallic surfaces is best represented by a general relationship that differs from the fourth-power dependence on absolute temperature. However, no analytical explanation of this result was offered. By use of a simple spectral emittance spectrum, which is valid at long wavelengths, it is possible to obtain some clarification of Branstetter's results.

From the single-electron theory (12, 13), the normal spectral emittance is given by

$$\epsilon(\theta_N, \lambda, T) = (8)^{1/2} \left(\frac{\lambda_1}{\lambda}\right) \left[\left(1 + \frac{\lambda^2}{\lambda_2^2}\right)^{1/2} - 1 \right]^{1/2} \tag{1}$$

where

$$\lambda_1 = \left[\frac{\pi m c^2}{N e^2}\right]^{1/2} = \left[\frac{c \lambda_2}{2 \sigma}\right]^{1/2}, \quad \lambda_2 = \frac{2 \pi m c \sigma}{N e^2} = 2 \pi c \tau_0 \tag{2}$$

and m is the mass of the charge carrier, c the speed of light, N the number of carriers per unit volume, e the carrier charge, σ the electric conductivity, and τ_0 the relaxation time.

Equation (1) is based upon a single set of charge carriers. It applies to the infrared part of the spectrum and is applicable to relatively low temperatures. For moderate and high temperatures, expressions based on the two-electron theory have been developed (13, 14), but their applications have been severely limited due to the complexity involved. The spectral hemispherical emittance may be obtained from the spectral normal emittance through use of expressions presented by Dunkle (15). In general, the ratio of these two quantities is dependent on the complex refractive index and, consequently, is a function of wavelength. For metals at moderate temperatures, the hemispherical emittance is approximately 1.30 times larger than the normal emittance value obtained from Eq. (1). For the platinum samples investigated during this program, the ratio of hemispherical to normal emittance was approximately 1.2. (See Section V.)

Even though Eq. (1) is the simplest form available for prediction of spectral emissivity, it is still sufficiently complicated so that no simple closed form result can be obtained for total emissivity. Therefore, simpler approximate forms were sought that contained the functional dependence of Eq. (1). Numerous approximate forms can be derived that in some degree match the numerical values of Eq. (1) for the same values of independent variables. However, no single simple expression was found that did so over the entire range of the ratio λ/λ_2. Final selection of an approximate form led to the expression

$$\epsilon(\theta_N, \lambda, T) = (8)^{1/2}(\lambda_1/\lambda_2)\left[(\lambda_2/\lambda)^{1/2} - 0.32(\lambda_2/\lambda)\right] \qquad (3)$$

This relation matches the behavior of Eq. (1) with satisfactory accuracy for the range $0.4 \leq \lambda/\lambda_2 \leq \infty$ which for most metals corresponds to wavelengths beyond 8 μ. Figure 3 compares the approximate form with a computer solution of Eq. (1).

The total normal emittance, $\epsilon(\theta_N, T)$, is obtained from

$$\epsilon(\theta_N, T) = \frac{1}{\sigma_o T^4} \int_0^\infty \epsilon(\theta_N, \lambda, T) \, E_b(\lambda, T) \, d\lambda \qquad (4)$$

where

$$E_b(\lambda, T) = c_1 \lambda^{-5} \left[\exp(c_2/\lambda) - 1\right]^{-1} \qquad (5)$$

Although Eq. (3) is a simple expression, it is still necessary to introduce an additional approximation to obtain a useful closed form result from the integration of Eq. (4). This approximation requires substitution of the Wien distribution for $E_b(\lambda, T)$. Use of the Wien distribution to approximate Planck's equation is a valid procedure for the range of interest since this distribution closely approximates the energy content given by the Planck distribution through most of the spectral range (10). Where the approximation fails to give close correspondence, i.e., at large values of (λT), there remains but a small portion of the total blackbody energy. Therefore, the final expression obtained provides numerically useful results that require a minimum of computational procedure.

Performing the integration of Eq. (4), with $\epsilon(\theta_N, \lambda, T)$ and $E_b(\lambda, T)$ given respectively by Eq. (3) and the Wien distribution, gives

$$\epsilon(\theta_N, T) = 3.96 \, b_2 \left(1 - 0.525 \, b_3^{1/2}\right) \qquad (6)$$

8
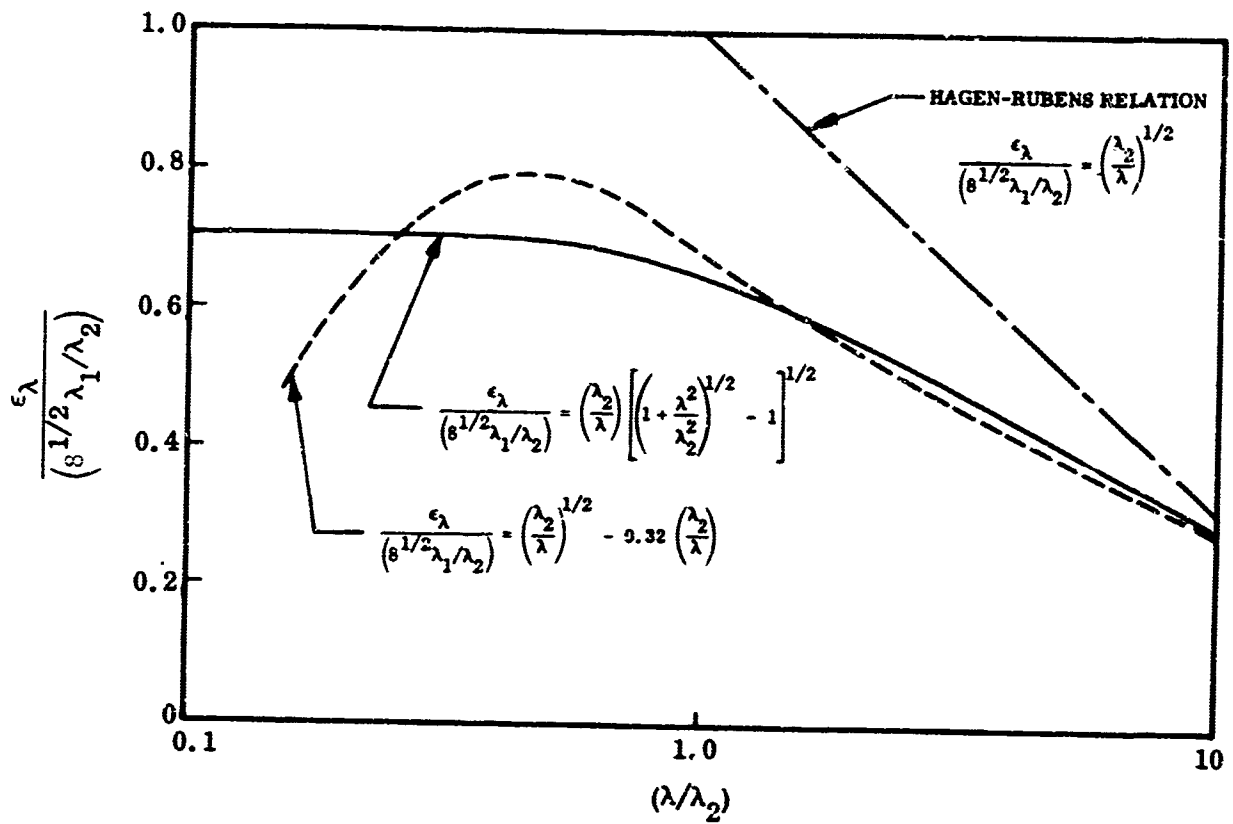
Figure 3. Approximate Expressions for Spectral Normal Emittance Based on Single Electron Theory

9

b_2 and b_3 characterize the effects of electrical conductivity and relaxation time and are given by (16)

$$b_2 = (c_3 k_0 T/2h\sigma)^{1/2} \quad , \quad b_3 = (2\pi c_3 k_0 T \tau_0/h) \quad , \quad c_3 = \pi(15)^{-1/4} = 1.601 \quad (7)$$

This result is simple and compares very well with the numerical solution, as shown in Figure 4. This result was also compared to the results of Parker and Abbott (12) where series expansions were presented for solution of Eq. (4) basing $\epsilon(\theta_N, \lambda, T)$ on the original form of the single-electron theory. The comparison obtained with that work is excellent with better agreement for low values of b_3 than that shown in Figure 4.

The form of Eq. (6) is of particular value since b_3 may be considered independent of temperature (13). The value of b_2 depends upon the electrical conductivity and is linearly dependent on temperature as shown by consideration of the results presented in (17). For the region $(T/\Theta') > 0.5$, the electrical conductivity is closely represented by the limiting relation of the Bloch-Gruneisen formula.

$$\sigma = \frac{4M\Theta'^2}{KT} \quad (8)$$

where M is the atomic weight, Θ' is a characteristic temperature of the metal with values close to the Debye temperature, K is a constant characteristic of the metal and its volume, and T is the absolute temperature. Using this relation in the definition of b_2 gives

$$\frac{b_2}{T} = \left[\frac{c_3 k_0 K}{8hM\Theta'^2}\right] = (\Theta_0')^{-1} \quad (9)$$

where Θ_0' is a material constant with the dimensions of temperature. Table I presents values for the required constants determined from the room temperature data presented by Lenham and Treherne (18).

The utility of the form derived for spectral emittance, Eq. (3), is the ease of incorporating it into heat-transfer computations.

For example, the radiant heat exchange between parallel plates may be expressed by

$$q_{\alpha\beta} = \int_0^\infty \frac{F_b(\lambda, T_\alpha) - E_b(\lambda, T_\beta)}{\left[\epsilon(\lambda, T_\alpha)\right]^{-1} + \left[\epsilon(\lambda, T_\beta)\right]^{-1} - 1} \, d\lambda \quad (10)$$
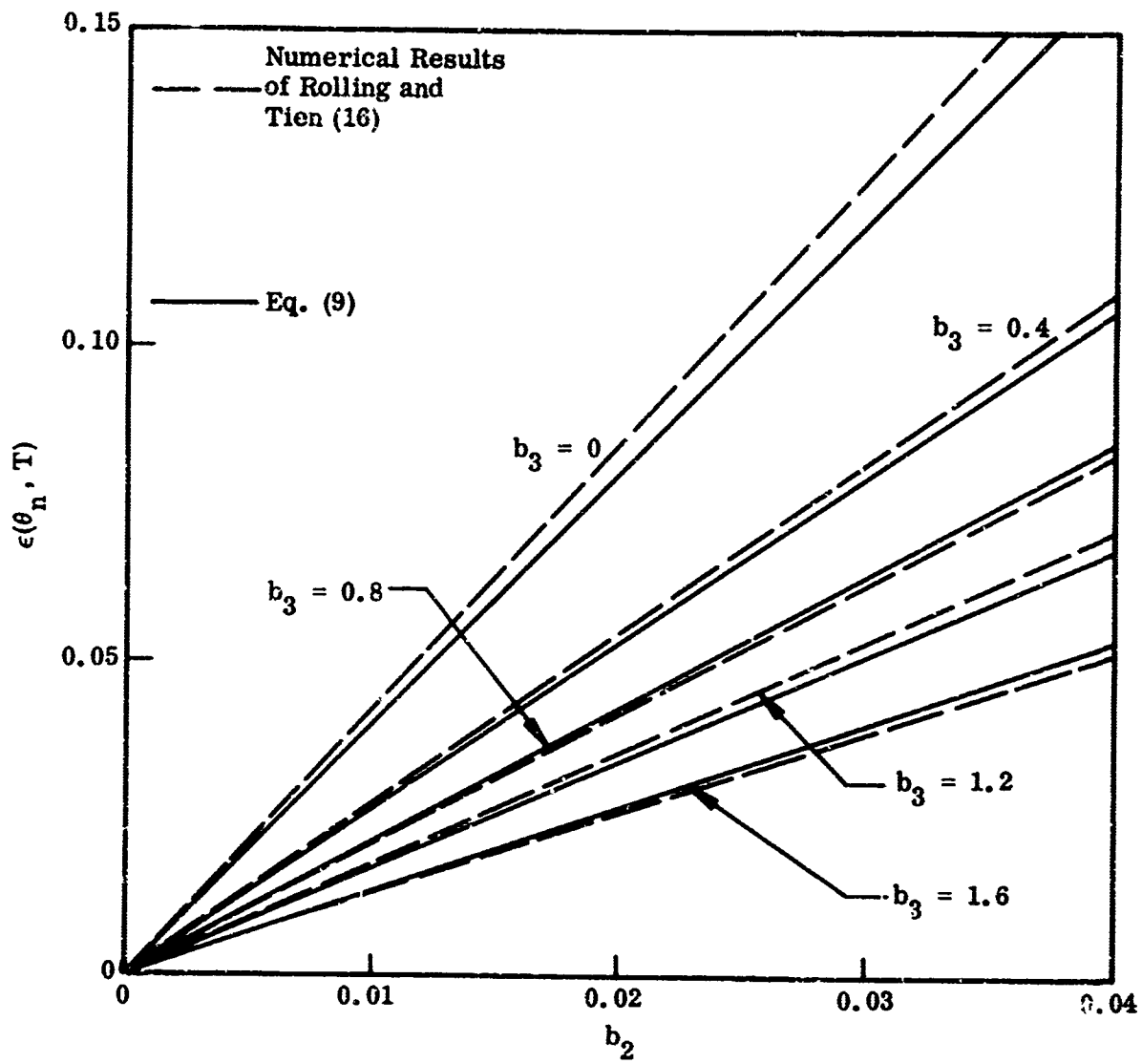
Figure 4. Total Normal Emittance as a Function of Characteristic
Dimensionless Groups

11

Table I. Values of Constants for Pure Metals at Room Temperature[a]

	20μ Properties[b]						
Material	N (cm$^{-3} \times 10^{-22}$)	τ_0 (sec $\times 10^{14}$)	σ^{-1} (ohm-cm $\times 10^6$)	λ_1 (μ)	λ_2 (μ)	b_2/T (°K$^{-1} \times 10^6$)	b_3
Al	4.3	2.1	3.94	0.161	39.5	15.6	1.32
Cr	1.1	0.73	44.3	0.018	13.7	52.2	0.458
Co	1.05	1.8	18.8	0.326	33.9	34.0	1.03
Cu	5.2	3.15	2.17	0.146	59.3	11.6	1.98
Au	4.9	1.1	6.59	0.151	20.7	20.2	0.690
Fe	1.3	1.2	22.8	0.293	22.6	34.7	0.753
Ni	1.6	1.9	11.7	0.264	35.8	26.8	1.19
Nb	1.55	0.9	25.4	0.268	16.9	39.6	0.565
Pt	2.6	0.75	18.2	0.207	14.1	33.5	0.471
Ag	6.3	2.5	2.26	0.133	47.1	11.8	1.57
Ta	0.8	0.75	58.2	0.373	14.1	60.4	0.471
Sn	3.0	0.8	14.8	0.193	15.1	30.2	0.502
Ti	0.8	0.3	14.8	0.373	5.65	95.6	0.188
W	1.3	1.35	20.2	0.293	25.4	35.3	0.847
	D. C. Properties[c]						
Al	5	2.8	2.56	0.149	52.7	12.5	1.76
Cr	1.15	2.05	15.1	0.311	38.6	30.5	1.29
Co	1.2	5.6	5.29	0.305	105.4	18.1	3.51
Cu	5.2	4.4	1.55	0.146	82.9	9.79	2.76
Au	4.9	3.6	2.02	0.151	67.8	11.1	2.26
Fe	1.3	3.16	8.65	0.293	59.5	23.1	1.98
Ni	1.6	3.4	6.54	0.264	64.0	20.1	2.13
Nb	1.6	0.95	23.4	0.264	17.9	38.0	0.596
Pt	2.5	1.5	9.48	0.211	28.2	24.2	0.941
Ag	6.3	3.7	1.52	0.133	69.7	9.70	2.32
Ta	0.8	3.6	12.3	0.373	67.8	27.6	2.26
Sn	3.2	1.24	8.95	0.187	23.3	23.5	0.778
Ti	0.8	1.06	41.9	0.373	20.0	50.8	0.665
W	1.3	5.6	4.88	0.293	105.4	17.3	3.51
Zn	1.5	4.3	5.51	0.273	81.0	18.4	2.70

(a) Values given are best averages for hand polished or evaporated film surfaces as reported by Lenham and Treherne (18).

(b) N and τ_0 computed from reflectance measurements using mass and charge of electron in free space.

(c) From D. C. conductivity measurements.

12

where $\epsilon(\lambda, T)$ is the spectral hemispherical emissivity, and the subscripts α and β refer to the hot and cold surfaces, respectively. Equation (10) includes the assumption of Kirchoff's law and negligible effects of polarization and directionality. At low and moderate temperatures, ϵ is small and Eq. (10) can be placed in the form

$$q_{\alpha\beta} = \overline{H} \int_0^\infty \frac{\epsilon(\lambda, T_\alpha)\,\epsilon(\lambda, T_\beta)}{\epsilon(\lambda, T_\alpha) + \epsilon(\lambda, T_\beta)} \left[E_b(\lambda, T_\alpha) - E_b(\lambda, T_\beta) \right] d\lambda \tag{11}$$

where $\overline{H}$ is the average ratio of hemispherical to normal emittance and has a value near 1.3 for most metals. The integration indicated by Eq. (11) can be performed in closed form using the Wien distribution and Eq. (3) or by a computer using the Planck distribution. In either case, the computation is considerably simplified compared to that required when using Eq. (1).

For computations of energy transfer through multiple shields, it is often desirable to define a radiation conductivity (13) so that the energy rate is given by the simple form

$$q = -(K_c + K_R) \frac{\partial T}{\partial X} \tag{12}$$

where K_c is the solid conductivity, and K_R is the radiation conductivity defined as

$$K_R(T) = \frac{S\overline{H}}{2} \int_0^\infty \epsilon(\theta_N, \lambda, T) \frac{\partial E_b(\lambda, T)}{\partial T} d\lambda \tag{13}$$

with S being the spacing between shields. In general, Eq. (13) results in a lengthy form that is of limited utility in engineering computations. However, by use of Eq. (3) and the Wien distribution it is easily integrated to the result

$$\left(\frac{2K_R}{S\overline{H}\sigma_o T^3} \right) = 252 b_2 \left[1 - 0.682 b_3^{1/2} \right] \tag{14}$$

where the parameter on the lefthand side is the dimensionless radiation conductivity. Equation (14) is shown in Figure 5 as a function of b_2 and b_3 in the range of practical interest. The dimensionless radiation conductivity varies with temperature. The simple form is very convenient for calculations of low-temperature radiation shields.

13
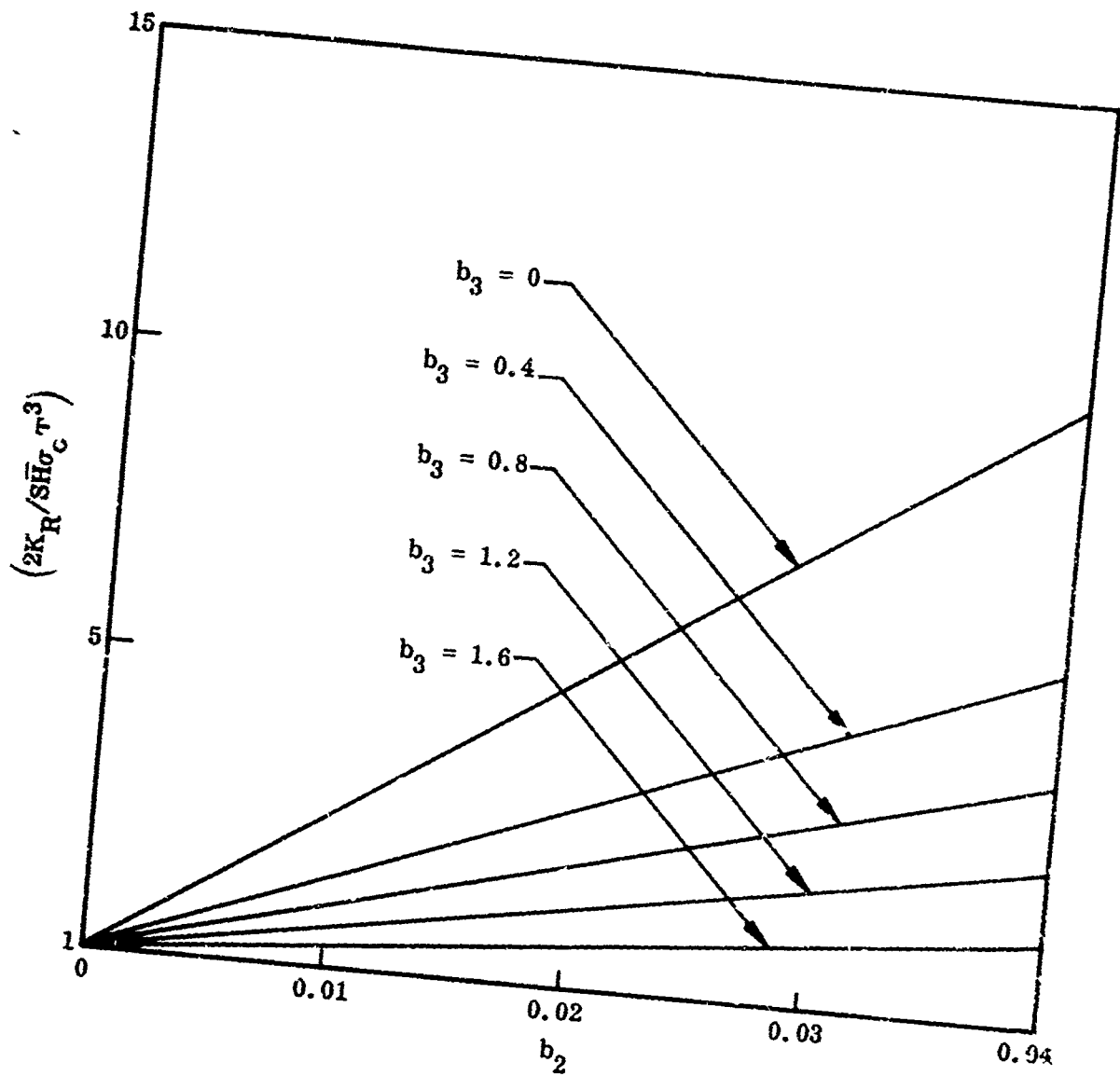
Figure 5 Dimensionless Conductivity of Multiple Radiation Shields

The approximations developed for prediction of spectral and total emissivity and radiation shield conductivity are applicable only to the range of wavelengths and temperatures which satisfy the assumptions made. Care should be exercised to avoid extreme extrapolations to shorter wavelengths or higher temperatures since a two-electron model is more applicable under these circumstances. Edwards (13) has derived approximate forms for the two-electron model that should be used where that model is more appropriate. However, his results are more complex and lead to computational difficulty. In either case, the results of measurements completed during this effort indicate that the theoretical predictions for a polished surface may be used under many circumstances where a clean, annealed, though slightly rough, surface exists. The possible variation in emittance for this type of surface, from the polished condition, will have less influence on the computation than is often assumed.

14

3. ROUGHENED SURFACES

The effects of roughness on a reflecting surface have been studied in considerable detail by numerous investigators. Of primary concern has been the bidirectional reflectance. There are several reasons for concentration of effort on this particular property in spite of its limited utility in heat-transfer computations. First, considerable early efforts had been expended on analyses of the bidirectional reflectance of radar and radio waves from rough terrain. This work has established a foundation which is easily extended to the problem on the rough reflecting surface in the infrared spectrum. Second, the specular component of reflectance is considerably altered by roughness and can be directly correlated with geometrical properties of the surface profile. This offers advantage to the experimentalist since large changes in specular properties will be observed. Finally, the preparation of rough reflecting samples and the radiometric techniques required for their measurement is straightforward.

The work accomplished on reflectance has conclusively shown that the reflectance of coherent energy from a randomly rough, perfectly reflecting surface may be described by a function which accounts for the coherent and incoherent energy separately. The energy in the coherent beams depends upon the optical roughness σ_m/λ and the angle of incidence θ. The incoherent energy distribution depends not only on σ_m/λ, but also on the parameter a/λ where a is the correlation distance and is determined from the rms slope and roughness. Analytical and experimental efforts are still continuing toward further development of the bidirectional reflectance theories.

For the rough emitting surface, the analytical treatment is considerably more difficult than for the rough reflecting surface. The interactions between electromagnetic waves and matter at the surface boundary are so complex that direct analytical considerations of emittance are not mathematically manageable. An indirect approach through calculation of the reflectance appears more feasible. However, such an indirect study of emittance requires a complete and comprehensive knowledge of both the specular and diffuse components and must include the effects of finite conductivity, shadowing, multiple reflections, and depolarization. These are often neglected in existing reflectance analyses since their influence introduces great difficulty in the mathematical treatment. In fact, it is reasonable to state that an analysis to properly include all of these effects is not possible within the present state of knowledge.

Attempts were made during this program to extend the exact approach of Rice to higher order terms than were considered during the first year's effort (1). The result, if successfully carried out, might indicate the extent of the effects previously mentioned, although this limited information would not be directly applicable to er ittances. However, the higher order analysis became so involved that its completion, while entirely possible, would require an intensive effort that could not be supported within the scope of this study.

15

At the present time, the only method available for correlation of data on rough emitting surfaces is a semi-empirical one which assumes the functional dependence of emittance to be of the form

$$\frac{\epsilon(\theta, \lambda, T)}{[\epsilon(\theta, \lambda, T)]_{polished}} = f\left(\frac{\sigma_m^2}{\lambda^2}, \frac{a^2}{\lambda^2}, \theta\right) \tag{15}$$

Attempts to correlate to these variables were made on the data presented in Section VII. However, no clear indication was obtained that these variables are sufficient for description of emittance properties. This failure could be an indication of the inadequacy or incompleteness of the groupings as well as an indication that the profilometer data on σ_m and a were not sufficiently accurate. Optical determinations of σ_m and a from bidirectional reflectance measurements were not made during this program since instrumentation was not available. However, such measurements are planned and may provide more realistic values of σ_m and a for purposes of further analysis of the emittance results.

4. OXIDIZED SURFACES

The effect of oxidation on the radiant properties of metal surfaces is of practical interest for several reasons. Because of their spectral emittance characteristics, the total emittance of clean metal surfaces is lowest at low temperatures and increases almost linearly with increasing temperature whereas the temperature variation of total emittance for oxides may be either positive or negative depending upon the location of spectral absorption bands. Also, the total hemispherical emittance of metal surfaces is generally from 20 to 30% higher than the total normal emittance whereas the total hemispherical emittance of oxides is from 0 to 10% lower than the total normal emittance. Between the low and high limits of emittance associated with these surfaces a wide variety of radiant characteristics is obtained depending upon the thickness of the oxide, its uniformity, and upon the optical properties of the oxide and the metal substrate. Those oxide coatings whose thickness is such that their radiant properties are influenced by the substrate metal are usually classified as thin films. Many of the oxide films that form on metal surfaces under ordinary exposure conditions fall into the thin film category.

With the development of vacuum deposition technology, a considerable amount of literature has been published concerning the optical properties of thin films [e.g., (3) and (19) through (21)]. The interest has concentrated, however, on the ultraviolet and visible reflectance properties of thin metal films. Very little attention has been given to the effects of absorbing oxide films on the infrared emittance characteristics of metal surfaces. Of the work that has been done with oxide films, most has been in connection with the effects of thin, weakly absorbing, protective films, such as silicon monoxide, on the reflectance properties of metallic mirror surfaces (22).

16

Calculations of the effect of a weakly absorbing dielectric film on the spectral normal reflectance of an opaque metallic reflector are reported by Turner in (21). His results for a high and a moderately high reflector are shown in Figures 6 and 7. For the case illustrated in Figure 6, the complex index of refraction of the metal reflector is taken as: $\bar{n} = 6.1 - i(36.4)$. This corresponds to the index for aluminum at $\lambda = 4\,\mu$. The index for the dielectric film is taken as $\bar{n} = 1.8 - ik$, and four cases corresponding to absorption coefficients of $k = 0,\ 0.05,\ 0.10$, and 0.20 are shown. The index for the first case, i.e., $\bar{n} = 1.8 - i(0)$ corresponds to that for SiO in the visible and infrared. The curves show the effect of film absorptance and film thickness on the spectral normal reflectance characteristics for SiO films on aluminum at $\lambda = 4\,\mu$. The reflectance is highly sensitive to slight increases in film absorptance. Correspondingly, significant increases in the emittance of the surface at this wavelength would be expected.

Figure 7 shows analogous curves for the same coating on a less highly reflecting metal with an index of $\bar{n} = 2.5 - i(28)$. This index corresponds to that for inconel at $\lambda = 0.546\,\mu$.

Although naturally occurring oxide films may significantly affect the reflectance of metal surfaces in the ultraviolet and visible spectral region, such films may have very little effect on the infrared emittance. As an example, Bennett (23) shows the calculated effect of thin (10 to 100 Å) oxide films on the spectral normal reflectance of aluminum at wavelengths from 0.5 to 5 μ. At wavelengths longer than 1.5 μ, the change in reflectance calculated for the 100 Å thick film is shown to be less than 0.1%.

Experimental data showing the effect of oxidation on the spectral normal reflectance of titanium have been reported by Edwards in (24). For films between 500 and 700 Å thick, a significant absorption band was observed in the 0.5- to 1.0-μ region. Beyond 1.5 μ, however, the observed drop in reflectance decreased from 20% to about 5% at 14 μ. By roughening the titanium substrate before oxidation, a wider but less deep absorption band was obtained which was attributed to the formation of a less uniform (variable thickness) oxide film.

For thicker films of Al_2O_3 which were vacuum deposited over aluminum, Hass (25) reports spectral reflectance data showing that significant increases in the infrared emittance can be obtained without changing the solar absorptance. The data presented by Hass include coating thicknesses of 0.5, 1.0, and 1.5 μ; the latter coating showing a marked drop in reflectance at wavelengths longer than 9 μ.

Thus far only the effect of different optical constants between the film and substrate has been considered. Additional complications are introduced when scattering occurs within the film.

Richmond (26) has derived equations for the spectral normal and hemispherical emittance of composite specimens consisting of partially transmitting, light scattering coatings over opaque substrates. The equations relate the emittance of the surface to the coating thickness, the reflectance properties of the coating and substrate, and
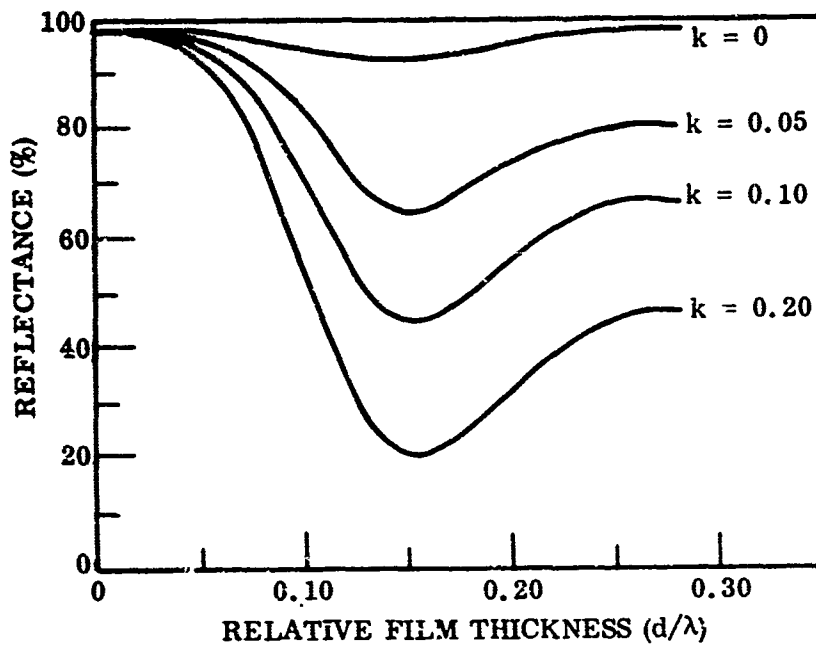
Figure 6 Calculated Reflectance of a Dielectric Film, $\bar{n} = 1.8 - ik$, on an Opaque Metal, $\bar{n} = 6.1 - i(30.4)$. [From Turner (21)]
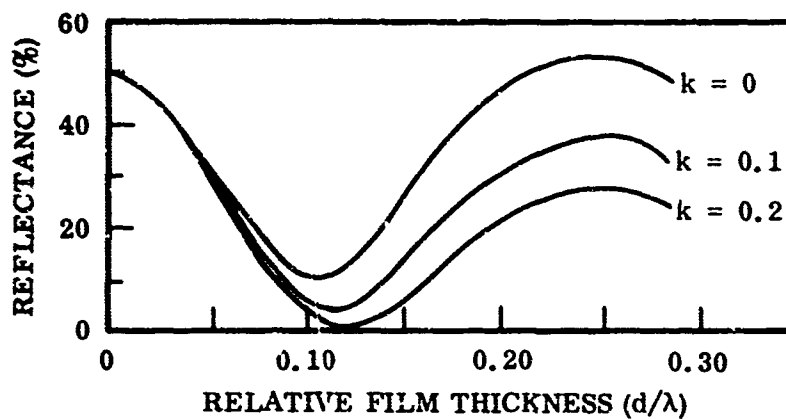
Figure 7 Calculated Reflectance of a Dielectric Film, $\bar{n} = 1.8 - ik$, on an Opaque Metal, $\bar{n} = 2.5 - i(2.8)$. [From Turner (21)]

18

the absorption and scattering coefficients of the coating.   Figure 8 shows the
effect of coating thickness on emittance for a specimen with properties which ap-
proximate those for a glossy gray paint coating over a polished metal substrate.
The family of curves designated by different values of $\bar{\sigma}$, show the effect of variations
in the absorption and backscatter coefficients for the coating $\left[\bar{\sigma} = \sqrt{K(K+2S)} \right]$. In a
later publication, Richmond (27) uses the same equation to demonstrate that the
emittance of nonmetallic surfaces should be essentially independent of surface rough-
ness. The analysis is supported by experimental data for the spectral normal emit-
tance of alumina.

The references above are cited to indicate that analytical treatments are available for
a simple, ideal, coating-substrate system, i.e., a system for which the surface inter-
faces are perfectly smooth, the coating thickness is uniform, and the optical proper-
ties of the coating and substrate are known. When these conditions are met, the
analyses provide values for the monochromatic reflectance. Edwards (24) presents an
extended analysis to account for irregular film thickness wherein he assumes a saw-
tooth surface profile. The results of the analysis indicate broadening of the absorption
bands due to the changing thickness; however, these results may only be used to indi-
cate probable trends. The actual geometry of oxide films is far more complex than
the analytical model and would require a detailed statistical analysis for prediction of
the radiative properties. The nonuniform geometry and frequently variable composi-
tion of most metal oxide films formed under natural exposure conditions, in combina-
tion with the almost complete lack of optical property data for oxides in the infrared,
presently require that the directional and total emittance characteristics of any par-
ticular oxide system be determined experimentally. This report contains the results
of such an experimental evaluation and demonstrates the complex surface conditions
that are created by surface oxidation. The trend of the results is in agreement with
the established analyses referred to above; however, direct analytical predictions of
the measured results were not possible.
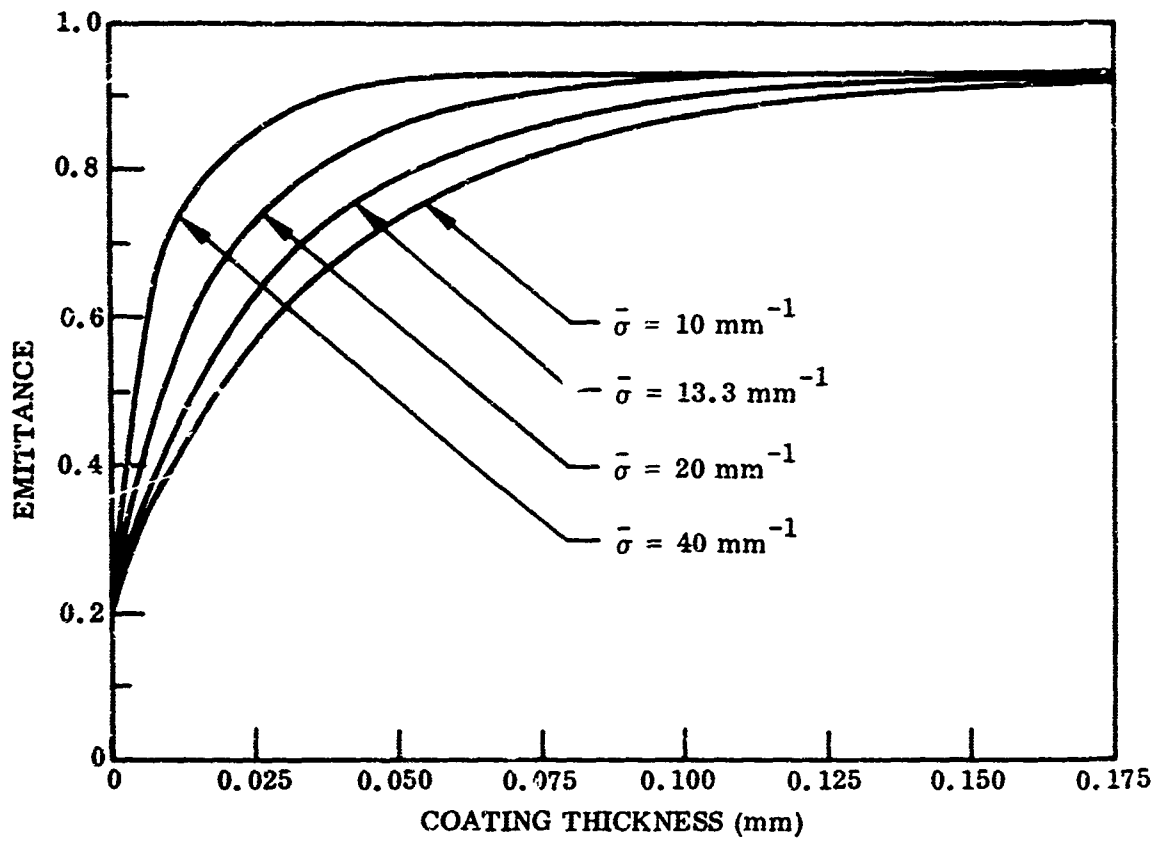
Figure 8. Calculated Emittance Versus Coating Thickness for Composite Specimen [From Richmond (26)]

Section III

SAMPLE PREPARATION AND CHARACTERIZATION METHODS

1. ROUGH (PLATINUM) SAMPLES

One of the important conclusions from test results of the first year was that rough metal surfaces with σ_m values as high as 200 μin. still retain directional, non-Lambertian, emittance characteristics. The observed changes in directional emittance characteristics for rough-surfaced samples relative to the directional characteristics for smooth-surfaced samples were most dramatic, however, for changes in σ_m between 0 and 100 μin. Additional studies of surfaces with σ_m values in this latter range were needed, therefore, to obtain a more complete understanding of the effect of roughness on directional emittance. Platinum was selected as the metal for further study because of its inherent chemical stability at the high temperatures required for the emittance tests and its amenability to preparation with controlled degrees of surface roughness.

Six 2 by 8 by 0.008 in. platinum strips were obtained with as-received surface characteristics similar to those for the three samples studied previously. The purity of the strips was certified to be 99.9+ % and special, highly polished rollers were used to provide a uniform thickness and a bright, smooth surface.

Faint longitudinal roll marks were just discernible on the as-received surfaces. Profilometer traces indicated rms roughness values of 4.3 μin. in the transverse direction (perpendicular to the rolling direction), and less than 0.5 μin. in the longitudinal direction. Surface interference micrographs indicated the roll marks were spaced between 100 and 400 μin. apart and were between 5 and 20 μin. deep. X-ray diffraction patterns indicated a highly preferred orientation of (200) and (220) crystal planes for the rolled platinum surface. These characteristics are discussed in more detail in subsection V.1.a, along with changes that occurred as a result of the high-temperature emittance-test exposures.

a. Sample Preparation

The glass hot blast method described in (1) was used to prepare the platinum sample surfaces. This method was selected because of its following desirable features:
(1) high surface purity is maintained and contamination by embedded material is minimized relative to such alternate methods as sand blasting or grinding; (2) large surface areas can be uniformly roughened to obtain σ_m values between 10 and 150 μin. with relatively good control over the parameters used to achieve the different degrees of roughness; (3) the roughness profiles produced by this technique, are independent of direction (i.e., are isotropic), and the distribution of profile heights is approximately Gaussian.

21

Five of the platinum strips were roughened using glass shot with diameters between 0.0005 and 0.0021 in.(13 to 53 μ). The shot-blast chamber was specially equipped with a filter and circulation system for removing used beads from the air stream, an adjustable regulator for controlling the air stream pressure, and a manual control for maintaining a fixed distance between the sample and the shot-blast nozzle. Each sample was roughened on both sides to within 1/4 in. of each end. The samples were supported on a heavy steel block while they were blasted to prevent excessive deformation and warpage. For the treatments used in this year's program, sample deformation due to the peening action of the shot was not a serious problem. After being roughened, each sample was cleaned for 10 min in an ultrasonic bath of trichlorethylene, rinsed in alcohol, dried, then stored in a desiccated belljar until ready for instrumentation and testing.

A summary of the shot-blast parameters used to prepare each sample and the resulting rms roughness obtained is shown in Table II. Sample identification numbers are followed by the letter B to differentiate them from similarly numbered samples tested last year. Sample 1B was tested as received to provide comparative data for the emittance characteristics of essentially smooth platinum.

Table II

SURFACE PREPARATION PROCEDURES FOR PLATINUM SAMPLES

Sample No.	Shot-Blast Pressure (psi)	Shot-Blast Distance (Nozzle to Sample) (in.)	rms Roughness[a]	
			(μin.)	(μ)
1B[b]			4.3	(0.11)
2B	5	12	15	(0.38)
3B	10	12	28	(0.70)
4B	20	6	49	(1.23)
5B	30	6	39	(0.98)
6B	60	6	127	(3.18)

(a) Determined from initial profilometer traces for each sample.
(b) Tested as received. Roughness values are for direction perpendicular to the roll marks.

It will be noted later that no test data were obtained from platinum sample No. 2B. During a pre-emittance test anneal treatment of this sample at 1645°K, an air blister formed in the center of the strip which made the sample unsuitable for testing. It will also be noted from Table II that the initial rms roughness of sample 5B was less than

22

that of sample 4B, even though a higher blast pressure was used to prepare this sample. The rms roughness of sample 5B was intended to be on the order of 70 to 80 μin. and no reason was discovered for the lower σ_m value actually obtained. This discrepancy indicates the need for further improvements in the shot-blast technique in order to produce surfaces with specific roughness values.

b. Surface Characterization Methods

Profilometric, photomicrographic, x-ray diffraction, and spectrographic methods similar to those described in (1) were used to evaluate the surface characteristics of each platinum sample. By these methods, a fairly complete description is obtained of the geometrical, physical, and chemical characteristics important to the process of thermal emission from a metallic surface. Experience gained during the study of the previous year had shown that the surface characteristics of metallic samples changed significantly during the high-temperature emittance tests in a vacuum environment. Since these thermally induced changes could not be avoided, the surface characteristics of each sample were determined both before and after the emittance tests whenever possible. The emittance-test procedure was such that each sample was first annealed at the maximum test temperature (1645°K) until a stable emittance was indicated before collecting emittance data at the lower test temperatures. A discussion of the changes observed between the initial and final surface characteristics of each sample is contained in Section V. A brief discussion of the methods used to evaluate the surface characteristics of the samples is contained in the following paragraphs.

(1) Profilometry

Profilometer traces were the principal source of information about the geometrical characteristics of each sample surface. A complete description of the profilometer used for this program has been given in (1). Profile traces were obtained before and after each emittance test to determine the initial and final surface characteristics of the samples. Each time, several longitudinal and transverse traces were made to ensure that the traces were representative of the sample test area, and to check the uniformity and nondirectional characteristics of the surface profile. The length of each sample trace was 0.25 in. and the horizontal scale for the recorded profile was 1000 μin. per 0.5 in. chart division. Vertical scale factors of 5, 25, and 100 μin. per 0.25 in. chart division were used depending on the roughness of the sample. At least 100 profile height measurements were made to calculate the surface roughness parameters, using the methods described in (1).

Microscopic examinations of each sample surface were also made to check on the accuracy of the profilometer traces. No evidence of surface scratching by the profilometer stylus was detected nor did any of the profile irregularities appear to be incapable of measurement by the stylus except possibly for those on the as-received platinum surface. The relatively close spacing of the roll marks on this latter surface may have prevented stylus contact with the deeper valleys, thereby causing the recorded profile to appear smoother than the true surface profile. Evidence of this

23

error was obtained from surface interference photomicrographs of the sample which indicated peak-to-valley depths two to three times larger than were indicated by the profilometer traces. Profile traces for the remaining samples are believed to be free of the errors associated with the size and weight of the stylus; consequently, the roughness parameter values calculated from these traces should be accurate descriptions of the true surface profiles. Repeated determinations from separate traces indicated variations in the calculated values of σ_m of less than $\pm 5\%$.

(2) Photomicrography

As mentioned above, microscopic examinations of the sample surfaces were made to verify the height and spacing of the profile features indicated by the profilometer traces. Photomicrographs also provided supplemental information about the uniformity and topography of the surface finishes and about the crystallinity of the surface metal. Various micrographic techniques were used including surface photomicrographs, surface interference photomicrographs, and taper section photomicrographs. The methods and apparatus used were essentially the same as described in (1). Illustrations and results obtained by these methods are discussed in Section V of the report.

Surface interference micrographs provided valuable information about the irregularities on the as-received and annealed surfaces of the unroughened platinum sample (No. 1B), but meaningful interference patterns were not obtained for any of the roughened platinum surfaces. Similar results were reported for this method in (1). The relatively close spacing of the randomly distributed surface irregularities on the roughened samples produces a highly complex pattern of interference fringes which cannot be resolved by our microscope. Some success in overcoming this difficulty has been reported by other investigators (28,29) using the Zehender method of fringe demagnification. However, development of the technique required to utilize this method was not attempted for this program. For the interference micrographs shown later in Section V, $0.487\text{-}\mu$ monochromatic light was used. Therefore, fringe deviations equal to one fringe separation interval on the interference pattern correspond to surface height variations of $0.24\ \mu$ (10 μin.).

Taper-section photomicrographs provided supplemental information about the characteristic peak-to-valley depths of the profile irregularities on the roughened platinum surfaces. Measurements from the photomicrographs and from the profilometer traces for each surface were in good agreement; thereby reaffirming the accuracy of the profilometer data for these surfaces. The photomicrographs were not suitable, however, for the statistical determination of σ_m values because of their limited field of view and the complex appearance of the profiles of randomly rough surfaces. The taper sections shown in Section V were prepared with a taper angle of $5°45' \pm 15'$. This angle gives an additional magnification of $10 \pm 0.4\times$ to the vertical scale of the photomicrographs. Before preparing the taper-section mounts, each specimen was coated with a 3- to 5-mil electroplated layer of nickel to help preserve the profile boundary while the specimen was sectioned and polished.

24

(3) X-Ray Diffraction and Spectrographic Methods

These methods were routinely used to examine the surfaces of the as-received and roughened platinum samples. Although quantitative methods were not available for determining specific surface properties, the qualitati~ results obtained provided useful additional information about the physical and chemical characteristics of the surfaces before and after their preparation and testing.

X-ray diffraction patterns were of value primarily for their indication of the lattice orientations of the as-received and roughened platinum samples. A highly preferred orientation of (200) and (220) lattice planes was indicated for the as-received platinum. This characteristic was not appreciably affected by the shot-blast treatments used on samples 2B through 5B; however, the pattern for sample 6B indicated that the more severe treatment used to prepare this surface did cause some reorientation of the surface lattice. Annealing and grain growth that occurred during the high-temperature emittance test exposures had no measurable effect on the orientation of any of the samples.

Spectrographic analyses were made to confirm the initial purity specification for the platinum samples and to check for possible contamination of the roughened samples by the glass shot. This method is extremely sensitive to the presence of minute quantities of inorganic impurities in a metal. Therefore, the absence of the persistent (sensitive) lines for Si, the principal constituent of the glass shot, from the spectra of the roughened platinum samples was interpreted to confirm that no significant contamination of the surfaces resulted from the shot-blast treatments.

2. OXIDIZED (STAINLESS STEEL) SAMPLES

In addition to the study of roughened platinum surfaces, a second objective of this year's program was to determine the effect of oxidation on the directional emittance properties of a common, high-temperature alloy. Type 304 stainless steel was selected for this phase of the study because of its widespread use as a high-temperature alloy and its known susceptibility to oxidation.

Several 2 by 8 by 0.015 in. sample strips were obtained with a type 2B (bright, annealed) surface finish. The chemical analysis of the sheet from which the samples were obtained was certified as follows:

Chromium	18.37%	Carbon	0.058%
Nickel	8.89%	Phosphorus	0.025%
Manganese	1.50%	Sulfur	0.007%
Silicon	0.50%	Iron	Balance

The surface condition of the as-received samples was smooth ($\sigma_m \approx 5~\mu$in.) but dull gray in appearance. To obtain clean, bright surfaces to enhance the formation of uniform reproducible oxide films, all of the stainless steel samples were electropolished and cleaned using the following procedure:

- Step 1. Soak for 5 min in a $Na_4P_2O_7$ solution (60 g/liter) at 130°F.

- Step 2. Electropolish for 20 min in a H_3PO_4-H_2SO_4 solution (Electrogleam 55 by MacDermid, Inc.) at 80°F. Lead cathodes, 15 A per strip, no agitation.

25

- Step 3. Rinse with distilled water.
- Step 4. Dip in solution of nitric acid (100 ml per liter) and sodium dichromate (20 g per liter).
- Step 5. Rinse and dry.

After electro polishing, several of the sample strips were roughened by glass-shot blasting using a blast pressure of 30 psi and a blast distance of 4 in. from the surface. To further aid in obtaining uniform and reproducible oxidation results, both the smooth and the roughened samples were then annealed for 10 min at 1040°C in a dry hydrogen furnace. Profilometer traces of the annealed surfaces indicated rms roughness values of 13 μin. for the electropolished samples and 20 μin. for the roughened samples. The initial characteristics of these unoxidized surfaces and changes due to their instability during the high-temperature emittance test exposures are discussed in more detail in subsection V.2.a.

a. Oxidization Procedures

Several methods were investigated for obtaining oxide films of suitable thickness and uniformity for this study. Initially, samples were oxidized in air using an open-end, muffle tube furnace. The results obtained were generally poor. The oxides formed were nonuniform in appearance and frequently spalled off the substrate when cooled. Reproducibility of results under duplicate exposure conditions was also poor. Subsequent tests in a controlled atmosphere furnace, using wet hydrogen, gave improved results and this method was finally selected for preparing the oxidized samples. The advantages of this method were: (1) uniform appearing oxide films were obtained; (2) the oxide films were strongly bound to the substrate, i.e., did not spall or flake off; (3) the oxidation rate was approximately the same for both the smooth and the roughened surfaces; (4) the repeatability of results was comparatively good; and (5) the composition of the oxide films was approximately the same for all samples regardless of thickness.

For the emittance tests, four pairs of smooth and roughened samples were oxidized in the wet-hydrogen atmosphere furnace, and one pair was retained for measurements of the emittance properties of the unoxidized surfaces. A summary of the oxidation exposure conditions and results obtained is shown in Table III. The sample identification numbers have been given the suffix S or R to designate a smooth or rough substrate surface, respectively.

Three 1-in. diameter disk samples were also prepared concurrently with each sample test strip to provide samples for the following pre-emittance test characterization studies of the oxide films:

- Spectral normal reflectance at room temperature
- Electron micrographs of the initial oxide films
- Electron diffraction patterns of the initial oxide films

26

Table III

OXIDATION EXPOSURES FOR 304 STAINLESS STEEL SAMPLES

Sample No.	Oxidation Temperature and Time[a]	Average Weight Gain (μg/cm^2)	Approximate Film Thickness[b] (μ)	Color of Oxide Film
1S 1R	Not oxidized	–	–	--
2S 2R[c]	600°C for 30 min	2.1 2.9	0.015 0.020	Gold
3S 3R	800°C for 30 min	24.3 23.6	0.170 0.165	Purple
4S 4R[c]	1000°C for 30 min	135.7 136.0	0.95 0.95	Dull gray
5S 5R	1000°C for 90 min	200 219	1.40 1.53	Dark brownish gray

Notes:

    (a) Wet hydrogen atmosphere. Hydrogen flow rate of 25 cfm through humidifier of the controlled atmosphere furnace.

    (b) Approximate film thickness values are based on sample weight gain data and the assumption of a uniform film of Fe_3O_4 with an average density of 5.2 g/cm^3.

    (c) Samples 2R and 4R not tested.

After oxidation, each sample was stored in a desiccated belljar until ready for instrumentation and testing.

In the discussion of results in Sections V and VII, it will be noted that because of surface instability of the samples at test temperatures above 950°K three separate samples of the smooth, unoxidized stainless steel were tested to obtain suitable data for this surface. These samples were designated 1S-1, 1S-2, and 1S-3 to indicate the chronological order in which they were tested. Of these samples, only the test data for samples 1S-2 and 1S-3 are presented. Because of the observed similarity of results for the roughened and smooth substrate samples, samples 2R and 4R were not tested.

b. Oxide Characterization Methods

Root-mean-square roughness values for the smooth and roughened, unoxidized, stainless steel surfaces were determined from profilometer traces by the same procedures as described in subsection III.1.b. To investigate the thickness, composition, and morphology of the oxide films, considerable emphasis was placed on the use of electron micrographic and diffraction techniques. Except for the most heavily oxidized samples, the oxide films were too thin to be effectively studied by ordinary photomicrographic and x-ray diffraction methods. In the remainder of this section, the various methods used to examine the oxide film characteristics are described.

(1) Film Thickness Measurement Methods

Methods investigated for obtaining direct measurements of oxide film thickness included photomicrographic and electron micrographic techniques and the use of an electronic film thickness measurement gage (the Dermitron). Indirect estimates of average film thickness were also made from weight-gain data obtained by weighing each sample before and after its oxidation exposure, and from the colors of the oxide films. In general, none of the direct measurement methods provided reliable film thickness data. The primary reason for the failure of these methods was the nonuniformity of the oxide film thickness. Secondarily, the time and expense required to develop and refine the methods were beyond the scope of this program. Consequently, most of the thickness values cited in this report are estimates based on the weight-gain data for each sample.

Attempts to correlate the Dermitron gage readings with film thickness were totally unsuccessful and this method was abandoned early in the study. Some success was obtained in measuring the thickness of the more heavily oxidized samples (4S and 5S) from high-magnification photomicrographs of carefully prepared and polished cross-section mounts of these samples. (See subsection V.2.a.) However, the thinner oxide films were not detectable by this method.

Two different electron micrographic techniques were investigated for determining the thickness of thin films. The first involved replication of the metallurgical polished cross-section mounts used for the photomicrographic studies. Because of difference in the polishing characteristics of the mount material (bakelite), the oxide film, and the substrate metal, some relief existed at the oxide film boundaries which could be observed on the replica. The replicas obtained in this manner, however, were frequently marred by extraneous artifacts, e.g., cracks in the mount which caused tears in the replica and flakes of oxide which stripped off with the replica, which prevented the acquisition of clearly defined film boundaries. The reliability of film-thickness values obtained by this method was also impaired by the nonuniform nature of the films in combination with the small field of view covered by the electron micrographs. Typical electron micrographs obtained by this method are shown in subsection V.2.a. It will be noted that the film thickness values indicated by the electron micrographs of samples 4S and 5S are about 2 times larger than the thickness values indicated by the photomicrographs and inferred from the sample weight-gain data for these samples.

The second electron microscope technique investigated involved stripping the oxide film from the substrate, then obtaining a shadowgraph of the free film in cross section. Most of the films were easily stripped from their stainless steel substrates by immersing the sample in a solution of bromine and methanol for a few minutes. The method is essentially the same as reported by Mahla and Nielsen (30). The free film was then cast into a mold of epoxy resin and, after the mold had cured, a thin cross-section slice of the film and mold was obtained with a microtome. This specimen was then mounted in the microscope and a transmission micrograph taken. The micrograph shows a dark silhouette of the film in cross section, as a result of its high absorption relative to the surrounding epoxy. Typical shadowgraphs obtained in this manner are shown in subsection V.2.a. Film boundaries were not well defined in the shadowgraphs obtained in this program and the irregular thickness of the films made interpretation still more difficult.

Best estimates of average thickness for the initial oxide films are believed to be those based on the weight-gain data obtained when the samples were oxidized. Each sample was weighed on a laboratory balance before and after its oxidation exposure. The balance sensitivity was 10 μgrams, and since the total surface area of the samples was large (about 200 cm^2). weight changes on the order of 0.05 $\mu g/cm^2$ could be detected. To convert oxidant weights to equivalent oxide film thickness, it is necessary to assume a uniform film thickness of known composition and density. Based on the results of the oxide composition determinations described below, the oxide films on these samples were assumed to be Fe_3O_4 with a density of 5.2 g/cm^3, and a factor of 70 was calculated for the conversion of weight gain per unit area to thickness in angstroms.

Rough estimates of film thickness can also be inferred from the color of the film; however, this method is subject to considerable error depending upon the width of the interference bands and the characteristic colors of the metal and the oxide. A summary of color versus film thickness data for several metals and oxides is presented in (31) along with an explanation of the origin of colors for thin (interference type) films. The lack of agreement between investigators shows that color by itself does not provide an accurate measure of thickness. Color versus thickness data for oxide films on type 304 stainless steel, reported in (32), indicates that interference colors are produced by films with thicknesses ranging from 100 to 2500 Å. For thicker films, the characteristic color of the oxide predominates.

(2) Oxide Composition Determinations

The chemical composition of the oxide films was determined exclusively from electron diffraction patterns. Transmission patterns of the thin oxide films were obtained by stripping the films from the metal, as described earlier; and reflection patterns were obtained for the thicker oxide films. The effective wavelength for the patterns was calibrated using a gold foil standard. Interplanar "d" spacings for the oxide patterns were then determined and compared with those obtained by other investigators using x-ray diffraction methods (33). Typical diffraction patterns for the oxide films in this study are shown in subsection V.2.a.

29

In addition to providing information about the composition of oxide films, electron diffraction patterns may also serve to indicate the average grain size of the oxide crystallites. In general, sharp, uniform diffraction rings are obtained from fine-grained oxide films, and spotty, nonuniform rings indicate large-grained structures with preferred lattice orientations. Broad, diffuse rings generally indicate an amorphous structure.

(3) Surface Morphology

Variations in the surface morphology of the oxide films resulting from the different oxidation exposures were examined using both photomicrographic and electron micrographic methods. Examinations before and after the emittance tests also served to indicate the changes in surface morphology resulting from the high-temperature exposures in vacuum. Typical before and after micrographs for each sample are shown in subsection V.2.a. The electron micrographs were obtained using a double replication technique.

Section IV

EXPERIMENTAL APPARATUS AND PROCEDURES

1. APPARATUS

The experimental apparatus used to measure the emittance characteristics of the platinum and stainless steel samples is shown in Figures 9 and 10. The apparatus consists of a water-cooled, evacuated test chamber which surrounds an electrically heated sample. The sample may be rotated in azimuth while it is viewed by an external optical transfer system. The optical system focuses an image of the center portion of the sample either on a total radiation detector or on the entrance slits of a monochromator for spectral measurements. Provision is made to also view a reference blackbody source through the same optics for absolute emittance determinations.

Although a description of the apparatus is contained in (1), several modifications were made to improve the vacuum stability of the test chamber and the measurement accuracy of the sample azimuth angle before starting the experimental phase of this year's study. Additional instrumentation was acquired to permit calorimetric determinations of total hemispherical emittance, and the optical transfer system was modified to improve the total radiation measurements.

a. Vacuum Test Chamber

The vacuum chamber consists of a water-cooled stainless steel bell jar which is 12 in. in diameter and 14 in. high. The cylindrical chamber rests on a 1-in.-thick stainless steel base plate. Conduction from the chamber walls to the cooling coils was aided by the application of Thermon, a high-conductance cement, over the external surface of the chamber and cooling coils. The inner surface of the bell jar was coated with a low-reflectance, flat black paint, to minimize internal reflections. A potassium bromide window in the chamber view port transmitted emitted energy from the sample to the external optics and the radiation detectors. A sample view port with a quartz window was also provided for visual observation of the sample and optical pyrometer temperature measurements. Removable vacuum feed-throughs were mounted in the base plate for access to the sample instrumentation wires.

The chamber vacuum system was modified by replacing the original 2-in. oil diffusion pump with a high-speed, 4-in. pump and manifold connected to the base plate. This change, in conjunction with the elimination of the large O-ring seal for the rotating sample mount, improved the test chamber vacuum by more than an order of magnitude. Pressures on the order of 10^{-6} to 10^{-5} Torr were maintained inside the chamber even during the highest sample-temperature tests. A large liquid nitrogen cold trap and a water-cooled baffle were located between the diffusion pump and the test chamber to

Figure 9 Directional Emittance Apparatus
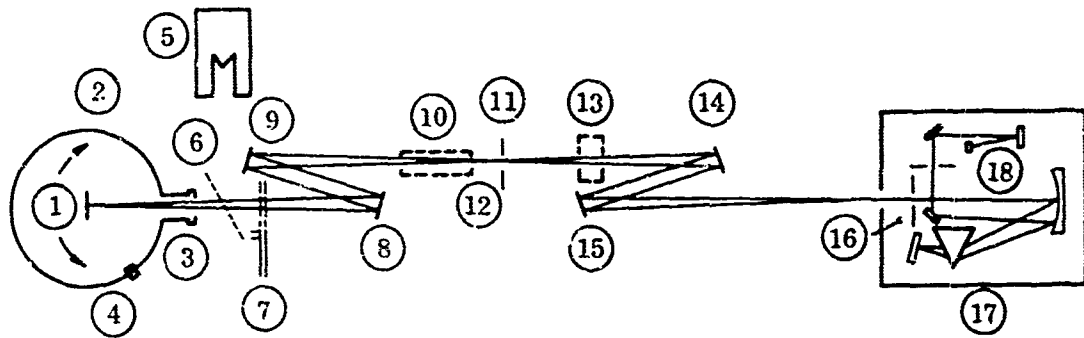
1. SAMPLE
2. VACUUM CHAMBER
3. KBr WINDOW
4. PYROMETER PORT
5. BLACKBODY
6. SELECTOR MIRROR
7. CHOPPER
8. 18-IN. FOCAL LENGTH SPHERICAL MIRROR
9. PLANE MIRROR
10. POLARIZER
11. ADJUSTABLE SLIT
12. IMAGE PLANE
13. VAC. THERMOCOUPLE – TOTAL DETECTOR
14. PLANE MIRROR
15. 11-IN. FOCAL LENGTH SPHERICAL MIRROR
16. INLET SLITS
17. MODEL 98 MONOCHROMATOR
18. VAC. THERMOCOUPLE DETECTOR

Figure 10 Schematic Layout of Directional Emittance Apparatus

33

minimize back-streaming of oil into the chamber. A zeolite trap was also located in the vacuum roughing line between the 5 cfm fore-pump and the chamber to remove oil vapors from this source. Chamber pressures were measured with a nude-type ionization gauge located in the base plate but shielded from the sample by a water-cooled plate.

b. Rotating Sample Mount and Angle Indication System

A considerable modification was made to the rotating sample mount to eliminate the large O-ring seal and flange arrangement used last year. The modified sample mount is shown in Figure 11. The sample is tightly clamped between two water-cooled copper electrodes. Both electrodes pass through a 1-3/4 in. diameter insulated rotatable vacuum seal located in the bottom of the vacuum manifold, 6 in. below the base plate. The electrodes are rigidly supported at the base plate level by an insulated steel yoke which turns on a 4-in. diameter ball bearing and race press-fitted into the base plate. The sample can be rotated about its longitudinal center-line axis to 95 deg on either side of the normal viewing angle. Variable tension can be applied to the sample by means of a bellows and spring-tension system in series with the lower electrode.

A new angle-indication system was also built to replace the previously used pointer and scale system. The new system consists of a 3-turn, precision potentiometer which is mechanically linked to the sample rotation shaft so that the resistance of the potentiometer varies linearly with the angular position of the sample. A small, constant current is passed through the potentiometer and the angular position of the sample is indicated by the voltage drop between the wiper arm and one end of the potentiometer. Voltages were read out on a four-place digital voltmeter.

In operation, the potentiometer current was adjusted through a variable resistor to 2.61 mA to obtain a signal of 10 mV per degree of sample rotation. This gave a readout sensitivity of 0.1 deg. The accuracy and repeatability of the system was calibrated using an eight-sided gage block to which mirrors were attached and whose angles between adjacent sides were known to within 0.1 deg. The calibration data indicated that the system was accurate and repeatable to within 0.2 deg over the entire angular range.

Electrical power to heat the sample was supplied by a variac-controlled, 10 kVA, stepdown transformer with a maximum current output of 1000 A at 10 V, or 500 A at 20 V. The current was measured with a 1000 A, 100 mV current shunt in series with the sample circuit. Voltage drops across the shunt were read to four-place precision with a Fluke Model 803B differential ac-dc voltmeter. The maximum power requirement for this study was 420 A at 8 V for heating the platinum samples to 1640°K.

c. Optical and Radiation Measurement System

Radiant energy from the sample was collected and focused on either the total or the spectral energy detectors by the optical system shown in Figure 10. All of the reflecting surfaces were front surface aluminized mirrors. The sample energy entered the optical

34

Figure 11 Rotating Sample Mount

system through a 1-1/2-in. diameter KBr window in the chamber wall. [3]* The window was tilted at an angle of 5 deg to the optical axis of the system to prevent interreflections between the sample and window surfaces at normal incidence. Radiant energy from the reference blackbody source [5] could be directed into the same optical path as the sample energy by means of a 45-deg mirror [6] located in front of the KBr window. The energy from either source was chopped at 13 cps by a Perkin-Elmer chopper [7] and collected by an 18-in. focal length spherical mirror [8] which was masked to limit the collecting half angle to 1.5 circular deg (2.1×10^{-3} sr).

Energy collected by the spherical mirror [8] was directed to the plane mirror [9] and then to the variable aperture slit [11]. At this position a real image of the sample was formed at a magnification of 1.6 × and the slit adjusted so that it was completely filled for viewing angles up to 88 deg from the normal. This condition was obtained for a slit-width setting of 0.035 in. After passing through the adjustable slit, the energy was either focused on the total radiation detector [13] or was directed to fill the entrance slits of a Model 13U Perkin Elmer monochromometer [16]. A real image of the adjustable aperture slit was formed at [16] at a reduced magnification of 0.75 ×. The monochromometer was equipped with a NaCl prism and a vacuum thermocouple detector. [18] Both the total and the spectral detector outputs were amplified and recorded by the Perkin-Elmer Model 107 amplifier.

With the exception of the KBr window and the blackbody selector mirror, the optical paths from the sample and the blackbody to the detectors were identical; consequently, the results were independent of the reflectance of the mirrors [8], [9], [14], and [15]. However, absolute emittance determinations required absolute values for the transmittance of the KBr window and the reflectance of the blackbody mirror. The spectral transmittance and reflectance characteristics of these components were measured periodically throughout the experimental phase of the study to assure their stability. The optical system from the KBr window to the entrance slits of the monochromometer was enclosed within a black enclosure to eliminate pickup of stray radiation.

The reference blackbody was an Infra-Red Industries Model 406 equipped with a Model 101 temperature controller. This source is designed to operate at temperatures between 100° and 1000°C with a temperature stability of ±1°C. The cavity temperature was read with a platinum/platinum-10% rhodium thermocouple embedded in the cavity wall. The blackbody was used as a reference source for absolute total and spectral normal emittance determinations and as a calibration source for checking the response of the total and spectral energy detectors.

An infrared polarizer was used to determine the directional emittance characteristics of the parallel and the perpendicular components of polarized spectral energy emitted by the samples. The polarizer consists of ten 0.010-in.-thick silver chloride plates mounted in a rotatable housing and inclined at a polarizing angle of 75 deg to the optical axis. The characteristics of this polarizer have been described by Newman and Halford in (34). The spectral transmission characteristics of the polarizer used in this study are shown in Figure 12.

---

*Numbers in brackets in this section refer to the optical system components shown in Figure 10.

36
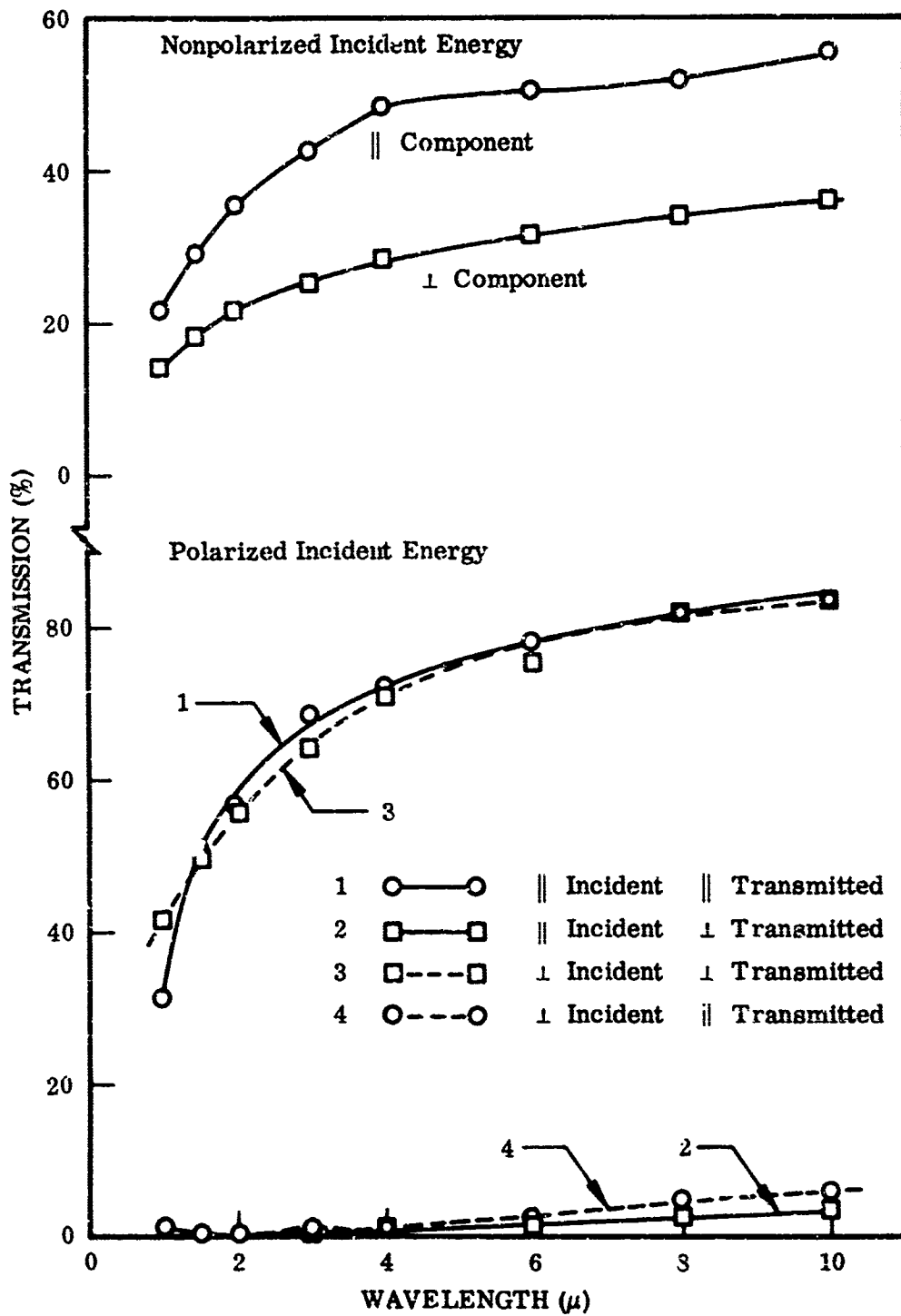
Figure 12 Polarizer Transmission Characteristics

2. EXPERIMENTAL PROCEDURES

With the exception of the calorimetric determinations of total hemispherical emittance, the emittance-measurement procedures used this year were the same as described in (1). Consequently, only the working equations used for the emittance calculations are summarized below.

a. Absolute Spectral Normal Emittance

For the arrangement shown in Figure 10 the spectral normal emittance is given by

$$\epsilon_s(\theta_N, \lambda, T) = \frac{\rho_m}{\tau_w} \frac{V_s(\theta_N)}{V_b} \left[\frac{E_b(\lambda, T) - E_a(\lambda, T)}{E_s(\lambda, T) - E_a(\lambda, T)} \right] \tag{16}$$

where $\epsilon_s(\theta_N, \lambda, T)$ is the absolute spectral normal emittance of the sample at wavelength λ; ρ_m is the spectral reflectance of the blackbody selector mirror [6] at wavelength λ; τ_w is the spectral transmittance of the KBr window [3] at wavelength λ; $V_s(\theta_N)$ is the detector signal when viewing the sample; V_b is the detector signal when viewing the reference blackbody; $E_b(\lambda, T)$ is the spectral emissive power of the reference blackbody; $E_s(\lambda, T)$ is the spectral emissive power of a blackbody at the temperature of the sample; and $E_a(\lambda, T)$ is the spectral emissive power of a blackbody at ambient temperature.

When the blackbody and sample temperatures are the same, Eq. (16) reduces to

$$\epsilon_s(\theta_N, \lambda, T) = \frac{\rho_m}{\tau_w} \frac{V_s(\theta_N)}{V_b} \qquad \text{(For } T_s = T_b) \tag{17}$$

In most cases, the sample and blackbody temperatures were not the same and Eq. (16) was evaluated using measured temperatures. Values for $E_b(\lambda, T)$, $E_s(\lambda, T)$, and $E_a(\lambda, T)$ were calculated with the aid of tables listed in (35). Values of $E_a(\lambda, T)$ were negligibly small except at wavelengths greater than 6μ.

The spectral normal emittance of the platinum samples at $\lambda = 0.65\mu$ was also determined from optical pyrometer readings by use of the pyrometer relation

$$\ln \epsilon_s(\theta_N, \lambda, T) = \frac{c_2/\lambda}{T_S - T_B} - \ln \tau_w \tag{18}$$

Here $c_2/\lambda = 22,135°K$; T_S is the true temperature of the sample; T_B is the brightness temperature of the sample; and τ_w is the spectral transmittance of the quartz viewing window at $\lambda = 0.65\mu$. T_S values were taken to be the temperatures indicated by the sample thermocouples. T_B values were the sample temperature readings obtained with a Micro Optical Pyrometer.

38

b. Relative Spectral Directional Emittance

As previously discussed in (1), the vertical refracting and reflecting surfaces in prism spectrometers introduce considerable polarization in the horizontal plane. Simon (36) found the degree of polarization for a Perkin-Elmer Model 12-B spectrometer to be about 30%. Because of the highly polarized nature of the radiation emitted by metal surfaces at off-normal direction angles, careful measurement procedures must be employed to eliminate the effects of apparatus polarization. The relative directional emittance cannot be measured directly without knowledge of the absolute polarization characteristics of the measuring apparatus.

To avoid this difficulty, measurements of the relative spectral directional emittance of each polarized component of the sample radiation were made, i.e.,

$$\epsilon_{\perp}(\theta, \lambda, T)/\epsilon_{\perp}(\theta_N, \lambda, T)$$

and

$$\epsilon_{\|}(\theta, \lambda, T)/\epsilon_{\|}(\theta_N, \lambda, T)$$

Emitted energy at the normal viewing angle, $\theta = \theta_N = 0$ deg is by symmetry circularly polarized; therefore, absolute values of emittance were determined only at that angle.

Relative spectral directional emittance for each of the polarized components were then determined from:

$$\frac{\epsilon_s(\theta, \lambda, T)}{\epsilon_s(\theta_N, \lambda, T)} = \frac{V_s(\theta)}{V_s(\theta_N)} \tag{19}$$

where $V_s(\theta)$ is the recorded detector signal obtained when viewing the sample at angle θ and $V_s(\theta_N)$ is the recorded detector signal obtained when viewing the sample at the normal viewing angle. Care was employed to maintain a constant sample temperature during the angular measurements since $V_s(\theta)$ and $V_s(\theta_N)$ are measured separately and small temperature variations could cause significant errors in their ratio. All of the relative spectral directional emittance data presented in Section VII have been normalized to a value of 0.5 at $\theta = \theta_N$ since

$$\epsilon_{\|}(\theta_N, \lambda, T) = \epsilon_{\perp}(\theta_N, \lambda, T) = 0.5 \, \epsilon_s(\theta_N, \lambda, T) \tag{20}$$

To obtain absolute values for the spectral directional emittance from these data, the normalized values for each polarized component must be added and then multiplied by the absolute spectral normal emittance value obtained at that temperature.

c. Absolute Total Normal Emittance

Absolute total normal emittance measurements are made by placing the total detector at position [13] in Figure 10. For this arrangement, the absolute total normal emittance is given by

$$\epsilon_s(\theta_N, T) = \frac{\rho_m}{\tau_w} \frac{V_s(\theta_N)}{V_b} \left[\frac{E_b(T) - E_a(T)}{E_s(T) - E_a(T)} \right] \tag{21}$$

where $\epsilon_s(\theta_N, T)$ is the absolute total normal emittance of the sample at temperature T: ρ_m is the reflectance of the blackbody selector mirror [6]; τ_w is the transmittance of the KBr window [3]; $V_s(\theta_N)$ and V_b are the recorded signals for the sample and the blackbody, respectively; $E_b(T)$ is the total emissive power of the reference blackbody; $E_s(T)$ is the total emissive power of a blackbody at the temperature of the sample; and $E_a(T)$ is the total emissive power of a blackbody at the ambient temperature of the surrounds. When the blackbody and the sample temperatures are the same, Eq. (21) reduces to:

$$\epsilon_s(\theta_N, T) = \frac{\rho_m}{\tau_w} \frac{V_s(\theta_N)}{V_b} \qquad (\text{For } T_s = T_b) \tag{22}$$

In most cases, the sample and blackbody temperatures were not the same and data were reduced by means of Eq. (21).

d. Relative Total Directional Emittance

Polarization of the total emitted energy is not a source of difficulty in these measurements since the collecting and detecting system does not influence the state of polarization. Polarized components were not determined for the total directional emittance measurements because of the nongray transmission characteristics of the polarizers. (See Figure 17.) The total energy emitted in each component is best obtained by integration of the spectral results.

The relative total directional emittance was determined from:

$$\frac{\epsilon_s(\theta, T)}{\epsilon_s(\theta_N, T)} = \frac{V_s(\theta)}{V_s(\theta_N)} \tag{23}$$

where $V_s(\theta)$ and $V_s(\theta_N)$ are the detector signals obtained at sample viewing angles of θ and θ_N, respectively. All of the relative total directional data presented in Section VII has been normalized to a value of 1 at $\theta = \theta_N$. To obtain values for the absolute total directional emittance, the normalized ratios must be multiplied by the absolute total normal emittance value at that temperature.

40

e. Spectral Hemispherical Emittance

As shown in (1), ratios of the spectral hemispherical emittance to the spectral normal emittance are obtained by integration of the directional results. Integration yields:

$$\frac{\epsilon(\lambda, T)}{\epsilon(\theta_N, \lambda, T)} = 2 \int_0^{\pi/2} f(\theta) \sin\theta \cos\theta \, d\theta = 2 \int_0^1 f(\theta) \cos\theta \, d(\cos\theta) \qquad (24)$$

where $f(\theta) = \epsilon(\theta, \lambda, T)/\epsilon(\theta_N, \lambda, T)$, i.e., $f(\theta)$ is the sum of the normalized relative spectral directional emittance values for the parallel and perpendicular polarized components. This form was used for numerical integration of the data to obtain the hemispherical results presented in Section V. By letting $f(\theta)$ represent the normalized relative total directional emittance values, defined in subsection IV.2.d, Eq. (24) gives the total hemispherical-to-total normal emittance ratio, $\epsilon(T)/\epsilon(\theta_N, T)$. These ratios are also presented in Section V.

f. Total Hemispherical Emittance

With the acquisition of an ac voltmeter for accurate measurement of the voltage drops across the current shunt and across the center uniform temperature region of the sample strips, calorimetric determinations of total hemispherical emittance were added to this year's experimental program. The method for determining $\epsilon(T)$ is analogous to the methods described by Richmond and Harrison in (37) and by Abbott et al. in (38). The total hemispherical emittance for the center region is given by

$$\epsilon(T) = \frac{VI - P_L}{A \sigma_0 \left(T_s^4 - T_a^4\right)} \qquad (25)$$

where V is the voltage drop across the center of the sample; I is the current flow; P_L is a power loss term to account for thermal conduction losses at each end of the center portion of the sample; A is the surface area; σ_0 is the Stefan-Boltzmann constant; T_s is the absolute temperature of the sample; and T_a is the absolute temperature of the surrounding chamber walls. V was measured between the platinum legs of the two thermocouples located on either side of the center line of the sample. P_L was determined from estimates of the temperature gradient at the location of the two thermocouples, from published data for the thermal conductivity of platinum and stainless steel, and from measurements of the cross sectional area of the sample. Estimates of the temperature gradients were obtained from inspection of graphical plots of the temperatures at the five different locations along the length of the sample strip. Except at the lowest test temperatures, both the P_L and T_a^4 terms were negligibly small. The surface area, A, was corrected for thermal expansion of the sample at each test temperature using published values for the expansion coefficients of platinum and stainless steel.

41

3. TEST PROCEDURE

a. Sample Instrumentation

Each sample was instrumented with five Pt/Pt-13% Rh thermocouples spot welded to the back surface of the test strip. Forty-gage thermocouple wire was used to minimize thermal conduction losses from the sample through the wires. The junctions were located approximately 1/2-in. from one edge of the strip and at vertical positions ±1, ±2, and ±3 cm from the center line of the strip. Care was taken to attach both wires of each junction at the same vertical location to avoid pickup of the ac voltage gradient along the strip. Between the junctions and the vacuum feed-through header, each wire was insulated with fiber-glass sleeving to prevent short circuits. (See Figure 11.) After passing through the vacuum feed-through, the leads were individually terminated in a reference-junction ice bath. Sample temperatures were determined from measurements of the thermocouple emfs with a Leeds and Northrup portable potentiometer.

b. Sample Test Procedures

Each sample was clamped into the rotating sample mount, the thermocouple wires attached to the vacuum feed-through leads, and the test chamber was evacuated to a pressure of 10^{-6} Torr. Each of the roughened platinum samples was then annealed at 1645°K (the highest test temperature) until a stable emittance was indicated by the sample heating power and temperature data. Except for platinum sample 6B, no significant change in emittance was observed over a 20-min anneal period. Sample 6B was annealed for 1 hr as the emittance of this sample appeared to decrease slightly during the first 1/2 hr. The smooth platinum sample (1B) was annealed for 6 hr at a lower temperature (1365°K) to minimize recrystallization of the sample before the first set of emittance data was obtained. No pre-test anneal was given to the stainless steel samples because of their nonstable surface characteristics at temperatures above 950°K.

Emittance tests of the platinum samples were made at five temperatures: nominally 865°, 1090°, 1225°, 1365°, and 1645°K (1100°, 1500°, 1750°, 2000°, and 2500°F). Complete sets of emittance data were taken at each temperature except 1225°K as permitted by the available sample energy. The 1225°K relative directional emittance measurements were omitted for samples 3B, 4B, and 5B. The stainless steel samples were tested at 535°, 670°, 810°, and 950°K (500°, 750°, 1000°, and 1250°F), starting at the lowest temperature, and samples 1S-3, 2S, and 3S were also tested at 1090°K (1500°F). Retests of most of the samples were made after completion of the measurements to check the stability of the sample emittance characteristics. A summary of the thermal history for each of the samples is presented in Section VII.

Absolute spectral normal emittance measurements were made with the variable aperture slit width set at 0.075 in. and the monochromator inlet slit width set at 0.30 mm to collect the maximum possible amount of sample energy at the lower test temperatures. For the high-temperature platinum sample tests it was necessary to reduce the monochromator slit width setting to 0.50 mm to avoid saturation of the detector. During

42

each sample-to-blackbody ratio measurement, care was taken to maintain constant values for such variables as optical alignment, monochromator slit width and wavelength settings, and amplifier gain.

Absolute total normal emittance measurements were made with the variable aperture slit width set at 0.015 in. and with an additional, horizontal aperture, 1/4-in. wide, in front of the vertical slit. This arrangement was employed to avoid saturation of the total detector system while at the same time obtaining uniform and complete irradiation of the total detector element. (See remarks for platinum samples 1B and 6B in subsections VII.1 and VII.5.)

Section V

RESULTS

i. PLATINUM SAMPLES

a. Surface Characteristics

Photom'~rographs of the five platinum sample; before and after emittance tests are shown in Figure 13. These pictures illustrate the sample-to-sample variations in surface appearance achieved by the various shot-b⸱s⸱ t treatments and show the changes in surface appearance due to the annealing, th⸱rmal etching, and thermal faceting which occurred during the high-temperature emittance tests. Very little quantitative surface profile data can be deduced from surface photomicrographs because of the small peak-to-valley dimensions relative to the lateral (peak-to-peak) dimensions. However, the photographs do provide a qualitative measure of increasing roughness and are presented here for that purpose. All the micrographs in Figure 13 were taken using dark-field (oblique) illumination of the surface, as opposed to bright-field (direct) illumination. The former type of illumination best indicates variations in surface appearance between samples and provides increased contrast between the recrystallized grain boundaries and the roughened grain faces.

Figure 13 shows the progressively more extensive surface pitting obtained on the platinum samp..s as a result of increased shot-blast pressure. Even the mild shot-blast treatment for sample 3B is sufficient to obscure the roll marks that are the pre-dominant feature of the as-received surface. The post-test surface micrographs show that recrystallization and thermal etching become less apparent as the initial roughness of the surface increases. Grain boundaries, which are the dominant feature of the unroughened surface, are still a significant feature of the surface of sample 3B. Grain boundaries are also detectable on the surfaces of samples 4B and 5B but are obscured on the surface of sample 6B. In all cases where grains were visible, it appeared that they were of the same average size for each sample, although sample 1B appeared to have a greater number of smaller grains and suffered considerably more thermal etching and faceting. The effects of the increased etching were clearly visible to the unaided eye because under various lighting angles the grains appeared to be blue and yellow. The roughened samples exhibited a more uniform gray appearance, even though grains could be observed without magnifying optics.

A summary of roughness characteristics for the platinum surfaces is presented in Table IV. Except for the approximate values for the as-received surface of sample 1B, shown in parentheses, all the parameters were determined from profilometer traces of the surfaces. Typical portions of these profilometer traces are shown in Figure 14. Samples 1B and 6B were the only two for which significant changes in

44

Before Emittance Tests

$\sigma_m = 4.3\ \mu\text{in.}$ 1B $\sigma_m = 28\ \mu\text{in.}$ 3B $\sigma_m = 49\ \mu\text{in.}$ 4B $\sigma_{in} = 39\ \mu\text{in.}$ 5B $\sigma_m = 127\ \mu\text{in.}$
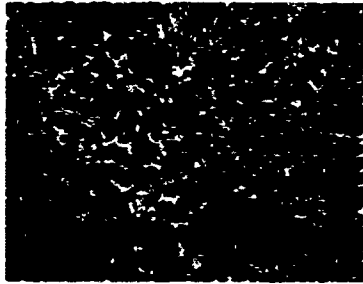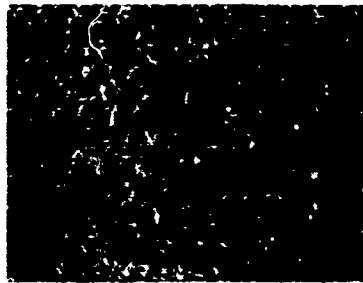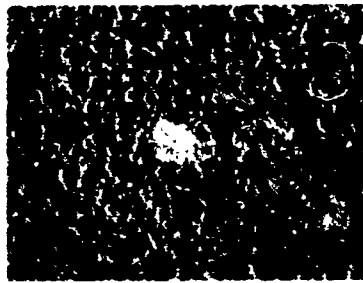
After Emittance Tests
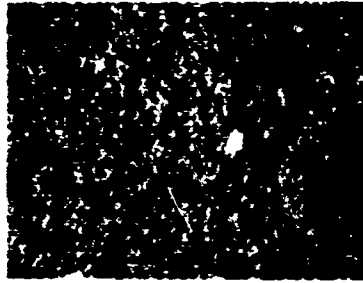
$\sigma_m = 8.0\ \mu\text{in.}$ $\sigma_m = 27\ \mu\text{in.}$ $\sigma_m = 43\ \mu\text{in.}$ $\sigma_m = 40\ \mu\text{in.}$ 6B $\sigma_m = 95\ \mu\text{in.}$

Mag.:   200 μ
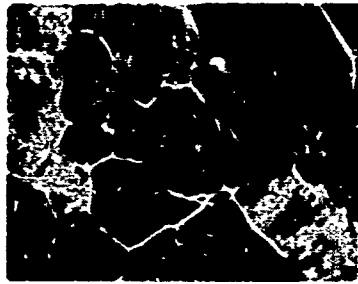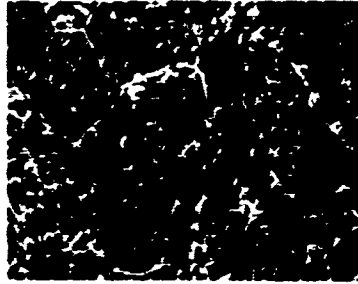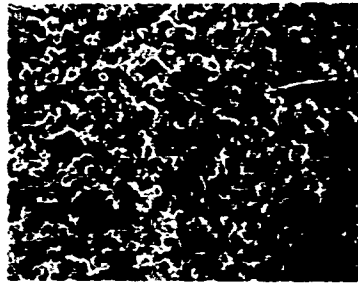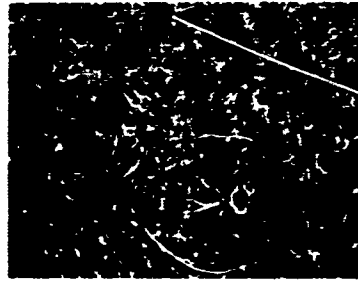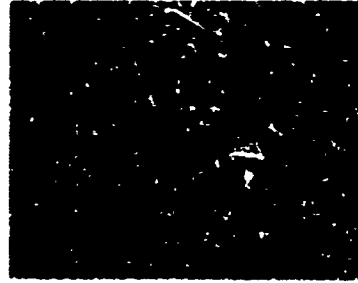
Figure 13   Surface Photomicrographs of Platinum Samples Before and After 1645°K Emittance Tests

45

Table IV. Surface Roughness Parameters for Platinum Samples Before and After 1645°K Emittance Tests

Sample	Mean Peak Height (µin.)	Mean Valley Depth (µin.)	Mean Peak-to-Valley Distance (µin.)	Mean Peak-to-Peak Spacing (µin.)	Mean Surface Slope (deg)	RMS Roughness (µin.)	AA Roughness (µin.)	Remarks
1B, Before	—	—	(14)	(300)	(5.5)	4.3	3.6	(a)
	—	—			(0)	<0.5	<0.7	(b)
1B, After	—	—	64	7,140	1	23	18.5	(c)
	—	—	12	1,430	1	8.0	6.0	(d)
3B, Before	31	25	56	1,310	5	28	22	(d)
3B, After	26	25	51	1,180	5	27	22	
4B, Before	62	53	115	1,650	9	49	40	
4B, After	40	37	77	1,140	8	43	36	
5B, Before	31	34	65	760	9.5	39	31	
5B, After	35	21	56	1,180	5.5	40	30	
6B, Before	153	116	269	2,020	15	127	99	
6B, After	94	59	153	1,280	13.5	95	76	

(a) For direction perpendicular to roll marks. Approximate values shown in parentheses are estimated from surface interference photomicrographs.

(b) For direction parallel to roll marks.

(c) For long-period roughness attributed to "slips" at the recrystallized grain boundaries. Calculated using a mean centerline for entire length of profilometer trace.

(d) For short-period roughness of grain faces. Calculated using adjusted centerlines for each section of profilometer trace over an apparent grain face.

46
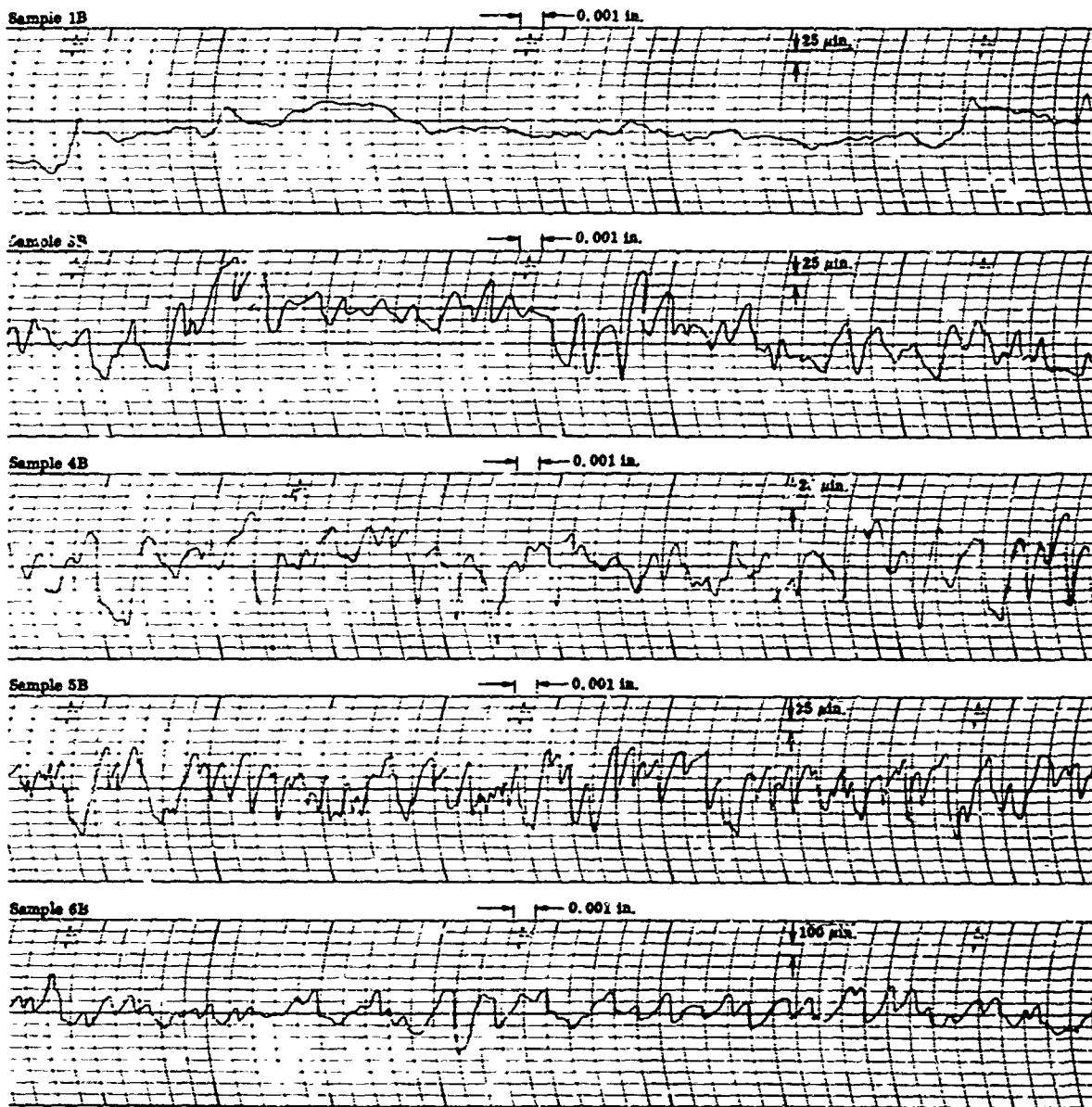
Figure 14 Typical Profilometer Traces of Platinum Sample Surfaces After 1645°K Emittance Tests

47

roughness occurred during the emittance tests. The increased roughness values for sample 1B were directly attributable to the recrystallization shown in Figure 13. The decreased roughness for sample 6B was due to high-temperature annealing effects which cause the rougher surface asperities to slump or level off. Similar large drops in roughness were observed for samples tested in last year's program, when the initial rms roughness exceeded 100 μin. The relative geometric stability of samples 3B, 4B, and 5B indicates, for the temperature-time histories of these samples, that neither recrystallization nor annealing changed the roughness from the initial rms values between 20 and 50 μin.

The emittance characteristics of the samples remained reasonably stable after the high-temperature anneal treatment given each sample before the emittance tests. Therefore, it is assumed that the changes in surface characteristics indicated in Figure 13 and Table IV occurred before emittance determinations were made.

Many analytical treatments of the effect of surface roughness on the scattering of electromagnetic energy from a surface include the assumptions that the surface irregularities are isotropic and are normally distributed about a mean surface plane. Profile traces of the platinum samples, made both parallel and perpendicular to the longitudinal axis, indicated isotropy in these directions except for the as-received platinum surface. Histograms showing the frequency distribution of profile heights about the mean surface plane were prepared for the four roughened samples and are shown in Figure 15. These distributions are based on 100 profile height measurements from the post-test profilometer traces and roughly indicate a Gaussian distribution of surface asperities. A larger sampling of data would undoubtedly result in a more nearly Gaussian form; however, the procedure would require considerable improvement over the manual techniques used for this evaluation.

Additional information about the surface topography of the unroughened platinum sample (1B) was obtained from surface interference micrographs similar to those shown in Figure 16. The interference pattern for the pre-test surface indicates that the roll marks are spaced about 300 μin. apart and are from 5 to 20 μin. deep (1/2 to 2 green fringe spacings). This close spacing suggests the possibility that the 500 μin. (radius) stylus for the Proficorder was too large to properly indicate the valley depths for this surface. Consequently, the roughness values determined from the profilometer traces are probably low. The interference pattern for the post-test surface shows a dramatic change in the surface characteristics of this sample. No trace of the original roll marks remains. The dominant surface features after high-temperature exposure are the grain faces and boundaries. The grains are irregularly shaped polygons with diameters ranging from 0.02 to 0.2 in. (500 to 5000 μ). Each grain appears to have its own unique surface topography with no preferred orientation or irregularities. Some of the grains appear flat and smooth while others appear hilly and rough. In addition, many grains are tilted relative to those adjacent to them. These features were corroborated by the profilometer traces and taper-section photomicrographs of the surface.

48
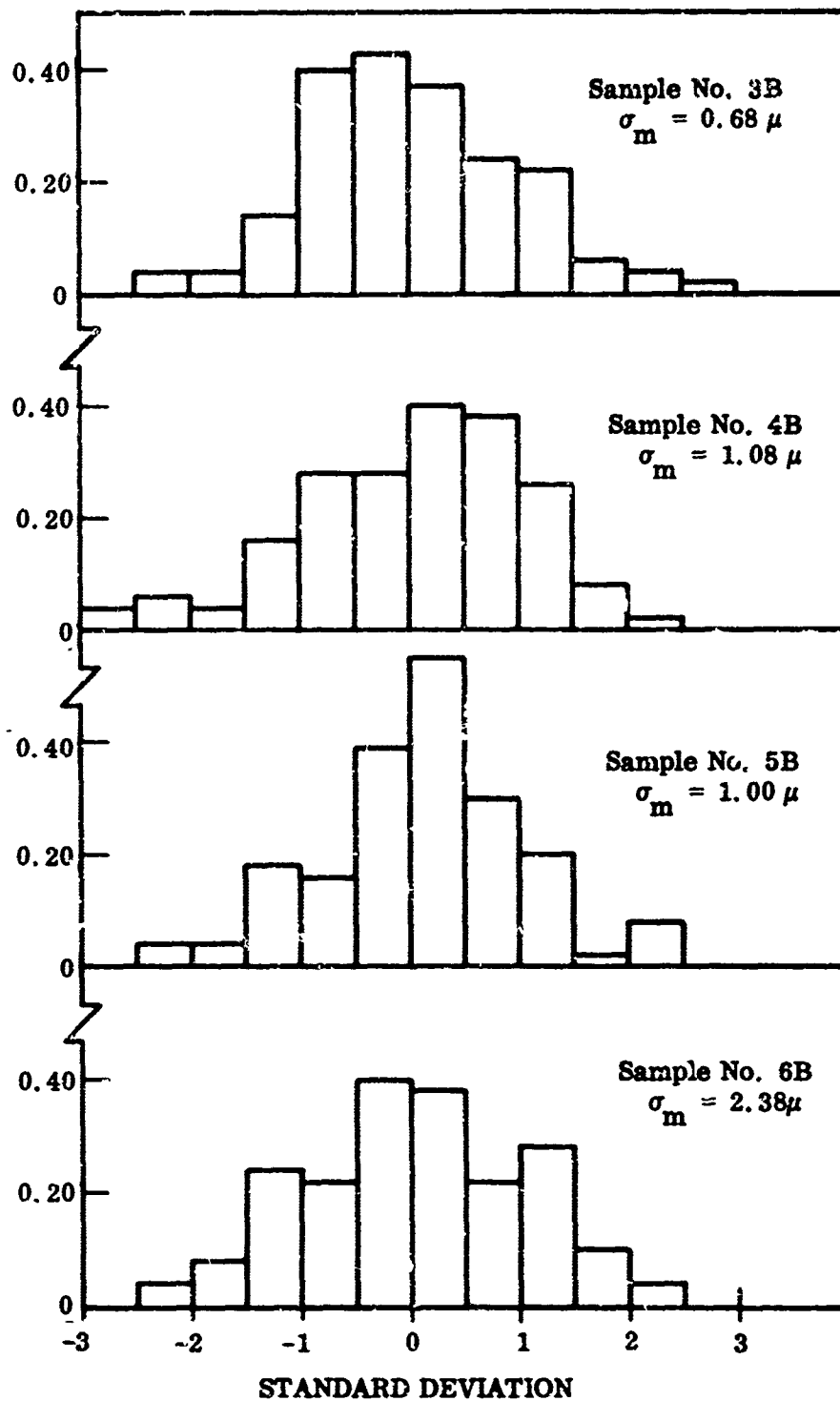
Figure 15 Distribution of Surface Heights for Roughened Platinum Samples, After Emittance Tests
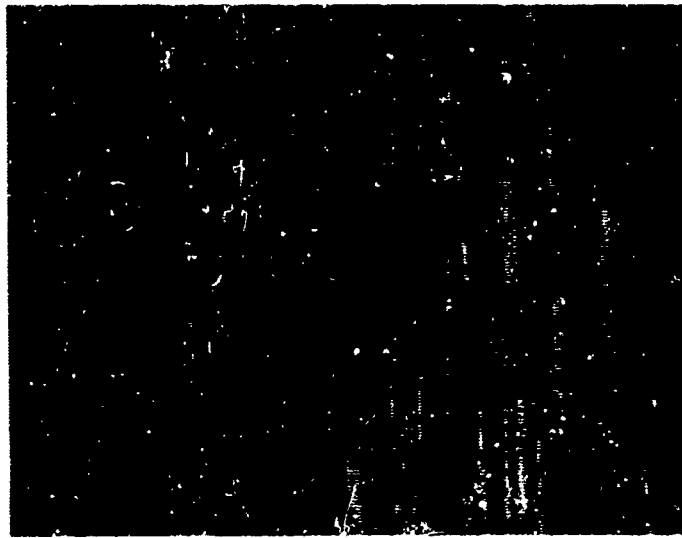
Before |— 100 µ —|
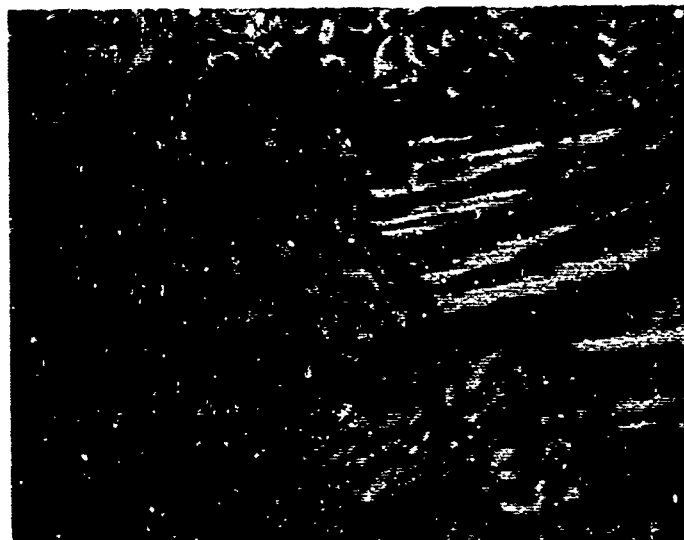
After |— 100 µ —|

Figure 16   Surface Interference Photomicrographs of Platinum Sample 1B
Before and After 1645°K Emittance Tests

Profilometer traces of the post-test surface of sample 1B indicated that the mean surface planes for adjacent grains were frequently displaced from one another by as much as 50 to 75 μin. This characteristic was evidenced by sudden vertical displacements of the centerline of the profilometer trace which occurred at intervals corresponding to the distance between grain boundaries indicated by the surface photomicrographs. Using an average centerline for the entire length of one profilometer trace, an rms roughness value of 23 μin. was calculated for the surface. This value includes the roughness contribution of the long-period (i.e., infrequent) grain boundary slips. By adjusting the centerline of the same profilometer trace to "fit" each apparent grain face, an rms roughness value of 8 μin. was calculated. The latter value represents the rms roughness of the grain faces only.

Vertical displacements of the profilometer centerline were also detected in the traces for sample 3B; however, the profile between the slips was signi   .tly rougher. The post-test roughness parameters for this surface were also calculated by adjusting the centerline to fit each apparent grain face. The profilometer traces for samples 4B, 5B, and 6B indicated no boundary displacements.

Taper-section photomicrographs of the post-test surfaces of platinum samples 1B, 4B, and 6B are shown in Figure 17. These micrographs indicate the same range of roughness parameter values as were determined from the profilometer traces for these surfaces. The sudden vertical displacements of 50 to 75 μin. on the profilometer traces of sample 1B correspond directly to the abrupt "slips" shown in Figure 17. The roughness across the grain faces, as indicated in Figure 17, is barely detectable and is about one order of magnitude less than the displacements at the grain boundaries. For sample 4B, peak-to-valley depths of from 10 to 150 μin. with an average peak-to-peak spacing of about 1300 μin. are indicated in Figure 17. Both of these characteristics are in agreement with those indicated by the profilometer traces. The taper section of sample 6B indicates a maximum peak-to-valley depth of about 480 μin. and an average depth of about 160 μin. Again, both values correspond with the profilometer data for this surface. The dark areas at the surface of sample 6B are indications of surface damage (e.g., crystalline fractures and reorientation) caused by the more severe shot-blast treatment of this surface. This interpretation is supported by the x-ray diffraction data, which indicated a change in the crystalline orientation at the surface of this sample caused by the roughening process.

Arc spectrographic analyses of each sample were made after the emittance tests to check for evidence of surface contamination. No evidence of contamination was indicated by these analyses. Similarly, no evidence of embedded glass-shot fragments was detected during the microscopic examinations of the surfaces.

X-ray diffraction patterns were obtained after the emittance tests for determination of the crystalline orientation of each surface. The pattern obtained from sample 1B indicated a strongly preferred orientation of (200) and (220) crystal planes parallel to the surface. This characteristic was also observed for the as-rolled platinum and was evidently not affected by the annealing and thermal etching that occurred during the high-temperature tests.
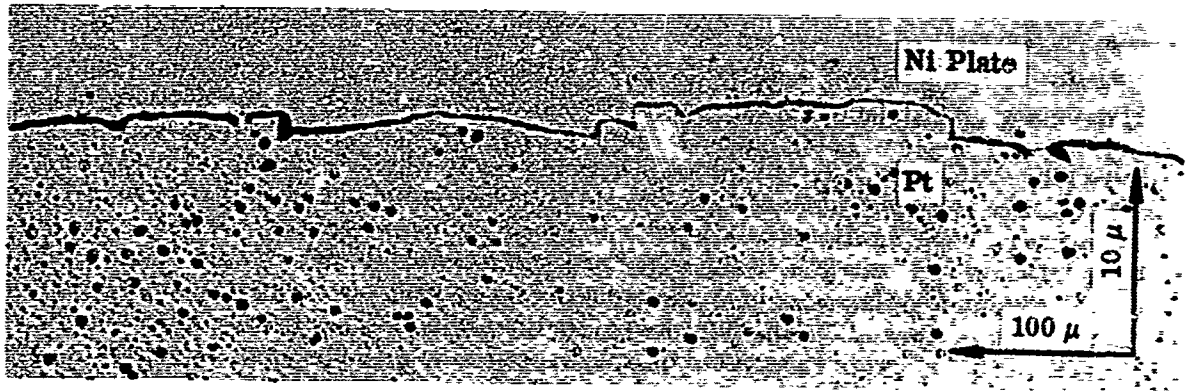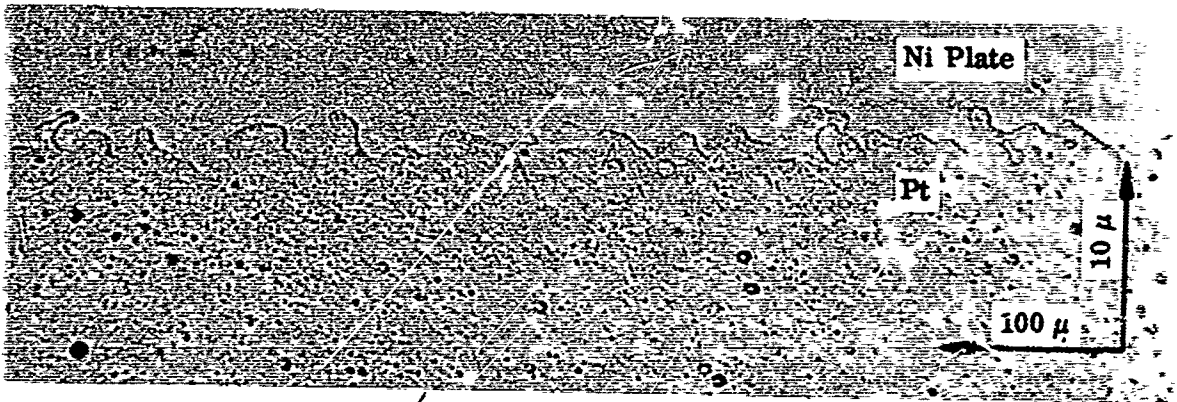
Figure 27 Taper Section Photomicrographs of Platinum Samples 1B, 4B, and 6B After 1645°K Emittance Tests (Taper Angle = 5°45')

52

The diffraction patterns for samples 3B, 4B, and 5B were identical to the pattern for sample 1B. This indicates that the shot-blast treatment of these samples did not alter the original crystalline orientation at the surface. The pattern for sample 6B, however, contained "d-lines" characteristic of the (111) and (311) crystalline planes. Thus, the more severe shot-blast treatment of this sample was sufficiently damaging to alter the original crystalline orientation. A comparison of the diffraction patterns for the emittance samples with a standard powder pattern for platinum (completely randomized orientation) is shown in Table V.

An overall evaluation of the results of the surface characterization provides the following conclusions:

- Exposure of platinum samples to high temperatures for extended periods results in thermal damage, as evidenced by etching and faceting of individual crystals. The extent of thermal damage is time dependent and was most severe on the as-rolled specimen (1B), where the sample was held at elevated temperatures in excess of 20 hr. (For details, see Section VII.) This resulted in creation of both fine structure (faceting) and coarser grain surface elevation shifts (due to etching) that increased the emittance of the sample.

- The annealing procedure used on the roughened samples provided a relatively stable surface geometry for the short duration of the emittance tests. Roughness values obtained at the conclusion of the emittance measurements are reliable indications of the surface geometry that existed during the measurements.

- Roughened surfaces up to 50 μin. rms created by shot-blasting platinum are relatively stable for the thermal conditions used in this program. For higher initial values of roughness, it is probable that high-temperature annealing has a smoothing effect on the surface.

- The samples used in the program were of high purity and free of surface contamination; they were thoroughly annealed before measurement of emittance and had a preferred crystal orientation at the surface.

Table V. X-Ray Diffraction Data for Platinum Samples After 1645°K Emittance Tests

Standard (Powder) Pattern for Platinum (33) (Face-Centered Cubic, a = 3.9231)			Pattern for Samples 1B, 3B, 4B, and 5B		Pattern for Sample 6B	
d	(hkℓ)	I/I_o	d	I/I_o	d	I/I_o
2.265	(111)	100			2.262	10
1.962	(200)	53	1.959	100	1.966	100
1.387	(220)	31	1.388	50	1.390	10
1.183	(311)	33			1.182	5
1.133	(222)	12				
0.981	(400)	6				
0.900	(331)	22				
0.877	(420)	20				
0.801	(422)	29				

54

b. Emittance Characteristics

(1) Total Normal and Total Hemispherical Emittance

A complete tabulation of the total normal and total hemispherical emittance values for each platinum sample at each test temperature is provided in Tables XIV through XVIII in Section VII. A summary of these data is shown in Figure 18 along with comparative data for polished platinum reported by Abbott et al. in (38).

The hemispherical and normal results clearly show a trend of increasing emittance with roughness for all samples with the exception of the smoothest sample (1B) which had the highest emittance of all samples tested. The reason for this apparent anomaly is attributed to the extended period of high temperature ($\approx 1650°K$) operation to which this sample was subjected during alignment and calibration of the apparatus. This caused a considerable increase in emittance of the sample due to thermal etching and faceting of the surface grains. Such phenomena have been frequently observed for platinum and are reported in detail in (38) where increases in emittance on the order of 20% occurred after 12-hr aging at 1310°K. It is apparent from Figure 18 that this same order of change must have been experienced by sample 1B since its emittance would normally be slightly less than that shown for sample 3B if it had received the same thermal treatment.

For the remaining samples it is apparent that roughening from 0.20 to 2.38 μ rms results in an increase of total normal emittance of from 5% at 870°K to 6% at 1360°K. Corresponding increases in total hemispherical emittance are 10% at 870°K and 13% at 1360°K.

Absolute values for the total normal and hemispherical emittance of sample 3B compare well with predictions based upon single electron theories and with the experimental observations of Abbott et al. (38) as shown in Figure 19. Agreement between experimental results for hemispherical emittance at temperatures below 1200°K is excellent while at higher temperatures greater divergence is apparent. For the normal emittance results, agreement is excellent throughout the entire temperature range. These results substantiate the expectation that very slight surface roughness ($\sigma_m/\lambda < 0.1$) will have little effect on absolute values of emittance. However, as reported later, slight roughness does significantly change the distribution of energy above the surface plane.

It is doubtful that initial values of emittance will remain stable during long-term, high-temperature exposure since the effects of recrystallization, thermal etching, and thermal faceting will alter the surface and result in significant changes in surface geometry. In fact, grain boundary slips and faceting may cause geometric changes that overshadow effects introduced by the roughening procedure. Examples of differences in the surface geometry of platinum samples 1B and 3B resulting from their high-temperature, emittance-test exposures are shown by the high magnification photomicrographs in Figure 20. Photomicrographs (a) and (b) show the surface of sample 1B. Differential evaporation from the surface has caused formation of continuous, step-like features, shown in (a), over most of the exposed crystal faces.
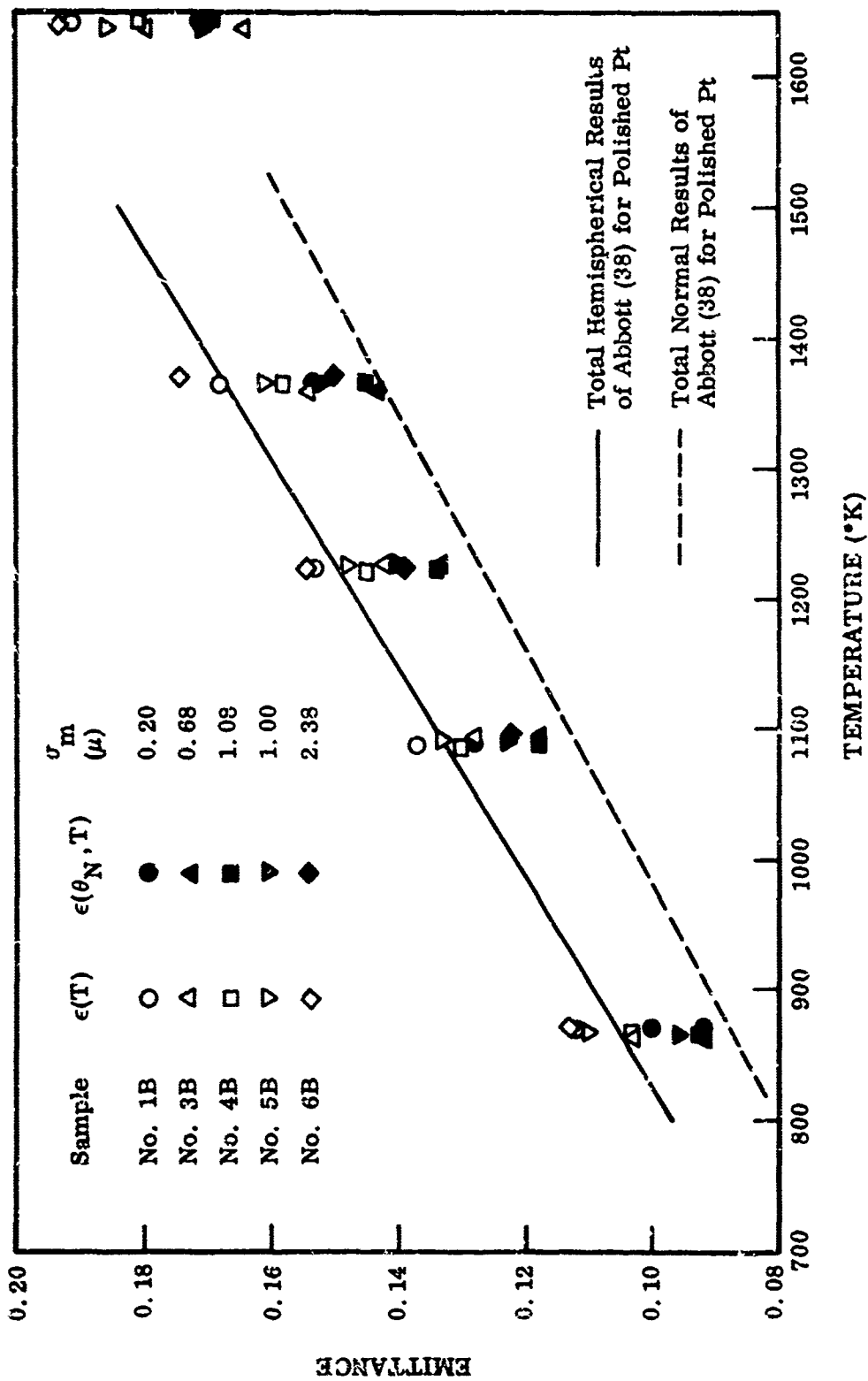
Figure 18 Total Hemispherical and Total Normal Emittance of Platinum Samples
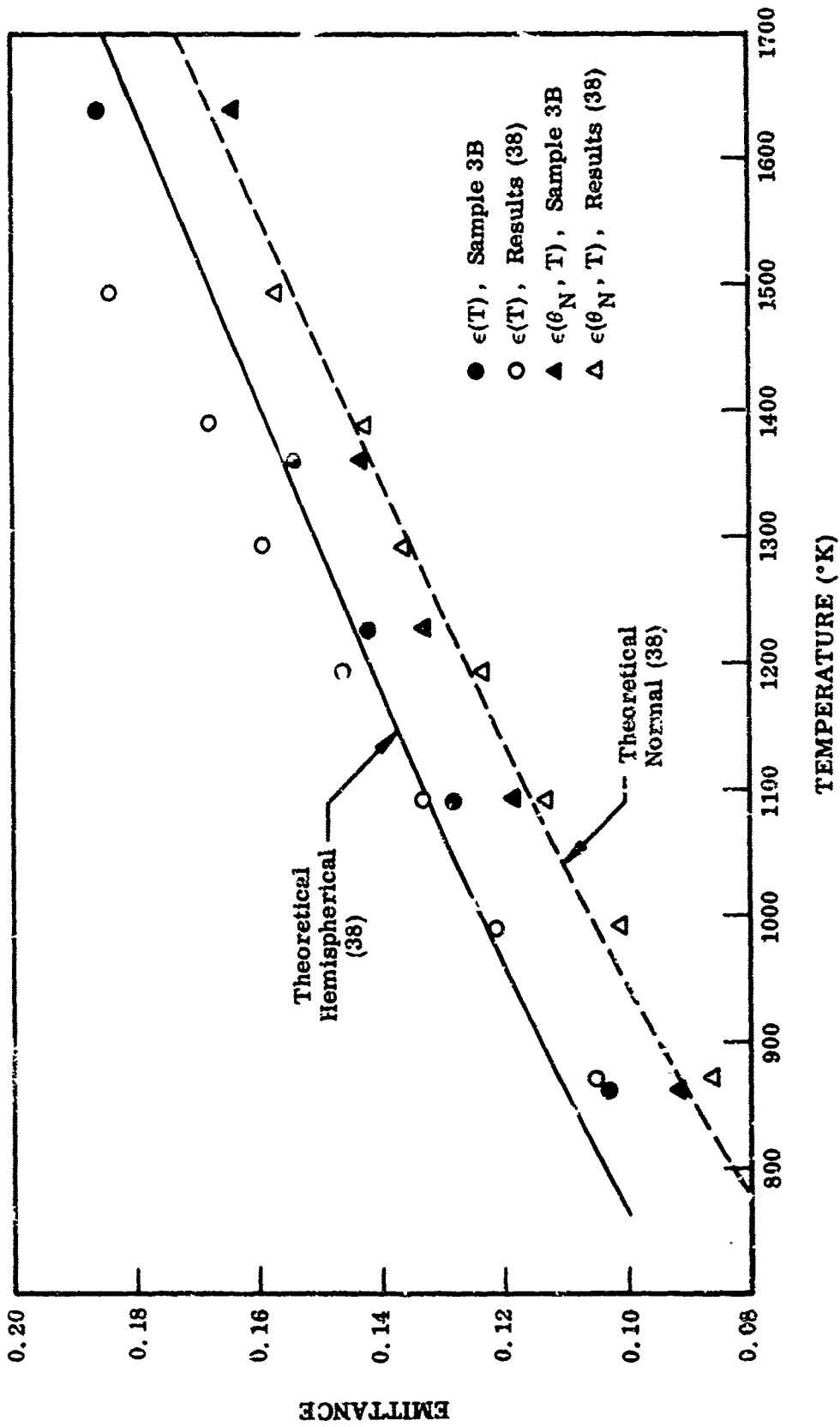
Figure 19 Total Emittance Characteristics of Polished Platinum

57

(b)

(d)

Sample 1B

Sample 3B

(a)

(c)
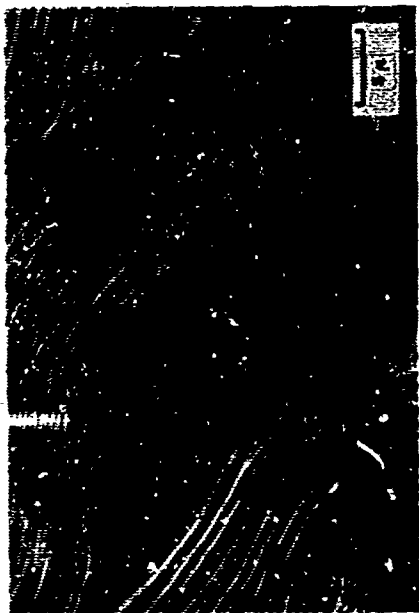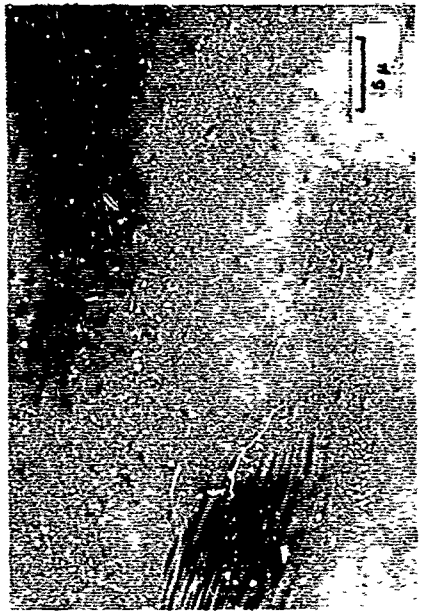
Figure 20 Surface Photomicrographs of Platinum Samples 1B and 3B After 1645°K Emittance Tests, Showing Effect of Thermal Etching on Surface Geometry

58

Only a few smooth crystal faces, such as shown in (b), were observed on this surface. In contrast the surface of sample 2B, shown in photomicrographs (c) and (d), is observed to nave entirely different geometric features. On this surface evaporation has produced features similar to those shown in (c) over most of the exposed surface area. Only a few of the crystals, as shown in (d), appear to have the step-like features that were characteristic of the surface of sample 1B. These comparisons clearly demonstrate the differences in surface geometry that existed on the samples during the emittance measurements and indicate the difficulty involved in maintaining a prepared surface condition at high temperatures. Such changes undoubtedly affect the absolute emittance characteristics of the surfaces; consequently, the meaningfulness of the data when compared with that of other investigators is of questionable value.

A comparison between the absolute values obtained this year and those reported after the first year's effort indicates that the previous total normal emittance results were high by approximately 10%. The reason for this error was determined early in the second year's program and was traced to amplifier saturation and detector non-linearities. Both sources of error were thoroughly investigated and operational procedures implemented which circumvented the difficulties. Consequently, the results obtained this year are in better agreement with those of previous workers over the full temperature range, in contrast with those obtained last year where emittances above 900°K were high. An assessment of the experimental procedure, thermometry, blackbody source, and detection system lead to the conclusion that the present experimental error is on the order of 5%. The precision is estimated on the order of 1% based on the ability to repeat data on identical samples at different times. Comparisons between samples are estimated to be of this same order of precision.

(2) Spectral Normal Emittance

Results obtained for the spectral normal emittance of each platinum sample at each test temperature are presented in detail in Tables XIV through XVIII in Section VII. The measurements were made point-by-point at nine wavelengths between 1.0 and 12.0 μ, as permitted by available sample energy levels at each temperature. The spectral normal emittance at 0.65 μ was determined by the optical pyrometer method. Comparisons of the data lead to the same conclusions as reached for the total emittance data; namely, that sample-to-sample variations caused by surface roughness were on the order of 10% with greater roughness producing higher emittance. A comparison of data obtained at 865°K and 1645°K is presented in Table VI, and is typical of comparisons at the other temperatures. The high emittance values for sample 1B correlate with the total emittance results and again indicate that the as-rolled specimen suffered high temperature, thermally induced, surface modification. Samples 3B through 6B show an overall increase of emittance with increasing roughness, though from one sample to the next rougher sample the difference is small.

Sample energy limited the wavelength range of each determination to the extent that integration of the spectral results for comparison to total normal results is not an accurate procedure. However, some integrations were performed using extrapolations

59

Table VI. Spectral Normal Emittance of Platinum Samples

λ (µ)	Sample No.				
	1B	3B	4B	5B	6B
At T = 865°K					
2	0.115	0.105	0.123	0.135	0.138
3	0.105	0.102	0.101	0.107	0.112
4	0.085	0.082	0.081	0.084	0.090
6	0.068	0.062	0.066	0.068	0.074
8	0.057	0.052	0.050	0.058	0.065
10	0.050	0.041	0.043	0.039	0.058
At T = 1645°K					
0.65[a]	0.30	0.30	0.28	0.30	0.33
1.0	0.244	0.255	0.254	0.253	0.253
1.5	0.197	0.197	0.212	0.209	0.203
2	0.165	0.166	0.180	0.172	0.167
3	0.140	0.141	0.144	0.146	0.144
4	0.118	0.118	0.119	0.122	0.123
6	0.098	0.097	0.100	0.102	0.107
8	0.086	0.085	0.087	0.089	0.094
10	0.076	0.074	0.072	0.079	0.087
12	0.065	0.067	0.070	0.070	0.080

(a) Determined by optical pyrometer method.

of the available data to obtain emittance values at the short and long wavelength ends of the energy spectrum. Comparison of these results with the measured total normal values show the integrated values to be approximately 10% low. This disagreement is within the inherent accuracy of the experimental and analytical procedures.

Changes in spectral normal emittance with increasing temperature are shown in Figures 21 and 22 for samples 3B and 5B respectively. A comparison between these figures demonstrates that surface roughness has less influence on the spectral emittance than does the sample temperature. Roughening in this range did not cause significant increases in $\epsilon(\theta_N, \lambda, T)$ nor did it influence the functional dependence of emittance on wavelength. A similar result is obtained by comparison of data from the other samples.

(3) Relative Total Directional Emittance

The results obtained from relative total directional emittance measurements are presented in Figures 48, 55, 62, 69, and 76 in Section VII. These results, along with the spectral measurements discussed in the next section, satisfy the primary objective of this program. It was anticipated that absolute emittance values would be influenced by numerous factors that could not be precisely controlled during the experimental effort. Additionally, it was expected that surface roughness would not provide large, demonstrative changes in absolute emittance properties for the range of roughnesses used. These expectations are adequately substantiated by the results discussed in the previous sections. However, it was also anticipated that slight roughness would strongly influence the spatial distribution of energy leaving the surface. These data provide the most sensitive measure of surface geometry. In addition, the inherent precision of relative measurements is of considerable assistance where accurate comparisons of the effects of roughness are desired.

The directional emittance of a polished metallic surface may be predicted with reasonable certainty from classical reflectance theories that utilize known values of the optical constants. These theories have frequently been presented in detail in previous literature and were discussed in last year's final report. The results reported in Section VII are in essential agreement with analytical predictions in terms of the effect of temperature on total directional emittance. Three characteristics are noticeable for all of the platinum samples. First, the maximum relative directional emittance value, designated $[\epsilon(\theta)_{max}]$, decreases as the sample temperature increases. Second, the angle at which the maximum relative directional emittance occurs, designated θ_{max}, tends to shift slightly towards the normal as the sample temperature increases. Finally, the area beneath each curve, which is a measure of the total hemispherical-to-total normal emittance ratio [see Eq. (24), subsection IV.2.e], decreases as the sample temperature increases. These general trends are all in agreement with anticipated changes in n and k with temperature and wavelength. A summary of the values obtained for these three parameters is presented in Tables VII and VIII.

Changes in $\epsilon(\theta)_{max}$ and $\epsilon(T)/\epsilon(\theta_N, T)$ with temperature are evident for all samples with the strongest temperature dependency existing for the smoother samples. Rough
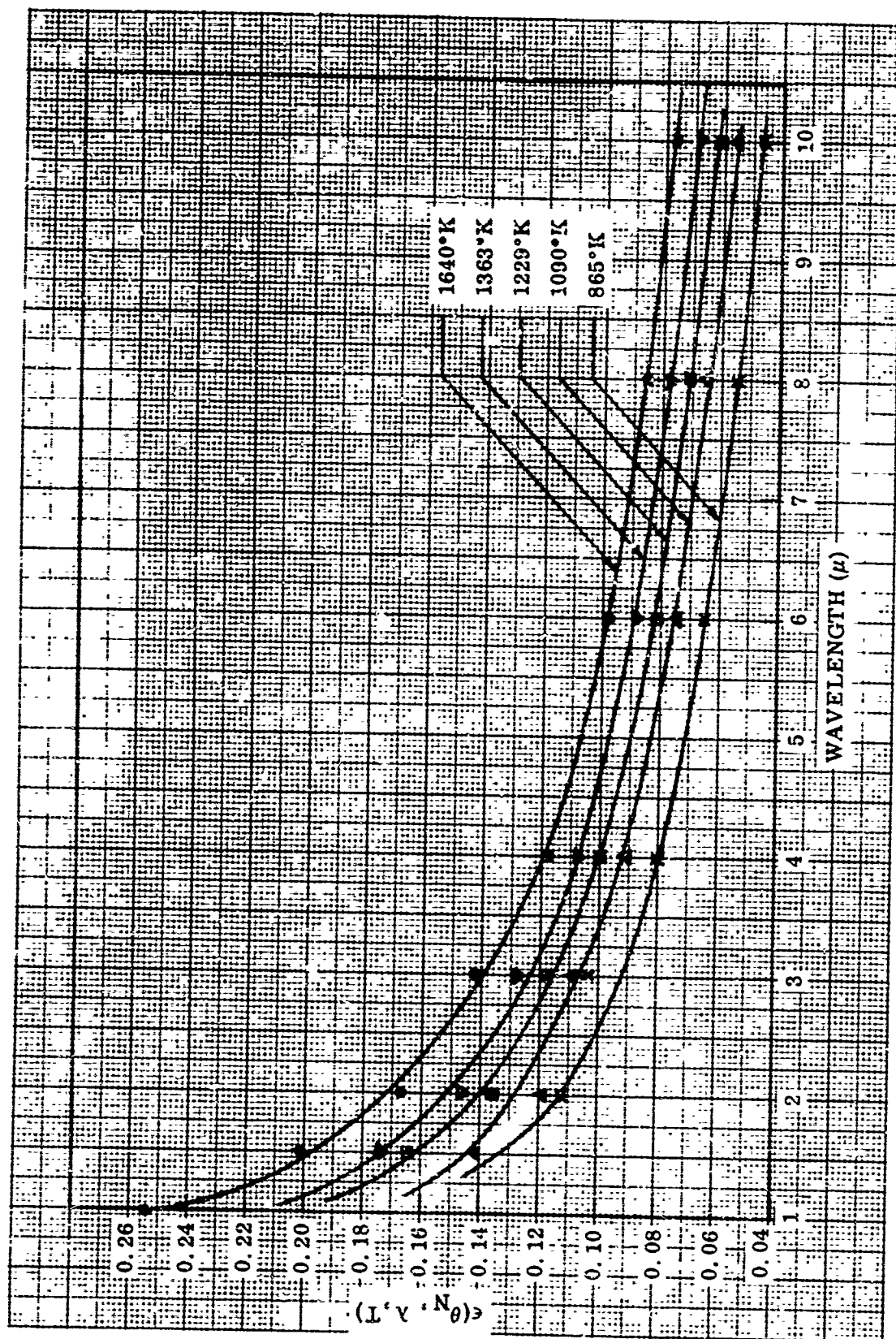
Figure 21 Spectral Normal Emittance of Platinum Sample 3B (σ_m = 0.68 μ)
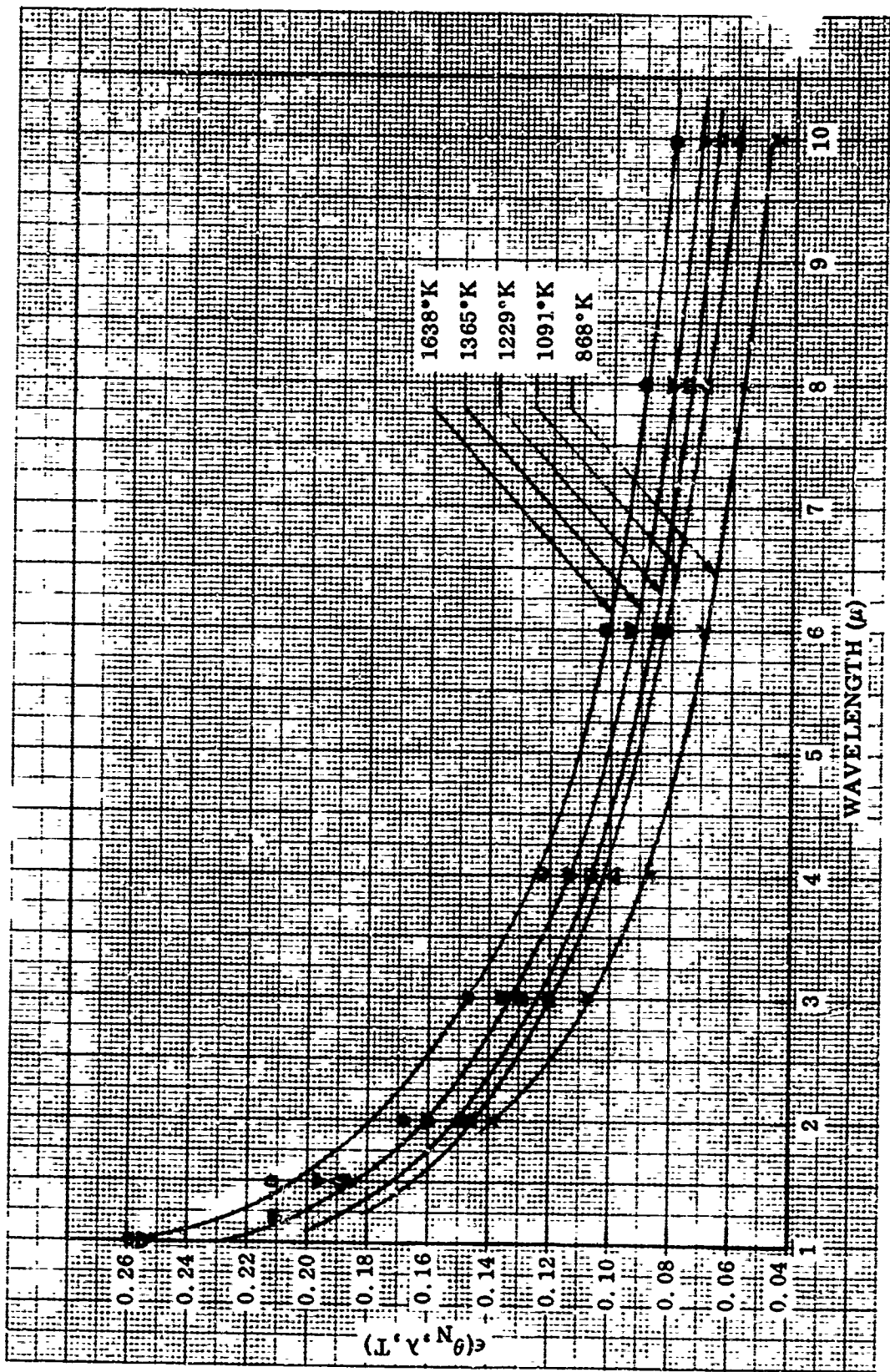
Figure 22 Spectral Normal Emittance of Platinum Sample 5B ($\sigma_m = 1.0\ \mu$)

63

Table VII. Temperature Dependence of θ_{max} and $\epsilon(\theta)_{max}$ for the Total Emitted Energy From Platinum Samples

Nominal Temperature (°K)	Sample 1B		Sample 3B		Sample 4B		Sample 5B		Sample 6B	
	θ_{max} (deg)	$\epsilon(\theta)_{max}$	θ_{max} (deg)	$\epsilon(\theta)_{max}$	θ_{max} (deg)	$\epsilon(\theta)_{max}$	θ_{max} (deg)	$\epsilon(\theta)_{max}$	θ_{max} (deg)	$\epsilon(\theta)_{max}$
865	87.0	2.99	87.0	3.01	86.0	2.58	87.0	2.78	83.5	1.91
1090	86.5	2.66	86.5	2.64	85.5	2.21	84.0	2.04	83.0	1.83
1225	86.0	2.44	—	—	—	—	—	—	84.0	1.75
1365	85.5	2.36	85.5	2.24	84.0	1.94	84.0	1.86	84.0	1.78
1645	83.5	1.91	83.5	1.79	82.5	1.76	84.0	1.75	83.5	1.70

Table VIII. Temperature Dependence of $\epsilon(T)/\epsilon(\theta_N, T)$ for Platinum Samples

Nominal Temperature (°K)	Sample No.				
	1B	3B	4B	5B	6B
865	1.181	1.213	1.224	1.231	1.252
1090	1.174	1.208	1.202	1.177	1.235
1225	1.160	—	—	—	1.218
1365	1.160	1.172	1.188	1.169	1.216
1645	1.137	1.132	1.169	1.159	1.211

surface effects tend to smooth out the temperature dependence. The effect of surface roughness on the relative total directional emittance characteristics of platinum is illustrated by the curves shown in Figures 23 and 24 for the highest and lowest test temperature used in this study. These figures show that for a fixed temperature, the value of $\epsilon(\theta)_{max}$ decreases as surface roughness increases. The decrease caused by roughness is largest for low temperature surfaces due to the highly directional emittance characteristics at long wavelengths as shown in the following section.

Attendant with the lower $\epsilon(\theta)_{max}$ values obtained for rougher surfaces there is an increase in $\epsilon(\theta, T)/\epsilon(\theta_N, T)$ at viewing angles between 20 and 70 deg. Integration of the distributional data shows the ratio of hemispherical to normal emittance to increase with increasing roughness even though $\epsilon(\theta)_{max}$ has decreased. This is clearly demonstrated by comparison of the values listed in Table VIII for each temperature. Except for the 865°K data, however, the trend is not a smooth function of roughness. For the range of surface roughness values represented by these samples, little or no effect on the relative total directional emittance at viewing angles between 0 and 20 deg was observed.

(4) Relative Spectral Directional Emittance

A complete compilation of spectral directional emittance data for each of the platinum samples is presented in graphical form in subsections VII.1 through VII.5. The data include angular distributions for the parallel and perpendicular components of polarized radiation emitted at wavelengths of 1.5, 2, 3, 4, 6, and 8 μ. An inspection of the data indicates that for each sample, the relative angular distribution of the perpendicular polarized component of emitted energy at each of the above wavelengths is a very weak function of sample temperature between 865 and 1645°K. It is also observed that the angular position of maximum emittance for the parallel polarized component does not change measurably with temperature. These two observations lead to the conclusion that the optical constants of platinum (n and k) in the infrared are nearly constant with temperature throughout this temperature range. The result for θ_{max} and $\epsilon(\theta)_{max}$ are summarized in Table IX. The general trend of the results is for a slight decrease in $\epsilon(\theta)_{max}$ as the temperature increases. This implies, on the basis of single electron theories, that the ratio k/n is increasing and the sum $(n^2 + k^2)$ is decreasing as a function of increasing temperature. The absolute values of the changes were not determined though they are obviously small. Optical constants were not computed from the results on sample 1B since the technique, as reported last year, is insensitive to small changes in directional characteristics.

The behavior of each sample, as a function of wavelength at fixed temperature, demonstrates the effect of increasing n and k with wavelength. Figures 25 and 26 present the directional results for sample 1B. The maximum emission angle $(\theta)_{max}$ and maximum relative emittance, $\epsilon(\theta)_{max}$, for the parallel polarized component both increase with wavelength, indicating larger values of the optical constants in the infrared. These changes were apparent for all samples and were not eliminated by increasing surface roughness, although the wavelength dependence for the rougher samples is
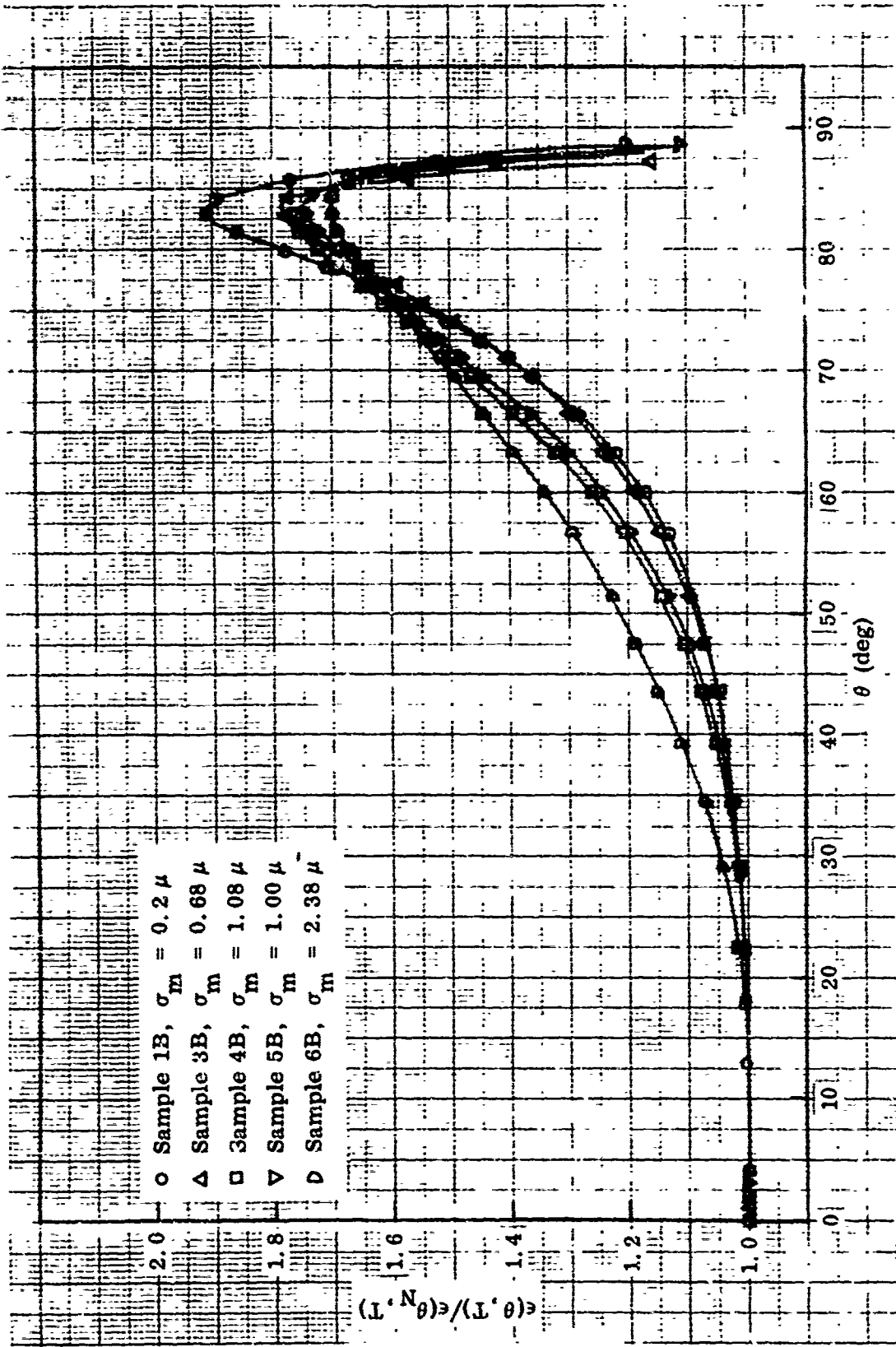
Figure 23 Effect of Roughness on Relative Total Directional Emittance of Platinum at 1645°K

Legend (within figure):

o   Sample 1B, σ_m = 0.2 μ
△   Sample 3B, σ_m = 0.68 μ
□   3ample 4B, σ_m = 1.08 μ
▽   Sample 5B, σ_m = 1.00 μ
D   Sample 6B, σ_m = 2.38 μ

Y-axis: $\epsilon(\theta, T)/\epsilon(\theta_N, T)$

X-axis: θ (deg)

66
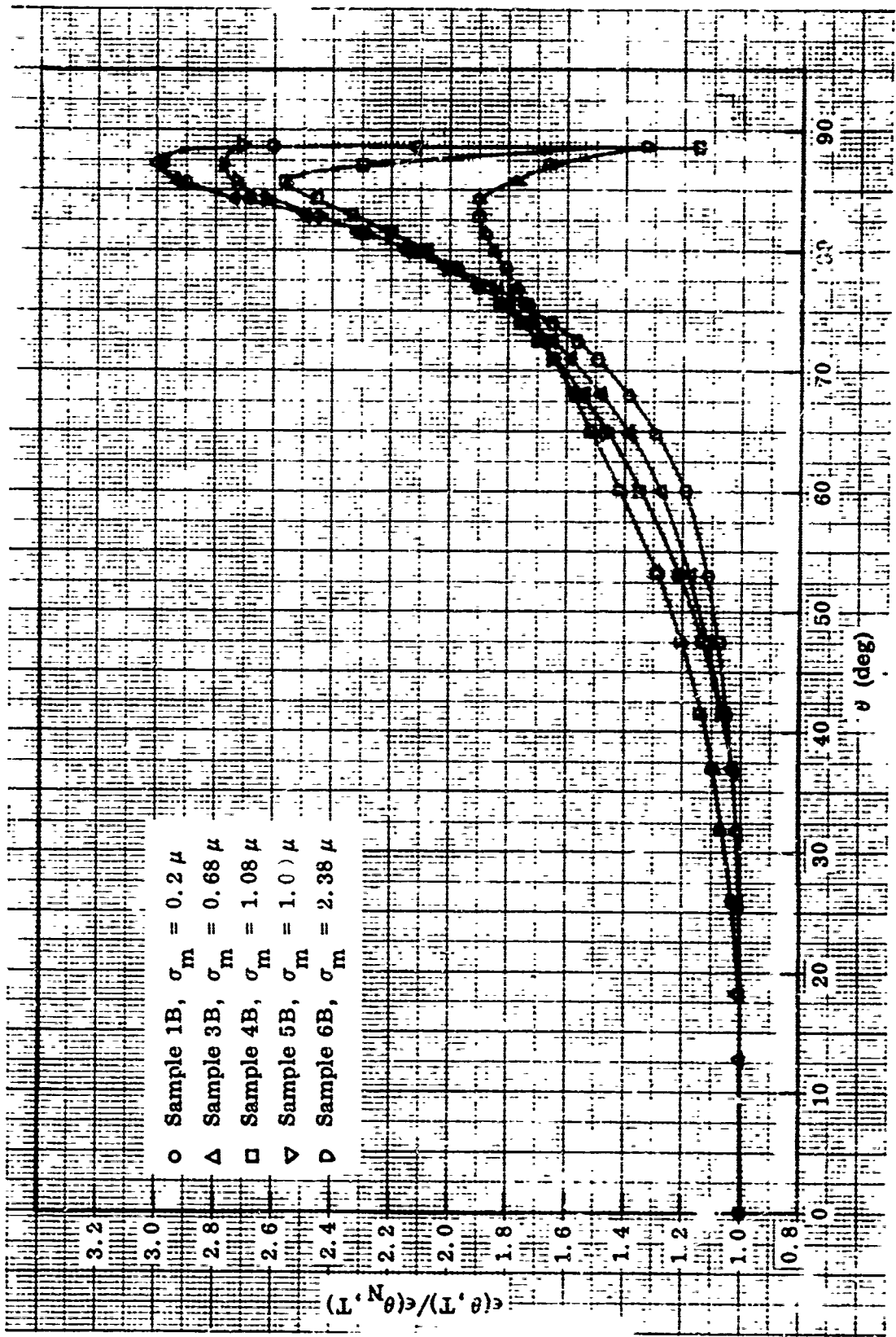
Figure 24 Effect of Roughness on Relative Total Directional Emittance of Platinum at 865°K

The y-axis is labeled $\epsilon(\theta, T)/\epsilon(\theta_N, T)$, and the x-axis is labeled θ (deg).

Legend:
o Sample 1B, σ_m = 0.2 μ
△ Sample 3B, σ_m = 0.68 μ
□ Sample 4B, σ_m = 1.08 μ
▽ Sample 5B, σ_m = 1.0) μ
◇ Sample 6B, σ_m = 2.38 μ

67

Table IX. Wavelength and Temperature Dependence of θ_{max} and $\epsilon(\theta)_{max}$ for the Parallel Polarized Component of Emitted Energy From Platinum Samples

Wavelength (μ)	Temp. (°K)	Sample 1B		Sample 3B		Sample 4B		Sample 5B		Sample 6B	
		θ_{max}	$\epsilon(\theta)_{max}$	θ_{max}	$\epsilon(\theta)_{max}$	θ_{max}	$\epsilon(\theta)_{max}$	θ_{max}	$\epsilon(\theta)_{max}$	θ_{max}	$\epsilon(\theta)_{max}$
1.5	1225	81.5	1.78	–	–	–	–	–	–	80.0	1.37
	1365	83.0	1.71	81.0	1.57	80.5	1.50	82.0	1.50	81.0	1.36
	1645	82.5	1.66	83.5(a)	1.58	80.5	1.45	81.5	1.51	81.5	1.37
2	865	84.0	2.03	82.5	1.84	81.0	1.65	83.5	1.72	81.5	1.50
	1090	84.0	2.00	83.0	1.82	81.5	1.62	83.5	1.73	81.0	1.42
	1225	83.5	1.97	–	–	–	–	–	–	81.5	1.46
	1365	84.0	2.02	82.0	1.79	81.5	1.62	83.5	1.66	81.0	1.46
	1645	84.0	1.97	82.0	1.69	82.0	1.54	83.0	1.62	81.0	1.44
3	865	84.0	2.52	82.5	2.23	81.5	1.93	84.5	2.05	81.0	1.59
	1090	84.5	2.43	82.5	2.14	82.5	1.85	84.5	1.99	82.5	1.57
	1225	85.5	2.59	–	–	–	–	–	–	81.5	1.55
	1365	85.5	2.51	82.0	2.03	82.0	1.80	84.5	1.90	82.0	1.54
	1645	85.5	2.42	83.0	1.98	82.0	1.71	84.0	1.85	81.5	1.46
4	865	84.5	2.83	83.5	2.50	82.5	2.16	85.0	2.32	82.5	1.62
	1090	84.5	2.75	83.5	2.38	82.5	2.08	84.5	2.16	83.5	1.60
	1225	85.5	2.86	–	–	–	–	–	–	82.0	1.56
	1365	84.0	2.73	83.0	2.33	83.0	1.99	84.0	2.06	82.5	1.54
	1645	85.0	2.65	83.5	2.16	82.5	1.89	84.0	2.06	81.5	1.48
6	1225	86.0(a)	3.47	–	–	–	–	–	–	83.5	1.66
	1365	83.0(a)	3.00	83.0	2.60	83.5	2.23	84.5	2.35	83.5	1.64
	1645	85.5	3.15	84.0	2.53	83.0	2.09	84.5	2.30	83.5	1.58
8	1645	86.0	3.10	84.0	2.70	83.5	2.22	84.0	2.44	83.0	1.62

(a) θ_{max} values questionable because of sample warpage.

68
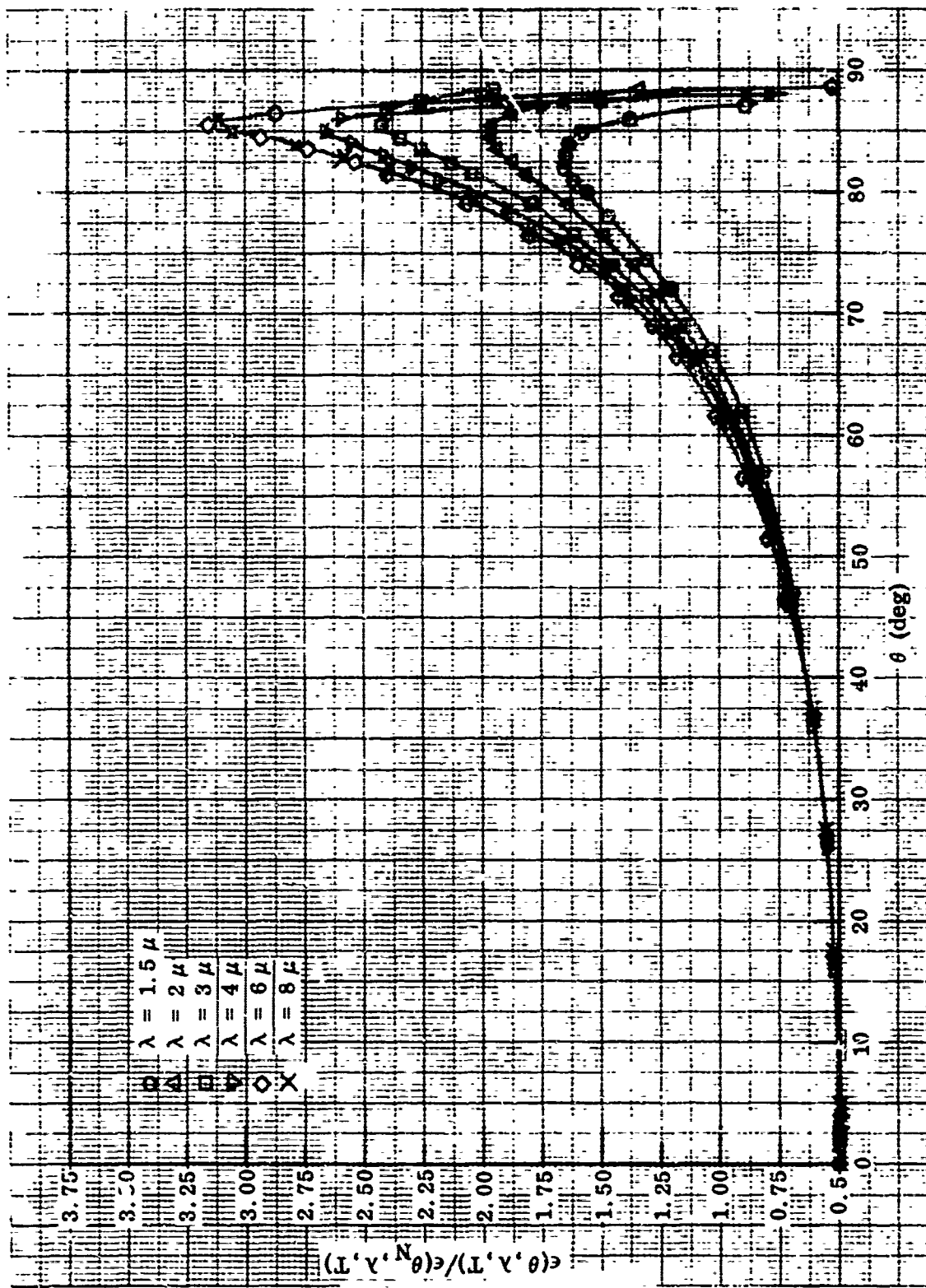
Figure 25 Wavelength Dependence of Parallel Polarized Component of Relative Spectral Directional Emittance of Platinum (Sample 1B at 1645°K)
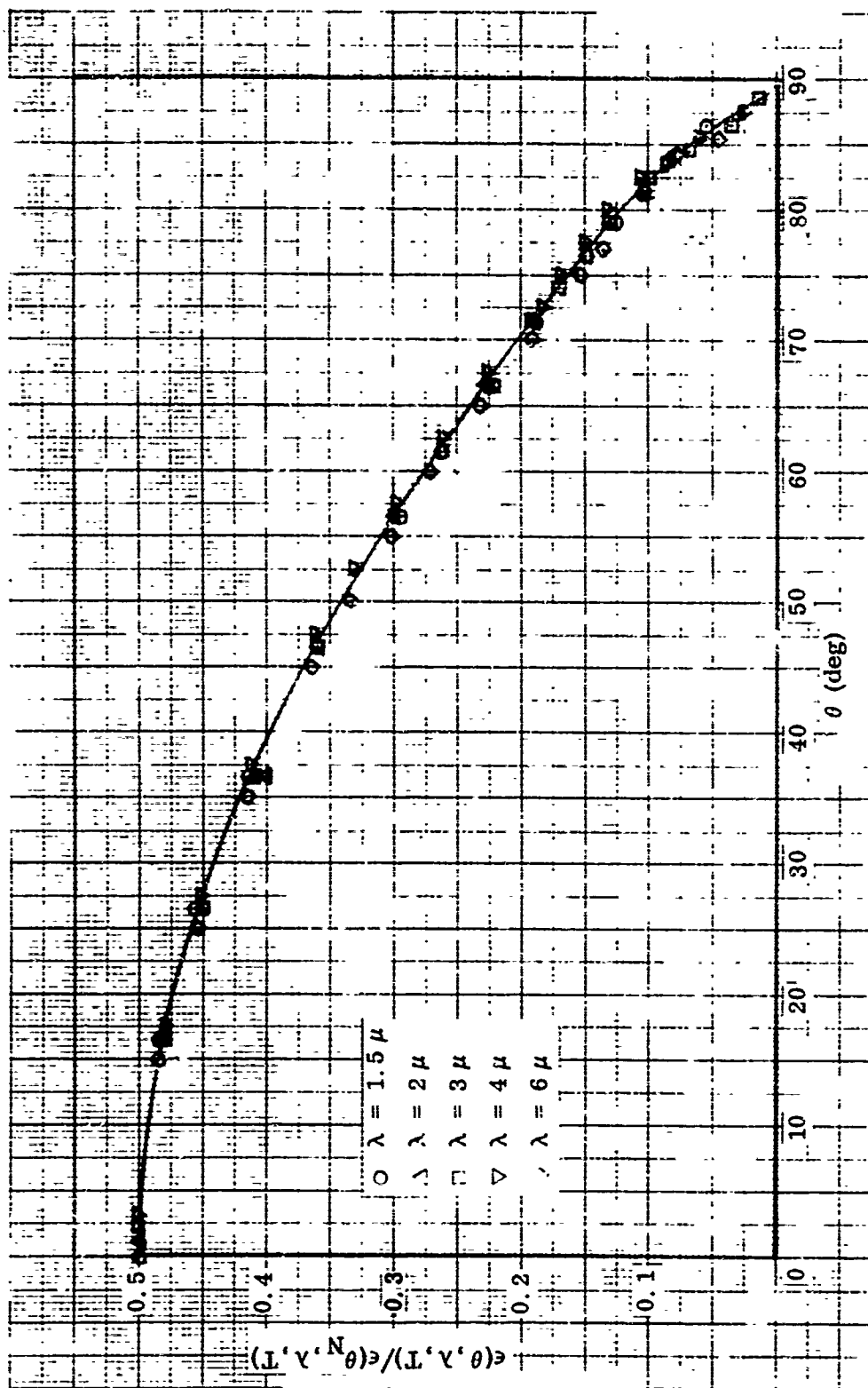
Figure 26 Wavelength Dependence of Perpendicular Polarized Component of Relative Spectral Directional Emittance of Platinum (Sample 1B at 1645°K)

70

less dominant. Figure 26 shows spectral changes in the perpendicular directional component for sample 1B and indicates a negligible wavelength dependence for this component. This is in agreement with predictions from the Fresnel equations.

Spectral hemispherical-to-spectral normal emittance ratios for all the platinum samples, determined using Eq. (24), subsection IV.2.e, are listed in Table X for the lowest and highest test-temperature data. The hemispherical-to-normal emittance ratios obtained at the intermediate test temperatures were intermediate to those reported here. Although the values for $\epsilon(\theta)_{max}$ tend to decrease slightly with increasing temperature, as noted from the data in Table IX, the effect of this decrease on the hemispherical-to-normal emittance ratio is small because of the large angle at which $\epsilon(\theta)_{max}$ occurs. The change in the relative spectral directional emittance characteristics of the parallel polarized components illustrated in Figure 25, however, is sufficiently large to produce detectable changes in the hemispherical-to-normal emittance ratio with wavelength. As shown by the data in Table X, this ratio tends to increase with wavelength.

Table X. Wavelength and Temperature Dependence of $\epsilon(\lambda, T)/\epsilon(\theta_N, \lambda, T)$ Ratios for Platinum Samples

Nominal Temperature (°K)	Wavelength (μ)	Sample No.				
		1B	3B	4B	5B	6B
865	2	1.153	1.151	1.175	1.171	1.191
865	3	1.180	1.188	1.204	1.217	1.267
865	4	1.183	1.220	1.220	1.235	1.264
1645	1.5	1.110	1.131	1.130	1.143	1.170
1645	2	1.153	1.136	1.153	1.156	1.191
1645	3	1.170	1.163	1.177	1.186	1.232
1645	4	1.183	1.179	1.200	1.202	1.240
1645	6	1.201	1.214	1.198	1.223	1.236
1645	8	—	1.235	1.214	1.220	1.234

The temperature and wavelength effects described above are observed to generally hold true for each of the platinum samples, regardless of its surface condition. The relative spectral directional emittance characteristics of platinum, however, are modified by the roughness of the surface, as illustrated by the data shown in Figures 27 and 28. These figures compare the directional results for each of the polarized components at 1.5 and 6 μ for samples 1B, 3B, 5B, and 6B. The effect of increasing roughness is to decrease the strongly directional character of the polished surface. This is most apparent at the longer wavelengths where the polished surface is most directional. The overall effect of roughening is to decrease $\epsilon(\theta)_{max}$ and θ_{max} of the parallel component and to increase $\epsilon(\theta,\lambda,T)/\epsilon(\theta_N,\lambda,T)$ of the perpendicular component. The integrated spectral directional results for $\epsilon(\theta,T)$ are in good agreement with those reported in the previous section.

As was the case for the total hemispherical to normal emittance ratio, it is seen that increasing roughness increases the ratio $\epsilon(\lambda,T)/\epsilon(\theta_N,\lambda,T)$ for all temperatures and wavelengths. While this is not immediately apparent from an initial inspection of Figures 27 and 28, it is easily discerned when the results are plotted as

$$\frac{\epsilon_{||}(\theta,\lambda,T) + \epsilon_{\perp}(\theta,\lambda,T)}{\epsilon(\theta_N,\lambda,T)}$$

versus $\cos\theta$. In this form it becomes apparent that the shift of parallel component energy from extreme angles ($\theta > 80$ deg) to less grazing angles (30 deg $< \theta <$ 80 deg) combined with an overall increase in the perpendicular component results in the trend of values reported in Table X.

As previously mentioned in subsection II.3, attempts at correlating the directional emittance data with the parameters σ_m/λ and a/λ were made; however, no definite correlating functions were established. The effects of polarization that are clearly observable on the previous figures are not accounted for by the reflectance theories; therefore, complete correlations based on parameters from that theory are not anticipated. However, it is interesting to note that the maxima of the spectral distributional curves for the parallel component are strongly influenced by the parameter σ_m/λ. It was found that these maxima could be described by a single plot similar to that shown on Figure 29 for T = 1645°K. Similar results were obtained for the other temperatures. In each case, sample 1B was observed to deviate considerably from the remaining samples due apparently to the different nature of its surface profile. The grain displacements, thermal etching, and thermal faceting that introduced roughness into this surface provide a geometry that is far from irregular or Gaussian.

For the other samples, the correlation with σ_m/λ was distinct for each temperature though no single analytical form was found to describe the correlation function. In most cases the curves are best described by an inverse power of (σ_m/λ) rather than the exponential function used to describe the decay of specularly reflected energy.

72

Figure 27 Effect of Roughness on the Relative Spectral Directional Emittance of Platinum at $\lambda = 1.5\ \mu$, $T = 1645°K$
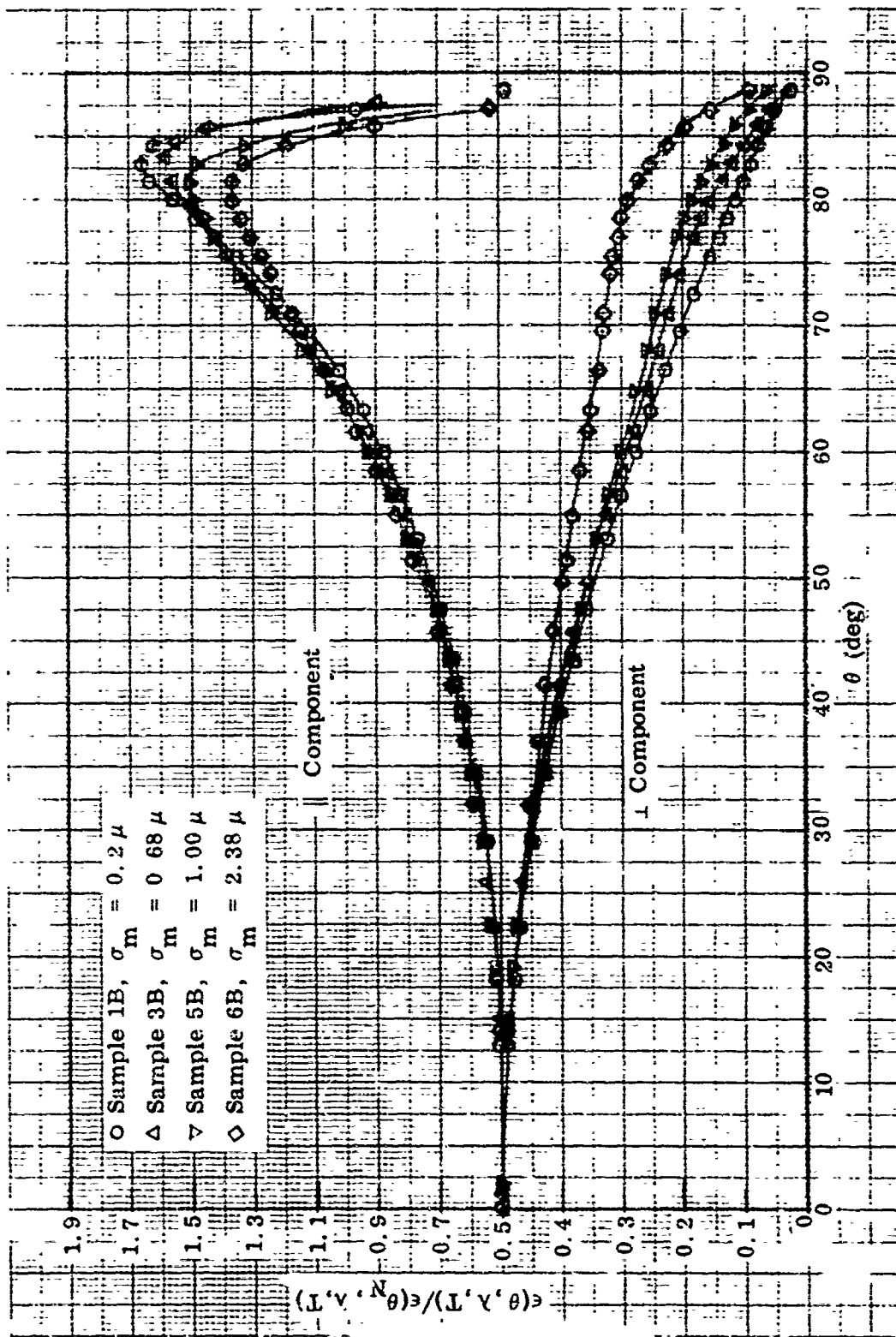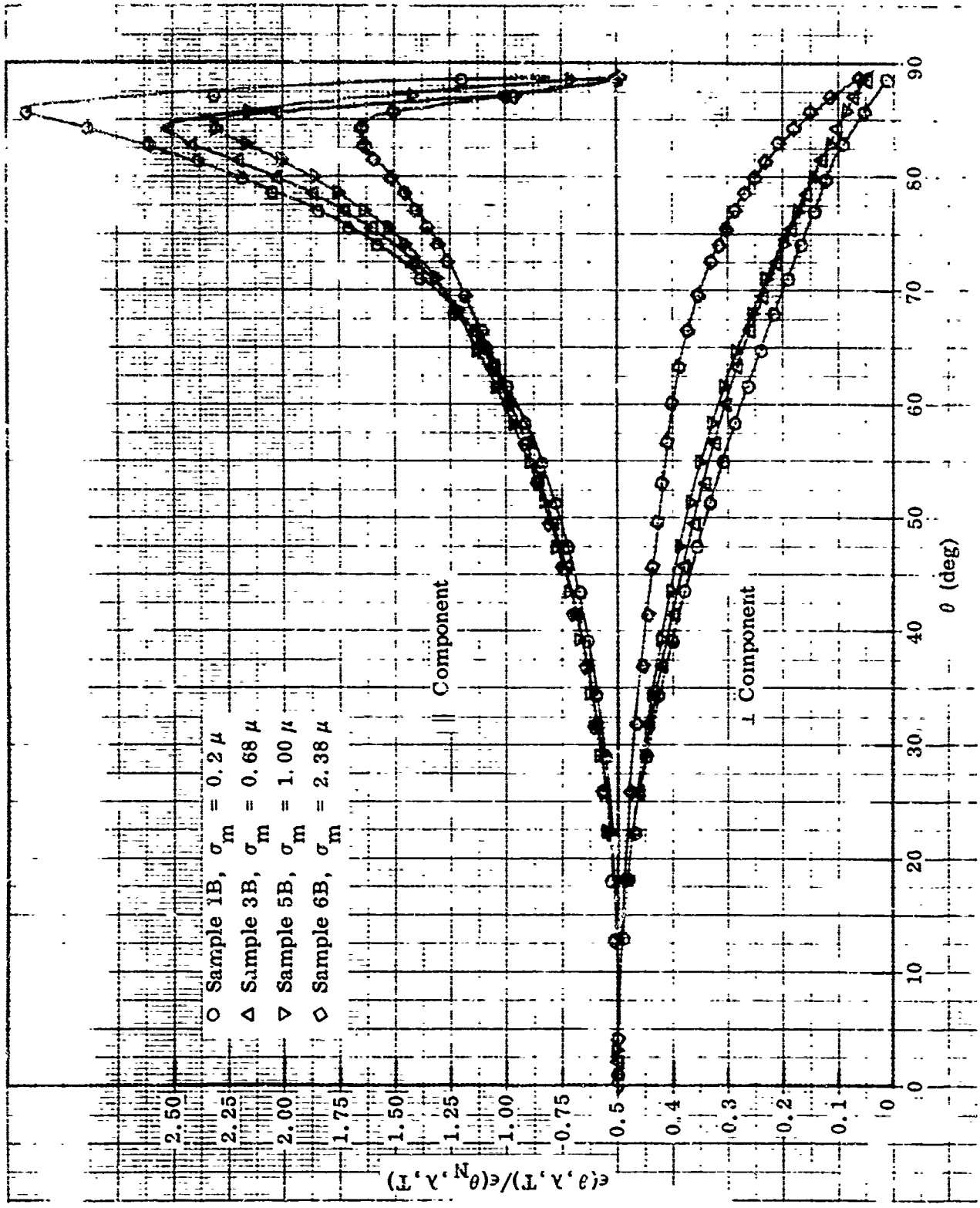
Figure 28 Effect of Roughness on the Relative Spectral Directional Emittance of Platinum at $\lambda = 6\ \mu$.
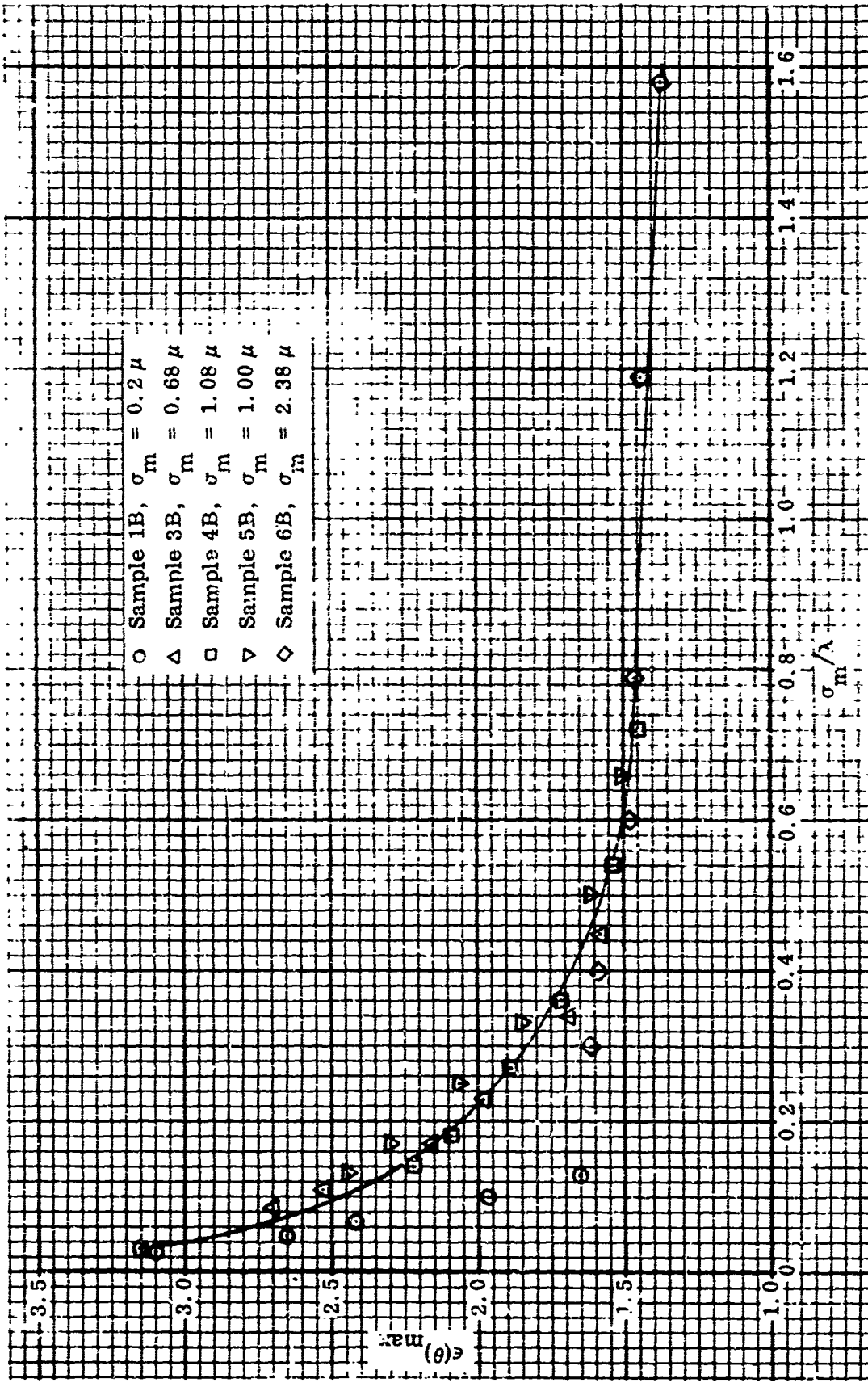$T = 1645°$ K

74

Figure 29   Correlation Between rms Roughness-to-Wavelength Ratio and Maximum Relative Directional Emittance Values for the Parallel Polarized Component at T = 1645°K

75

2. STAINLESS STEEL SAMPLES

a. Surface Characteristics

Surface photomicrographs of the stainless steel samples before and after their emittance tests are shown in Figure 30. Electron micrographs of the same surfaces are shown in Figure 31. Micrographs of sample 1S-3 are not shown since its surface appearance, both before and after the emittance tests, was nearly identical to those shown for sample 1S-2. No after-test micrographs of sample 3S were taken because the oxide apparently dissociated and evaporated during its test at 1090°K, leaving a bright, unoxidized surface.

The initial electropolished and annealed surface condition of all smooth samples was identical to that shown for sample 1S-2. Similarly, the initial electropolished, glass-shot blasted and annealed surface of sample 1R is representative of all the roughened sample surfaces before they were oxidized. The rms roughness of the latter samples was 20μin. before oxidation. No roughness measurements were made of the samples after oxidation since the substrate roughness produced by the shot-blast treatment was completely obscured by the oxide films.

The thickness of the oxide films on each sample increased during the high-temperature emittance tests with the exception of the film on sample 3S which disappeared from the surface during the tests at 1090°K. No satisfactory explanation for this oxide removal is known since its composition was the same as for the other samples and the dissociation pressure for Fe_3O_4 at 1090°K is low — on the order of 10^{-11} Torr (39). To prevent a recurrence of the phenomenon, the maximum test temperature for the remaining samples was lowered to 950°K. Changes in the thickness of the oxide films, even at this lower temperature, caused significant changes in the emittance characteristics of the samples.

Continued oxidation of the stainless steel samples during emittance tests was not anticipated since the test chamber pressure was maintained at pressures less than 5×10^{-6} Torr during all high-temperature measurements. It is possible that the sample surfaces acted as "getters" for residual oxygen and/or water vapor in the test chamber. A phase transition occurs for Fe_3O_4 at 900°K (40). However, the influence of this transition on the surface oxidation is uncertain. Richmond (41) has reported a similar occurrence for an Inconel specimen which oxidized when heated to between 850 and 950°K in a vacuum of 10^{-5} Torr.

The initial surface photomicrographs of sample 1S-2 show that crystallization of the stainless steel samples occurred during their pre-oxidation anneal treatment at 1300°K (10 min) in the dry hydrogen furnace. Grain boundaries are clearly evident on the initial surfaces of samples 1S-2 and 2S (also on 1S-3), but are obscured by the roughness on sample 1R. These grain boundaries are also evident in the electron micrographs (Figure 31), including the one of sample 1R. Small spherical nodules appear to be scattered over the surfaces of samples 1S-2 and 1R. Gulbransen and Andrew (32)

76

Before Emittance Tests

(Unoxidized)	Gold	Purple	Dull Gray
$d = 0$	$d = 0.015\,\mu$	$d = 0.17\,\mu$	$d = 0.95\,\mu$
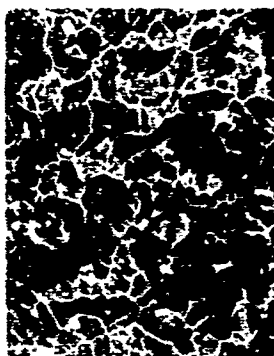
1S-2	2S	3S	4S
$T_{max} = 950°K$	$T_{max} = 1090°K$	$T_{max} = 1090°K$	$T_{max} = 950°K$

Not Photographed;
Oxide Disappeared
During 1090°K
Emittance Tests
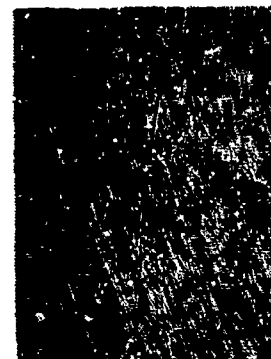
Light Blue   Silver-Gray   Dull Gray

After Emittance Tests

$$200\,\mu$$

Mag.: |_____|

Figure 30 Surface Photomicrographs of 304 Stainless Steel Samples Before and
After Emittance Tests (I)

77

Before Emittance Tests

Brown-Gray	(Unoxidized)	Purple	Brown-Gray
$d = 1.40 \mu$	$d = 0$	$d = 0.165 \mu$	$d = 1.50 \mu$
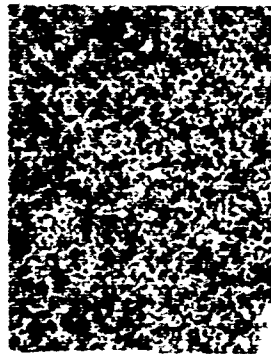
5S	1R	3R	5R
$T_{max} = 950°K$	$T_{max} = 950°K$	$T_{max} = 950°K$	$T_{max} = 950°K$
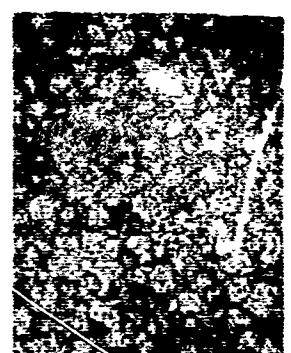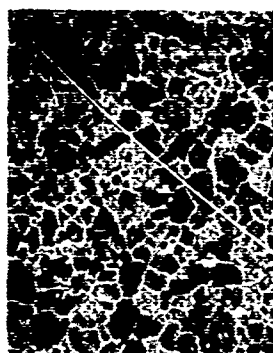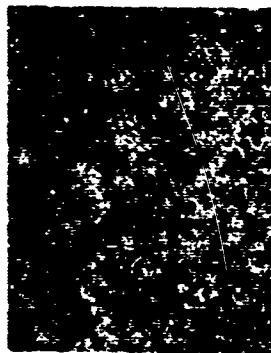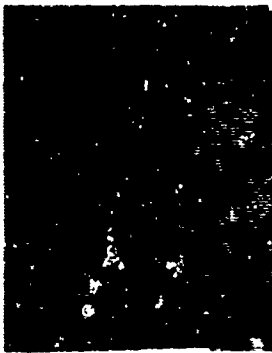
Brown-Gray	Red-Gold	Blue-Gray	Brown-Gray

After Emittance Tests

Mag.: $\underset{}{\underline{\qquad}}$ 200 μ

Figure 30 Surface Photomicrographs of 304 Stainless Steel Samples Before and After Emittance Tests (II)

78

Before Emittance Tests

1S-2   2S   3S   4S

Oxide Disappeared
During 1090°K
Emittance Tests
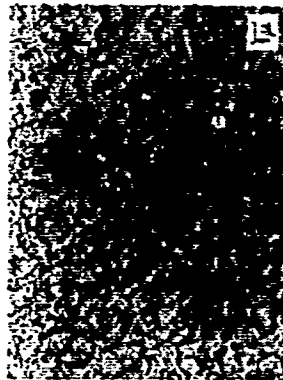
After Emittance Tests

Figure 31 Electron Micrographs of 304 Stainless Steel Surfaces Before and After Emittance Tests (I)

79

Before Emittance Tests

After Emittance Tests

5R

3R

1R

5S

Figure 31 Electron Micrographs of 304 Stainless Steel Surfaces Before and After Emittance Tests (II)

80

point out that the annealing of stainless steel at temperatures above 1050°K is known to precipitate carbides and nitrides which might also occur during normal oxidation at these temperatures. The nodules on these surfaces are assumed to be these precipitates.

The photomicrograph of the initial surface of sample 2S fails to show the thin, gold-colored oxide film that covered this surface; however, the oxide film is clearly evident in the electron micrograph. The latter micrograph also indicates a difference in the formation rate, and possibly in the composition of the oxide at the grain boundaries.

Photomicrographs of the initial surfaces of samples 3S, 4S, 5S, 3R, and 5R indicate that the thicker oxide films hide the substrate and that the oxide morphology changes considerably as film thickness increases from 0.015 to about 1.0 μ. The changes in morphology are shown more dramatically by the electron micrographs of these surfaces. Large oxide nodules begin to appear on the surfaces of samples 3S and 3R with major diameters of up to 2 μ. These nodules continue to form and grow to where they cover over 50% of the surface area of sample 4S and have major dimensions up to 4 μ. On the surface of sample 5S, the nodules are merging together, forming relatively smooth-looking lumps of oxide up to 8 or 10 μ long.

Emittance data for the stainless steel samples at temperatures less than 950°K are attributed to oxide films having the initial properties described above. However, at 950°K all the surfaces (except for sample 1S-3) experienced further oxidation which resulted in significant changes of the emittance characteristics on both oxidized and unoxidized samples. Micrographs of the after-test surfaces in Figures 30 and 31 show the changes in surface appearance of the samples caused by high temperature exposure and attendant oxidation. The most dramatic change occurred on the unoxidized sample surfaces (1S-2 and 1S-3). A light blue-colored oxide film formed on sample 1S-2 during its 950°K tests which appeared entirely different from the prepared oxides. Small grained crystals completely hid the substrate and were brightly multicolored when viewed through a microscope. A light gold-colored oxide film formed on sample 1S-3 during its 1090°K tests in the hydrogen-purged atmosphere and appeared practically identical in structure to the initial film on sample 1S-2. A light reddish-gold-colored film formed on sample 1R during its 950°K tests that appeared more fine-grained than the thicker oxides, but did not have the bright, multicolored appearance of the smooth surface oxides. Electron micrographs of the films that formed on samples 1S-2 and 1R indicate the smoother and more uniform films that formed on these samples.

Electron micrographs of the remaining samples in Figure 31 show that significant changes in the morphology of all the oxides occurred during the emittance tests. These changes were not generally detected in the surface photomicrographs, except in the case of sample 2S.

Only one clear surface interference photomicrograph was obtained from the stainless steel samples and it is shown in Figure 32. This was obtained on sample 1S-2 and is representative of all the smooth, electropolished, and annealed stainless steel surfaces

81

$\vdash$— 100 μ —$\dashv$
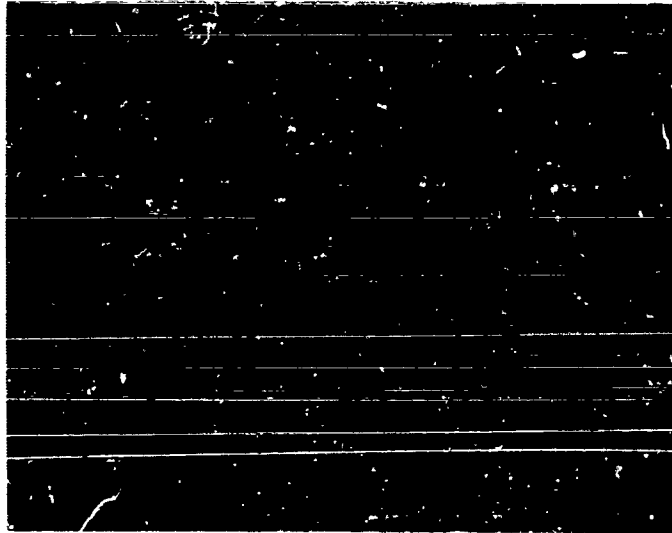
Figure 32 Surface Interference Photomicrograph of
Electropolished, Annealed 304 Stainless
Steel Before Oxidation

before oxidation. Because of the nonuniform appearance of the pattern, it is not possible to specify quantitative values of roughness parameters by analyses of the patterns. However, the photograph does show closed fringes around each precipitate nodule which indicate their height to be between 1/2 and 1 μ (2 to 4 fringes). This dimension agrees with the diameter measurements from the electron micrograph in Figure 31, and indicates the nodules to be approximately spherical in shape.

Attempts to obtain direct measurements of film thickness by the techniques described in Section III were generally unsuccessful. Best estimates of the average initial oxide film thickness are believed to be those from weight-gain data obtained before and after sample oxidation. However, this method was not applicable for determining the changes in thickness during the emittance tests because of the weight of the thermocouple attachments.

Attempts to measure film thickness from micrographs of metallurgical cross-section mounts of the samples were unsuccessful for the thin films on samples 2S and 3S. However, some success was obtained by metallographic cross-sectioning for the thicker films on samples 4S and 5S. Photomicrographs and electron micrographs of the films on these latter two samples are shown in Figure 33. The photomicrographs indicate average film thicknesses of approximately 1.25 μ for sample 4S and 1.5 μ for sample 5S. These values are slightly larger than those from the weight-gain estimates for the initial thickness of these films. Average film thickness estimates obtained from the electron micrographs of the same cross-section mounts, are 2.3 μ for sample 4S and 3.8 μ for sample 5S. These values are about twice as large as those obtained from microscopic examination, but are highly questionable since the oxide boundaries are so poorly defined and the lateral field of view is so small at this high magnification. Definition of the oxide boundaries on the electron micrographs of the cross-sectioned thinner oxide films of samples 2S and 3S was so poor that no definitive estimate of thickness could be established.

Attempts were also made to determine oxide film thickness from electron shadow-graphs of "free" films. These were stripped from the stainless steel substrate, cast in epoxy, and cross sectioned [see subsection III.3.b.(1)]. Typical shadowgraphs obtained by this method are shown in Figure 34. The procedure required to obtain a suitable cross-section was tedious and the results were erratic and nonrepeatable from one region to another on the same film sample. The thinner films usually appeared to be discontinuous, which is not surprising in view of the uneven profiles indicated by the surface micrographs shown in Figure 31. From the shadowgraphs shown for the thin films in Figure 34, it is apparent that film thickness estimates would be highly unreliable. The thicker oxide film stripped from sample 5S, was more uniform and its thickness agreed fairly well with that indicated by the weight gain data and the photomicrograph shown in Figure 33.

The discontinuous nature of the thinner films indicated by the electron shadowgraphs was also apparent on normal transmission shadowgraphs of one of the "free" films. Two of these latter shadowgraphs are shown in Figure 35. Another example of the preferred oxidation in the vicinity of a grain boundary is indicated in the lower

83

Photomicrographs

lite M

Oxide

Stainless Steel Substrate

Sample 4S

Electron Micrographs
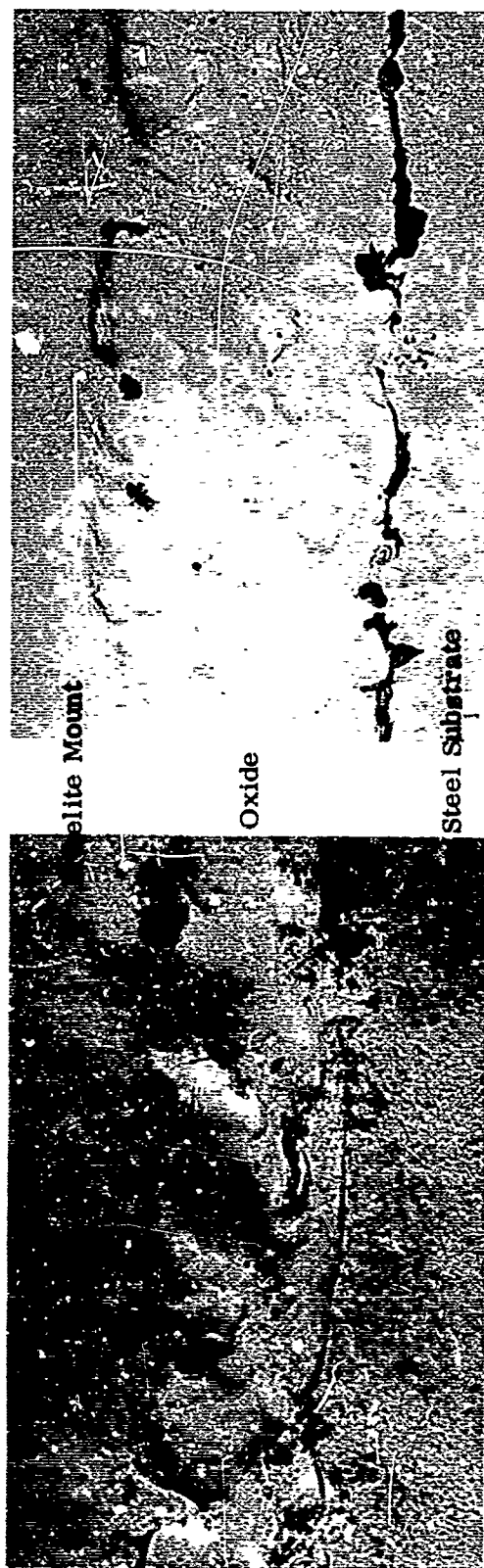
lite Mount

Oxide

Steel Substrate

Sample 5S   Mag.: 5μ

Mag.: -1μ

Figure 33   Cross-Section Micrographs of Oxide Films on Stainless Steel
Samples 4S and 5S, After Emittance Tests

84

a. Oxide Film Stripped From
Sample Oxidized at 800°C
for 20 min (Similar to
Sample 3S)

$\overline{2\mu}$

b. Oxide Film Stripped From
Sample 3S (Control Disk),
Before Emittance Tests
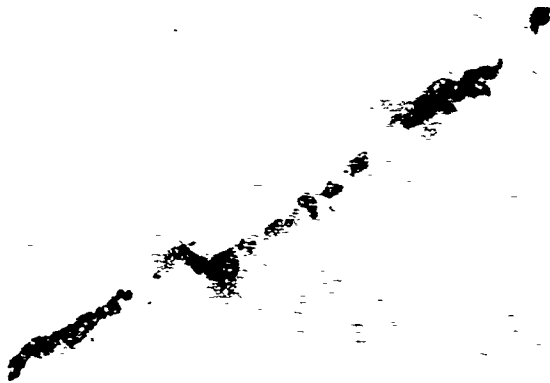
$\overline{1\mu}$

c. Oxide Film Stripped From
Sample 5S (Control Disk),
Before Emittance Tests

$\overline{1\mu}$

Figure 34 Cross-Section Electron Shadowgraphs of Stainless Steel
Oxide Films

85
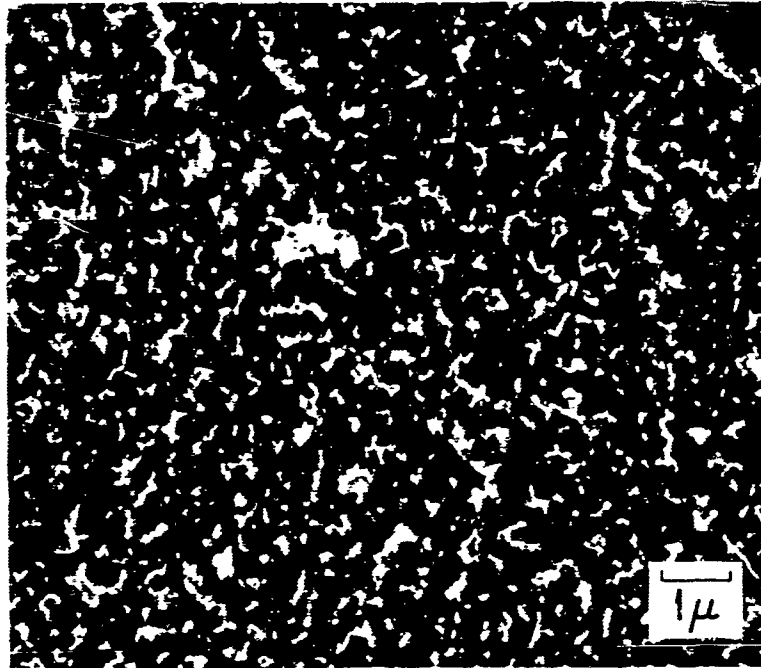
a.
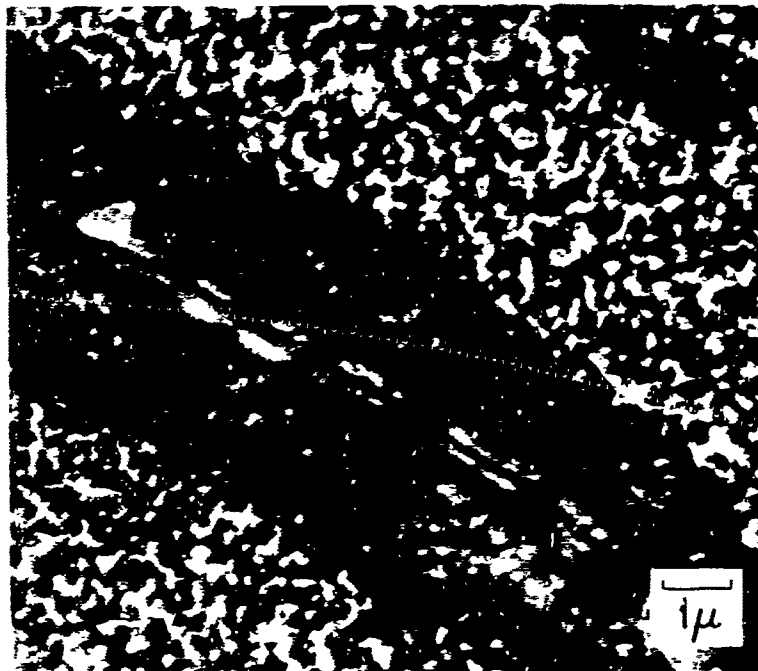
b.

Figure 35   Surface Electron Shadowgraphs of Stainless Steel Oxide
Film From Sample 3S, Before Emittance Tests

shadowgraph in this figure. The results obtained from weight gain measurements and from the various photomicrographic and electron micrographic examinations clearly indicate the complex nature of the films examined during this study. The films were irregular, suffered changes in morphology with temperature, and had thicknesses which from point-to-point varied by an order of magnitude. It is obvious that the average film thickness values computed from weight gain data have little meaning for such heterogeneous surfaces. However, the other inspection techniques also fail to provide the information required for analysis of the effect of oxide films on emittance due to the limited field of view of the micrographs (this severely limits the statistical sample available), and the need for considerable interpretation of the photographic evidence obtained. These results indicate the need for further development of film thickness measuring techniques and also show that, for the stainless-steel samples used in this program, a single specification of film thickness cannot be established for the purpose of describing the emittance results.

Oxide film composition determinations were made exclusively from electron diffraction patterns of the films. Transmission patterns were obtained for the thin films on samples 2S and 3S and of the light blue-colored film that formed on sample 1S-2 during its emittance tests. Reflection patterns were obtained for the films on samples 4S and 5S since these were too thick to be analyzed by the transmission method. Samples of the initial oxide films used for analysis were obtained from 1-in. diameter control disks that were oxidized along with the emittance-test samples. Samples of the after-test oxide film were obtained from the center portion of the test strips themselves. Typical diffraction patterns are shown in Figure 36 along with a pattern of the gold-foil standard used for calibration. From these patterns, the composition of all the oxide films was determined to be primarily Fe_3O_4; however, a large number of weaker diffraction lines were observed which could not be accounted for.

The formation of Fe_3O_4 on the stainless steel samples is consistent with the findings reported by Hickman and Gulbransen in (42) for other 18/8 type stainless steels. For oxide films formed on a type 301 stainless steel in a 1-mm atm of oxygen at temperature from 300 to 900°C the most common oxide structure is reported to be Fe_3O_4. It is further reported that a Cr_2O_3 structure predominates at the 800°C formation temperature and at 900°C a spinel formation, probably of Fe, Cr, and Mn, occurs. Depending on the size and orientation of the oxide crystals, various degrees of sharpness of the pattern lines results, with intense arcs or spots generally indicating preferential growth of the oxide crystals on the surface. Based on the above report, it is assumed that the additional lines that appeared in the patterns obtained from the emittance test samples probably resulted from the spinel structure obtained at the higher formation temperature, since they are not accounted for by the Cr_2O_3 pattern. No significant change in the patterns was detected as a result of the emittance test procedures.
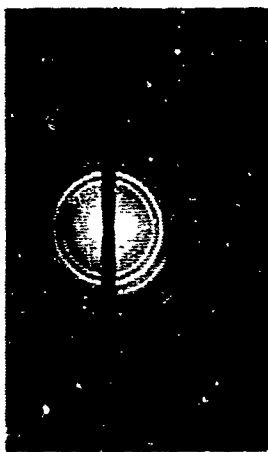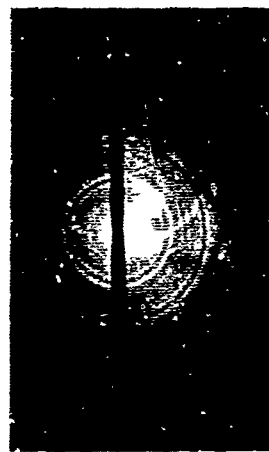
a. Blue Oxide Film on Sample 1S-2, After Emittance Tests.
b. Initial Gold Oxide Film on Sample 2S.
c. Initial Purple Oxide Film on Sample 3S.
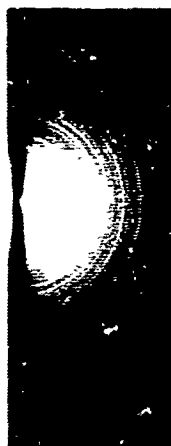
d. Initial Gray Oxide Film on Sample 4S.
e. Initial Brown-Gray Oxide Film on Sample 5S.
f. Gold-Foil Standard for Calibration.

Figure 36 Electron Diffraction Patterns of Stainless Steel Oxide Films
and Gold Standard

b. Emittance Characteristics

(1) Total Normal and Total Hemispherical Emittance

Absolute total normal and total hemispherical emittance values for each stainless steel
sample at all test temperatures are listed in Tables XIX through XXVII in Section VII.
A comparison of the data for the unroughened samples is shown in Figure 37. A similar
comparison for the roughened samples is not included since a study of the data tabu-
lated in Section VII indicates that roughening of the samples did little to change their
total or spectral absolute emittance. The oxide growth was by far the dominant influ-
ence causing changes in absolute properties.

The data shown in Figure 37 are the initial emittances for the samples which were
measured during the first test-temperature cycle. Therefore, these properties are
representative of the initial oxide films before they changed as a result of further
oxidation during the high temperature tests. Total hemispherical results for the
smooth, electropolished sample (1S-2) are in good agreement with those reported
by Deitch and Plunkett (43) for electropolished 304 stainless steel, whereas the results
for sample 5S are representative of those for fully oxidized stainless steel. The
absolute accuracy of the total normal emittance results for all the samples is on the
same order as that reported for the platinum samples, i.e., ±5%.

The absolute total emittance of sample 2S, whose initial gold-colored oxide film was
estimated to be about 0.015 μ thick, was found to be just slightly higher than that for
the unoxidized sample. Although the increase in absolute emittance is small, it repre-
sents a large percentage increase (25%). [Approximately the same change in total
emittance was observed for the light-blue oxide film that formed on sample 1S-2 while
it was tested at 950°K (see Table XIX.]

Total emittance values for sample 3S, whose initial purple-colored oxide film was
estimated to be about 0.17 μ thick, were observed to be significantly higher than those
for samples 1S-2 and 2S. The increase of emittance with temperature was also
observed to be significantly more positive, indicating a relatively higher increase in
the spectral emittance of this film at the short wavelengths (i.e., $\lambda < 4\,\mu$) than at
the longer wavelengths. This charac eristic was confirmed by the spectral normal
emittance data which are presented in the following section. Further large increases
in total emittance were observed for samples 4S and 5S whose initial oxide films were
estimated to be 0.95 and 1.4 μ thick, respectively. The emittance of the latter sam-
ple is close to that for fully oxidized stainless steel indicating that a film thickness of
approximately 1.5 μ constitutes an opaque film. No further increase in emittance at
these temperatures would be expected for films thicker than about 1.5 μ, except as
might occur because of changes in the chemical composition of thicker films. Interpre-
tations of these observations must take into consideration the fact that the quoted film
thicknesses are based on weight-gain data which provide a crude averaging of actual
film thicknesses. Point to point variations on the oxide films must be considered if
these results are to be used for direct comparison to theoretical predictions.

Figure 37 also shows the total normal emittance of the more heavily oxidized samples
to be higher than the total hemispherical emittance. This characteristic is expected

89
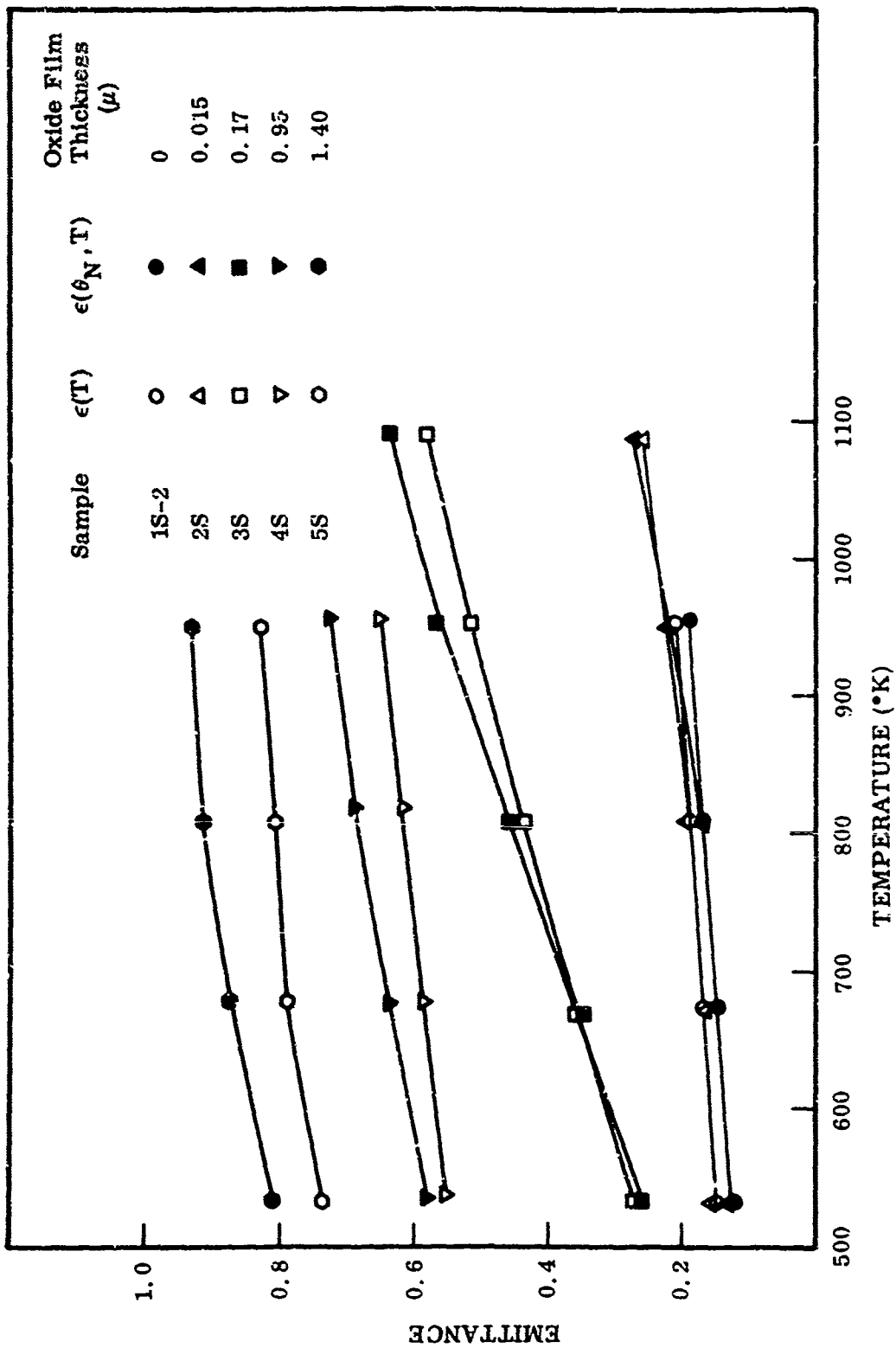
Figure 37 Total Hemispherical and Total Normal Emittance of 304 Stainless Steel Samples

as the film thickness becomes sufficient to provide an opaque, nonconducting surface. $\epsilon(T)/\epsilon(\theta_N, T)$ ratios obtained from the directly measured values of $\epsilon(T)$ and $\epsilon(\theta_N, T)$ are from 5 to 10% lower than the same ratios obtained by integration of the relative total directional emittance data. Similar differences were reported earlier for the platinum samples and are consistent with the estimated measurement errors for these tests.

The change in emittance caused by progressive oxidation during the measurements was evaluated by remeasuring $\epsilon(T)$ and $\epsilon(\theta_N, T)$ after the high temperature directional emittance tests were completed. A summary of the results obtained by this procedure is presented in Table XI, where the initial and final total emittances at $T = 535°K$ and $T = 950°K$ for each sample are compared. The data for sample 1S-3 are not included as the primary reason for testing this sample was to obtain the emittance characteristics of the unoxidized surface; therefore its emittance was not remeasured after oxidation at 1090°K. The tabulated data clearly show that the normal and hemispherical emittance of samples with oxide films less than $1\,\mu$ thick were significantly affected by the relatively small changes in oxide film thickness.

Table XI. Change in Total Emittance Due to Oxidation During Emittance Tests of Stainless Steel Samples

Sample No.	Color Change of Oxide Film	T = 535°K		T = 950°K	
		$\epsilon(T)$	$\epsilon(\theta_N, T)$	$\epsilon(T)$	$\epsilon(\theta_N, T)$
1S-2 (Initial)	Bright metal to	0.151	0.118	0.206	0.187
1S-2 (Final)	light blue	0.149	0.125	0.225	0.226
2S (Initial)	Gold to	0.152	0.130	0.222	0.216
2S (Final)[a]	silvery-gray	0.192	0.153	0.345	0.306
3S (Initial)	Purple to	0.272	0.261	0.517	0.564
3S (Final)[b]	bright metal	—	—	—	—
4S (Initial)	Dull gray,	0.554	0.580	0.648	0.725
4S (Final)	no change	0.586	0.599	0.691	0.769
5S (Initial)	Dark brownish gray,	0.735	0.813	0.826	0.928
5S (Final)	no change	0.764	0.841	0.828	0.938
1R (Initial)	Bright metal to	0.153	0.127	0.212	0.193
1R (Final)	reddish-gold	0.155	0.130	0.223	0.212
3R (Initial)	Purple to	0.259	0.249	0.439	0.490
3R (Final)	blue-gray	0.263	0.276	0.477	0.543
5R (Initial)	Dark gray,	0.755	0.799	0.836	0.899
5R (Final)	no change	0.757	0.799	0.838	0.901

(a) Maximum test temperature for sample 2S was 1090°K.
(b) Final emittance values for sample 3S not determined because oxide film disappeared during 1090°K tests.

(2) Spectral Normal Emittance

Spectral normal emittance data for each stainless steel sample at each test temperature above 800°K are listed in Tables XIX through XXVII in Section VII. Spectral emittance determinations were not possible at the two lower test temperatures because of inadequate energy at the detector. This same difficulty existed for the higher temperature tests at wavelengths below 3 μ, where the measurement uncertainty approaches ±10%. A comparison of the spectral emittance data from the five smooth (substrate) samples is shown in Figures 38 and 39 to illustrate the effect of oxide film thickness on spectral emittance. The data shown in Figure 38 were determined from room temperature spectral normal reflectance measurements, using 1-in.-diameter disk samples that were oxidized along with the emittance-test samples. Figure 39 presents the initial emittance data obtained at 810°K, which is most representative of the initial oxide films on these samples. Data for the roughened (substrate) samples were comparable to that shown in Figures 38 and 39, thereby indicating that roughening introduced no significant changes in the spectral properties of these samples.

A comparison of the results in Figures 38 and 39 shows that the spectral emittance characteristics determined from room temperature reflectance measurements agree closely with the directly measured emittance characteristics for the three samples with thin oxide films. This indicates that the effect of temperature on the spectral emittance of samples of this type is small. However, significant differences between the room temperature and elevated temperature data are apparent for the samples with the thicker oxide films. It is improbable that these differences are due entirely to thermal changes in the radiant properties of the coating material. While such effects are expected to cause band broadening in the emission spectrum, their influence would not be as dominant as that indicated in Figure 39. It is more probable that the observed differences were caused by changes in surface morphology during the elevated temperature exposures. Such changes, as shown by the surface micrographs presented earlier, were considerable and undoubtedly resulted in films of different average thickness and geometry than those present on the room temperature disk samples. Such changes would result in significant differences in the emittance characteristics of the sample and would be most apparent for the thick oxide films since their initial condition was more heterogeneous than the oxides on samples 1S-2, 2S, and 3S.

Figure 40 shows the influence of film thickness on spectral normal emittance at specific wavelengths. Since only five separate thicknesses were investigated, the data are somewhat incomplete. For this reason, no attempt was made to extrapolate smoothly between data points. The emittance at shorter wavelengths was strongly influenced by very thin oxide layers while at longer wavelengths a considerably thicker layer was required for a high emittance. No direct comparison of these results with those predicted from scattering theories is possible due to the complex geometrical nature of the oxide layers; however, it is apparent that the trend is in agreement with predictions where uniform dielectric films are assumed.

Increases in the spectral normal emittance of the samples also occurred as a result of oxidation during the directional emittance tests. The changes observed are presented for each sample individually in Section VII and compare favorably in
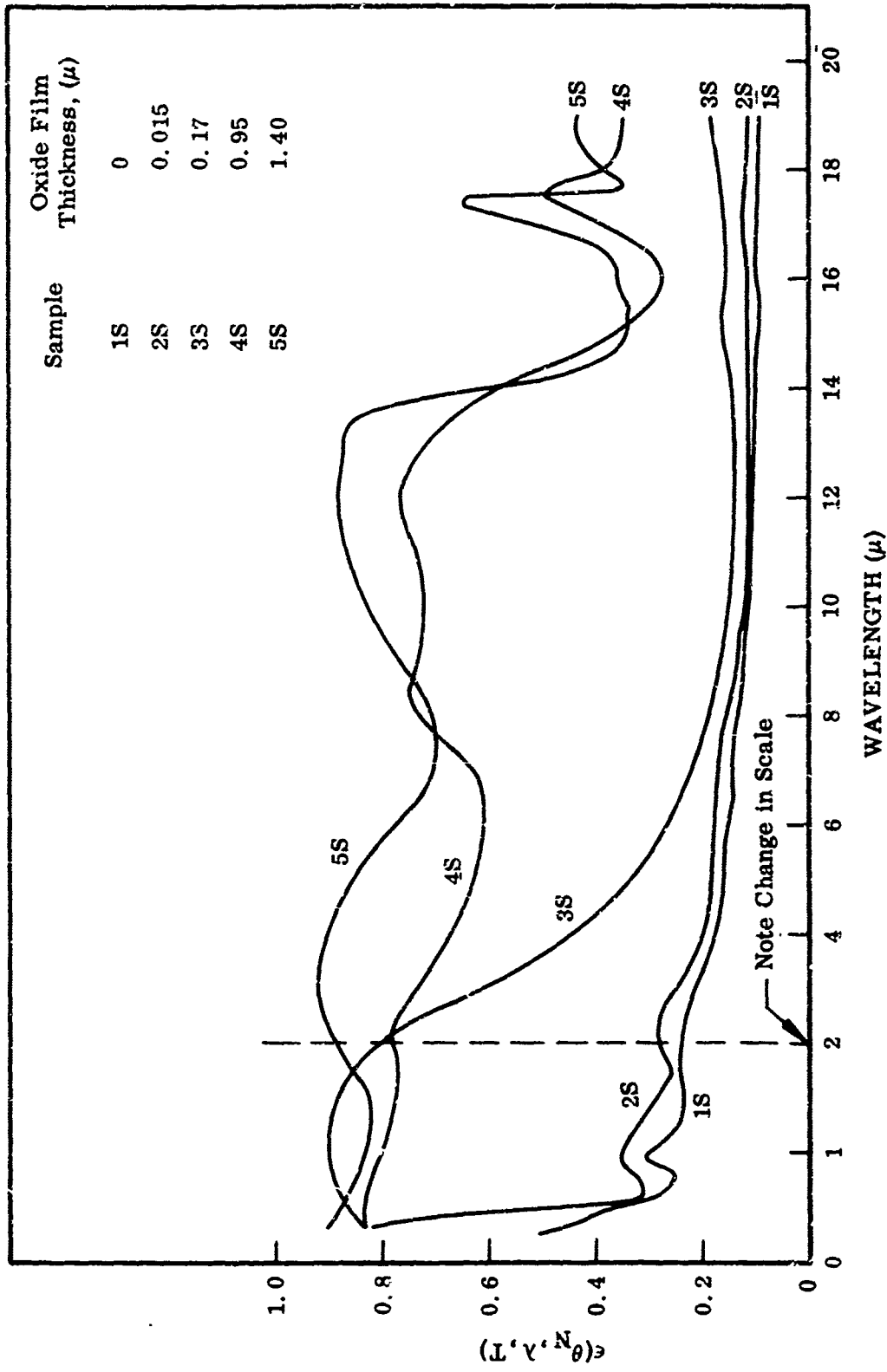
92

Figure 38 Spectral Normal Emittance of 304 Stainless Steel Samples at 300°K (From Spectral Reflectance Data)
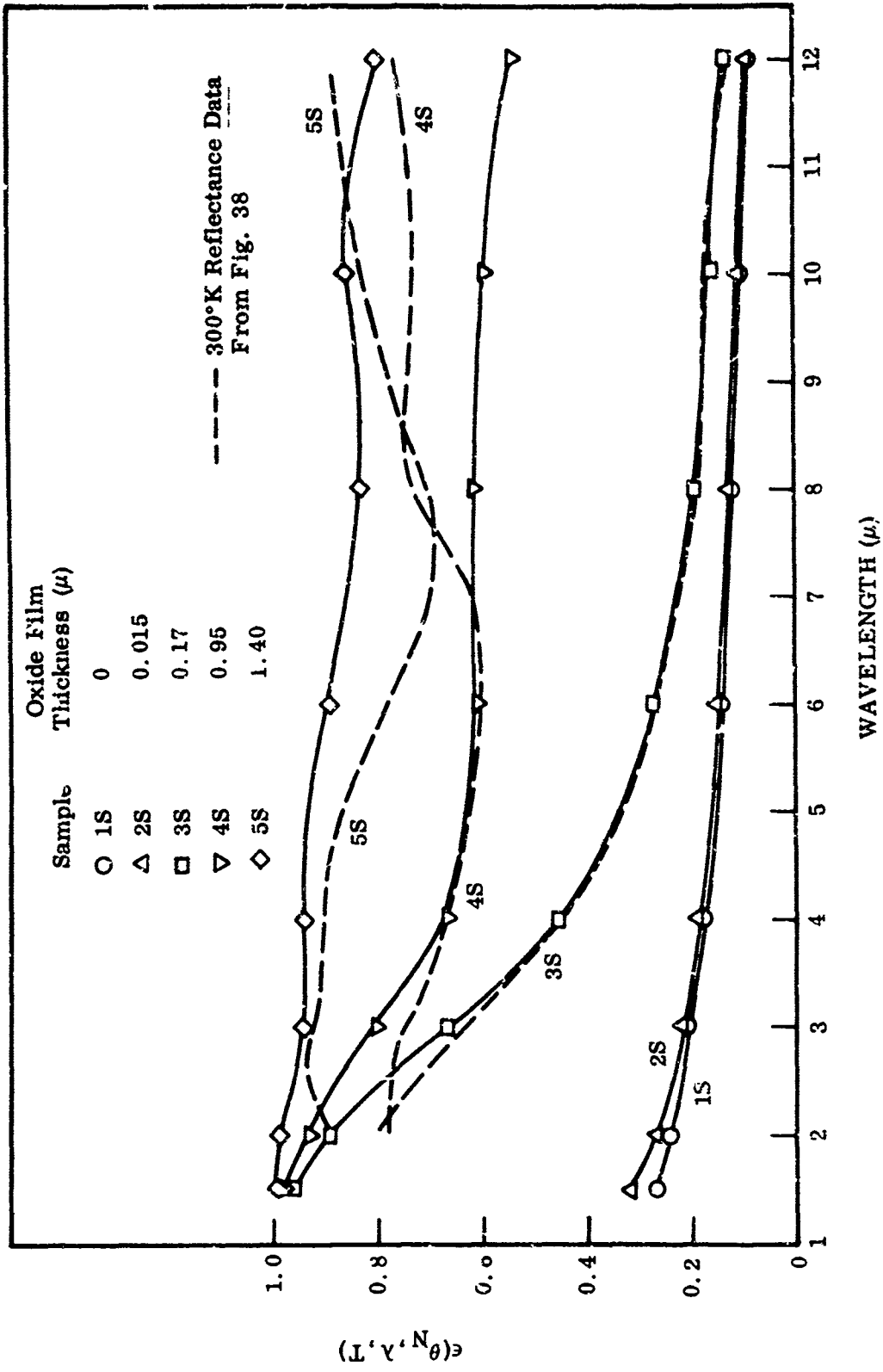
93

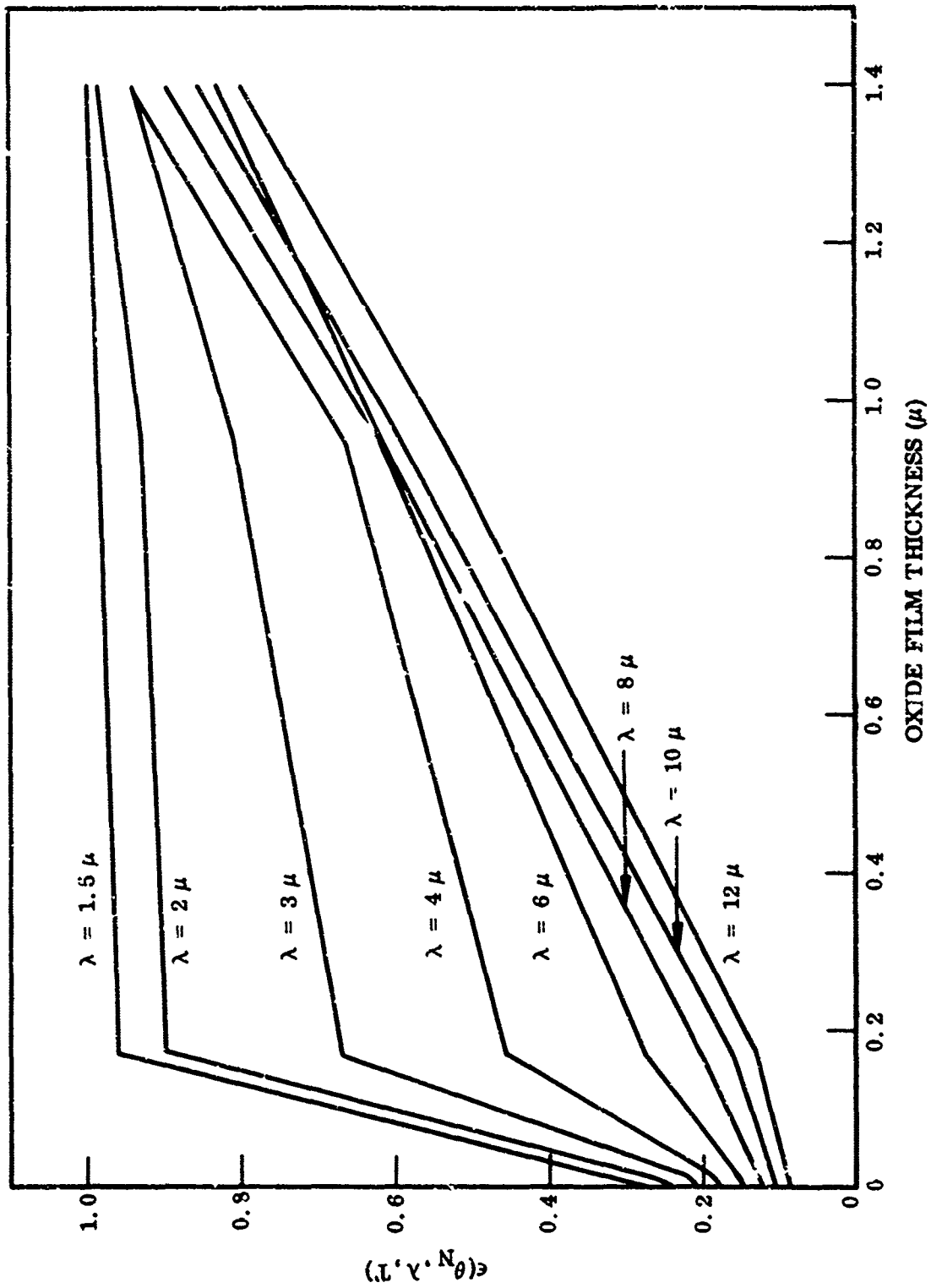Figure 39 Spectral Normal Emittance of 304 Stainless Steel Samples at 810°K

94

Figure 40 Effect of Oxide Thickness on the Spectral Normal Emittance of 304 Stainless Steel at 810°K

95

magnitude with those given in Table XI for the total properties. In view of the continual growth of the oxide film during testing, it is necessary to carefully consider the sample thermal histories presented in Section VII during interpretation of the absolute properties obtained from the test specimens.

(3) Re' ... Total Directional Emittance

The relative total directional emittance of each stainless steel sample is presented in graphical form in subsections VII.6 through VII.14. Interpretation of the results should consider that all of the stainless steel samples, except for 1S-3, experienced further oxidation during measurements at 950°K and higher. As a result, significant changes occurred in the initial emittance characteristics of the unoxidized and lightly oxidized test samples. These changes were determined at the conclusion of the high temperature measurements. Examples of the effect of this additional oxidation on the relative total directional emittance characteristics are shown in Section VII by Figure 90 for sample 2S, by Figure 118 for sample 1R, and by Figure 138 for sample 1S-3.

The relative total directional emittance data obtained at the three lowest test temperatures (535, 670, and 810°K), are believed to be representative of the initial surface condition for each sample. This is also true for most of the 950°K data since it was taken within 15 to 30 min after this temperature was attained. However, the 1090°K data obtained on samples 1S-3, 2S, and 3S were affected by oxidation during the 950°K tests. After loss of the oxide from sample 3S during its 1090°K tests, no further testing at this temperature was attempted except with sample 1S-3 in the special, hydrogen-purged atmosphere. Figure 97 in Section VII shows the effect of the oxide loss from sample 3S on its relative total directional emittance at 1090°K.

The effect of temperature on the relative total directional emittance parameters: θ_{max}, $\epsilon(\theta)_{max}$, and $\epsilon(T)/\epsilon(\theta_N, T)$ for each of the stainless steel samples is illustrated by the data in Tables XII and XIII. The data for samples 1S-2 and 1S-3 in these tables, and in subsections VII.6 and VII.14, show that increasing temperature has the following effects on the relative total directional emittance characteristics of electro-polished, unoxidized stainless steel:

- θ_{max} shifts slightly (1 to 2 deg) toward the normal as the temperature is increased from 535°K to 950°K. A further shift of another 2 deg at 1090°K is indicated by the data for sample 1S-3; however, this shift is probably due to the surface oxidation that occurred at this temperature.
- $\epsilon(\theta)_{max}$ and the $\epsilon(T)/\epsilon(\theta_N, T)$ ratio drops significantly with each increase in temperature.

These characteristics are consistent with the spectral directional results presented in the next subsection and are attributable to changes in the spectral energy content with temperature. The spectral properties are only a weak function of temperature, as shown in the next section.

96

Table XII. Effect of Temperature on θ_{max} and $\epsilon(\theta)_{max}$ for the Relative Total Directional Emittance of Stainless Steel Samples

Sample No.	Initial d. (μ)	T = 535°K		T = 670°K		T = 810°K		T = 950°K[a]		T = 1090°K[a]	
		θ_{max}	$\epsilon(\theta)_{max}$	θ_{max}	$\epsilon(\theta)_{max}$	θ_{max}	$\epsilon(\theta)_{max}$	θ_{max}	$\epsilon(\theta)_{max}$	θ_{max}	$\epsilon(\theta)_{max}$
1S-2	0	86.0	3.30	86.0	2.51	85.0	2.20	84.0	1.72	–	–
1S-3	0	85.5	2.86	86.0	2.40	85.0	2.10	84.5	1.99	82.5	1.62
2S	0.025	85.5	3.00	85.5	2.44	84.5	2.10	83.5	1.84	78.5	1.24
3S	0.17	74.0	1.12	62.0	1.03	0	1.00	0	1.00	0	1.03
4S	0.95	0	1.00	0	1.00	0	1.00	0	1.00	–	–
5S	1.4	0	1.00	0	1.00	0	1.00	0	1.00	–	–
1R	0	85.5	2.50	85.0	2.13	84.5	1.93	84.0	1.73	–	–
3R	0.17	71.0	1.11	60.0	1.02	0	1.00	0	1.00	–	–
5R	1.5	0	1.00	0	1.00	0	1.00	0	1.00	–	–

(a) See discussion in text on instability of sample surfaces at these temperatures.

Table XIII. Effect of Temperature on $\epsilon(T)/\epsilon(\theta_N, T)$ Ratios
for Stainless Steel Samples

Sample No.	Temperature (°K)				
	535	670	810	950[a]	1090[a]
1S-2	1.202	1.163	1.145	1.109	—
1S-3	1.199	1.159	1.140	1.125	1.099
2S	1.206	1.167	1.143	1.126	1.050
3S	1.027	1.002	0.965	0.947	0.940
4S	0.980	0.970	0.960	0.947	—
5S	0.947	0.947	0.947	0.947	—
1R	1.177	1.151	1.139	1.127	—
3R	1.035	0.995	0.978	0.965	—
5R	0.958	0.958	0.958	0.958	—

(a) See discussion in text on instability of sample surfaces at these
temperatures.

The effect of increasing film thickness on the directional emittance characteristics
above are apparent by comparison of the data at each temperature in Tables XII and
XIII. A graphical comparison of the data for two different temperatures is presented
on Figures 41 and 42. These figures show that abrupt changes in the directional
properties occur as the film thickness increases from 0.015 to 0.17 μ. The data for
sample 2S, whose initial gold-colored oxide film was estimated to be approximately
0.015 μ thick, indicates that this thin film had very little effect on the relative total
directional emittance of stainless steel at 535°K but produced a noticeable effect at
950°K.

The data for samples 3S and 3R, whose initial purple-colored oxide films were
estimated to be approximately 0.17 μ thick, show that this film thickness is sufficient
to produce directional properties that are characteristic of a dielectric at high tem-
peratures (950°K). For this same thickness, the directional emittance characteristics
at low temperatures (longer wavelengths) are intermediate to those for unoxidized and
heavily oxidized stainless steel at the lower temperatures. Similar characteristics
were observed for sample 4S, whose initial dull gray-colored oxide film was estimated
to be approximately 0.95 μ thick.

The data for samples 5S and 5R indicate no temperature dependence for the relative
total directional emittance characteristics of the opaque, or nearly opaque, oxide
film that covered these sample surfaces. This behavior is verified by the spectral
directional emittance of these samples where only minor changes in properties were
obtained as a function of temperature and wavelength.
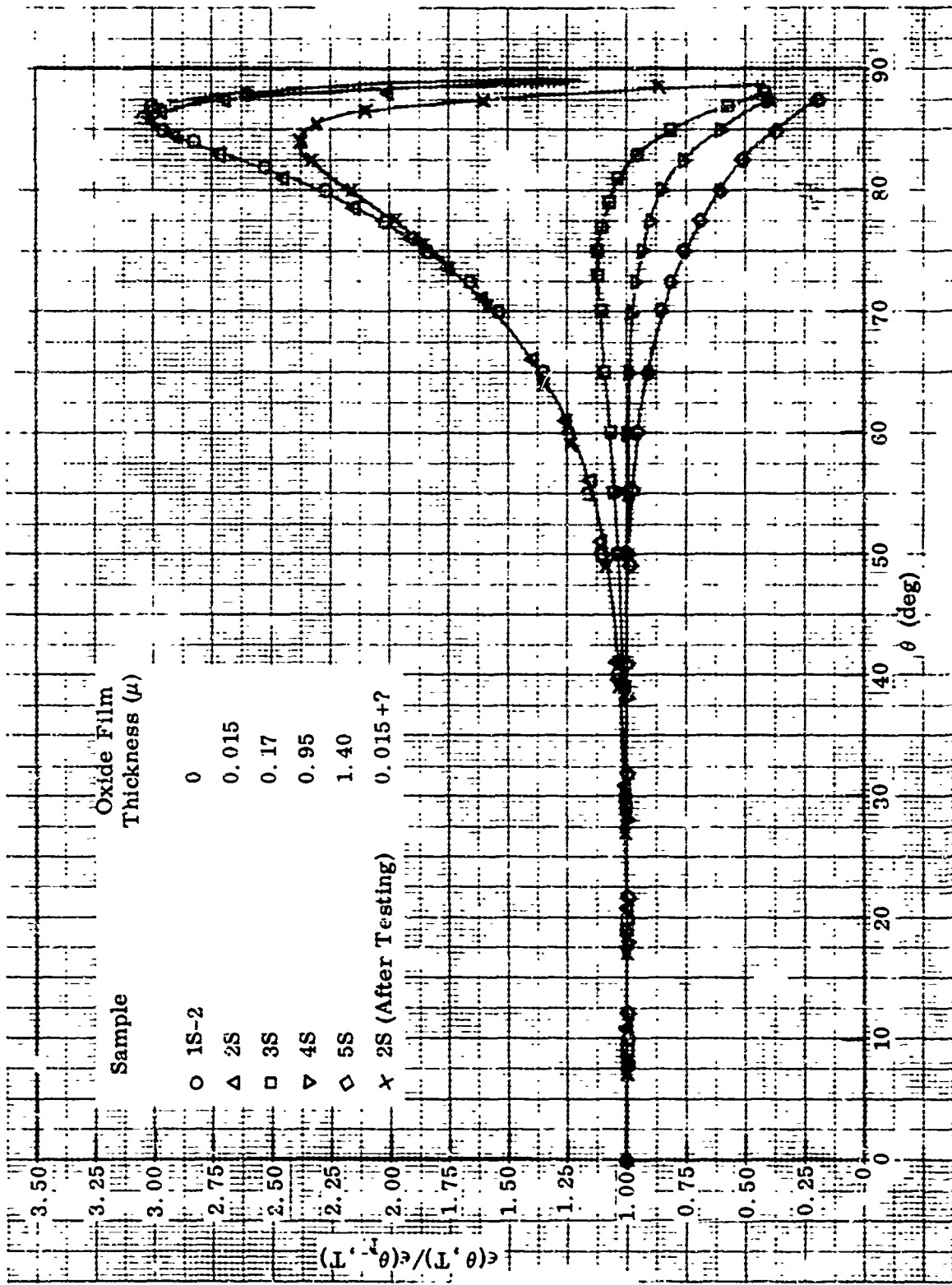
98

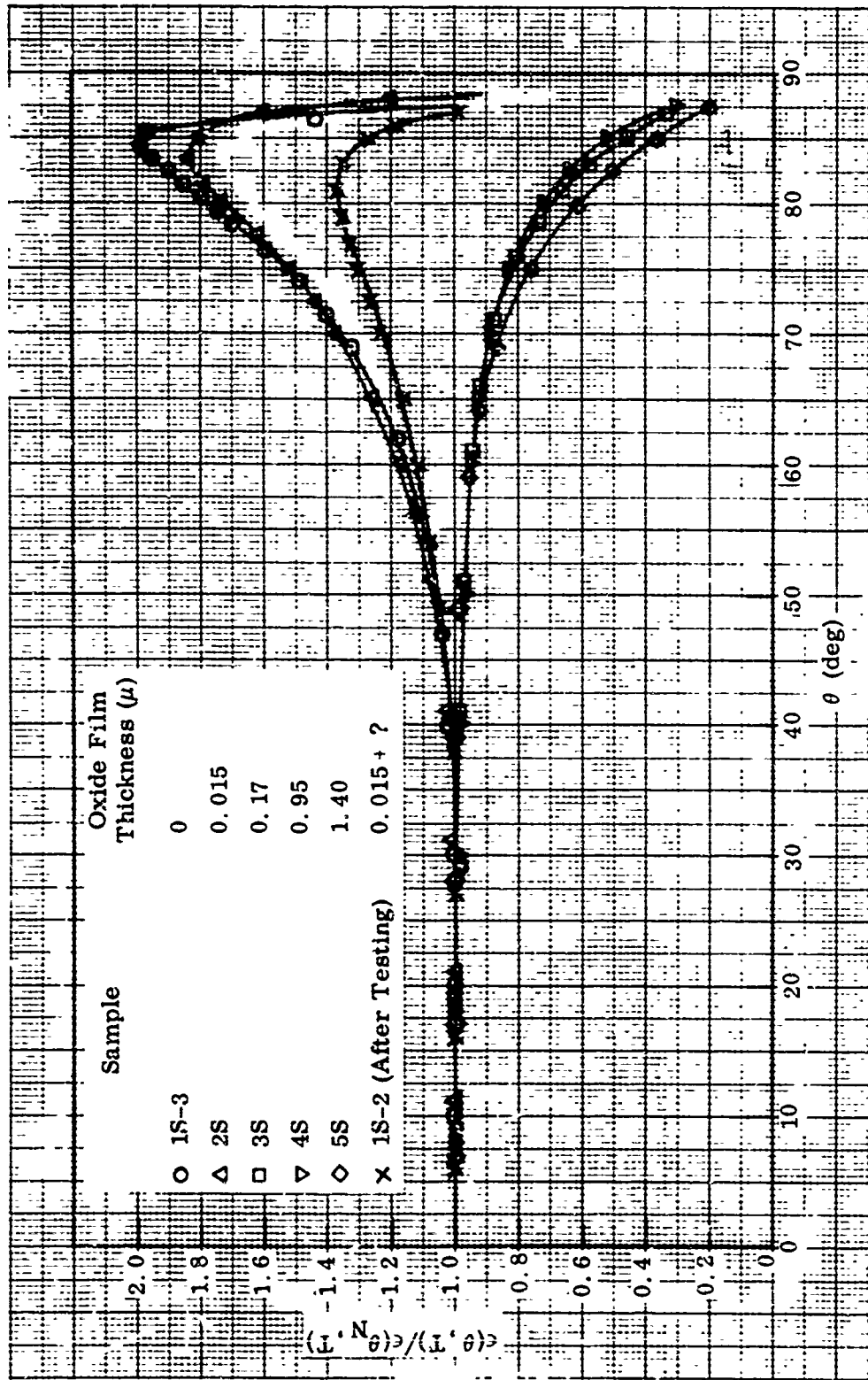Figure 41 Effect of Oxide Thickness on the Relative Total Directional Emittance of 304 Stainless Steel at 525°K

Figure 42   Effect of Oxide Thickness on the Relative Total Directional Emittance of 304 Stainless Steel at 950°K

100

(4) Relative Spectral Directional Emittance

Relative spectral directional emittance data for each of the stainless steel samples are presented in subsections VII. 6 through VII. 14. The data show angular distributions for the parallel and perpendicular components of radiation emitted at wavelengths of 1.5, 2, 3, 4, 6, and 8 μ. The lowest temperature at which data were obtained was 810°K, because of energy limitations. The highest temperature for which reasonably stable emittance data were obtained was 950°K. Even at 950°K the relative spectral directional emittance of the unoxidized and lightly oxidized samples (1S-2, 2S, and 1R) was significantly affected by the surface oxidation that occurred as the measurements were made. The surface of sample 1S-3, which was tested in the hydrogen-purged atmosphere, appeared to remain stable (i. e., unoxidized) throughout the 950°K tests, but then oxidized when measurements were attempted at 1090°K. Because of these problems, only a limited amount of data were obtained to show the effect of temperature on the relative spectral directional emittance characteristics of the surfaces.

On the basis of the data obtained from sample 1S-3 (subsection VII. 14) it is concluded that the relative spectral directional emittance characteristics of smooth, unoxidized stainless steel are essentia. independent of temperature between 810 and 950°K. It is further concluded that the differences in the directional emittance characteristics of samples 1S-2, 2S, and 1R at these two temperatures are due to surface oxidation that occurred at 950°K. Similarly, on the basis of the data obtained from samples 3S, 4S, 5S, 3R, and 5R, it is concluded that the directional emittance characteristics of the oxide films are essentially independent of temperature between 810 and 950°K. The assumption of temperature independence of the directional emittance characteristics of each sample has been used to obtain the 810°K spectral hemispherical-to-normal emittance ratios for most of the samples, since the perpendicular component at this temperature was usually too weak to be measured. This was done by combining the 950°K directional characteristics for the perpendicular polarized component with the 810°K directional emittance data for the parallel polarized component. The ratio of spectral hemispherical-to-normal emittance was computed by integration of these combined properties.

Variations in the spectral directional emittance characteristics of the unoxidized and heavily oxidized stainless steel surfaces with wavelength are shown in Figures 43 and 44, respectively. For the unoxidized stainless steel surface, the variations with wavelength are those expected for a pure metal. A summary of the results indicates that:

- The relative spectral directional emittance of the perpendicular polarized component is essentially independent of wavelength.
- The value of θ_{max} for the parallel polarized component shifts toward larger angles with increasing wavelength, and $\epsilon(\theta)_{max}$ values increase correspondingly.
- Spectral hemispherical-to-normal emittance ratios increase with wavelength.

Figure 44 shows the relative spectral directional emittance characteristics of the heavily oxidized surface of sample 5S. The figure shows the drastic modification
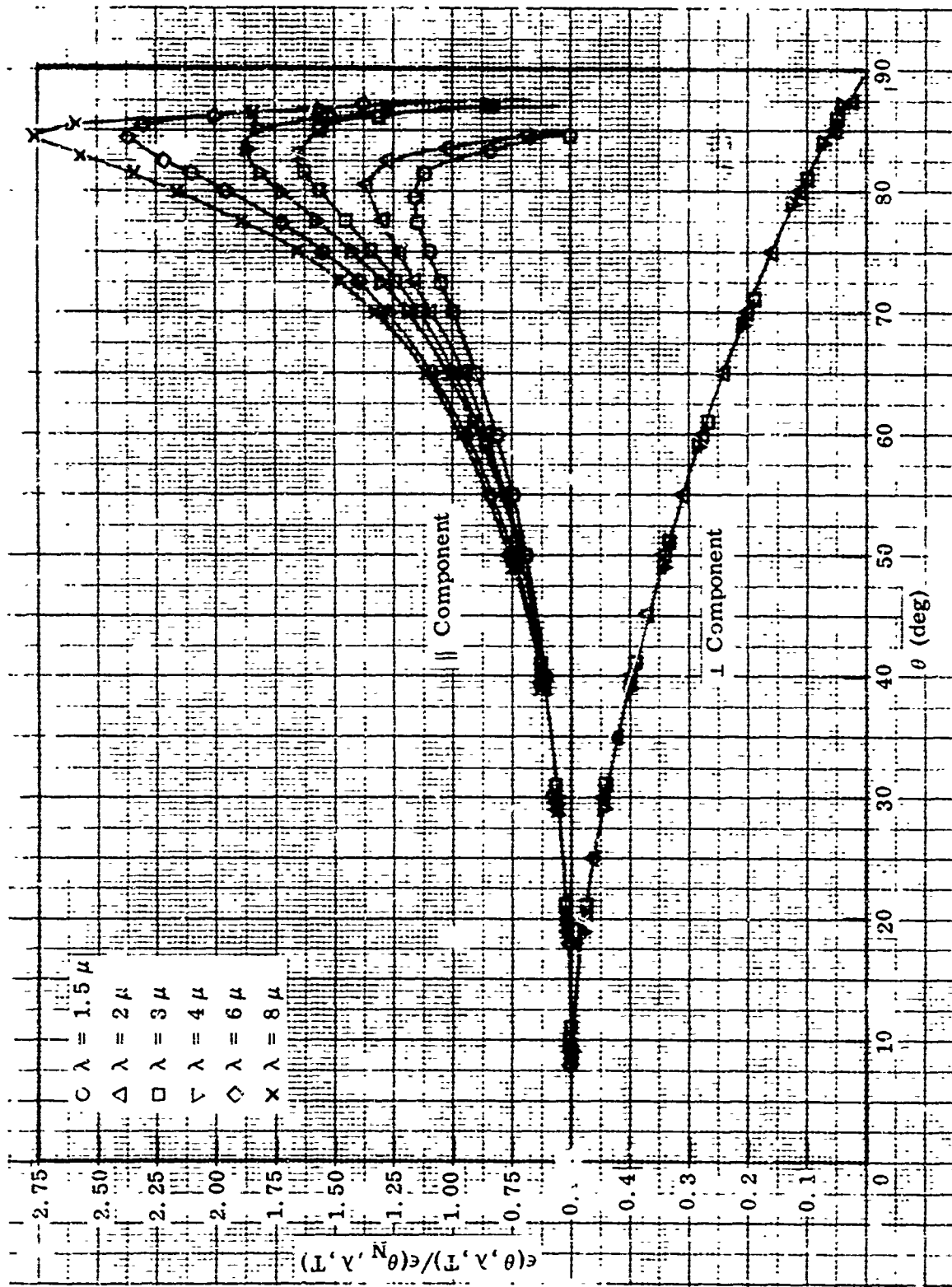
Figure 43 Change in Relative Spectral Directional Emittance of Unoxidized 304 Stainless Steel With Wavelength (Sample 1S-3 at 950°K)
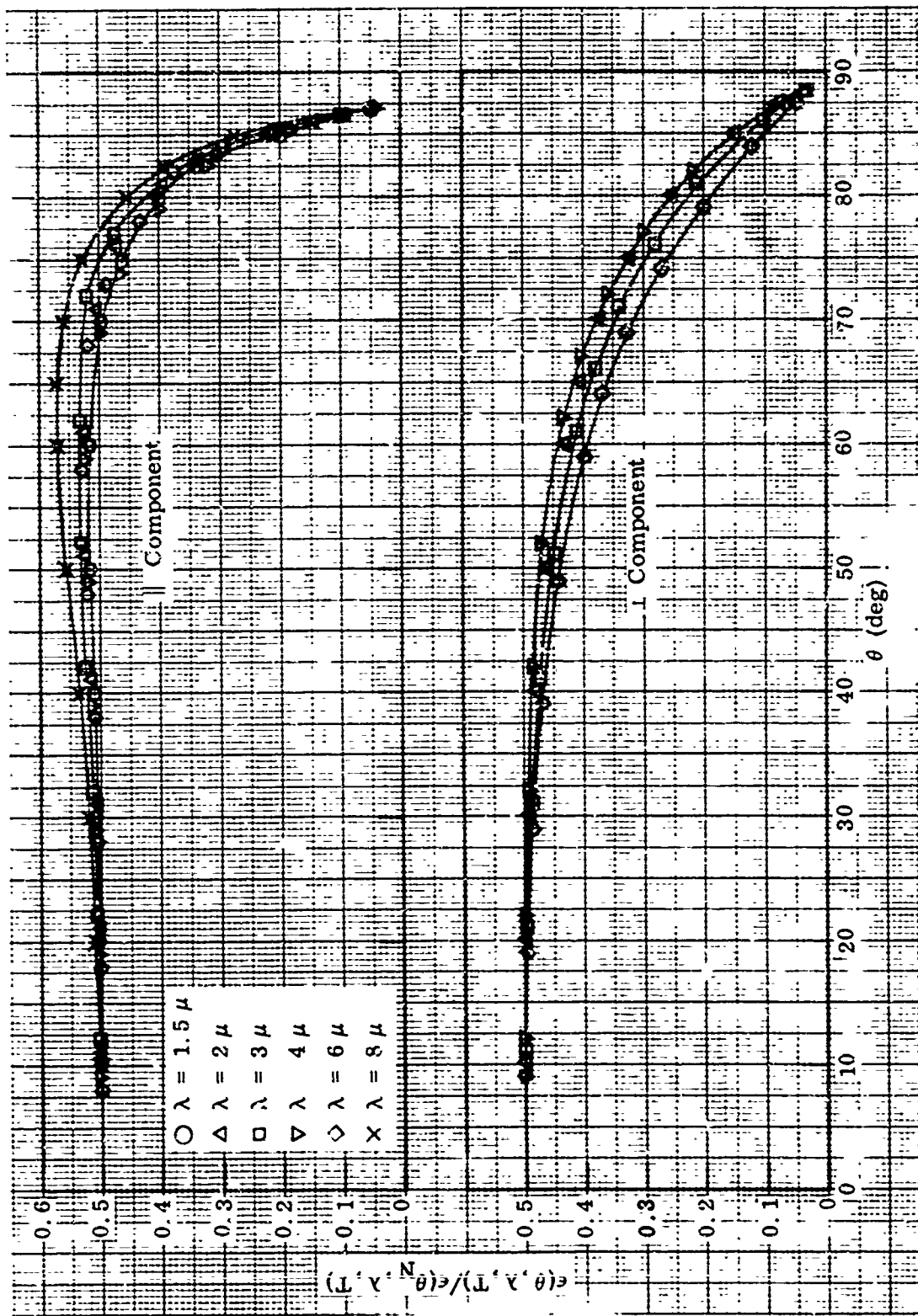
Figure 44   Change in Relative Spectral Directional Emittance of Oxidized 304 Stainless Steel With Wavelength (Sample 5S at 950°K)

103

caused by the oxide layer. The relative directional emittance ratios for the parallel polarized component increase only slightly with wavelength in the region between $\theta = 20$ and $\theta = 85$ deg. Corresponding ratios for the perpendicular component undergo a slight decrease resulting in constancy with wavelength for the sum of the polarized components. These deviations are consistent with the total directional characteristics reported in subsection V. 2. b. (3).

The effect of increasing film thickness on the distribution of energy about the normal is demonstrated in Figures 45, 46, and 47, for wavelengths of 2 and 6 μ. At 2 μ the energy content in the parallel component is drastically reduced by a film of 0. 17 μ thickness. The 0.015 μ film caused very little change in spatial distribution. At 6 μ the effect of increasing film thickness is also to reduce the relative energy in the parallel component, although the change occurs more gradually from sample to sample than at the shorter wavelength. For the perpendicular component, the relative energy at off-normal angles gradually increases at both 2 and 6μ, but the distribution for this component does not become as Lambertian as for the parallel component at comparable wavelengths and temperatures. This trend in directional properties with increasing film thickness is consistent with that predicted from consideration of the optical properties of metals and dielectrics. At short wavelengths it is expected that a film of given thickness will be more opaque than at longer wavelengths. That is, the effect of films having like values of thickness-to-wavelength ratios, (d/λ), will be comparable.

Computations were performed using the Fresnel equations to establish the directional emittance of an opaque film with $n = 1.3$ and $k = 0.4$. The resulting curves for directional distribution of the parallel and perpendicular component compare well with those in Figures 45 and 47 for the 1.40-μ film thickness. These results verify the measurements; however, the comparison was made only to verify the assumption of opacity of the film. The values of n and k used in the computation were selected on the basis of the measured normal emittance of the sample since published data for the optical constants of Fe_3O_4 could not be found.

It should be noted that the difference between the relative directional emittance properties of samples 1S-3 and 2S, on Figure 46, is due to the additional oxidation of sample 2S at the 950°K test temperature. For this reason, the initial film thickness value shown for this sample is questionable and is so designated on the figure. Similar designations are used in Figure 47; however, the effect of the change in film thickness on the relative directional characteristics of the perpendicular polarized component for each sample was quite small.

Figure 45   Effect of Oxide Thickness on the Parallel Polarized Component of Relative Spectral Directional Emittance of Stainless Steel at $\lambda = 2\,\mu$

105

Figure 46 Effect of Oxide Thickness on the Parallel Polarized Component of Relative Spectral Directional Emittance of Stainless Steel at $\lambda = 6\ \mu$

106

$\lambda = 2\,\mu$

Sample	Temp. (°K)	Oxide Film Thickness (μ)
○ 1S-3	950	0
△ 2S	950	0.015
□ 3S	950	0.17
▽ 4S	950	0.95
◇ 5S	950	1.40

$\lambda = 6\,\mu$

Sample	Temp. (°K)	Oxide Film Thickness (μ)
○ 1S-3	1080	0 ~ ?
△ 2S	1080	0.015+ ?
□ 3S	1080	0.17 - ?
▽ 4S	950	0.95
◇ 5S	950	1.40

$\epsilon(\theta,\lambda,T)/\epsilon(S_N,\lambda,T)$
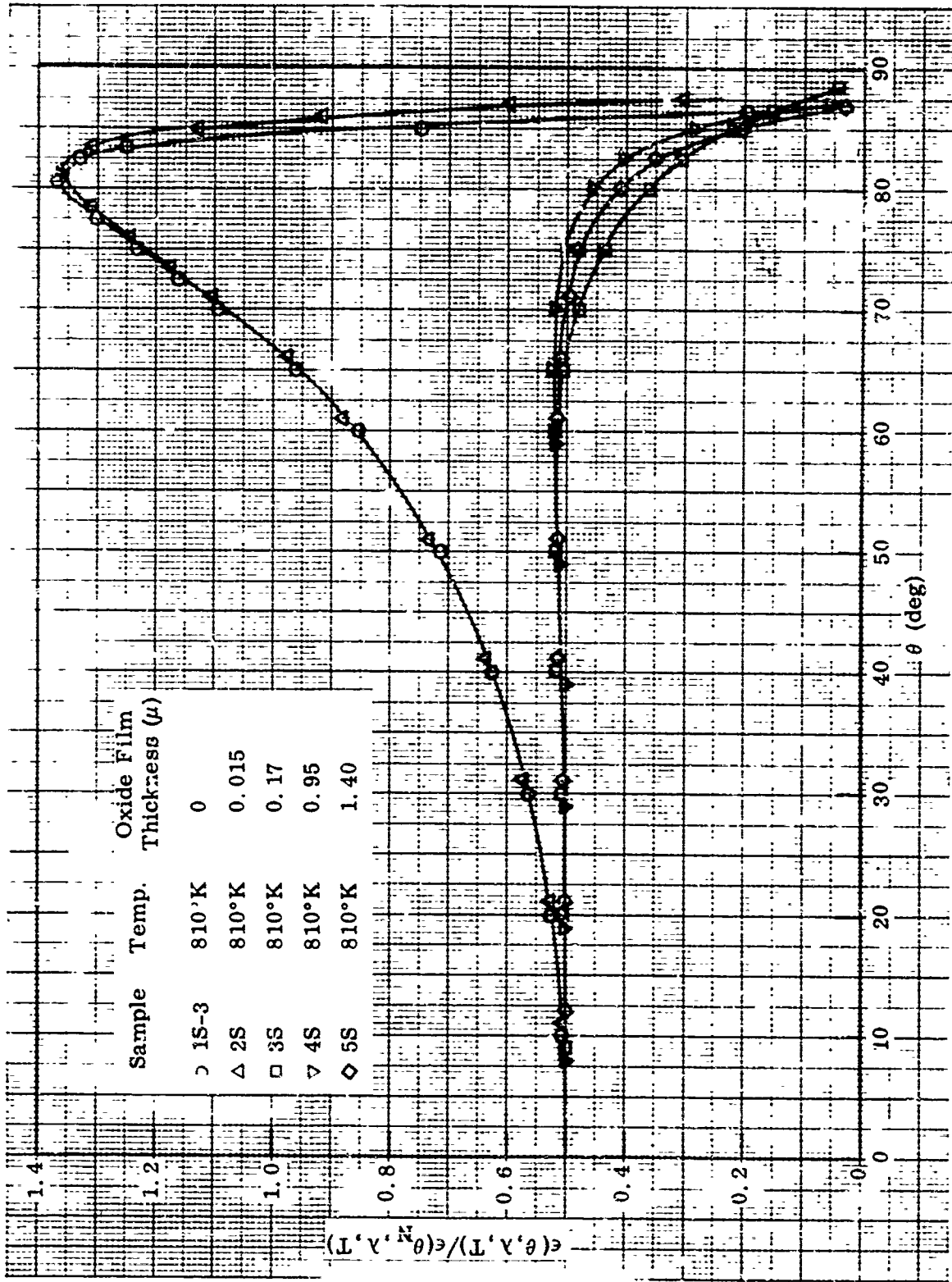
θ (deg)

Figure 47 Effect of Oxide Thickness on the Perpendicular Polarized Component of Relative Spectral Directional Emittance of Stainless Steel at $\lambda = 2\,\mu$ and $\lambda = 6\,\mu$
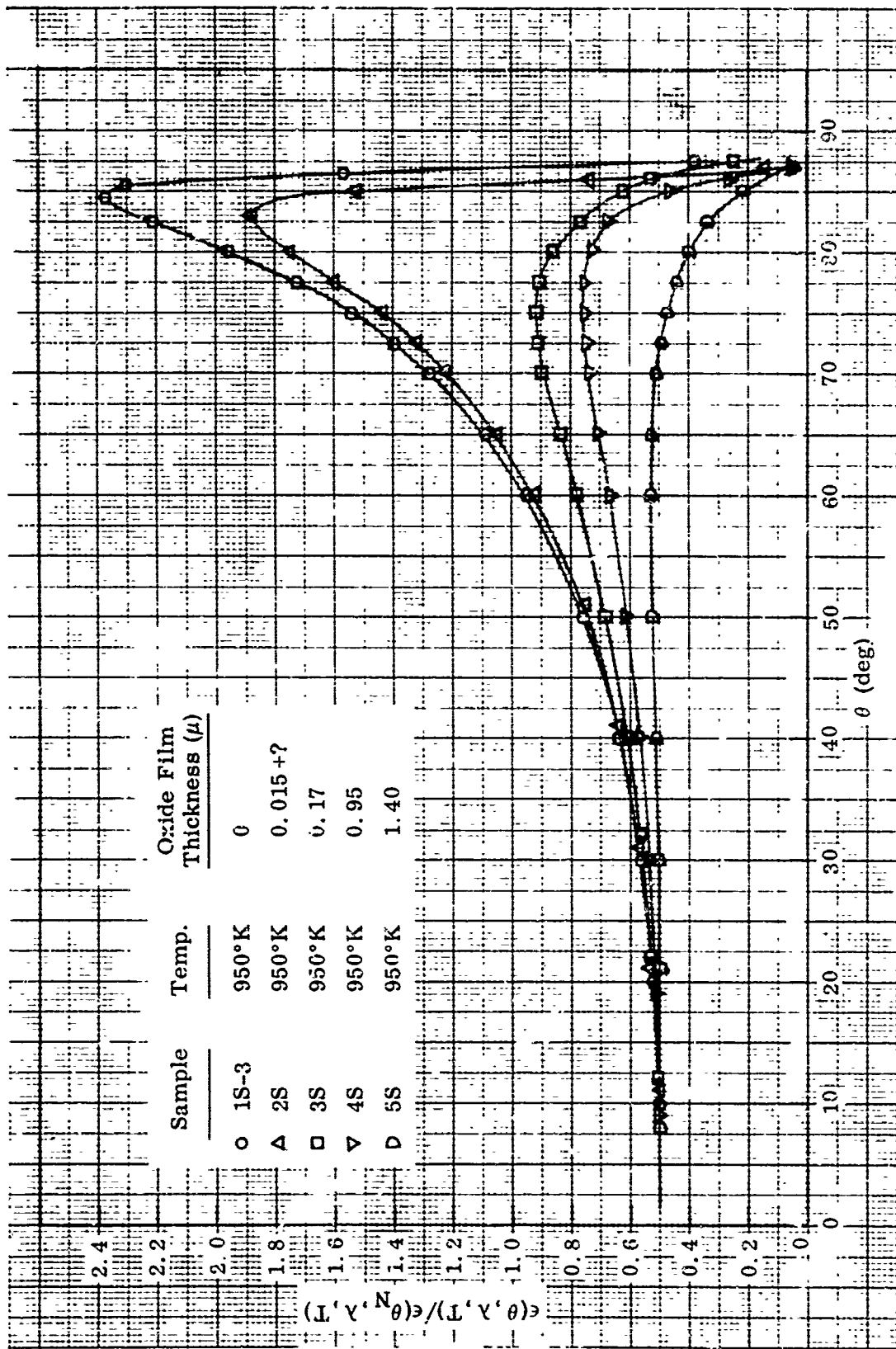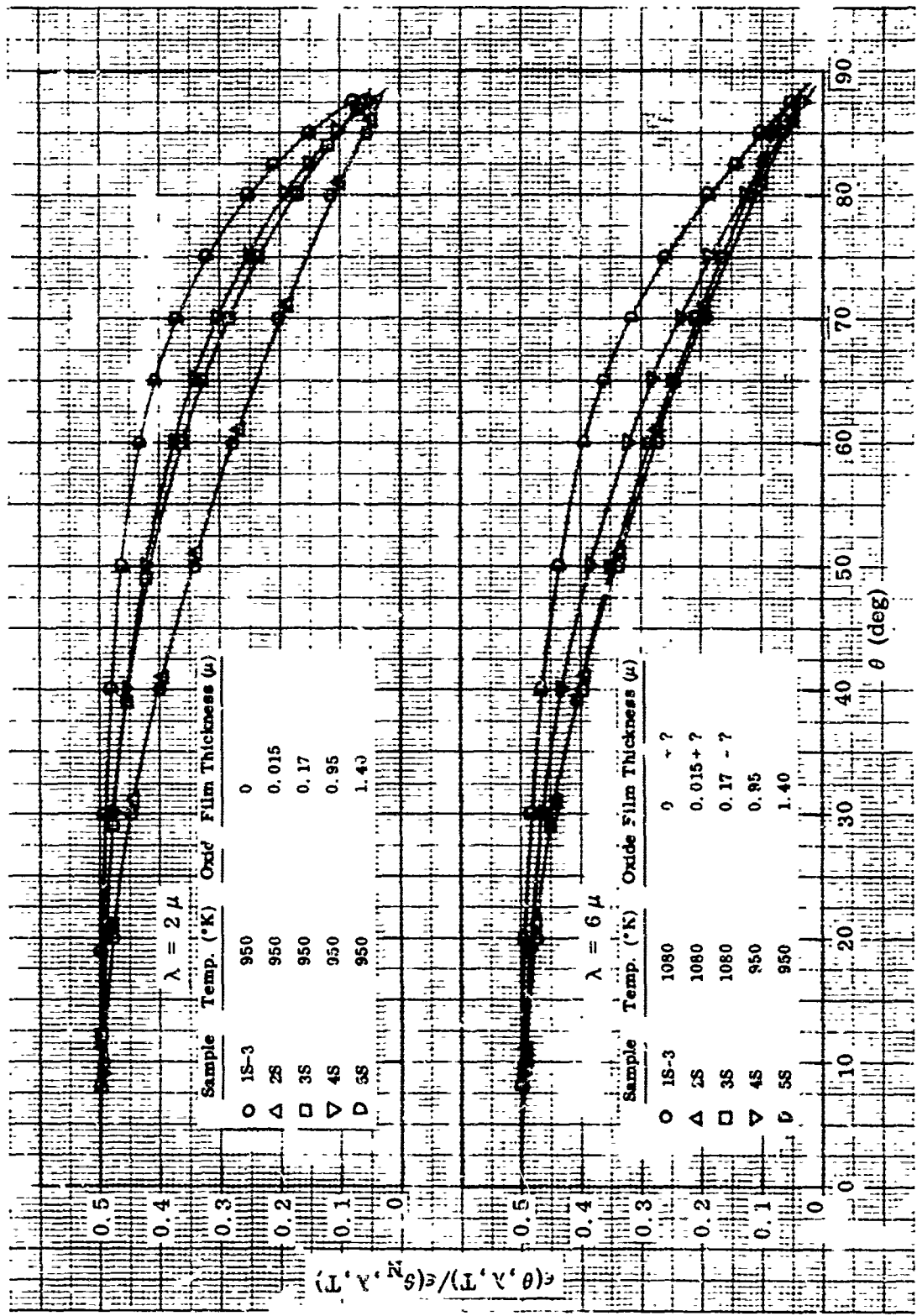
Section VI
SUMMARY

The analytical and experimental work completed during this program had as its primary objective a clarification of the effects of surface condition on the emittance of metallic surfaces. This objective was accomplished with varying degrees of success.

The effect of surface roughness on emittance was clarified to a large extent by the data obtained on the carefully prepared platinum samples. The stability of these samples proved to be a considerable asset to the program. Such was not the case with the oxidized stainless steel samples which tended to continuously oxidize during the emittance measurements and resulted in doubt that the sample examinations were truly indicative of the surface conditions existent during the test. Furthermore, the difficulties experience in obtaining meaningful data on film thickness for the oxidized specimens resulted in a less than adequate specification of surface condition for the majority of these samples. However, the results obtained from both sets of samples are sufficient to demonstrate that the effects of oxide films are far more of an influence on emittance than are the effects of surface roughness.

Previously published works on the total and spectral reflectance of roughened room temperature samples, and on the bidirectional reflectance of similar samples have shown significant decreases in reflectance for only slight increases in roughness. Such results infer that the emittance of these surfaces would be similarly increased. However, the results obtained on the platinum samples used in this program demonstrate conclusively that roughness alone, for σ_m up to $2.4\,\mu$, will not cause large increases in spectral or total emittance. For roughness in this range, the increase in emittance over that of the smooth sample was on the order of 10%. This small increase can often be neglected for the purpose of heat transfer computations. However, these computations should not neglect the more significant influences of wavelength and temperature on the spectral and total emittance. The simple relations presented in Section II provide working formulae that account for these stronger influences.

While slight surface roughness has a limited influence on the hemispherical and normal emittance, its effect on the distribution and polarization of energy about the normal is considerable. The maximum parallel component of emittance is reduced considerably as roughness is increased. This change is accompanied by an increase of energy in the perpendicular component at less grazing angles of incidence. While this redistribution of polarized energy is readily discernible, its influence on the ratio of hemispherical-to-normal emittance is relatively minor. The overall effect is to shift energy toward the normal and increase the ratio by approximately 7%. The fact that an increase of hemispherical-to-normal emittance occurs is easily explained by

consideration of the geometry involved. For a slightly rough surface, the tilted planes are, on the average, at a greater angle to the off normal viewer then for the smooth surface. Therefore, as the viewing angle is increased to large values, a portion of the viewed surface lies at grazing incidence where the maximum emittance occurs. Other effects including depolarization and multiple reflections are also present; however, it is reasonable to presume that the overall effect will be an increase in the hemispherical-to-normal emittance ratio for the gently sloped surfaces examined during this study.

The correlation between σ_m/λ and the maximum of the parallel component of emittance was the only correlation found between surface roughness and emittance. This is not surprising in view of the complex nature of the emission phenomena. Considerably more theoretical work must be accomplished to establish the guidelines required for even semi-empirical predictions of emittance for roughened surfaces. The results of such work would be of considerable assistance in correlating the significant amount of data presented herein. The major parameters used to describe the reflectance distribution of a roughened surface (i.e., σ_m/λ, slope, θ) are equally important for describing the emittance distribution. However, the functional dependence of emittance is more complex due to other effects. This dependence was not clarified during the present study since attempts to correlate the experimental results using the parameters established in directional reflectance theory were generally unsuccessful.

It is well known that thin dielectric films on metallic substrates cause considerable alteration of the emittance characteristics. The changes in spectral and total emittance will depend upon the optical properties of the oxide and substrate, the film thickness, uniformity, and scattering when the oxide creates this latter effect. Theoretical treatments of thin, uniform, films have established relationships that are adequate for prescription of radiative behavior when the required optical constant data are available for the temperature and wavelengths of interest. Unfortunately, the films created by oxidation of a free metal surface grow preferentially and result in nonuniform, nonhomogeneous, irregular oxide layers. Under these conditions, the analytical treatments serve only as a guide for prediction of trends. Satisfactory predictions of the radiative behavior of complex films appear feasible only through a statistical treatment wherein point by point variations in film properties are accounted for. The characterization techniques required for such a specification are generally available and were utilized during the program; however, the effort involved in completely characterizing a single randomly oxidized surface would be so extensive that it is doubtful that the results obtained would justify the expense.

It was found during this study that even a direct measure of film thickness is not straightforward. Cross-sectioned metallographic mounts, replication techniques, and weight gain measurements were all employed and yielded different results. For thin films (i.e., less than 0.25 μ) on the stainless steel, the replication techniques failed to give satisfactory samples for electron microscope examination. In this range, the simple method of visual color examination was as reliable as any of the more highly refined procedures. As film thickness increased, weight gain data provided predictions of film thickness that were judged to be as realistic as those obtained from metallographic inspection procedures. These findings indicate that considerable work

109

must yet be done to refine the techniques used for film thickness determinations. Equally difficult problems exist for determination of the chemical composition and physical state of the films.

The results obtained for 304 stainless steel showed that films as thin as 0.2 μ increase the spectral emittance at 1.5 μ from 0.27 to 0.96. At longer wavelengths this film is less important and results in only a slight increase. Thicker films increase the entire emission spectrum since effects of the substrate are masked and the surface properties are those of a dielectric. For the stainless steel this occurred for films having thicknesses on the order of 1.4 μ. Other oxidized metal surfaces are likely to have entirely different characteristics based upon their optical properties and film morphology.

In view of the many parameters influencing the emittance of a randomly oxidized surface, and the difficulty in obtaining detailed descriptions of these parameters, direct measurement of radiative properties remains as the only practical approach to specification of their thermal radiation characteristics.

Section VII

EXPERIMENTAL DATA

Because of the bulk of material, and for ease of use by other investigators, all the experimental data obtained in this program are presented separately in this section. Data for each of the 14 samples — the 5 platinum samples and the 9 stainless steel samples — are presented in individual subsections. Each subsection identifies the sample and presents a summary of the following information:

- Sample preparation method
- Surface roughness or oxide film characteristics, before and after the emittance tests
- Test procedure and thermal history
- Index to emittance data tables and figures
- Supplementary information regarding sample emittance stability, changes in sample characteristics during the emittance tests, and results of diffraction and spectrographic analyses

The absolute emittance data (i.e., total hemispherical, total normal, and spectral normal emittance values) are presented in tabular form, in the order in which they were obtained, and the time duration at each temperature is listed. The relative total and relative spectral directional emittance data are presented in graphic form. Relative total directional emittance ratios were obtained by normalizing directional signal ratios to a value of 1 at $\theta = 0$ deg. To obtain the absolute total directional emittance, the relative directional emittance ratio must be multiplied by the appropriate total normal emittance that is tabulated for the corresponding temperature and time. The relative spectral directional emittance ratios are presented for each polarized component of emitted radiation, and were obtained by normalizing directional signal ratios for each component to a value of 0.5 at $\theta = 0$ deg. To obtain the absolute spectral directional emittance, the relative directional emittance ratio of each polarized component must be added and multiplied by the appropriate absolute spectral normal emittance value at the corresponding wavelength, temperature, and time.

All relative directional emittance measurements were made with the aperture slit of the apparatus filled by the sample image out to viewing angles of ±88 deg from the normal. Measurements were actually made out to 90 deg on either side of normal in order to detect possible misalignment of the sample due to thermal warpage. For all but a few of the highest temperature test runs, sample warpage was not a serious problem and symmetry of directional data was obtained about the normal. In cases where sample warpage did occur, the sample edge was imaged at different viewing angles for each direction of rotation. In these cases, the relative emittance ratios at the

111

smaller viewing angles (0 to 70 deg) on either side of normal were matched to obtain a corrected zero setting, and the emittance ratios for the side viewed out to the largest off-normal angles were plotted. In no case did the correction exceed ±1.5 deg from the nominal zero setting of the sample angle-indication meter. The correction procedures used for warped samples and the calibrated accuracy of the angular measurement device provided an overall angular measurement accuracy of ±0.5 deg.

For the stainless steel samples, the data obtained at the highest test temperature are generally significantly different from those obtained at the lower temperatures. This is true for all but the most heavily oxidized samples (5S and 5R). These differences are primarily the result of surface instability during the measurements (oxidation, except for sample 3S), rather than actual temperature effects on the emittance properties of the surface. The data are included to illustrate the changes that can be expected during measurements of the type reported.

1. PLATINUM SAMPLE NO. 1D

Preparation: None; tested as received.

RMS Roughness: Before emittance tests: 4.3 μin. $\perp$ to rolling direction; <0.5 μin. $\parallel$ to rolling direction. After emittance tests: 8 μin.; variable centerline (see subsection V.1.a); large displacements of grain surface levels.

Test Procedure: Before testing, the sample was annealed at 1365°K for 6 hr in vacuum. Absolute normal, hemispherical, and relative directional emittance data were then obtained at 1370, 1226, 1093, and 863°K (first temperature cycle). Absolute and relative directional emittance data were next obtained at 1644°K (second temperature cycle), and several additional tests were made to correct the total normal emittance measurement procedure. Absolute emittance values were then remeasured at all test temperatures to check the stability of the sample. Test chamber pressures were maintained between 2 and 10 $\times$ 10^{-6} Torr throughout all tests.

Emittance Data. Absolute emittance values are shown in Table XIV; relative total directional emittance data in Figure 48; relative spectral directional emittance data at λ = 1.5, 2, 3, 4, 6, and 8 μ in Figures 49 through 54.

Remarks: After the 6-hr anneal at 1365°K, the emittance of the sample appeared to be stable. Total normal emittance values for the first five test temperatures, however, were erratic and inconsistent; therefore, several tests to check the measuring apparatus were made after the 1644°K tests. (See discussion of results in subsection V.1.b.) The trouble was eventually traced to nonuniform irradiation of the total detector element due to too narrow a setting of the aperture slit-width. To correct the problem, the aperture slit-width was reopened to 0.015 in. and a 1/4-in. horizontal aperture plate was attached to the front of the vertical aperture slit. This arrangement was used for the emittance determination during the third temperature cycle and for all the total emittance determinations for the remaining platinum and stainless steel samples.

Photomicrographs of the sample surface before and after the emittance tests are shown in Figure 13. Surface interference micrographs and a taper-section photomicrograph of the sample are shown in Figures 16 and 17, respectively. Changes in the surface characteristics as a result of the high-temperature emittance tests are discussed in subsection V.1. Most of the observed changes are believed to have occurred during the pretest anneal treatment.

An x-ray diffraction pattern of the sample, taken after the emittance tests, was identical to the pattern for the as-received platinum. Both patterns indicated a strong preferred orientation of the surface lattice structure which was unaffected by the high-temperature test. Diffraction data are presented in Table V.

No evidence of sample impurities or surface contamination was detected by the spectrographic analysis made after the emittance tests.

113

Table XIV. Absolute Emittance Data for Platinum Sample No. 1B

Temperature (°K)	Time at Temp. (hr, min)	ε(T)	ε(θ_N, T)	ε(θ_N, λ, T)									
				0.65 μ (a)	1 μ	1.5 μ	2 μ	3 μ	4 μ	6 μ	8 μ	10 μ	12 μ
1365	6,0	Sample annealed in vacuum											
First Temperature Cycle													
1370[b]	6,30	0.168	(c)	0.30	0.177	0.173	0.144	0.129	0.110	0.093	0.080	0.071	0.066
1226[b]	4,30	0.151	(c)	0.31	—	0.163	0.136	0.124	0.105	0.087	0.076	0.070	0.063
1093[b]	2,15	0.135	(c)	0.31	—	0.166	0.136	0.120	0.100	0.083	0.071	0.064	—
863[b]	3,30	0.106	(c)	—	—	—	0.130	0.107	0.087	0.071	0.062	0.058	—
Second Temperature Cycle													
1644[b]	10,15	0.191	(c)	0.30	0.244	0.197	0.165	0.140	0.116	0.098	0.086	0.076	0.055
Third Temperature Cycle													
871	1,30	0.112	0.100	—	—	—	0.115	0.105	0.085	0.068	0.057	0.050	—
1089	0,45	0.132	0.123	—	—	0.165	0.135	0.119	0.097	0.080	0.070	0.062	—
1225	1,0	0.153	0.140	0.32	—	0.164	0.136	0.122	0.101	0.082	0.072	0.059	0.059
1336	0,45	0.168	0.153	—	—	0.179	0.146	0.130	0.108	0.092	0.072	0.068	0.052
1664	0,30	0.191	0.171										

(a) Determined from optical pyrometer readings.
(b) Directional emittance; data obtained at these temperatures.
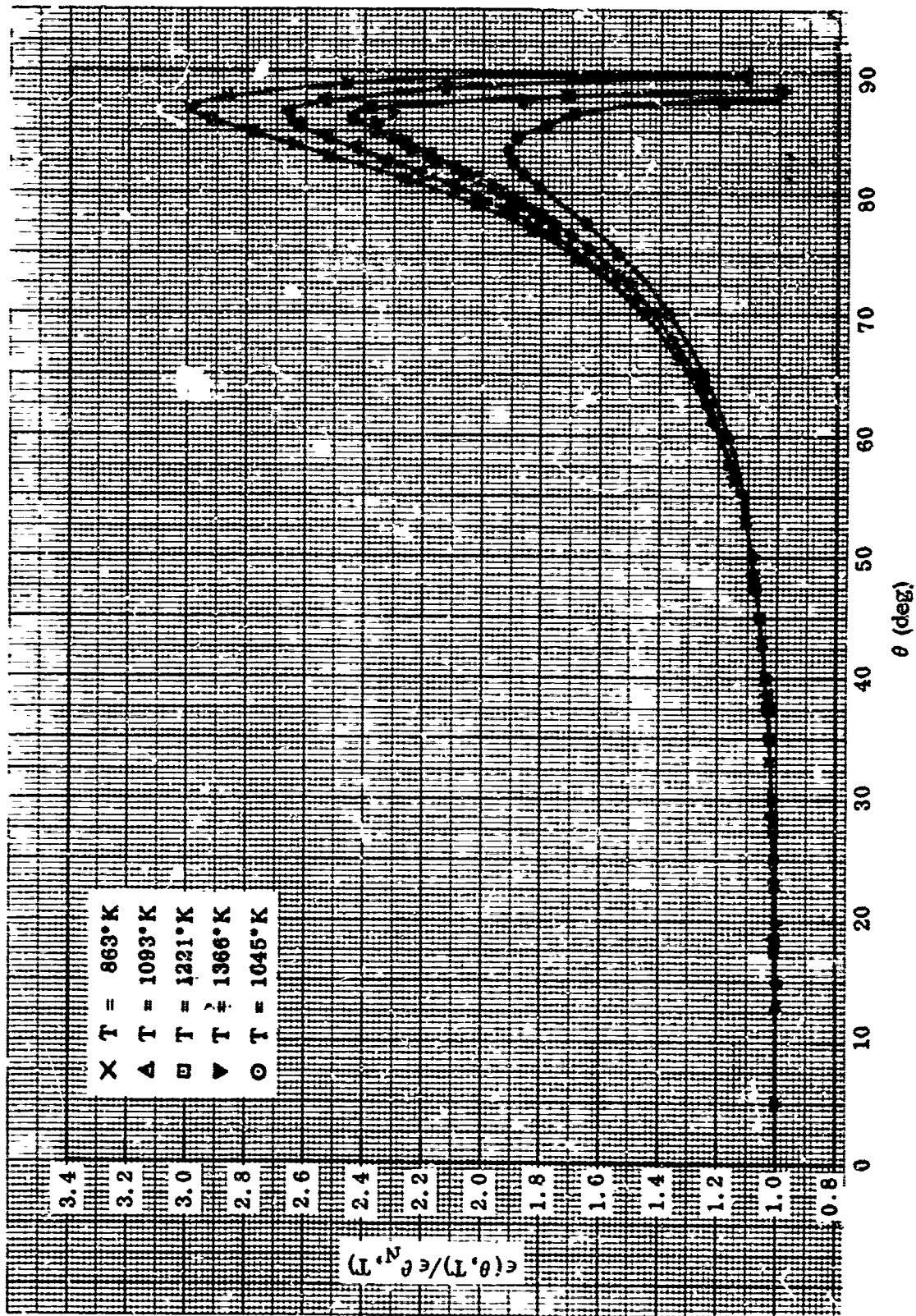(c) Erroneous data; see Remarks.

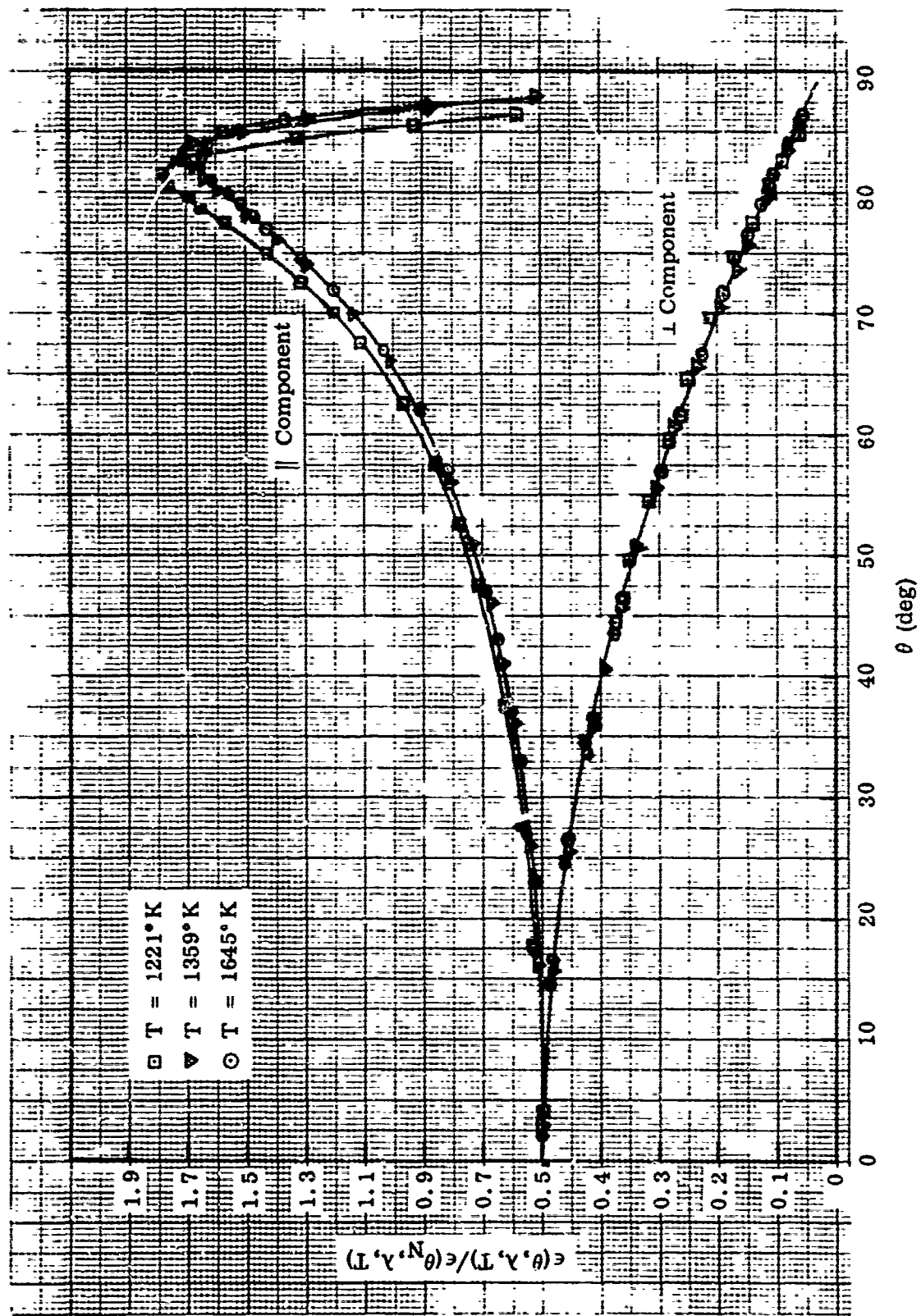Figure 48 Relative Total Directional Emittance, Platinum Sample No. 1B

115

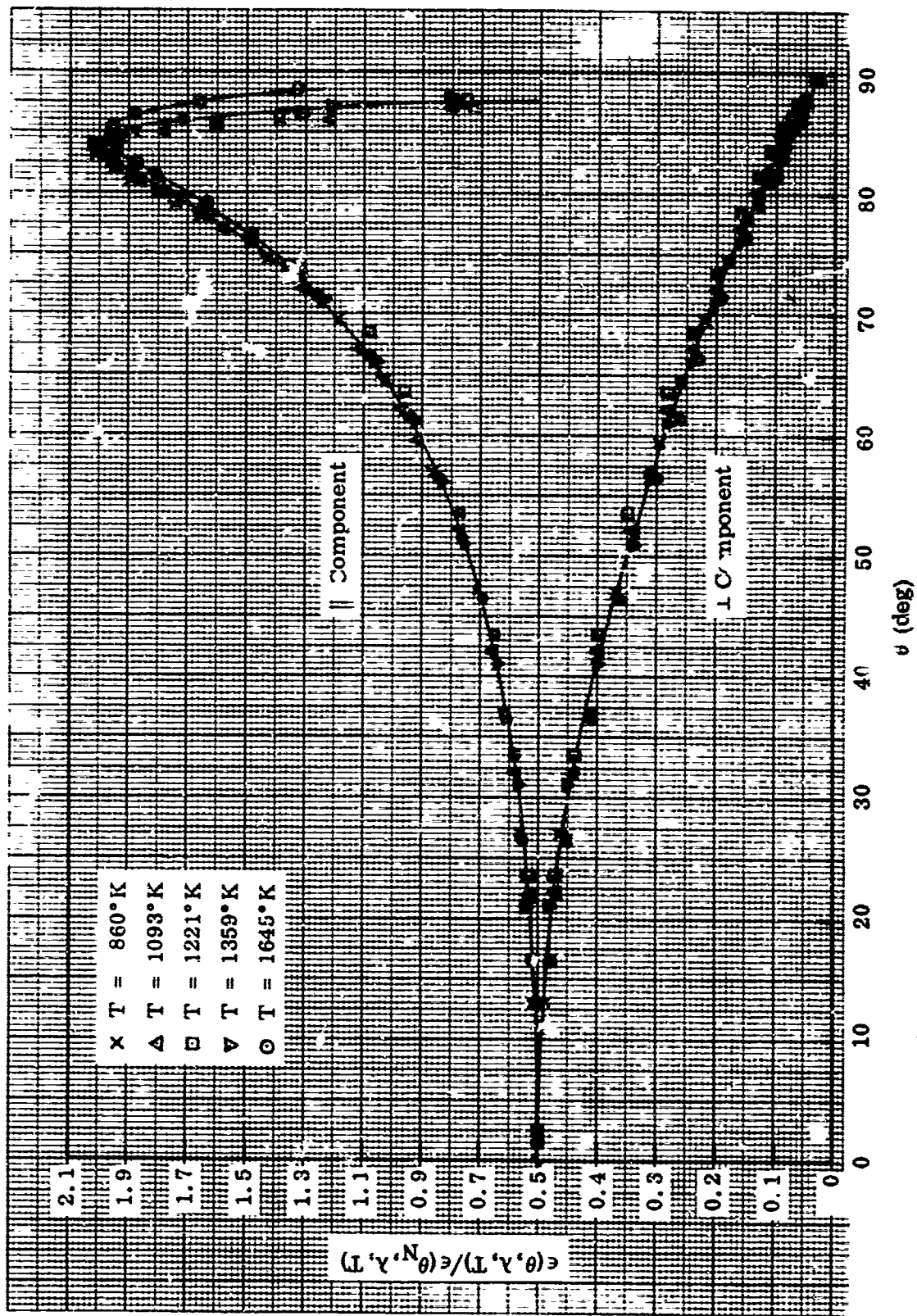Figure 49 Relative Spectral Directional Emittance at $\lambda = 1.5\ \mu$, Platinum Sample No. 1B

116

Figure 50 Relative Spectral Directional Emittance at $\lambda = 2\,\mu$, Platinum Sample No. 1B
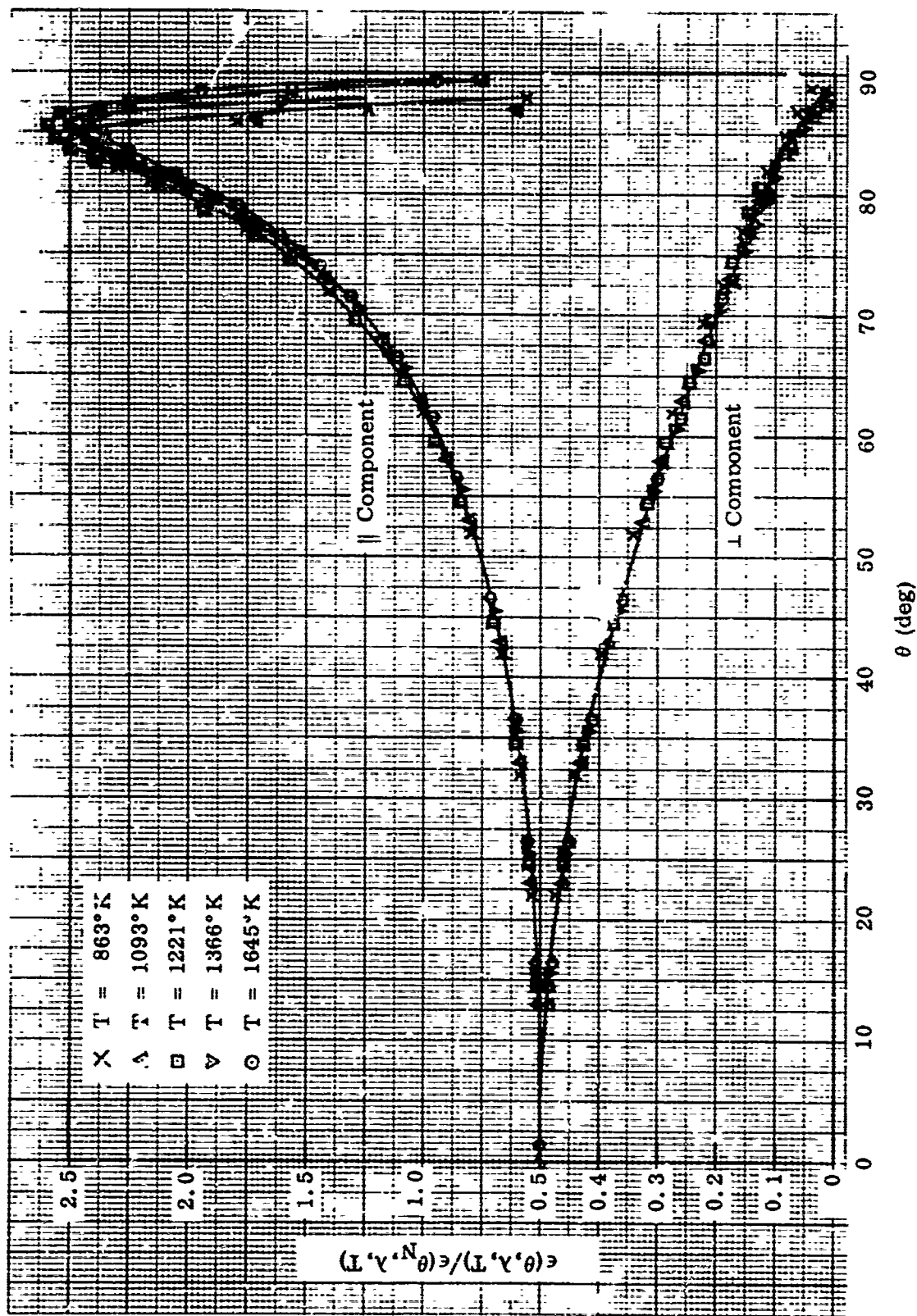
117

Figure 51 Relative Spectral Directional Emittance at $\lambda = 3\,\mu$, Platinum Sample No. 1B
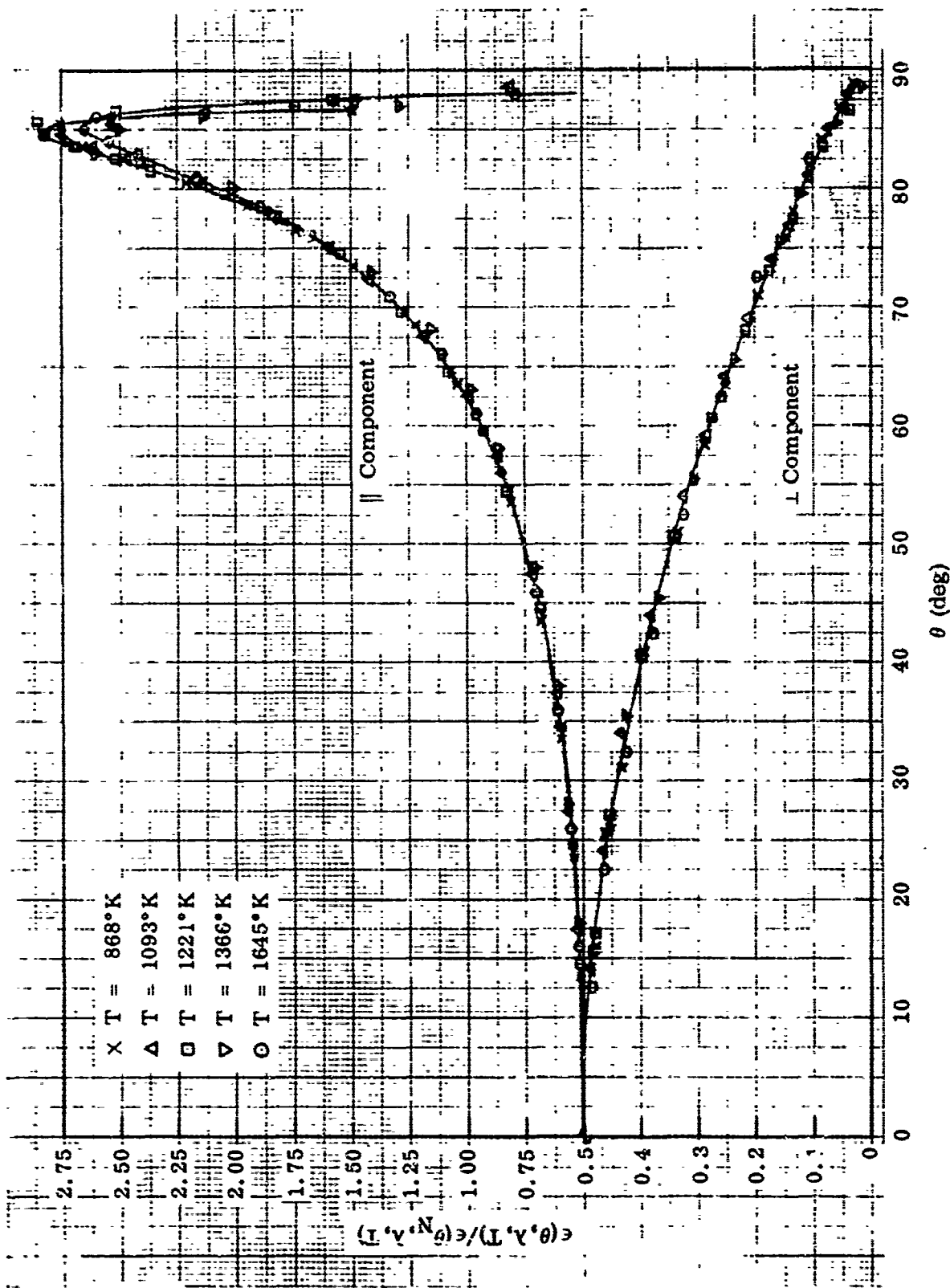
118

Figure 52 Relative Spectral Directional Emittance at λ = 4 μ, Platinum Sample No. 1B
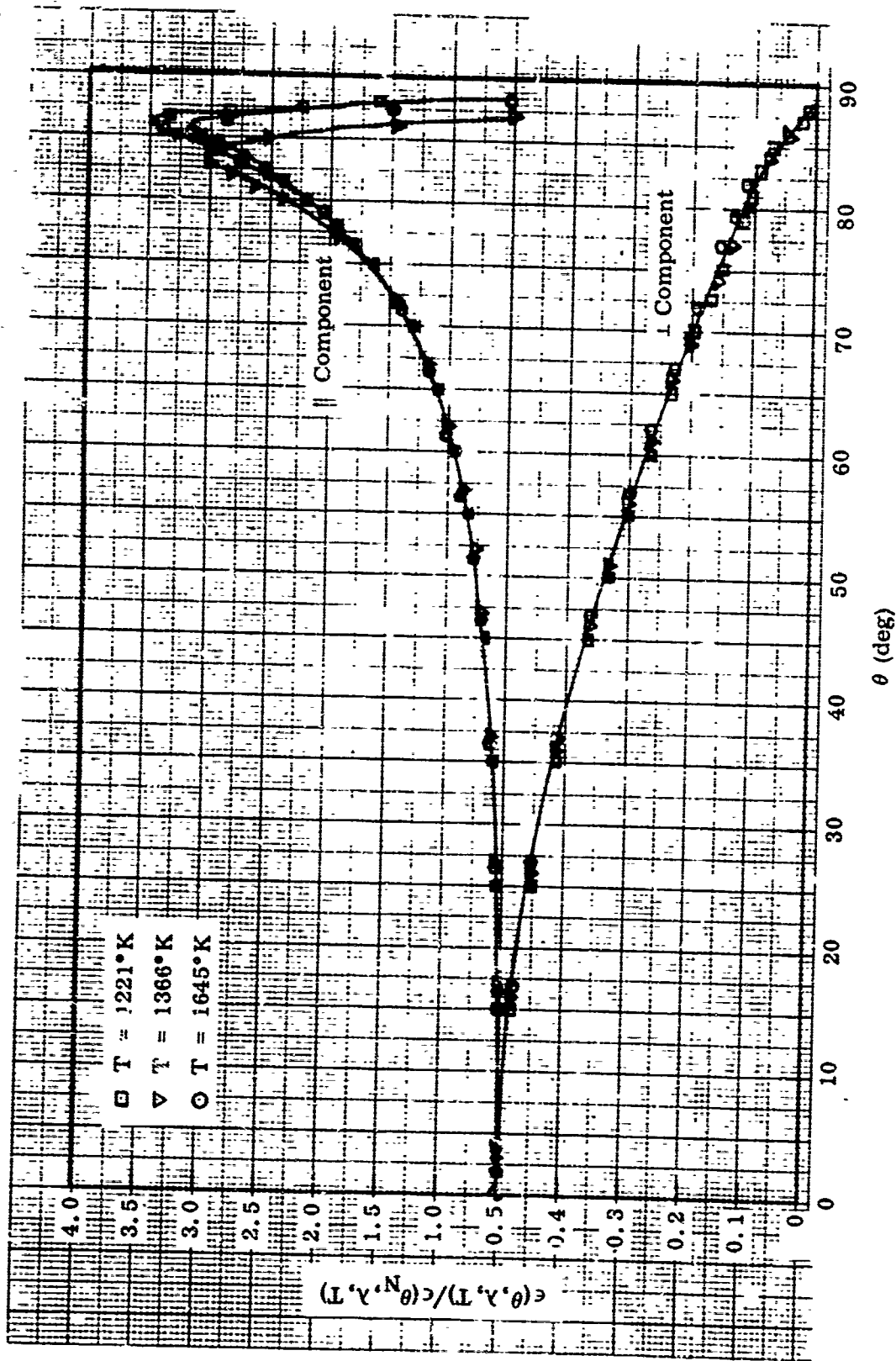
119

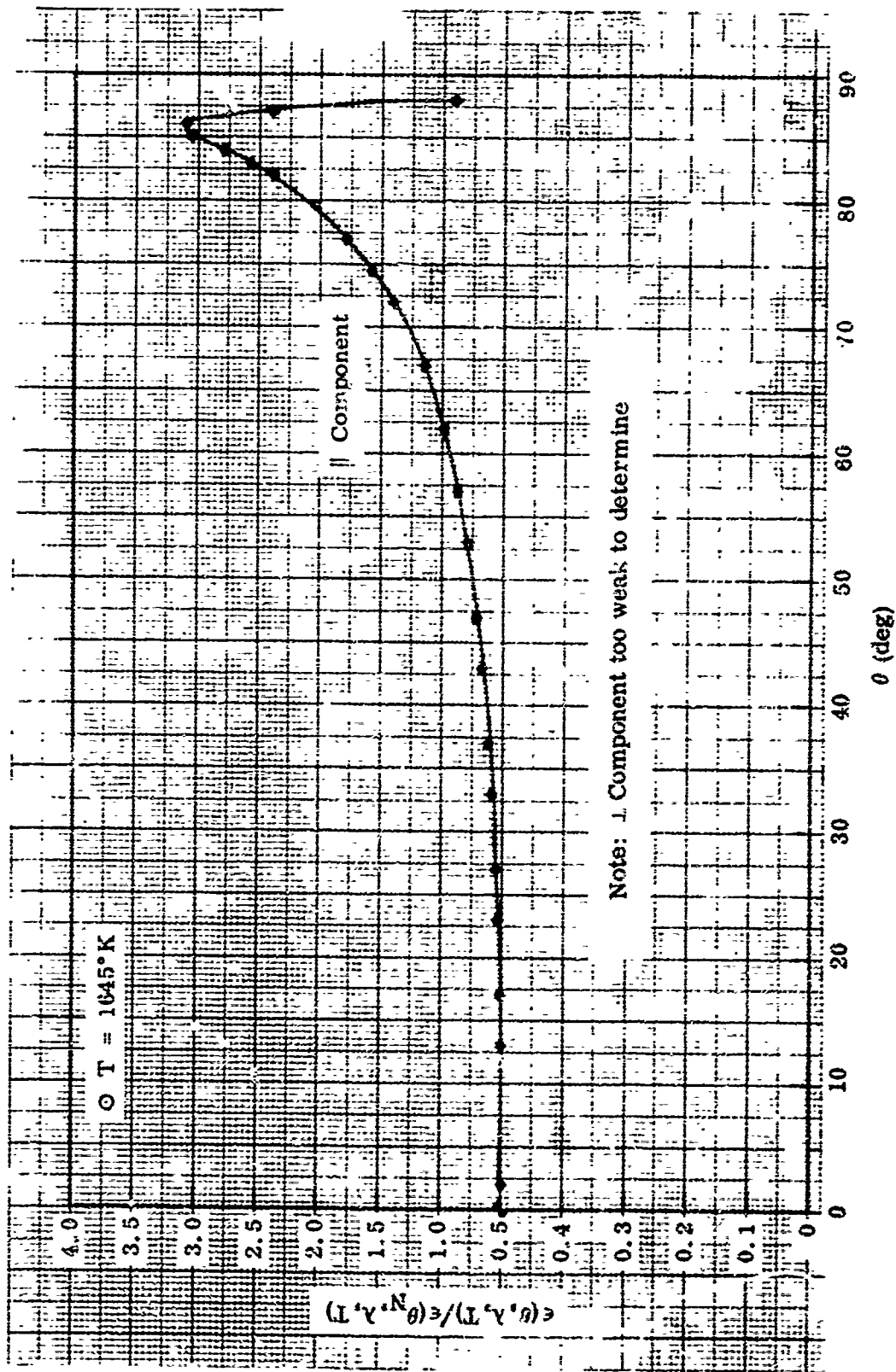Figure 53 Relative Spectral Directional Emittance at $\lambda = 6\ \mu$, Platinum Sample No. 1B

120

Figure 54 Relative Spectral Directional Emittance at $\lambda = 8\,\mu$, Platinum Sample No. 1B

121

2. PLATINUM SAMPLE NO. 3B

Preparation: Lightly shot blasted with size XL "Glas-Shot", pressure, 10 psi; distance, 12 in., normal to surface.

RMS Roughness: Before emittance tests, 28 μin.; after, 27 μin.

Test Procedure: Before testing, the sample was annealed at 1640°K for 15 min in vacuum. Absolute emittance values were then determined at 867, 1088, 1231, 1367, and 1642°K, and relative directional emittance data were obtained at 1642°K (first temperature cycle). Absolute emittance values were redetermined at all temperatures to check the stability of the sample, and the relative directional emittance data at 864, 1093, and 1360°K were obtained (second temperature cycle). The test chamber pressure was maintained between 5 and 10 x 10^{-6} Torr throughout all tests.

Emittance Data: Absolute emittance values are snown in Table XV; relative total directional emittance data in Figure 55; relative spectral directional emittance data at $\lambda = 1.5$, 2, 3, 4, 6, and 8 μ in Figures 56 through 61.

Remarks: During the 1642°K directional emittance tests, the sample was discovered to have a slight twist which noticeably affected the directional emittance data. (See data for $\lambda = 1.5 \mu$ in Figure 56.) The twist was removed by increasing the tension on the sample, and the directional emittance data were remeasured at all wavelengths except 1.5 μ. A post-test examination showed that the sample had stretched slightly at the center, presumably when the tension was increased.

Total hemispherical emittance values during the second test temperature cycle were redetermined using the stretched-sample dimensions but were still found to be about 6% lower than the values obtained during the first temperature cycle. A similar drop in the total and spectral normal emittance values was noted. The latter determinations are independent of the change in sample size; therefore, the lower absolute emittance values are due to either a real change in the sample emittance characteristics or to a systematic error during the second test temperature cycle. The second explanation is believed to be the most likely, since no significant change in the rms roughness of the sample was indicated by the post-test examinations.

Photomicrographs of the sample surface before and after the emittance tests are shown in Figure 13, and the changes in surface characteristics are discussed in subsection V.1.a. The x-ray diffraction and arc-spectrographic results were the same as for platinum sample 1B.

Table XV. Absolute Emittance Data for Platinum Sample No. 3B

Temperature (°K)	Time at Temp. (hr, min)	ε(T)	ε(θ_N, T)	ε(θ_N, λ, T)									
				0.65 μ (a)	1 μ	1.5 μ	2 μ	3 μ	4 μ	6 μ	8 μ	10 μ	12 μ
1640	0,15	Sample annealed in vacuum											
First Temperature Cycle													
867	2,0	0.110	0.095	–	–	–	0.108	0.106	0.078	0.067	0.057	0.052	–
1088	1,15	0.133	0.120	0.33	–	0.150	0.125	0.110	0.092	0.076	0.067	0.060	–
1231	0,45	0.148	0.131	0.32	–	0.169	0.141	0.119	0.099	0.083	0.073	0.063	0.057
1367	0,45	0.160	0.146	0.31	0.215	0.180	0.153	0.131	0.109	0.091	0.081	0.072	0.061
1642[b]	7,15	0.186	0.169	0.31	0.252	0.205	0.168	0.143	0.119	0.099	0.087	0.081	0.073
Second Temperature Cycle													
864[b]	3,30	0.103	0.092	–	–	–	0.105	0.102	0.082	0.062	0.052	0.041	–
1093[b]	3,0	0.128	0.118	0.30	–	0.131	0.113	0.106	0.090	0.074	0.063	0.051	–
1227	0,45	0.142	0.133	0.31	–	0.161	0.130	0.117	0.100	0.081	0.071	0.061	0.050
1360[b]	4,15	0.154	0.143	0.30	–	0.167	0.139	0.125	0.106	0.086	0.076	0.064	0.058
1638	0,45	0.180	0.164	0.30	0.255	0.167	0.166	0.141	0.118	0.097	0.085	0.074	0.067

(a) Determined from optical pyrometer readings.
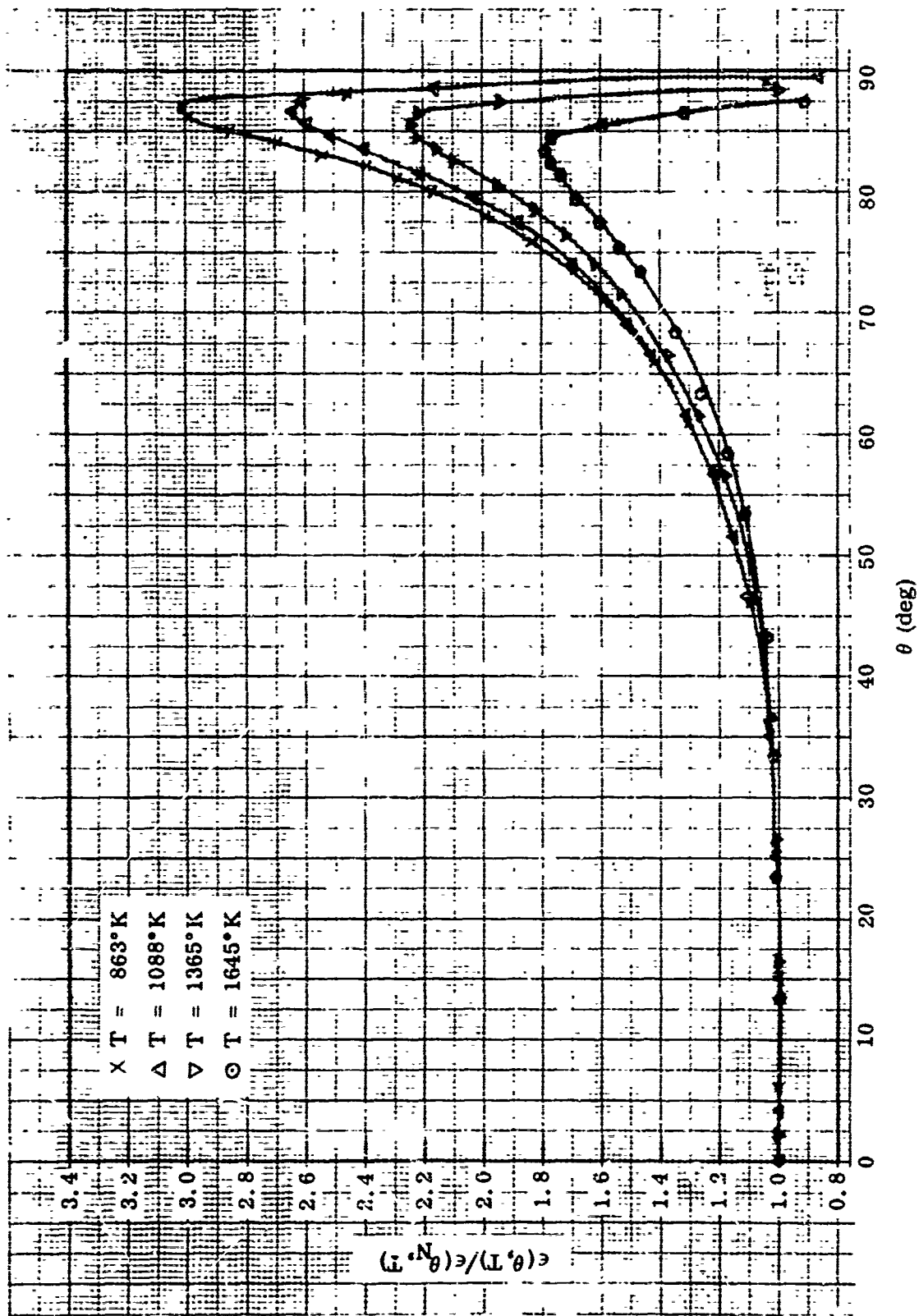(b) Directional emittance data obtained at these temperatures.

123

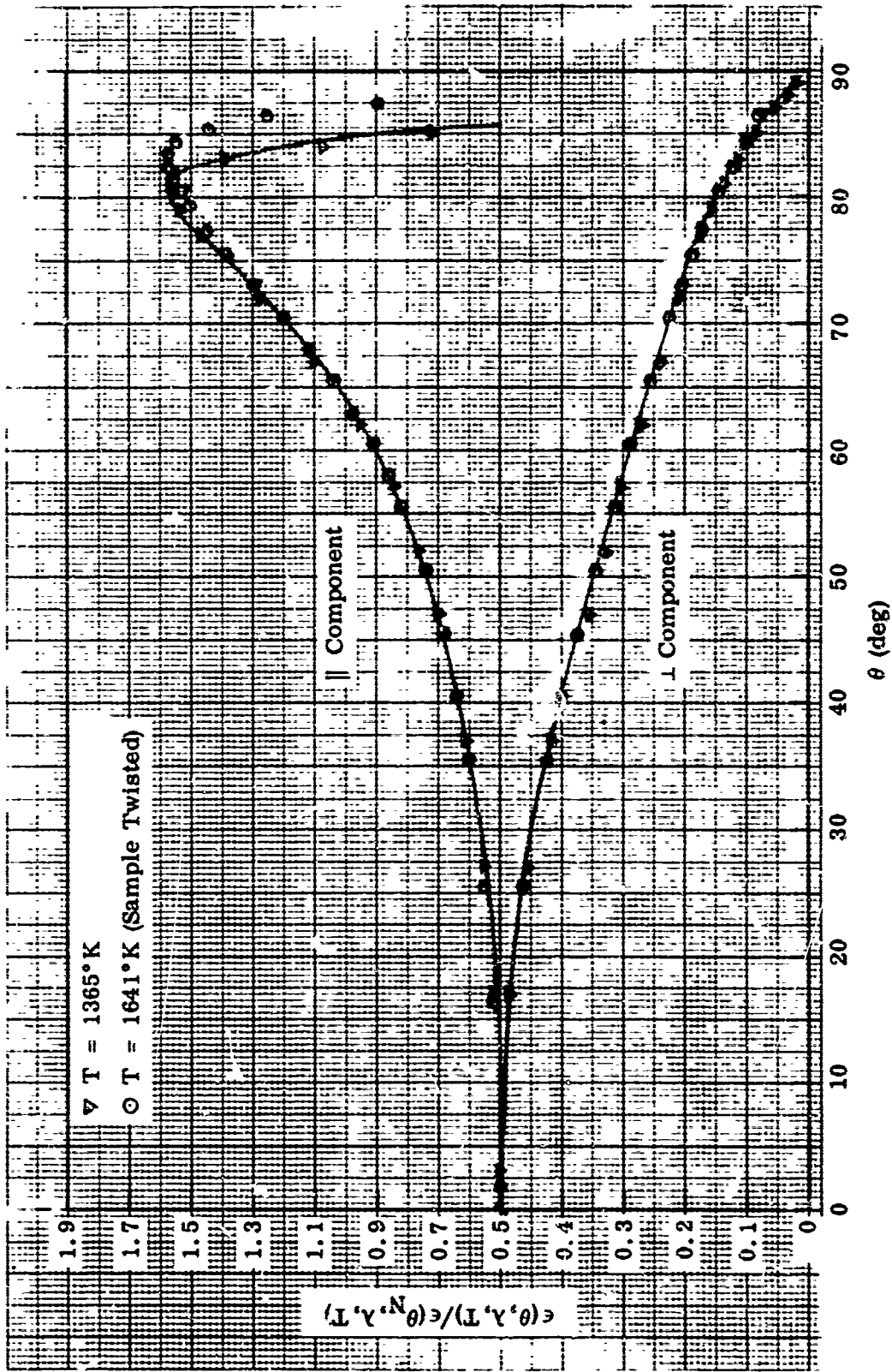Figure 55 Relative Total Directional Emittance, Platinum Sample No. 3B

124

Figure 56 Relative Spectral Directional Emittance at $\lambda = 1.5 \; \mu$, Platinum Sample No. 3B
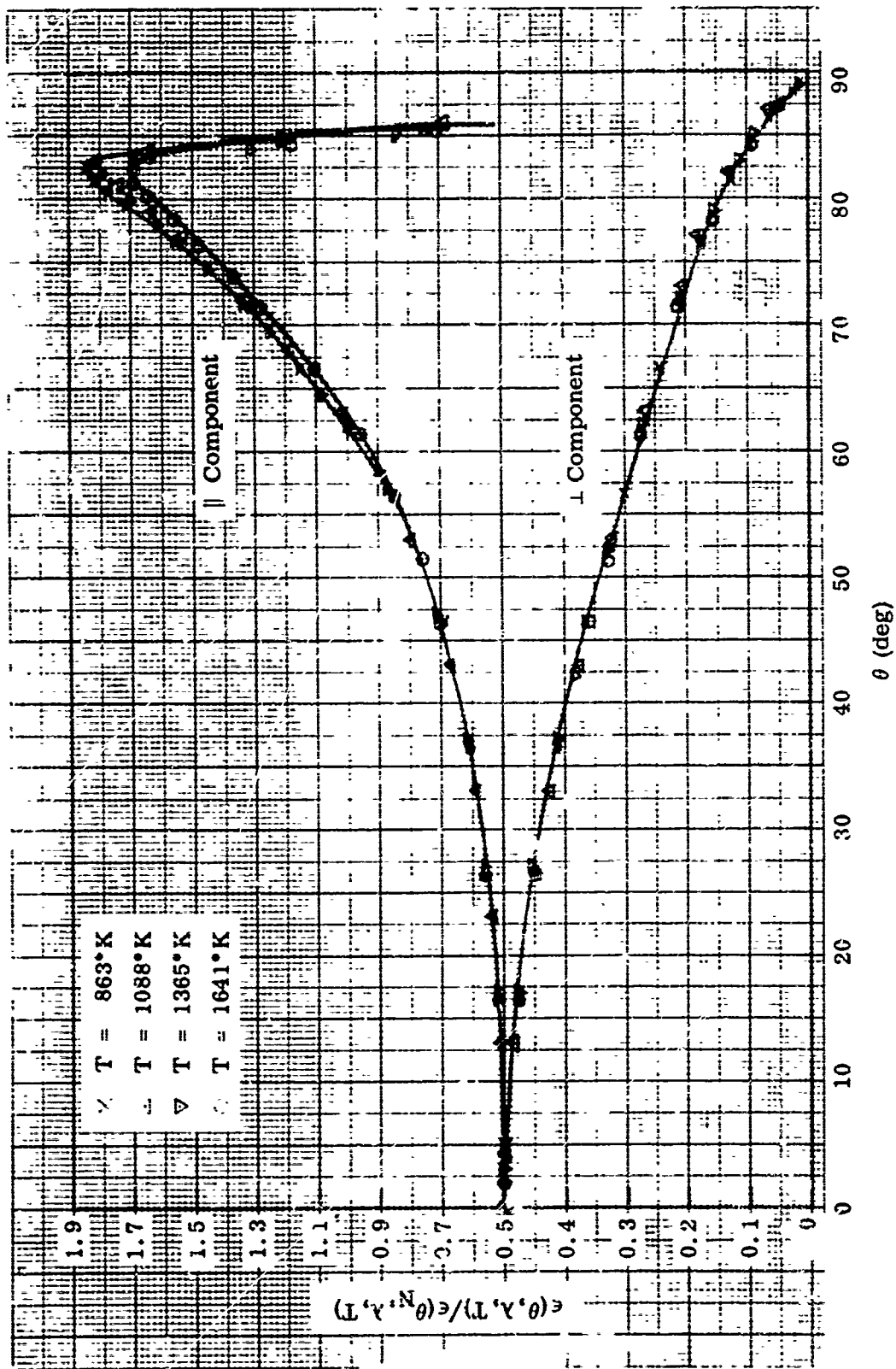
125

Figure 57 Relative Spectral Directional Emittance at $\lambda = 2\ \mu$, Platinum Sample No. 3B
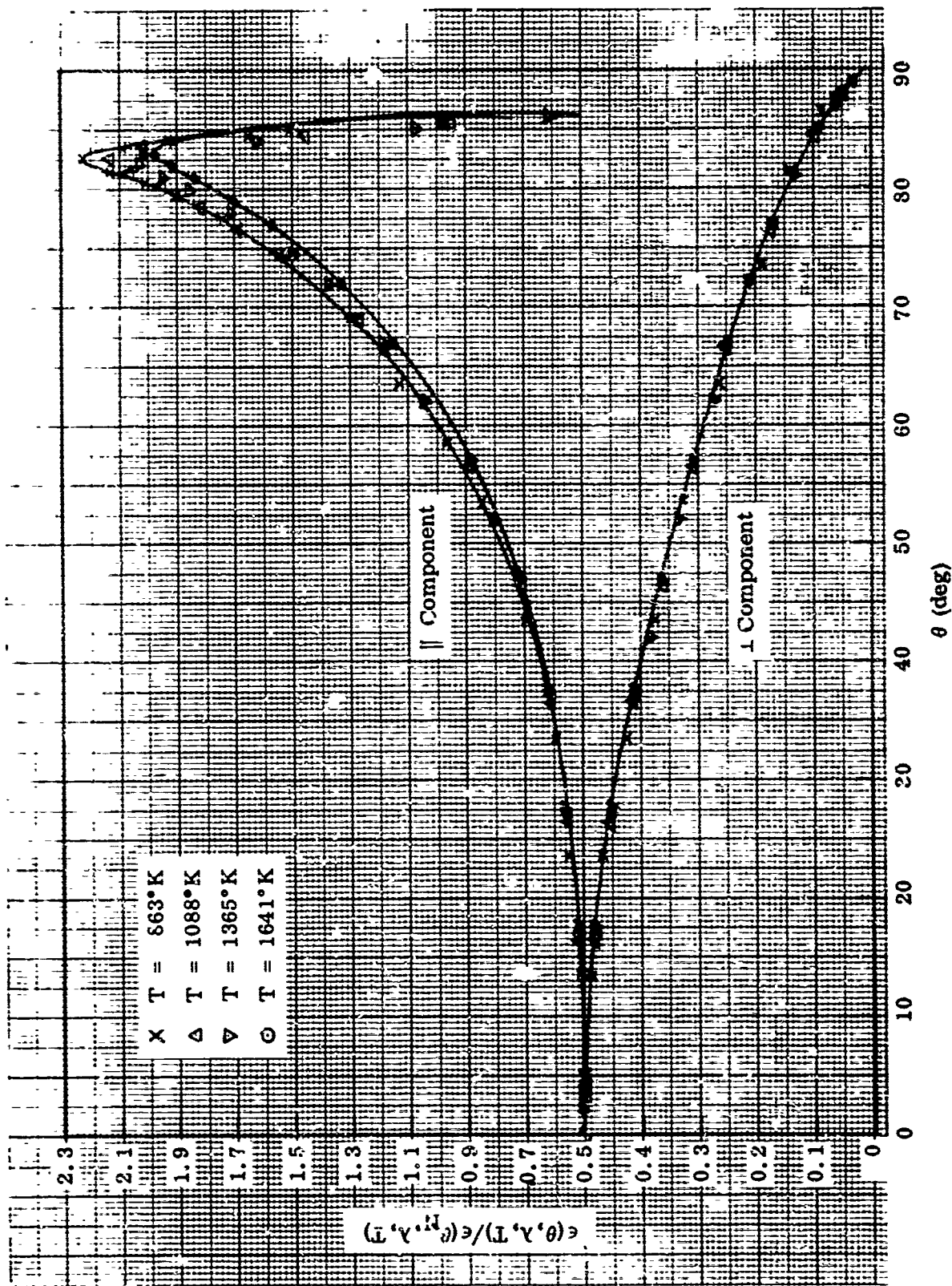
126

Figure 58 Relative Spectral Directional Emittance at $\lambda = 3\ \mu$, Platinum Sample No. 3B
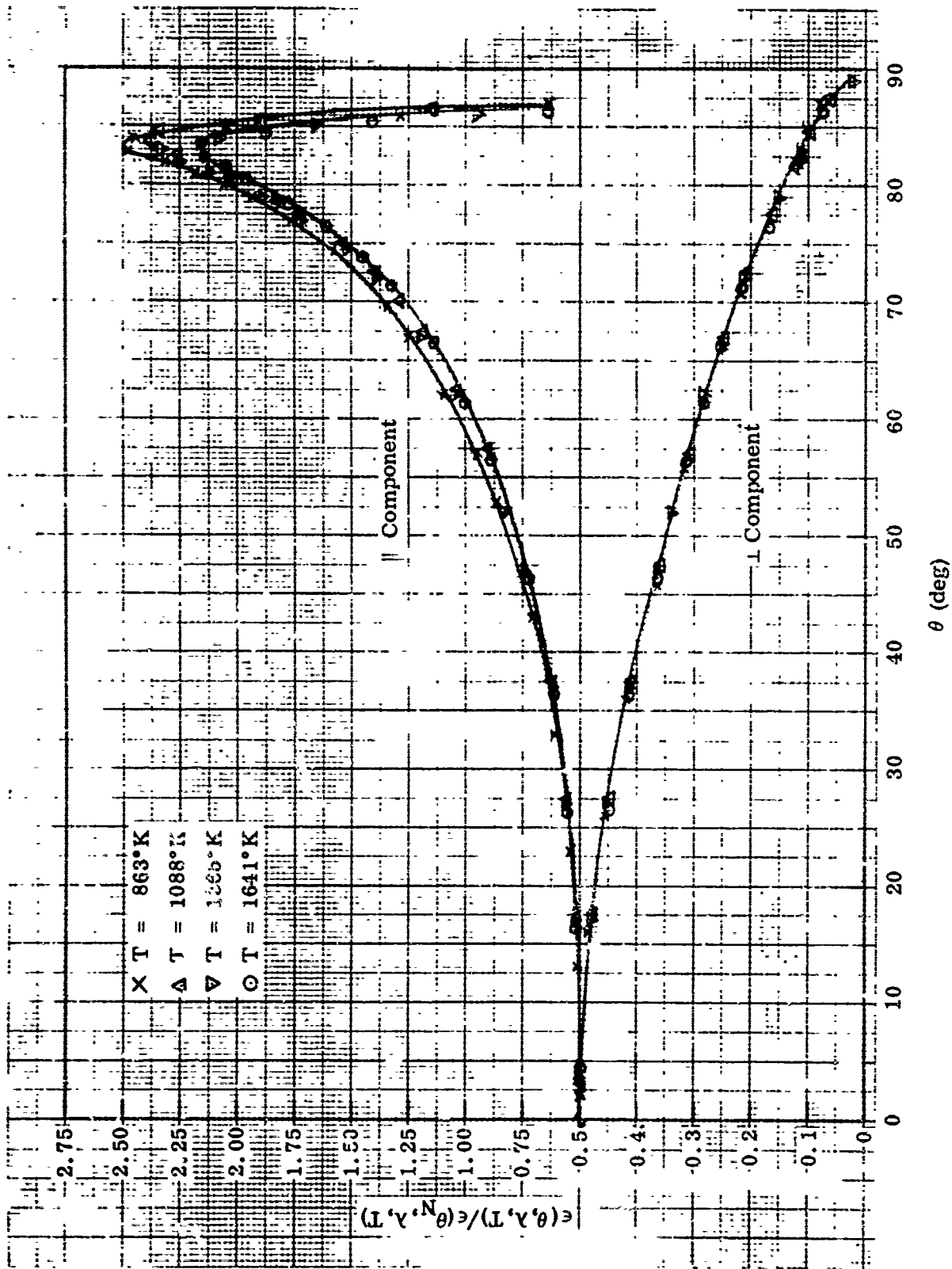
127

Figure 59 Relative Spectral Directional Emittance at $\lambda = 4\ \mu$, Platinum Sample No. 3B
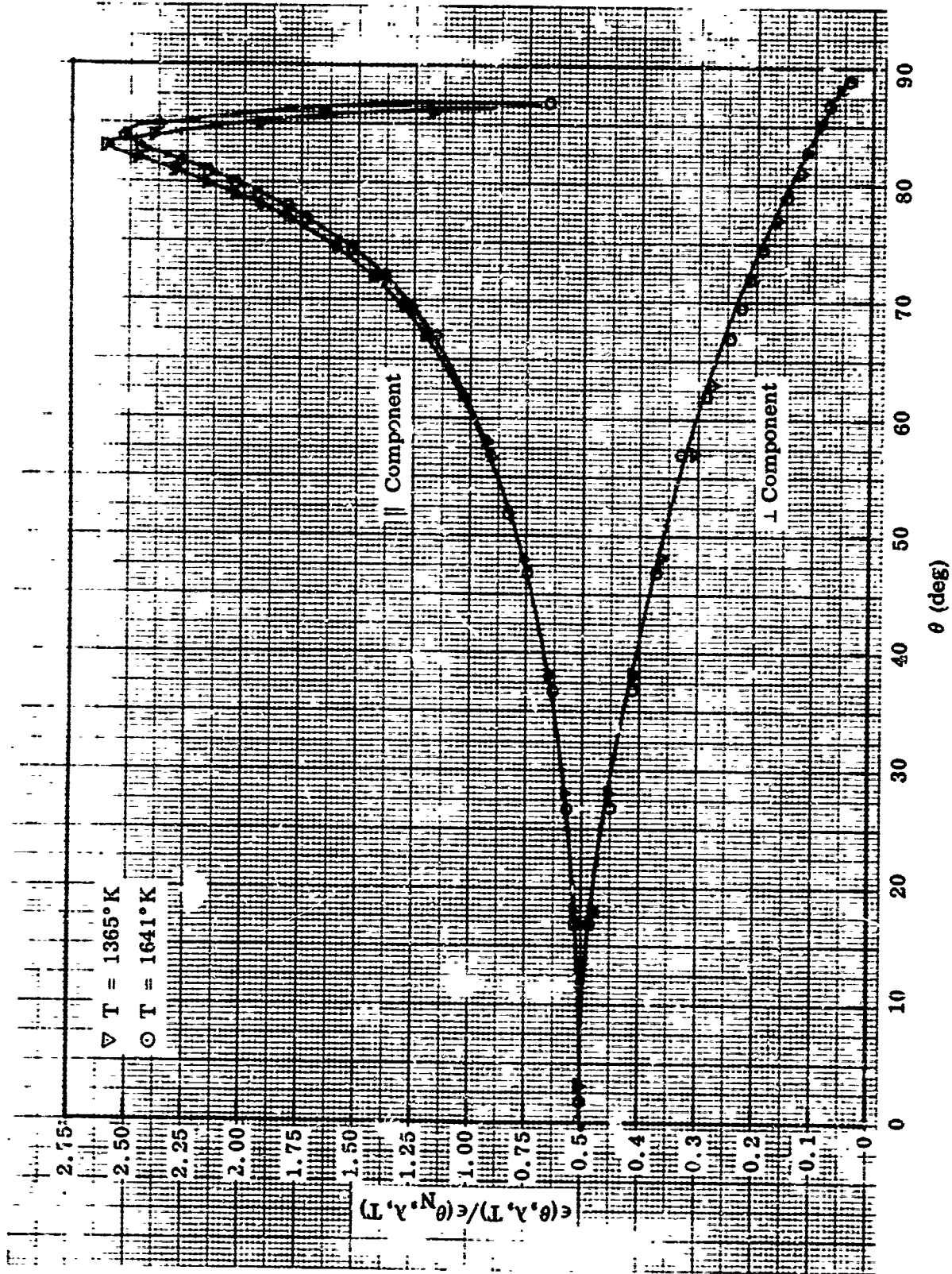
128

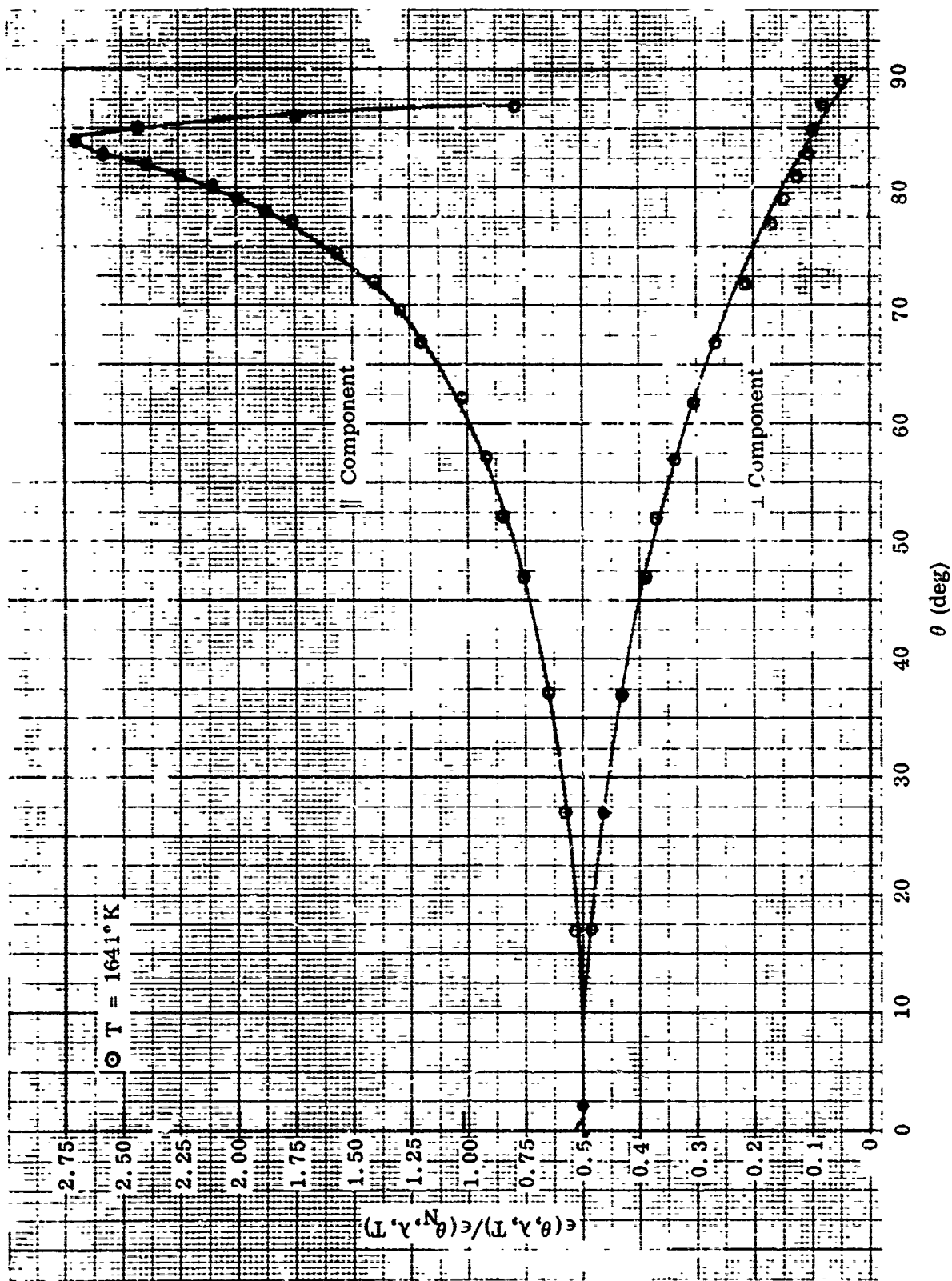Figure 60 Relative Spectral Directional Emittance at $\lambda = 6\;\mu$, Platinum Sample No. 3B

129

Figure 61 Relative Spectral Directional Emittance at $\lambda = 8\,\mu$, Platinum Sample No. 3B

130

3. PLATINUM SAMPLE NO. 4B

Preparation: Shot blasted with size XL "Glas-Shot"; pressure, 20 psi; distance, 6 in., normal to surface.

RMS Roughness: Before emittance tests, 49 μin.; after, 43 μin.

Test Procedure: Before testing, the sample was annealed at 1640°K for 20 min in vacuum. Absolute emittance values were then determined at 868, 1088, 1224, 1366, and 1644°K, and relative directional emittance data were obtained at 1644°K (first temperature cycle). Relative directional emittance data were then obtained at 1364, 1085, and 866°K, and the absolute values were remeasured at all test temperatures (second temperature cycle) to check the stability of the sample. The test chamber pressure was maintained between 4 and 10 x 10^{-6} Torr throughout the tests.

Emittance Data: Absolute emittance values are shown in Table XVI; relative total directional emittance data in Figure 62; relative spectral directional emittance data at λ = 1.5, 2, 3, 4, 6, and 8 μ in Figures 63 through 68.

Remarks: The total hemispherical emittance values were essentially the same before and after the 1644°K tests, but the total normal and spectral normal emittance values at the short wavelengths appeared to drop slightly. Slight changes in the surface characteristics of the sample due to further annealing during the 1644°K test are believed to be the cause for the changes in emittance.

Photomicrographs of the sample surface before and after the emittance tests are shown in Figure 13, and a taper-section photomicrograph is shown in Figure 17. Changes in the surface characteristics of the sample are discussed in subsection V.1.a. The x-ray diffraction and arc-spectrographic results were the same as for platinum sample 1B.

Table XVI. Absolute Emittance Data for Platinum Sample No. 4B

Temperature (°K)	Time at Temp. (hr, min)	$\epsilon(T)$	$\epsilon(\theta_N, T)$	$\epsilon(\theta_N, \lambda, T)$									
				0.65 μ (a)	1 μ	1.5 μ	2 μ	3 μ	4 μ	6 μ	8 μ	10 μ	12 μ
1640	0,20	Sample annealed in vacuum											
First Temperature Cycle													
868	0,45	0.105	0.095	–	–	–	0.110	0.099	0.079	0.066	0.055	0.041	–
1088	0,45	0.131	0.122	0.29	–	0.157	0.130	0.116	0.096	0.078	0.067	0.058	–
1224	1,30	0.145	0.135	0.28	–	0.168	0.138	0.123	0.102	0.084	0.074	0.066	0.057
1366	0,45	0.162	0.150	0.28	0.225	0.184	0.153	0.133	0.111	0.093	0.080	0.072	0.065
1644(b)	4,15	0.185	0.173	0.29	0.261	0.208	0.173	0.145	0.120	0.101	0.086	0.080	0.072
Second Temperature Cycle													
866(b)	3,45	0.103	0.093	–	–	–	0.123	0.101	0.081	0.066	0.050	0.043	–
1085(b)	3,15	0.130	0.118	0.29	–	0.153	0.128	0.114	0.094	0.075	0.065	0.055	–
1222	1,0	0.145	0.134	0.27	–	0.160	0.133	0.120	0.101	0.082	0.067	0.061	0.054
1364(b)	5,0	0.145	0.145	0.28	0.212	0.170	0.141	0.127	0.108	0.089	0.079	0.072	0.060
1639	0,45	0.181	0.169	0.28	0.254	0.212	0.180	0.144	0.119	0.100	0.087	0.077	0.070

(a) Determined from optical pyrometer readings.
(b) Directional emittance data obtained at these temperatures.
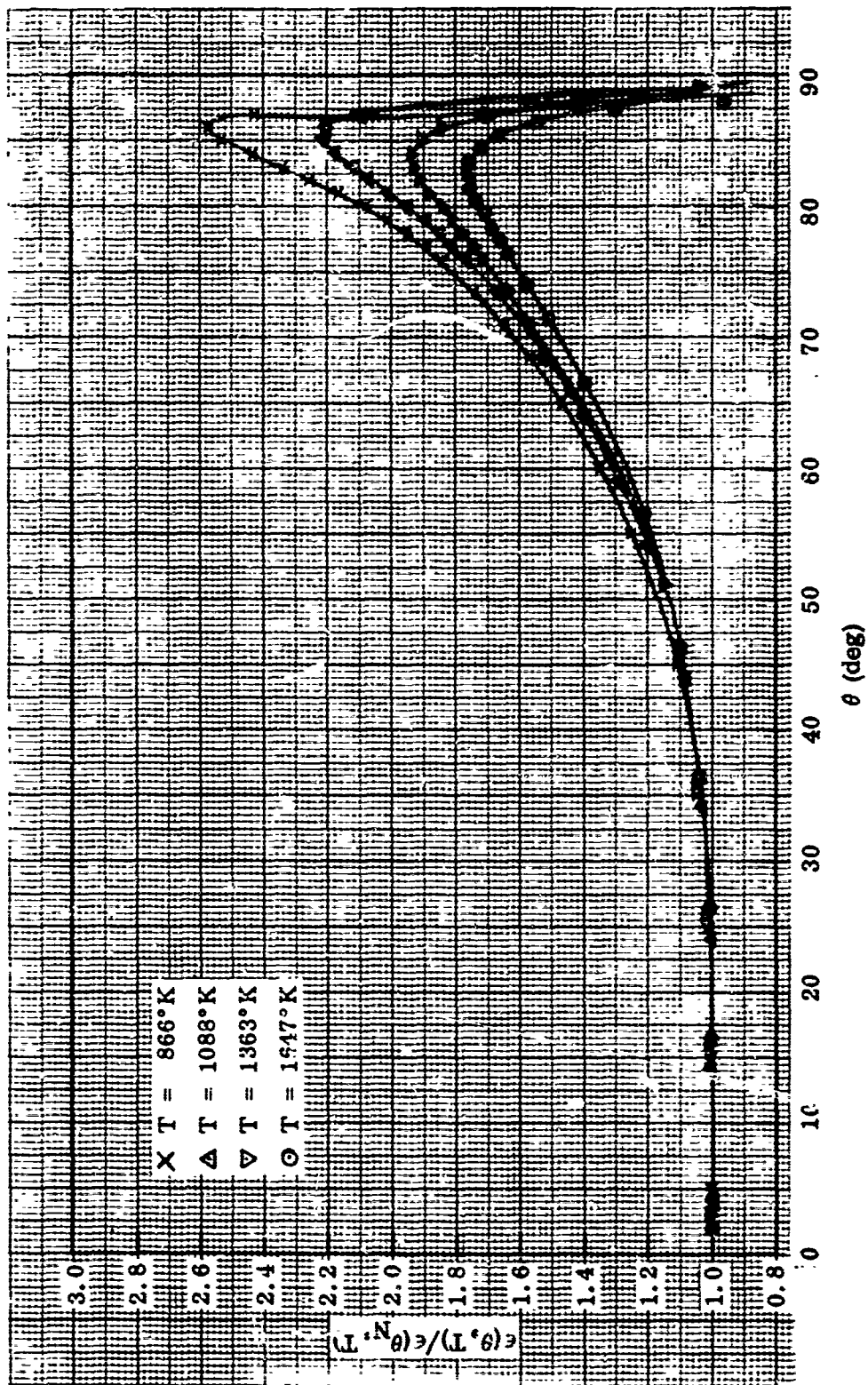
132

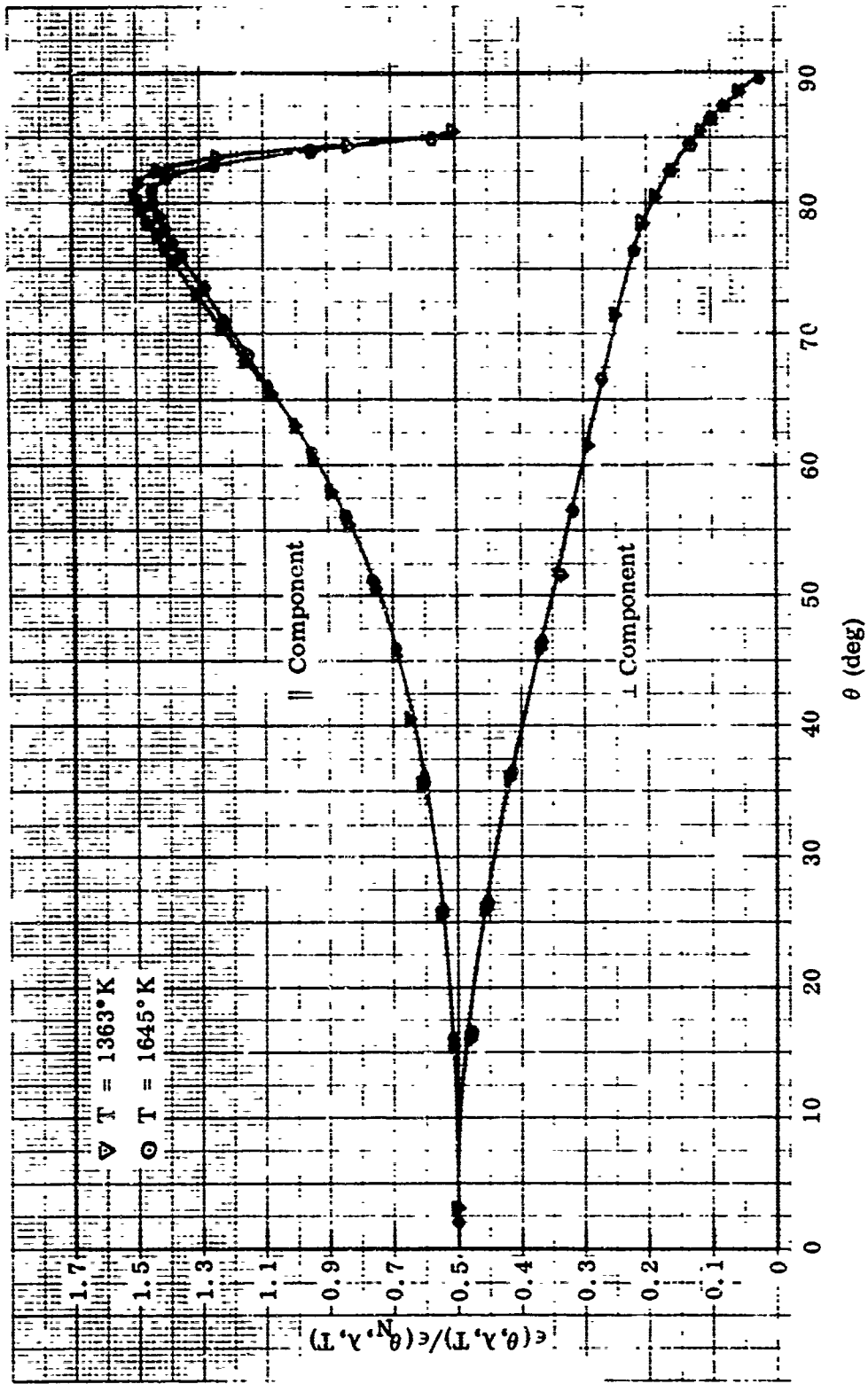Figure 62 Relative Total Directional Emittance, Platinum Sample No. 4B

133

Figure 63 Relative Spectral Directional Emittance at $\lambda = 1.5\ \mu$, Platinum Sample No. 4B
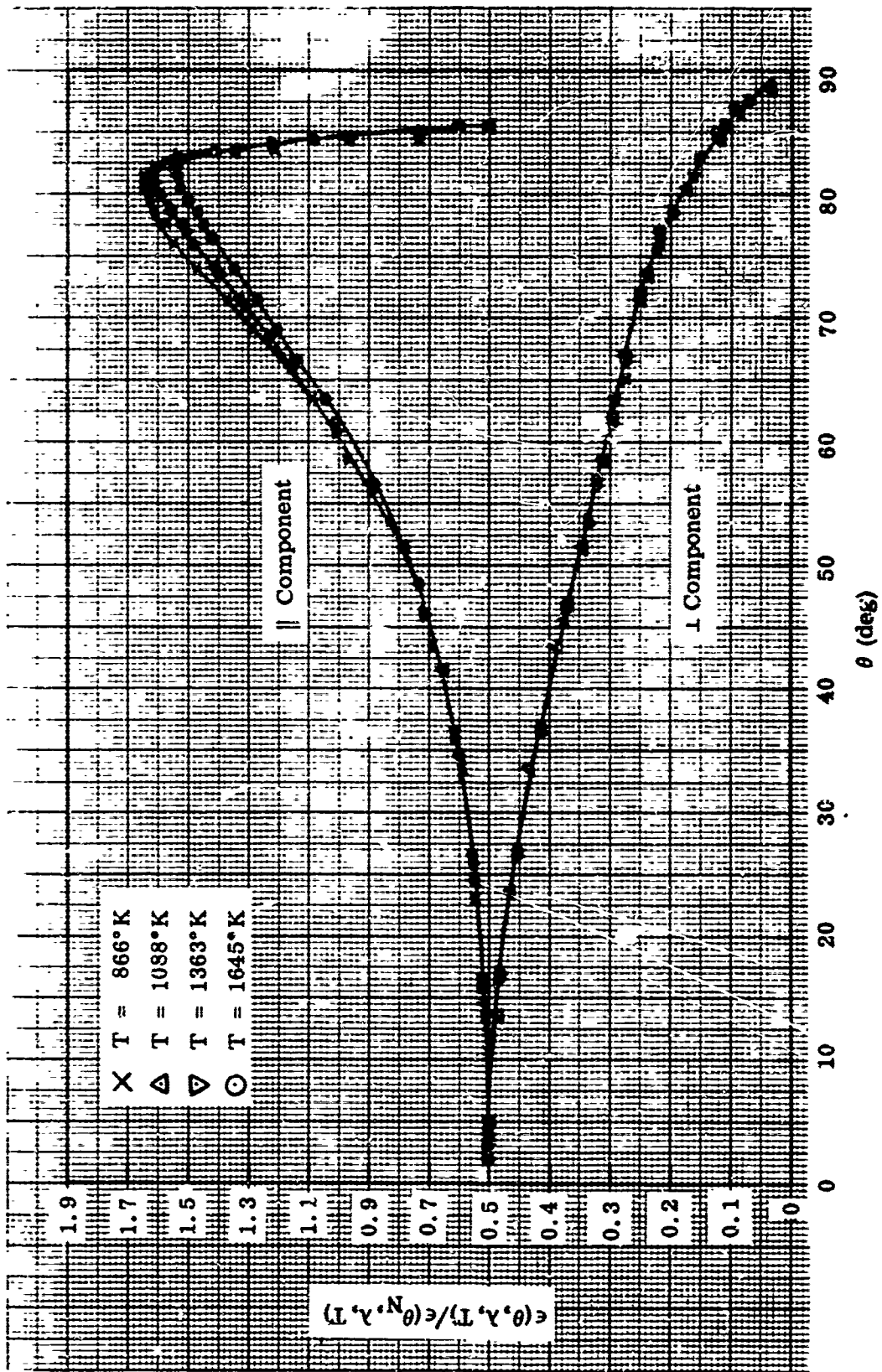
134

Figure 64 Relative Spectral Directional Emittance at $\lambda = 2\mu$, Platinum Sample No. 4B

135

Figure 65 Relative Spectral Directional Emittance at $\lambda = 3\,\mu$, Platinum Sample No. 4B
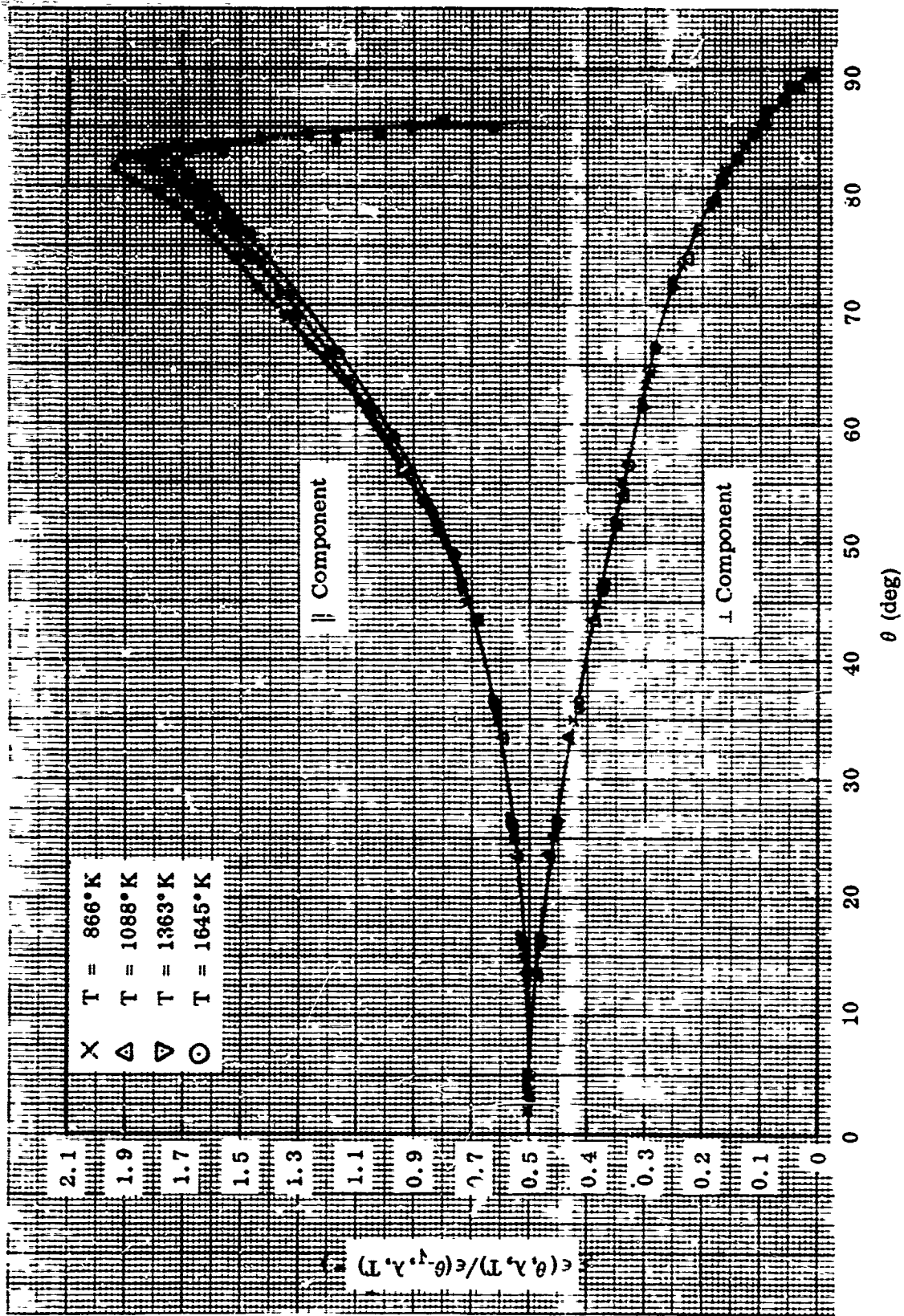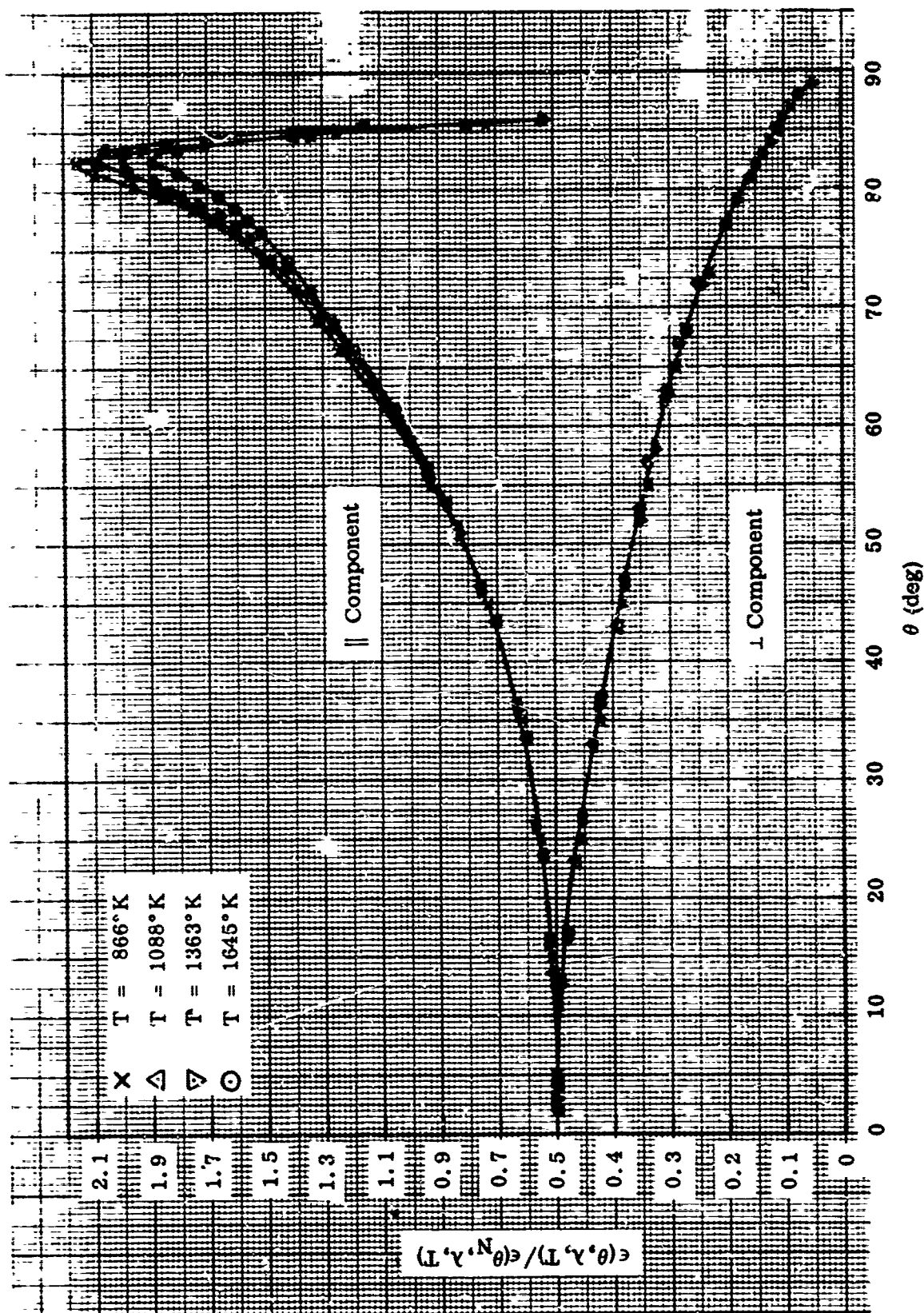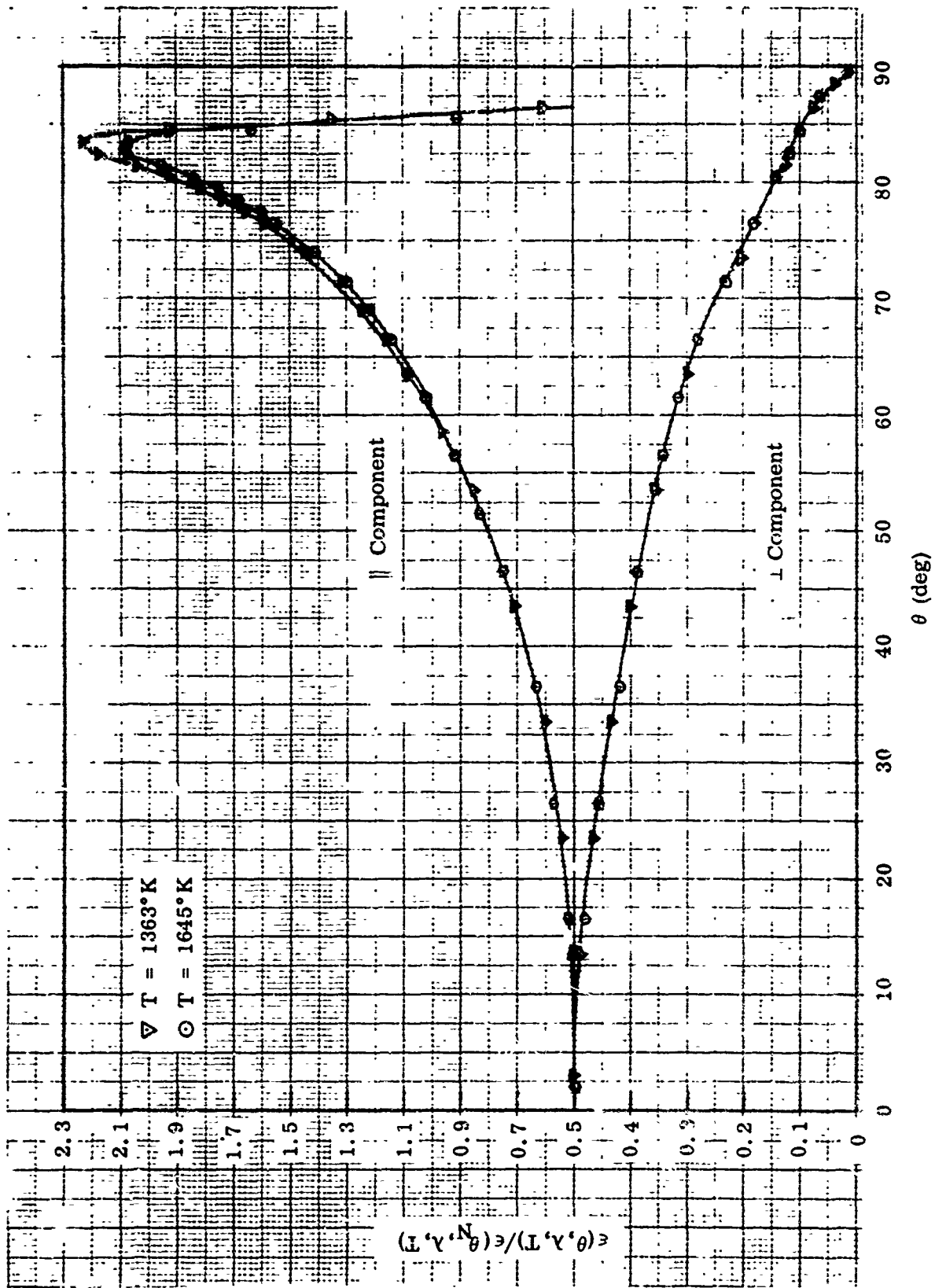
136

Figure 66 Relative Spectral Directional Emittance at $\lambda = 4 \mu$, Platinum Sample No. 4B

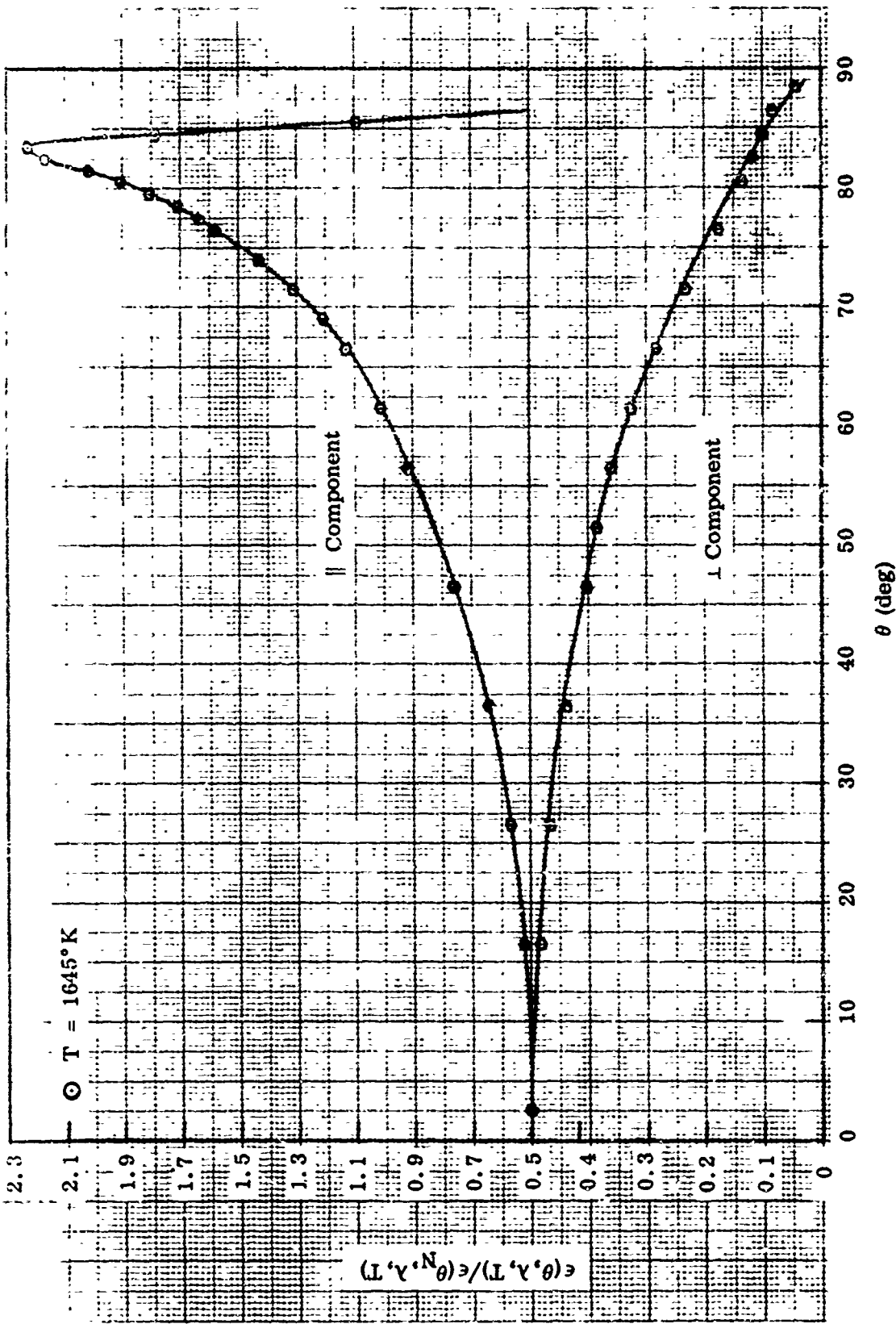Figure 67 Relative Spectral Directional Emittance at $\lambda = 6\,\mu$, Platinum Sample No. 4B

138

Figure 68 Relative Spectral Directional Emittance at $\lambda = 8\,\mu$, Platinum Sample No. 4B

139

4. PLATINUM SAMPLE NO. 5B

Preparation: Shot blasted with size XL "Glas-Shot"; pressure, 30 psi; distance, 6 in., normal to surface.

RMS Roughness: Before emittance tests: 39 μin.; after, 40 μin.

Test Procedure: Before testing, the sample was annealed at 1640°K for 20 min in vacuum. Absolute emittance values were then determined at 870, 1091, 1232, 1365, and 1639°K, and relative directional emittance data were obtained at 1639°K (first temperature cycle). Relative directional emittance data were then obtained at 1365, 1091, and 866°K, and the absolute emittance values were remeasured at all test temperatures (second temperature cycle) to check the stability of the sample. The test chamber pressure was maintained between 4 and 9 × 10^{-6} Torr throughout all tests.

Emittance Data: Absolute emittance values are shown in Table XVII; relative total directional emittance data in Figure 69; relative spectral directional emittance data at λ = 1.5, 2, 3, 4, 6, and 8 μ in Figures 70 through 75.

Remarks. Absolute emittance values determined after the 1639°K tests tended to be slightly lower than the initial values for this sample. The cause is believed to be a systematic measurement error during the second test-temperature cycle rather than a change in surface characteristics. No significant change in surface characteristics was indicated by the post-test examinations. A similar drop in absolute emittance was noted for sample 3B. A possible explanation is that the calibration of the fine (0.003-in. diameter) thermocouple wire changed slightly during the 1640°K test.

Photomicrographs of the sample surface before and after the emittance tests are shown in Figure 13, and the change in surface characteristics is discussed in subsection V.1.a. The x-ray diffraction and arc-spectrographic results were the same as for platinum sample 1B.

Table XVII. Absolute Emittance Data for Platinum Sample No. 5B

Temperature (°K)	Time at Temp. (hr, min)	$\epsilon(T)$	$\epsilon(\theta_N, T)$	$\epsilon(\theta_N, \lambda, T)$									
				0.65 μ (a)	1 μ	1.5 μ	2 μ	3 μ	4 μ	6 μ	8 μ	10 μ	12 μ
1640	0, 20	Sample annealed in vacuum											
						First Temperature Cycle							
870	2, 0	0.111	0.098	-	-	-	0.141	0.106	0.087	0.069	0.058	0.049	-
1091	1, 15	0.139	0.128	0.32	-	0.190	0.146	0.121	0.099	0.082	0.069	0.060	-
1232	1, 30	0.152	0.141	0.31	-	0.185	0.149	0.129	0.108	0.088	0.077	0.064	0.054
1365	1, 25	0.166	0.154	0.31	0.254	0.201	0.165	0.140	0.117	0.095	0.083	0.073	0.061
1639(b)	6, 0	0.192	0.178	0.31	0.264	0.214	0.164	0.147	0.122	0.103	0.091	0.082	0.072
						Second Temperature Cycle							
866(b)	4, 30	0.110	0.096	-	-	-	0.135	0.107	0.084	0.068	0.053	0.039	-
1091(b)	2, 50	0.133	0.123	0.29	-	0.180	0.147	0.123	0.099	0.080	0.068	0.057	-
1226	0, 40	0.148	0.140	0.30	-	0.188	-	0.129	0.105	0.086	0.074	0.065	0.051
1365(b)	4, 0	0.161	0.152	0.31	-	0.188	0.154	0.131	0.110	0.091	0.078	0.069	0.057
1638	0, 45	0.186	0.171	0.30	0.253	0.209	0.172	0.146	0.122	0.102	0.089	0.079	0.070

(a) Determined from optical pyrometer readings.
(b) Directional emittance data obtained at these temperatures.
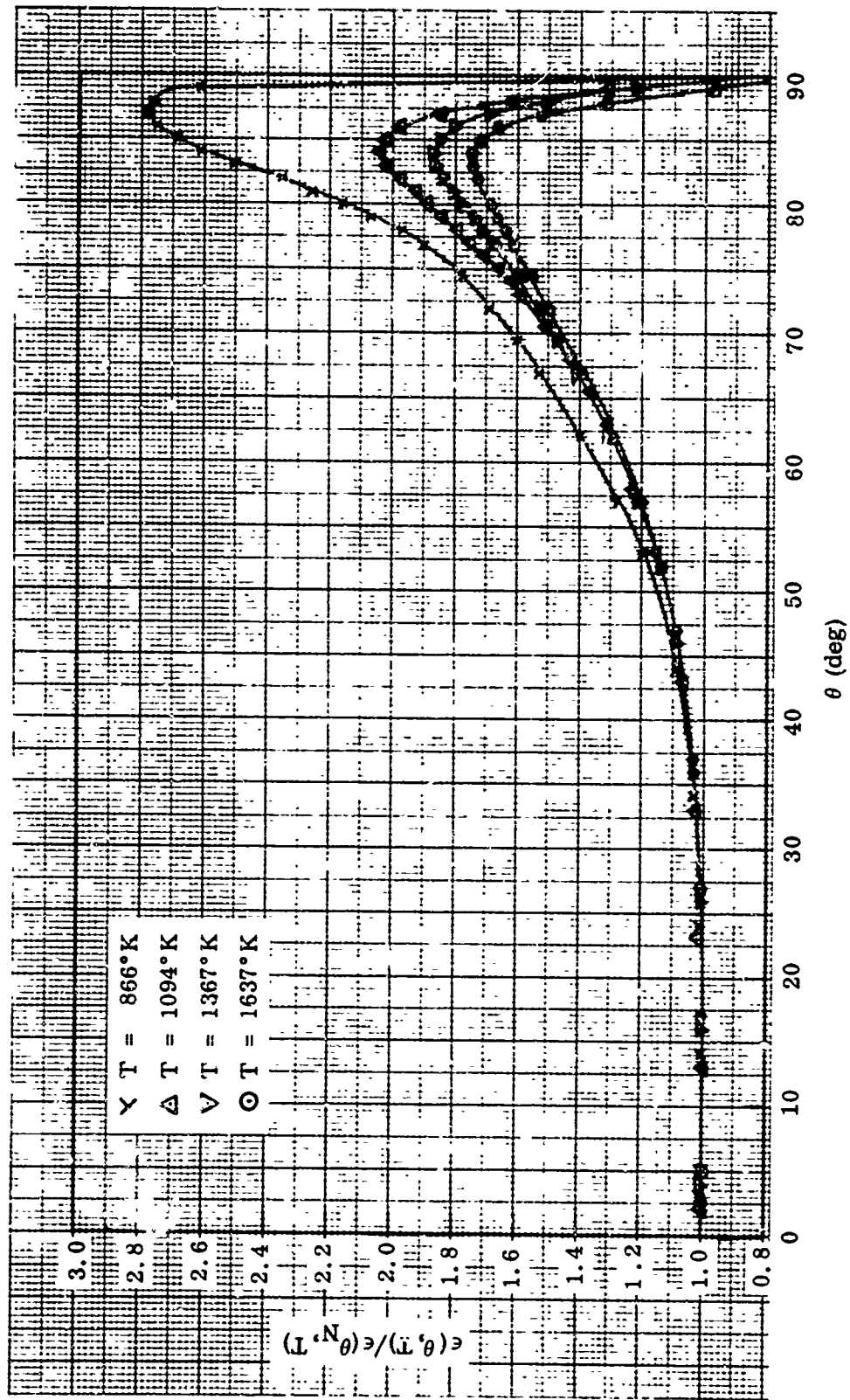
141

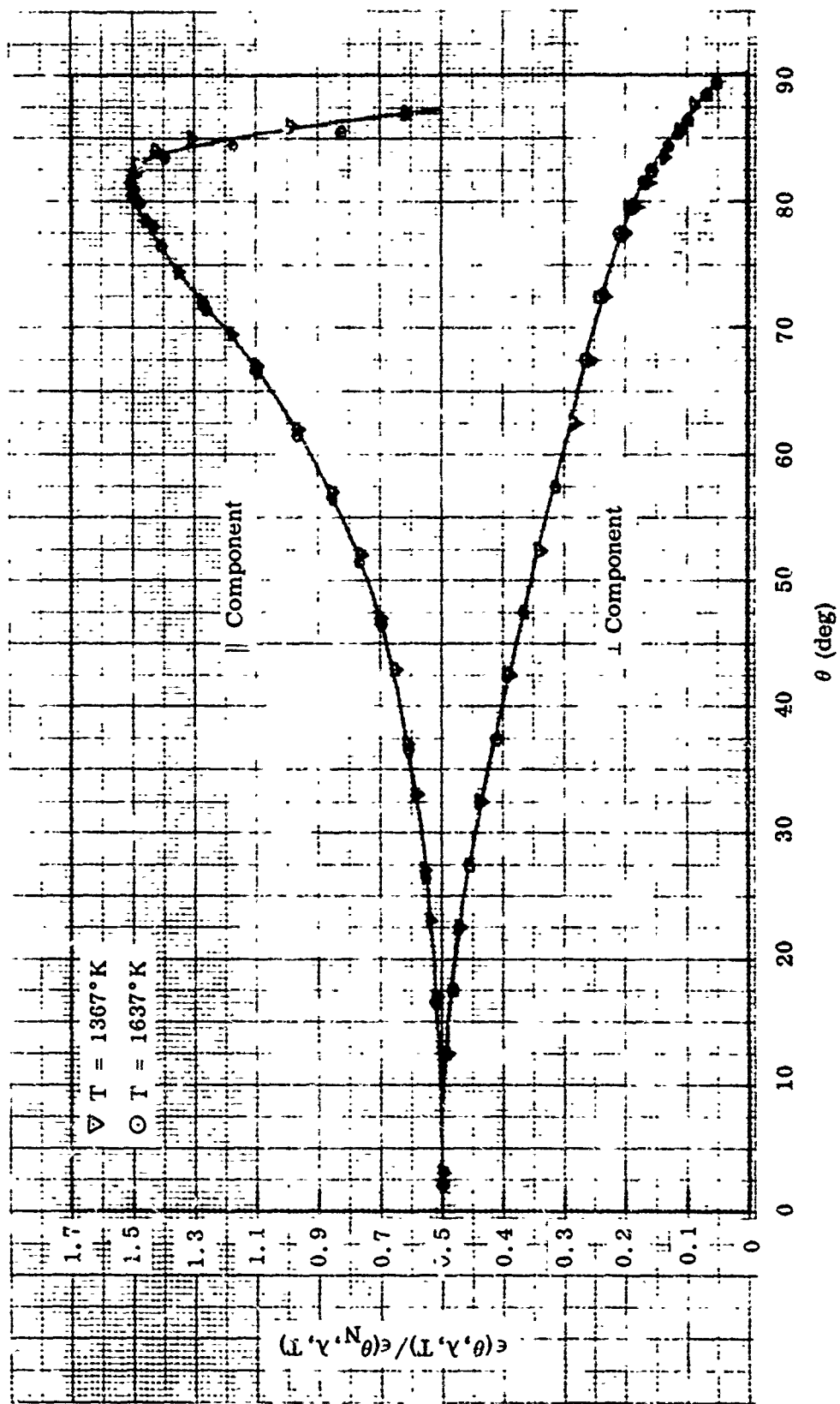Figure 69 Relative Total Directional Emittance, Platinum Sample No. 5B

142

Figure 70 Relative Spectral Directional Emittance at $\lambda = 1.5\ \mu$, Platinum Sample No. 5B
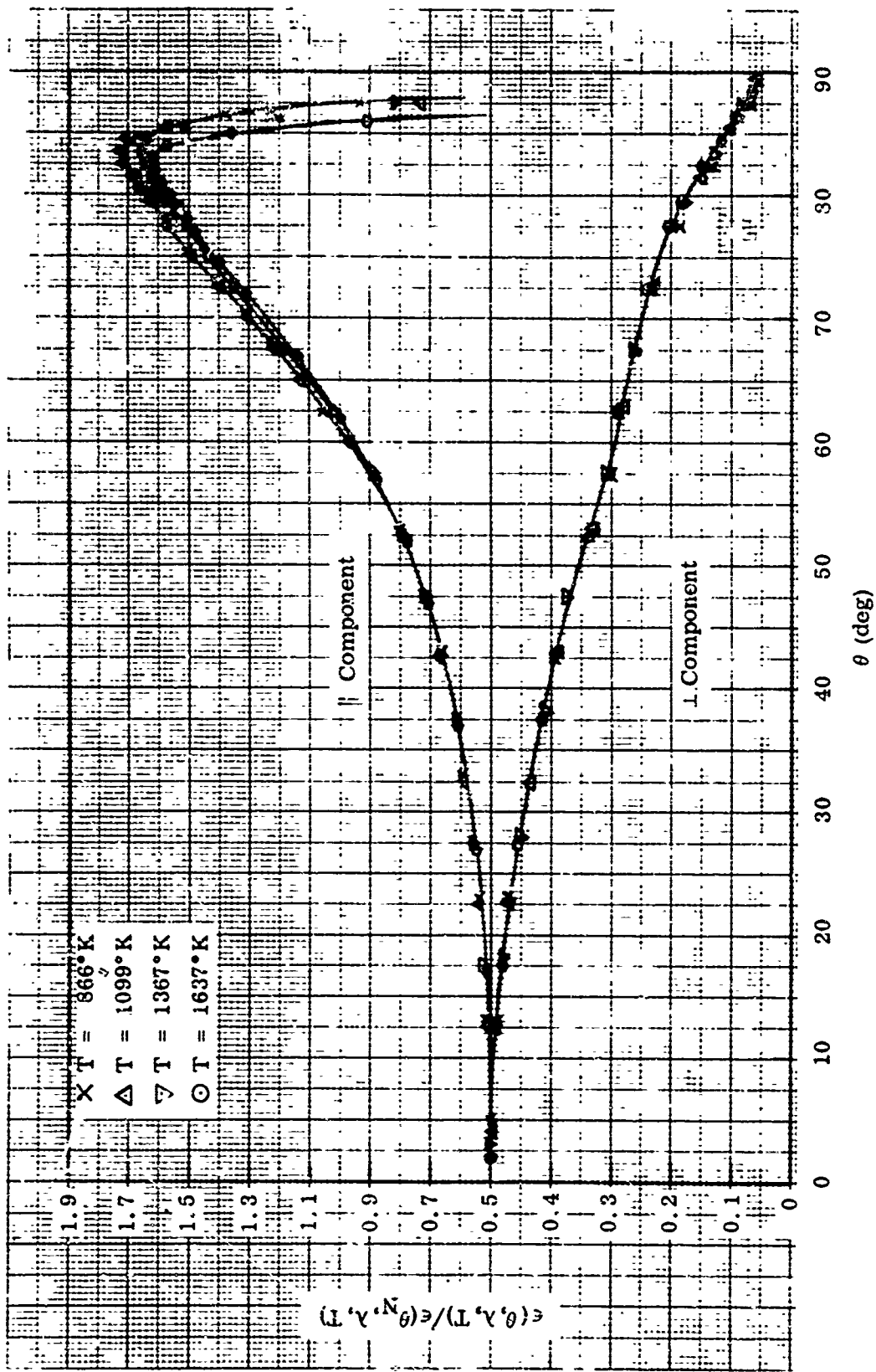
143

Figure 71 Relative Spectral Directional Emittance at $\lambda = 2\ \mu$, Platinum Sample No. 5B

Figure 72 Relative Spectral Directional Emittance at $\lambda = 3 \mu$. Platinum Sample No. 5B
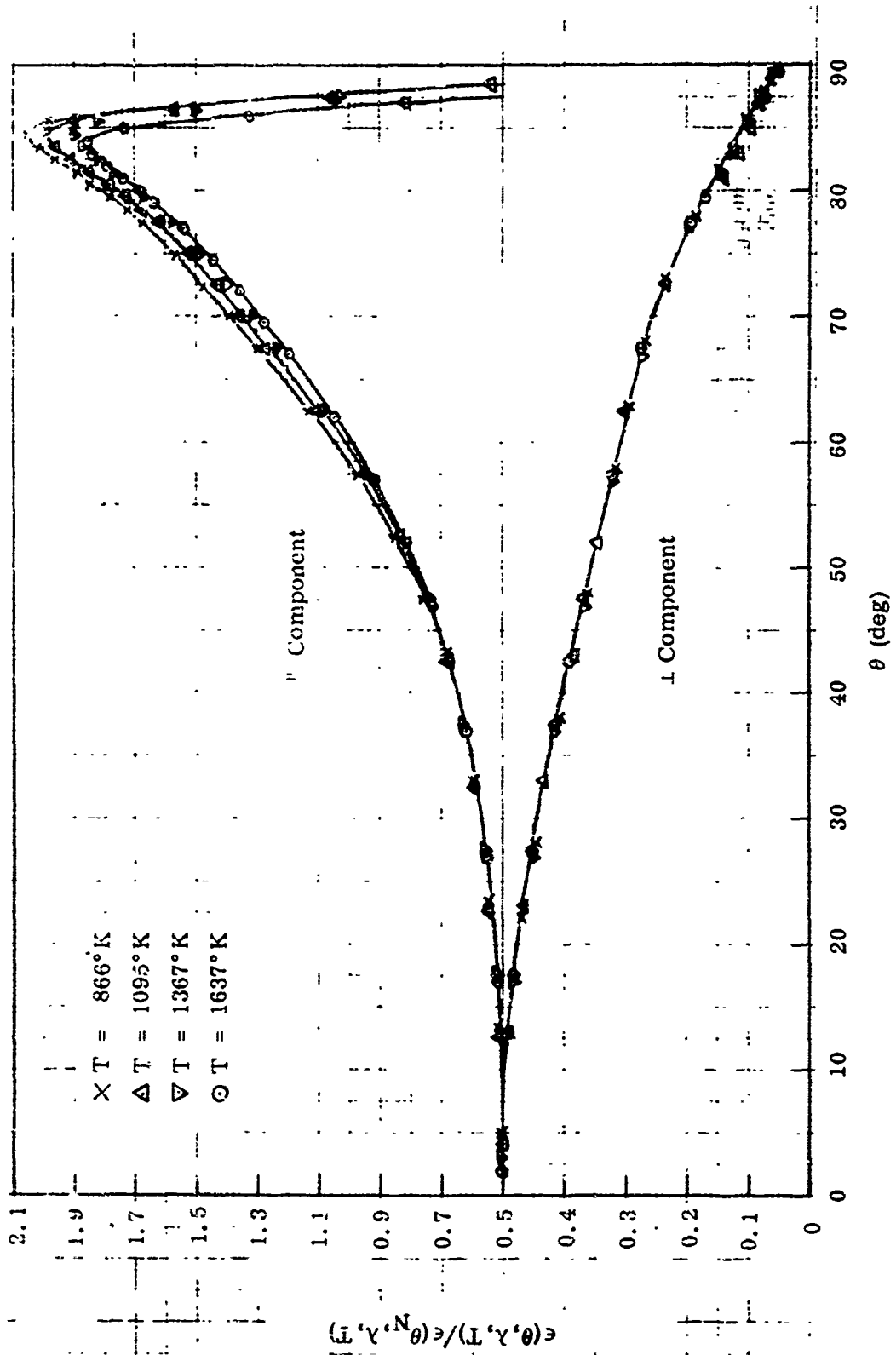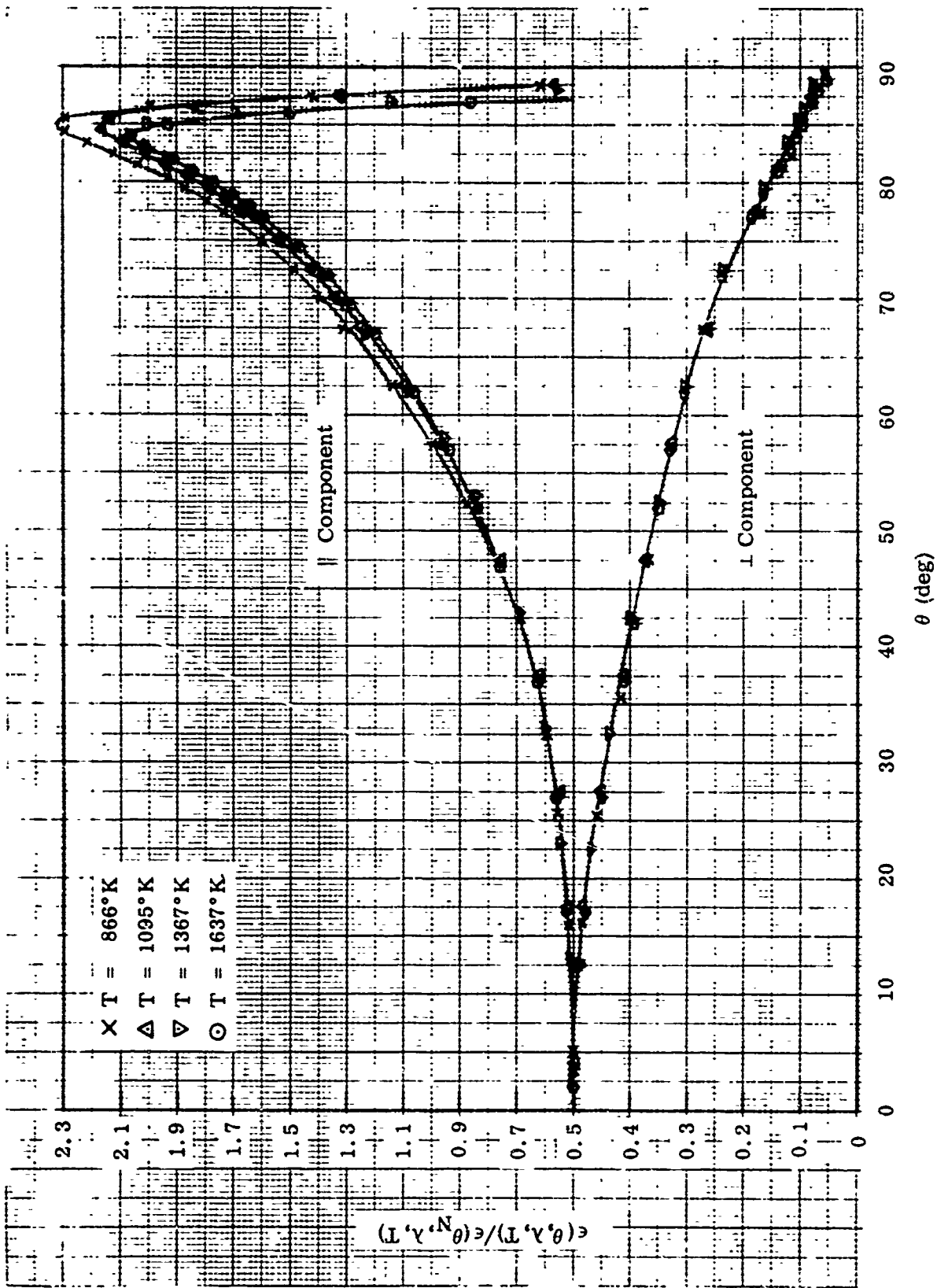
145

Figure 73 Relative Spectral Directional Emittance at $\lambda = 4 \mu$, Platinum Sample No. 5B
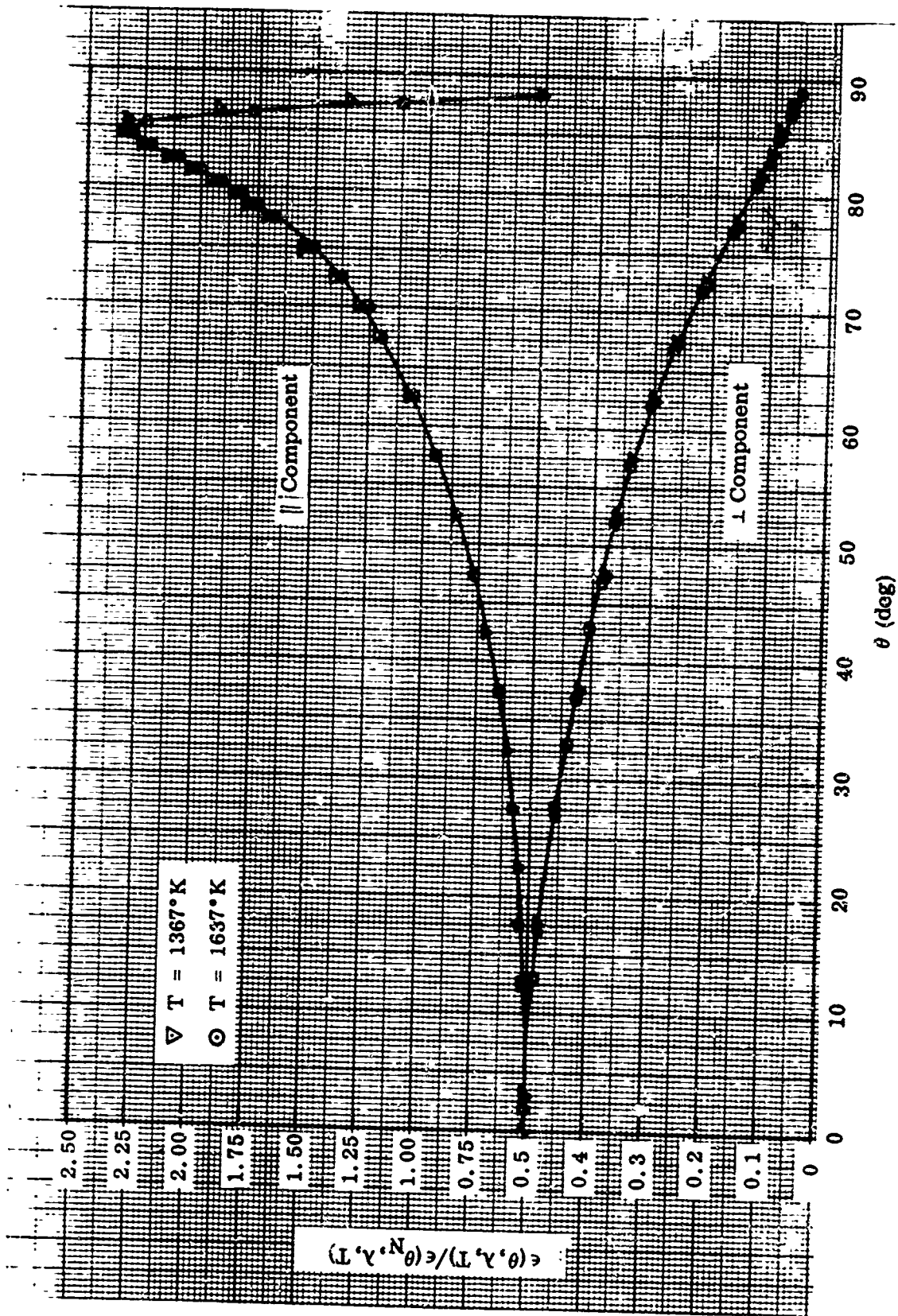
146

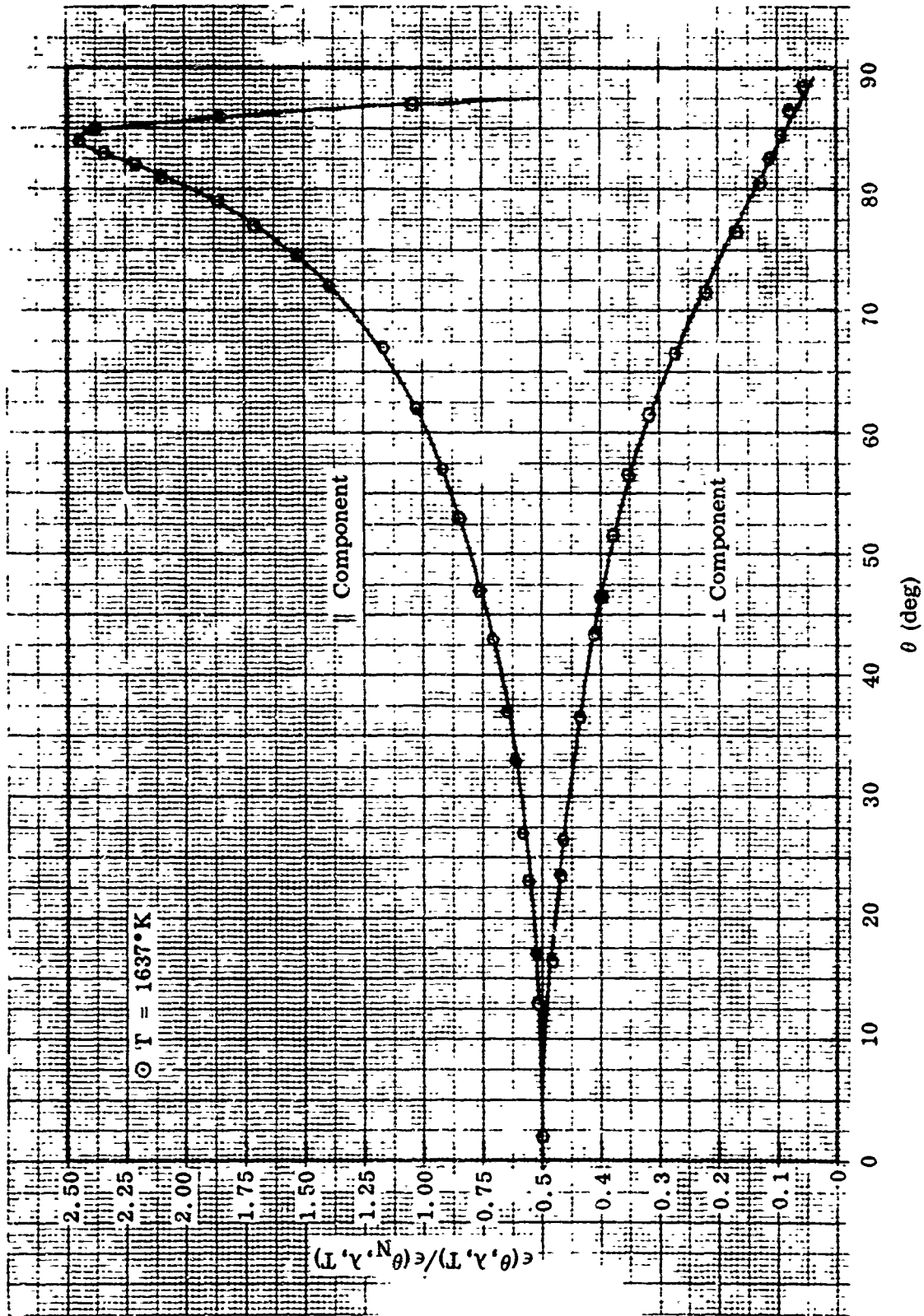Figure 74 Relative Spectral Directional Emittance at $\lambda = 6\,\mu$, Platinum Sample No. 5B

147

Figure 75 Relative Spectral Directional Emittance at $\lambda = 8~\mu$, Platinum Sample No. 5B

148

5. PLATINUM SAMPLE NO. 6B

Preparation: Shot blasted with size XL "Glas-Shot"; pressure, 60 psi; distance, 6 in., normal to surface.

RMS Roughness: Before emittance tests, 127 μin.; after, 95 μin.

Test Procedure: Before testing, the sample was annealed at 1640°K for 1 hr in vacuum. Absolute and relative directional emittance data were then obtained at 1635, 1365, 1225, 1088, and 870°K (first temperature cycle). Absolute and relative total directional emittance data were remeasured at 1095, 1223, 1370, and 1640°K (second temperature cycle) to check the sample stability. The test chamber pressure was maintained between 2×10^{-6} and 6×10^{-5} Torr throughout all tests.

Emittance Data: Absolute emittance values are shown in Table XVIII; relative total directional emittance data in Figure 76; relative spectral directional emittance data in Figures 77 through 82.

Remarks: This sample was the first tested in the modified emittance apparatus used for this year's study. After the first test-temperature cycle, analysis of the data showed the total normal emittance determinations to be erratic and unreasonably high at 1365 and 1640°K. Additional tests of the total detector alignment and response showed the problem to be saturation of the 13 cps detector-amplifier at the energy levels associated with these temperatures. To eliminate this error, the aperture slit width for the total normal emittance determinations was narrowed from 0.015 to 0.005 in., thereby reducing to acceptable levels the amount of energy received by the detector. Subsequent determinations were in good agreement with previous data at the lower test temperatures but were later found to be erratic and nonrepeatable. (See Remarks for platinum sample no. 1B.) A discussion of this problem and of the procedure for eliminating it is contained in subsection V.1.b. Since the problem was not satisfactorily solved during the testing of this sample, a complete set of total normal emittance data was not obtained. From the absolute emittance data that were obtained, however, the emittance characteristics of the sample do not appear to be significantly different from those of the other four platinum samples. The total hemispherical and spectral normal emittance values indicate that the sample remained essentially stable after the 1-hr, pretest anneal treatment.

Photomicrographs of the sample surface before and after the emittance tests are shown in Figure 13, and a taper-section photomicrograph of the sample is shown in Figure 17. Changes in the surface characteristics of the sample are discussed in subsection V.1.a.

X-ray diffraction data for the sample are presented in Table V. The diffraction pattern indicated that the more severe shot-blast treatment of this surface altered the orientation of the lattice structure somewhat, relative to the structure of the other four platinum samples. The spectrographic results were the same as for the other platinum samples, indicating no surface contamination by the Glas-Shot.

149

Table XVIII. Absolute Emittance Data for Platinum Sample No. 6B

Temperature (°K)	Time at Temp. (hr, min)	ε(T)	ε(θ_N, T)	$\epsilon(\theta_N, \lambda, T)$									
				0.65 μ (a)	1 μ	1.5 μ	2 μ	3 μ	4 μ	6 μ	8 μ	10 μ	12 μ
1640	1, 0	Sample annealed in vacuum											
First Temperature Cycle													
1635(b)	4, 45	0.195	(c)	0.33	0.250	0.199	0.164	0.141	0.123	0.107	0.096	0.087	0.080
1365(b)	5, 45	0.174	(c)	0.30	0.220	0.192	0.160	0.132	0.112	0.097	0.086	0.077	–
1225(b)	5, 30	0.148	0.143	0.34	–	–	–	0.113	0.105	0.090	0.081	0.074	–
1088(b)	2, 0	–	–	–	–	–	–	–	–	–	–	–	–
870(b)	4, 15	0.113	0.092	–	–	0.175	0.138	0.112	0.090	0.074	0.065	0.058	–
Second Temperature Cycle													
1095	1, 0	–	0.122	0.31	–	0.171	0.141	0.123	0.103	0.085	0.077	0.069	–
1223	1, 10	0.154	0.139	0.33	–	0.180	0.147	0.128	0.108	0.090	0.082	0.073	0.068
1370	1, 0	0.174	0.150	0.32	0.218	0.190	0.153	0.132	0.112	0.096	0.084	0.076	0.070
1640	1, 45	0.193	(c)	0.33	0.253	0.203	0.167	0.144	0.123	0.107	0.094	0.087	0.080

(a) Determined from optical pyrometer readings.
(b) Directional emittance data obtained at these temperatures.
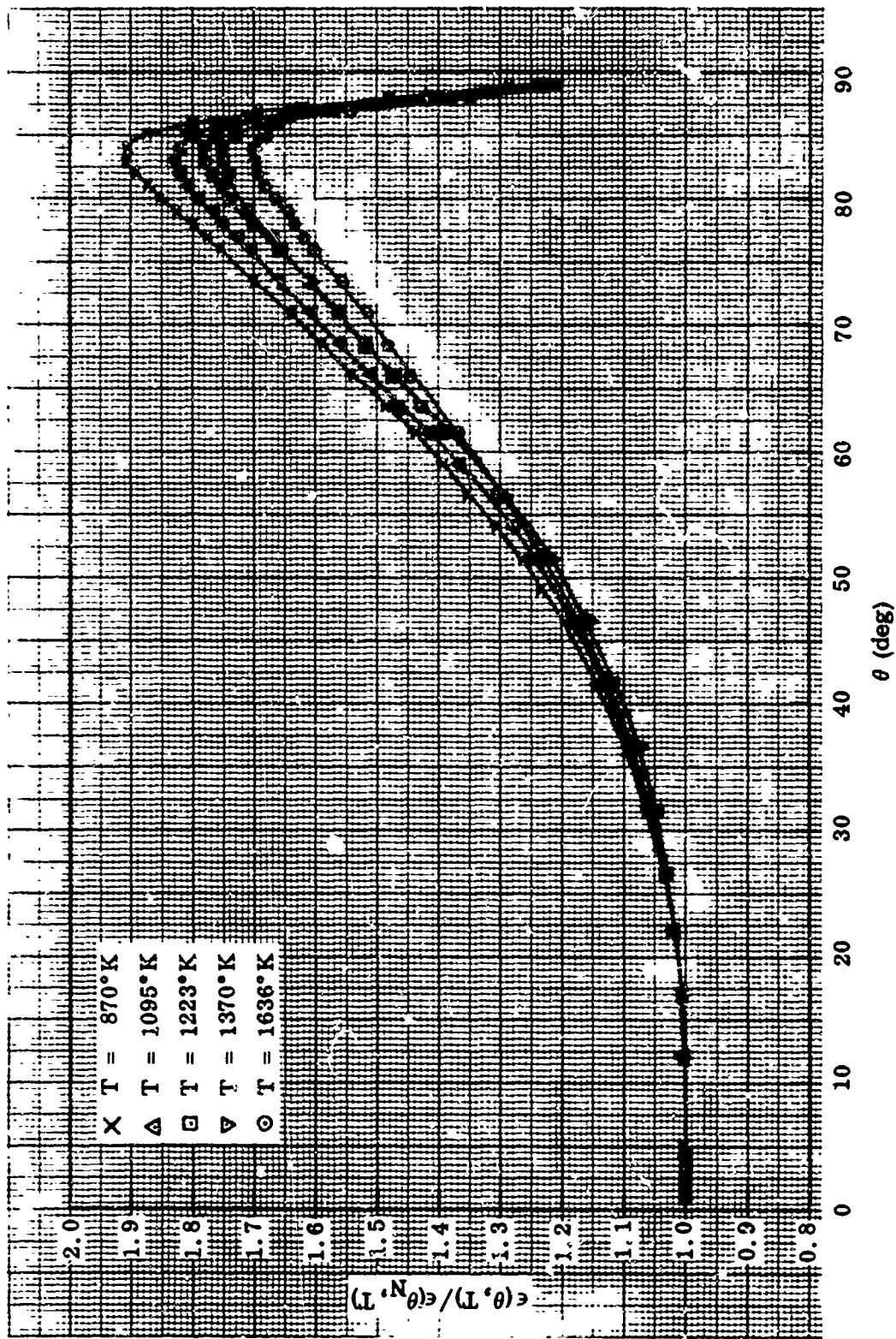(c) Erroneous data; see Remarks.

150

Figure 76 Relative Total Directional Emittance, Platinum Sample No. 6B
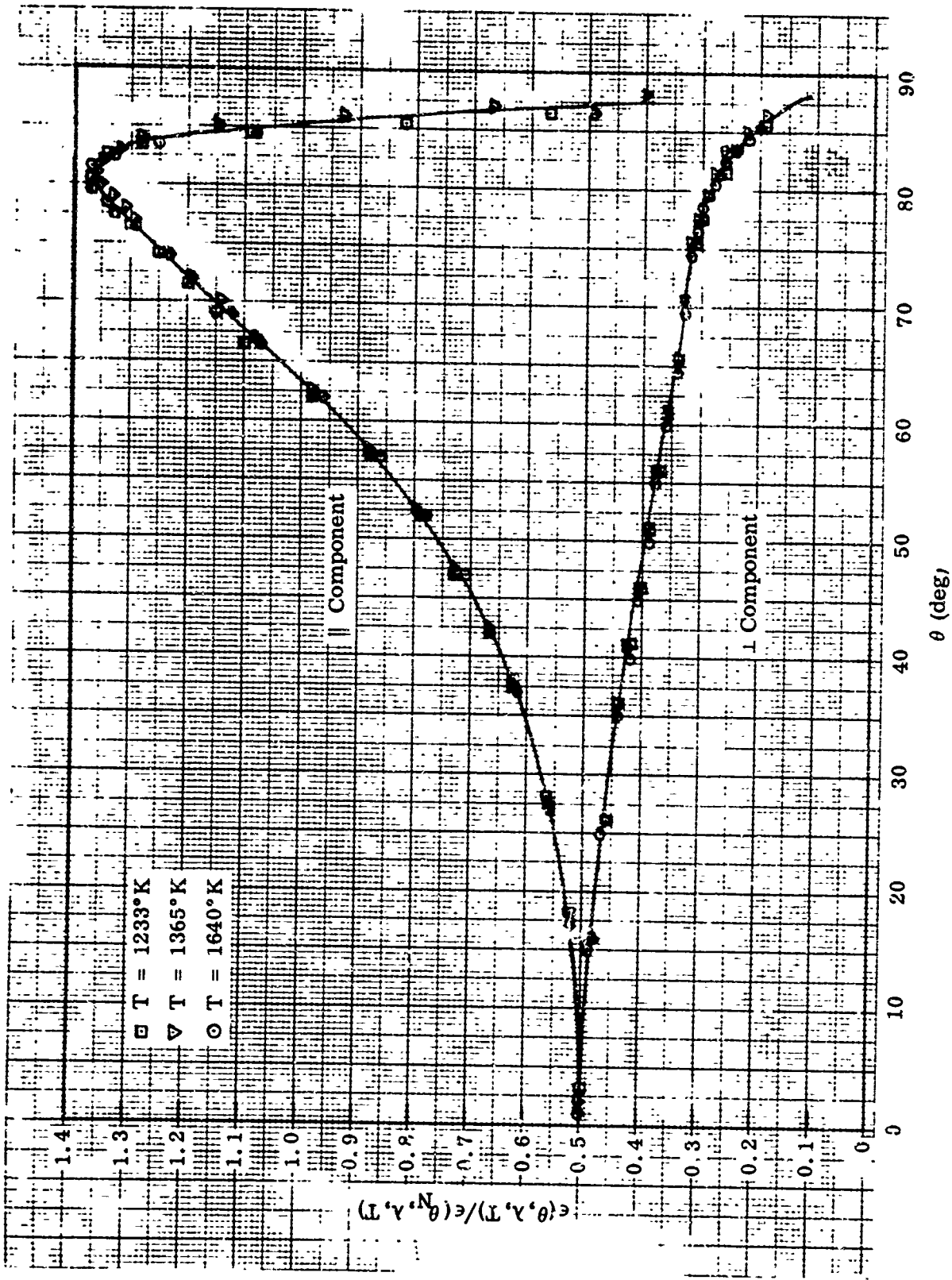
151

Figure 77 Relative Spectral Directional Emittance at $\lambda = 1.5\ \mu$, Platinum Sample No. 6B
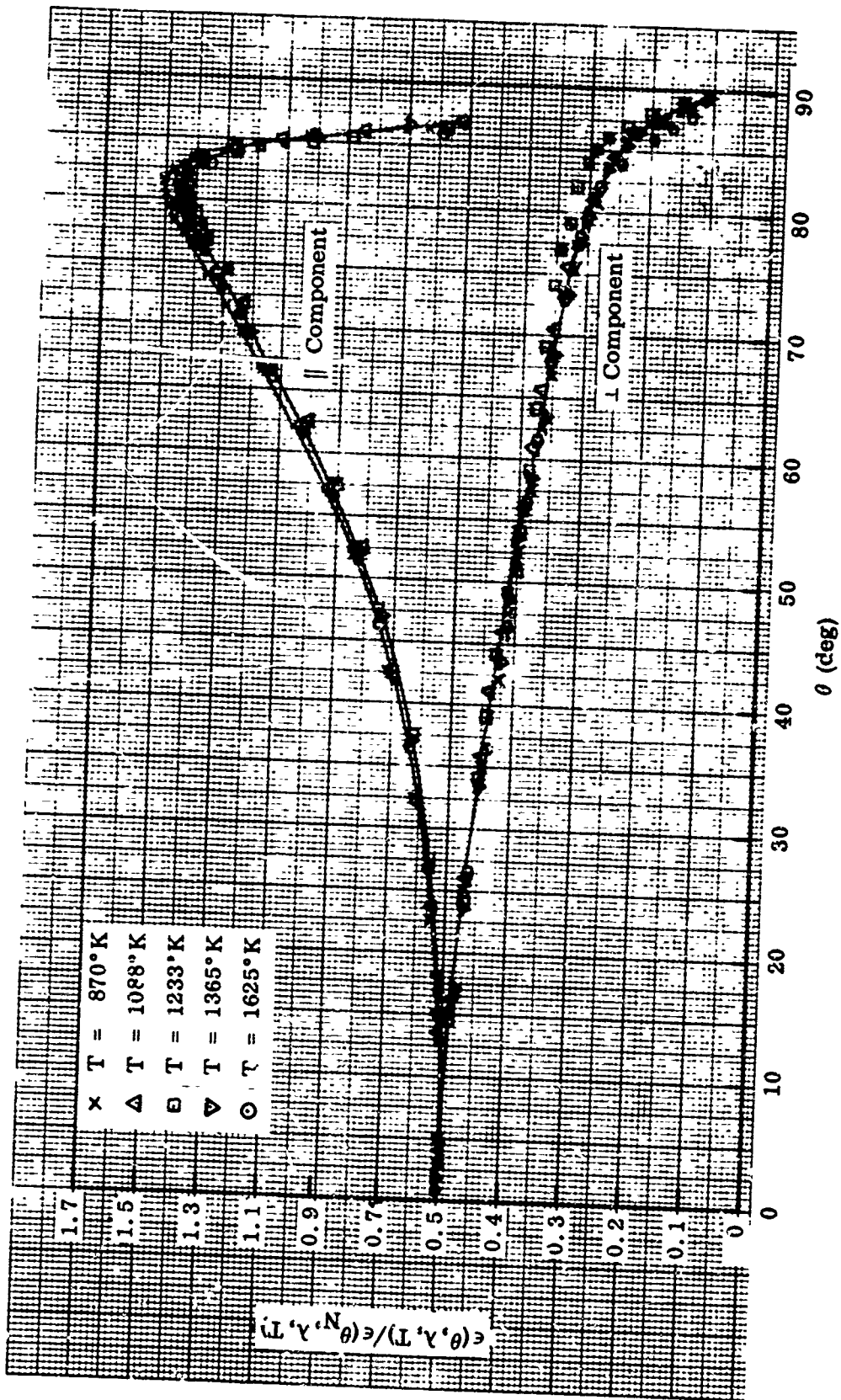
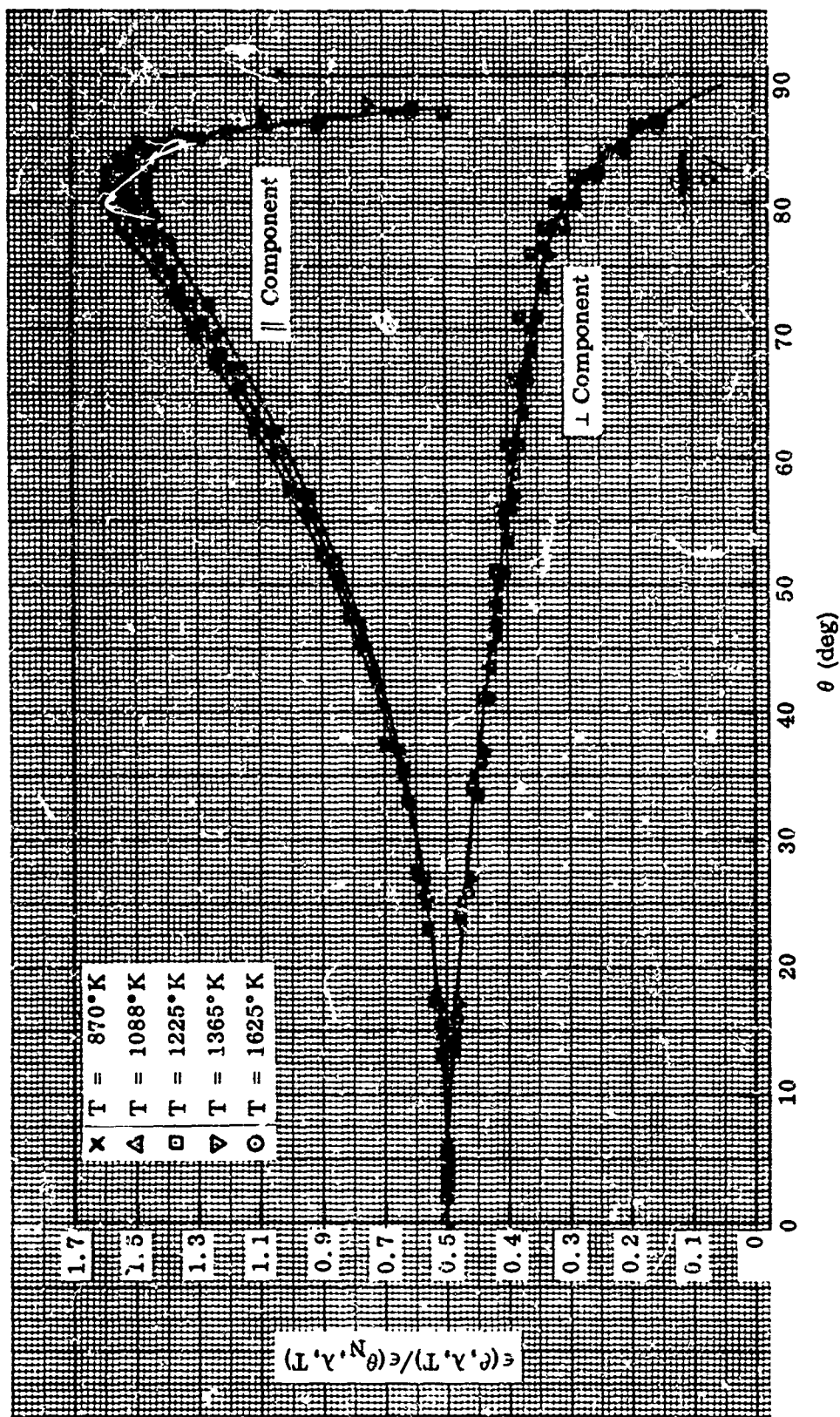Figure 78 Relative Spectral Directional Emittance at $\lambda = 2\,\mu$, Platinum Sample No. 6B

153

Figure 79 Relative Spectral Directional Emittance at $\lambda = 3\,\mu$, Platinum Sample No. 6B
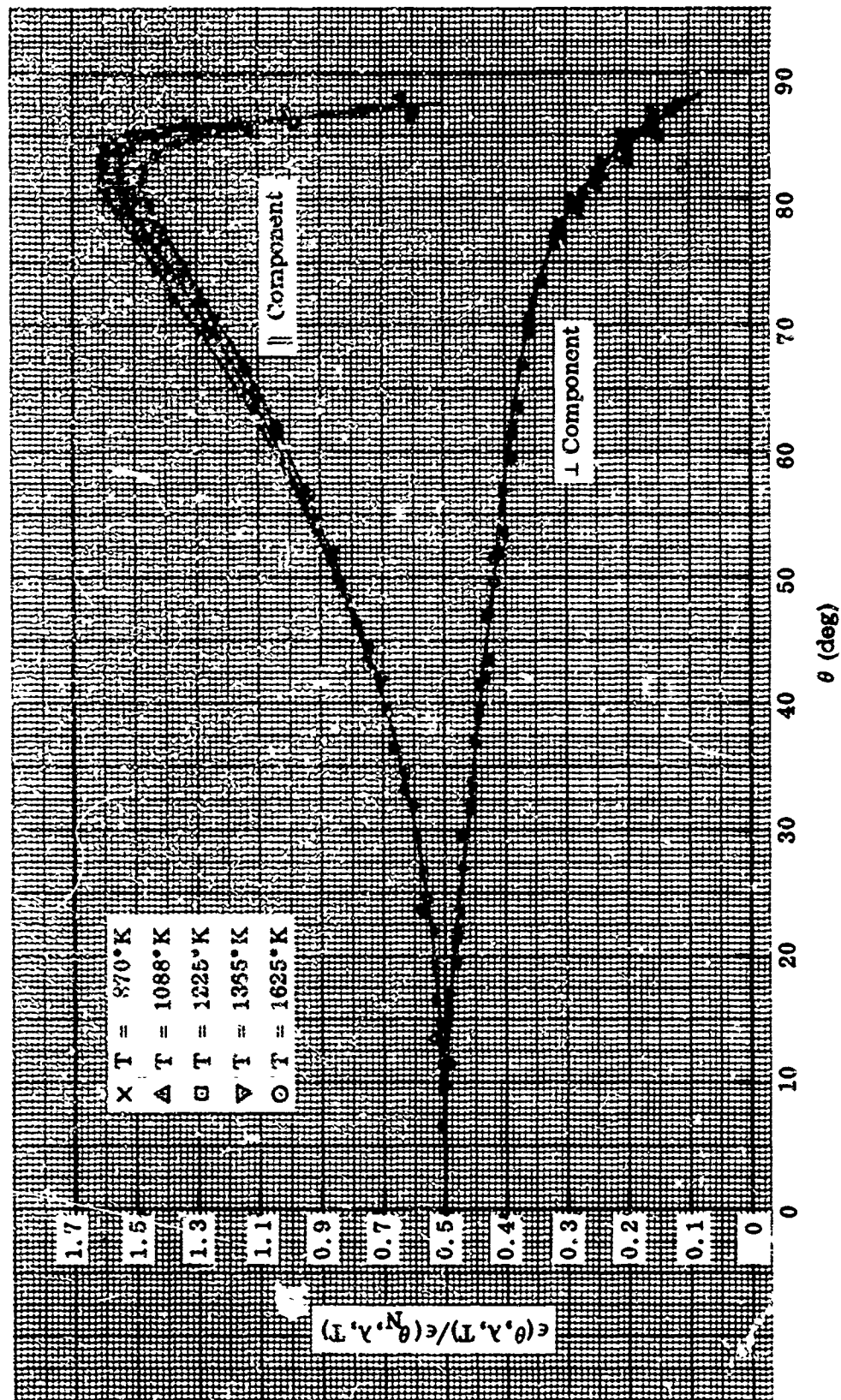
154

Figure 80 Relative Spectral Directional Emittance at $\lambda = 4\ \mu$, Platinum Sample No. 6B
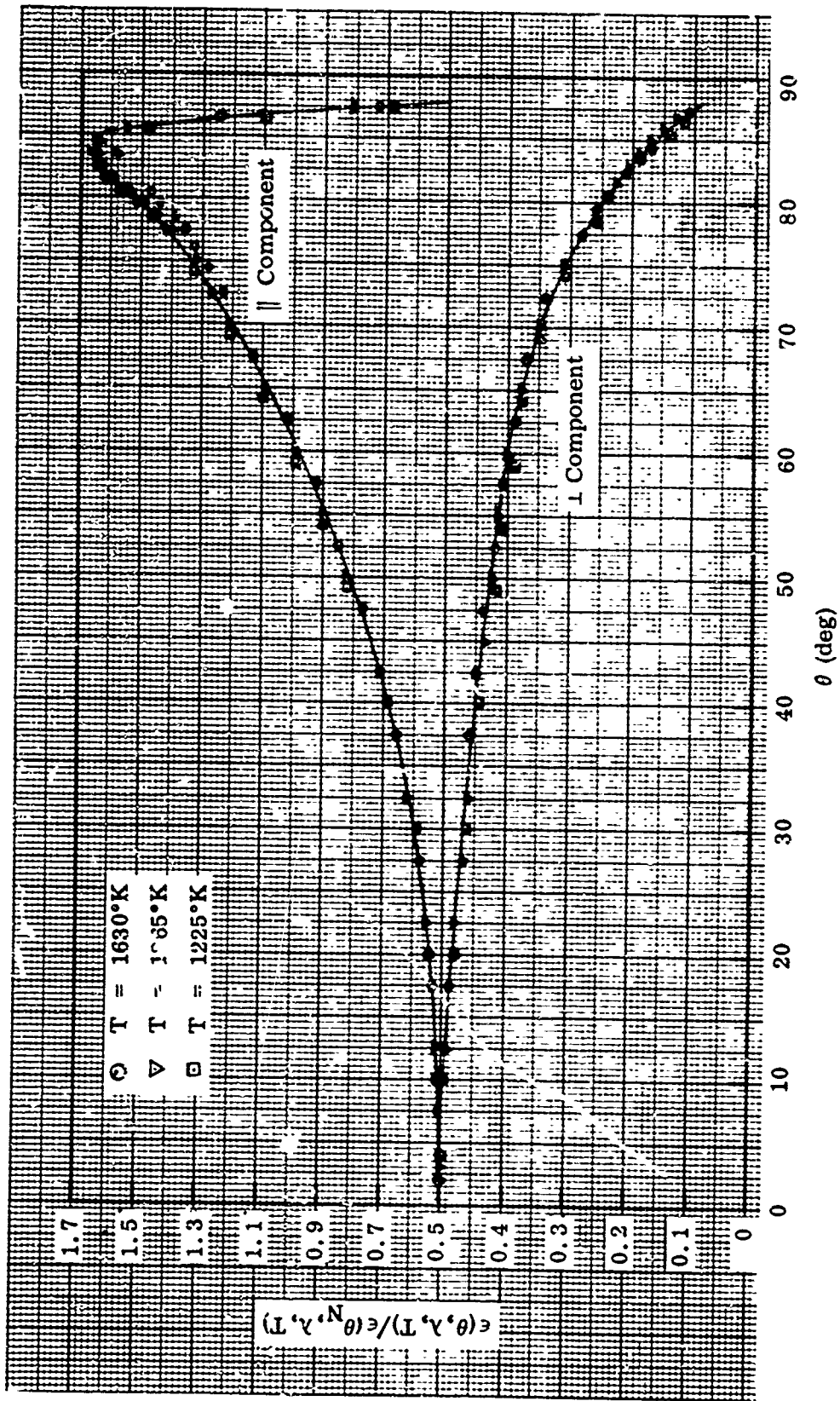
155

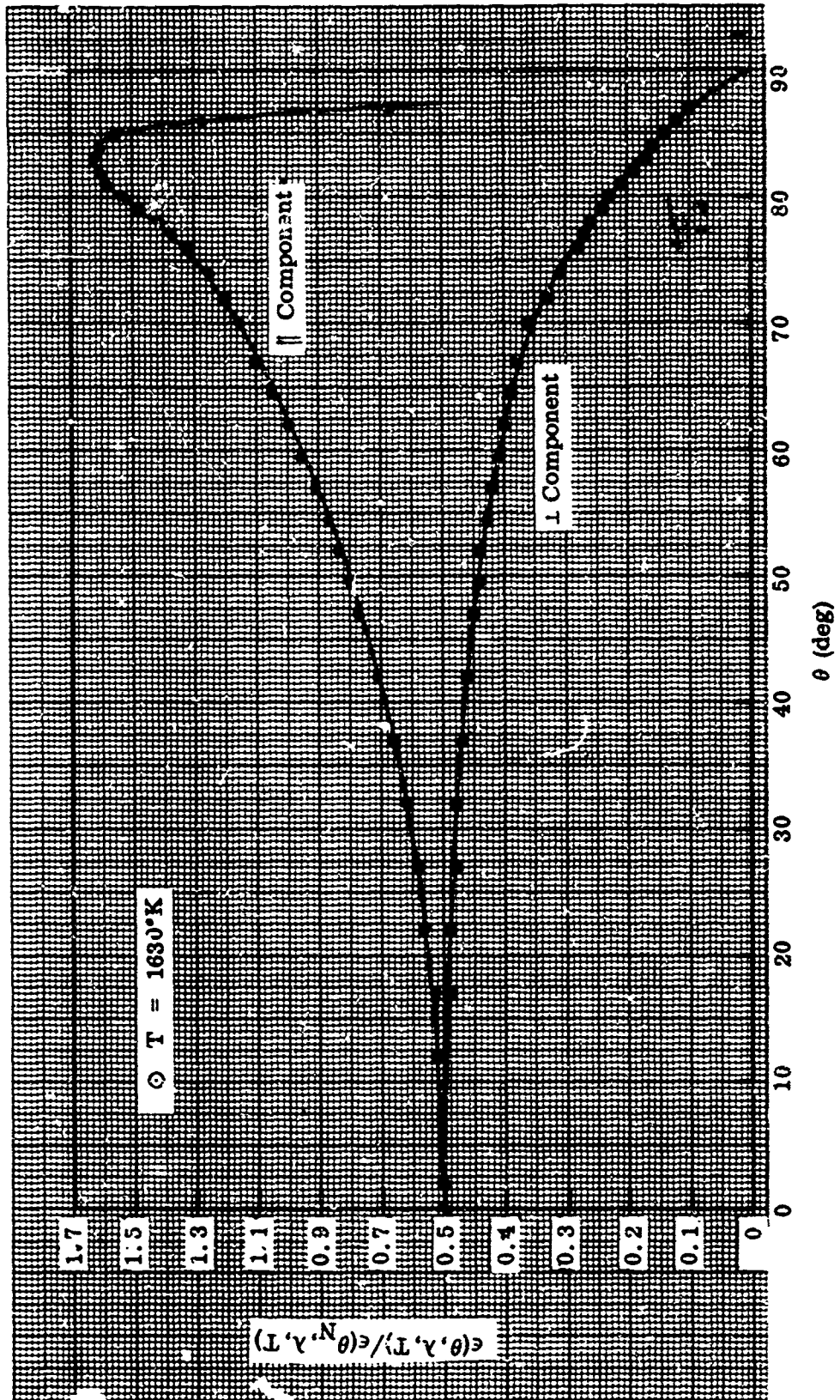Figure 81 Relative Spectral Directional Emittance at $\lambda = 6\,\mu$, Platinum Sample No. 6B

156

Figure 82 Relative Spectral Directional Emittance at $\lambda = 8\ \mu$, Platinum Sample No. 6B

157

6. STAINLESS STEEL SAMPLE No. 1S-2

Preparation: Unoxidized, electropolished and annealed by the method described in subsection III.2.a.

RMS Roughness: Before emittance tests: 13 μin. (independent of direction). After emittance tests: not measured; surface oxidized.

Test Procedure: Absolute emittance data were obtained at 532, 675, 811, and 955°K (first temperature cycle). The sample surface was visually inspected and appeared bright and clean, i.e., unoxidized. Absolute and relative directional emittance data were then obtained at the same test temperatures (second temperature cycle), and the absolute and relative total directional emittances of the sample at 946°K were rechecked after the directional emittance tests. An inspection of the sample surface showed that a light-blue oxide film had formed. Absolute emittance values at 537, 673, and 808°K were remeasured (third temperature cycle) to determine the change in sample emittance characteristics due to sample oxidation. A test chamber pressure of 2.5×10^{-6} Torr was maintained throughout all tests.

Emittance Data: Absolute emittance values are shown in Table XIX; relative total directional emittance data in Figure 83; relative spectral directional emittance data at $\lambda = 1.5$, 2, 3, 4, and 6 μ in Figures 84 through 88.

Remarks: This sample was the second of three smooth, unoxidized stainless steel samples tested; test data for the first are not presented because the surface oxidized during a pretest anneal at 1090 °K. The absolute emittance values obtained during the first test-temperature cycle of this sample are believed to be representative of electropolished, unoxidized stainless steel. After the first temperature cycle, the surface appeared to be unchanged from its initial bright finish. Spectral normal emittance values obtained during the second test temperature cycle, however, indicate that sufficient surface oxidation occurred to cause a slight rise in spectral normal emittance values at 1.5 and 2 μ. Following the 808°K tests, it appears that further oxidation occurred, sufficient to produce a significant rise in the total hemispherical, total normal, and spectral normal emittance values out to 4 μ. Still further oxidation occurred during the 946°K tests, as indicated by the emittance data obtained at the end of the second temperature cycle and during the third temperature cycle. After the emittance tests the center portion of the sample surface was covered with a uniform, light-blue oxide film.

The change in relative total directional emittance due to further oxidation during the 946°K tests is shown in Figure 83. Most of the change in relative spectral directional emittance is also attributed to the surface oxidation that occurred at this temperature. Absolute and directional emittance data characteristic of unoxidized stainless steel at 945°K were obtained later from a third sample. (See data for sample 1S-3, subsection VII.14.)

Photomicrographs, electron micrographs, and a surface interference micrograph of this sample are shown in Figures 30, 31, and 32, respectively, and are discussed in subsection V.2.a. The thickness of the light-blue oxide film was not determined but its relative total directional emittance characteristics indicate a thickness between 0.015 and 0.17 μ. From the color-versus-thickness data reported by Gulbransen and Andrew (Ref. 32) for oxide films on 304 stainless steel, the thickness of blue-colored films appears to be between 0.020 and 0.080 μ.

An electron diffraction pattern of the oxide is shown in Figure 36. Most of the principal diffraction lines were identified with the pattern for Fe_3O_4, but numerous additional lines were not identified.

Table XIX. Absolute Emittance Data for Stainless Steel Sample No. 1S-2

Temperature (°K)	Time at Temp. (hr, min)	$\epsilon(T)$	$\epsilon(\theta_N, T)$	$\epsilon(\theta_N, \lambda, T)$							
				1.5 μ	2 μ	3 μ	4 μ	6 μ	8 μ	10 μ	12 μ
First Temperature Cycle											
532	0,45	0.151	0.118								
675	0,30	0.168	0.145								
811	0,45	0.187	0.169	0.271	0.240	0.206	0.177	0.146	0.121	0.104	0.084
955	0,35	0.206	0.187	0.290	0.251	0.215	0.183	0.155	0.130	0.110	0.095
Second Temperature Cycle[a]											
539[b]	0,45	0.151	0.119								
677[b]	0,30	0.169	0.148								
807[b]	3,15	0.187	0.171	0.290	0.253	0.210	0.180	0.148	0.123	0.104	0.087
946[b]	3,50	0.211	0.205	0.353	0.289	0.230	0.195	0.157	0.130	0.111	0.098
948[b]		0.225	0.226	0.431	0.334	0.257	0.209	0.161	0.134	0.116	0.097
Third Temperature Cycle[c]											
537	0,45	0.149	0.125								
673	0,40	0.169	0.157								
808	0,25	0.198	0.196								

(a) Surface appeared to be unoxidized at start of second temperature cycle.
(b) Directional emittance data obtained at these temperatures.
(c) Sample oxidized during 946° K emittance tests at end of second temperature cycle.
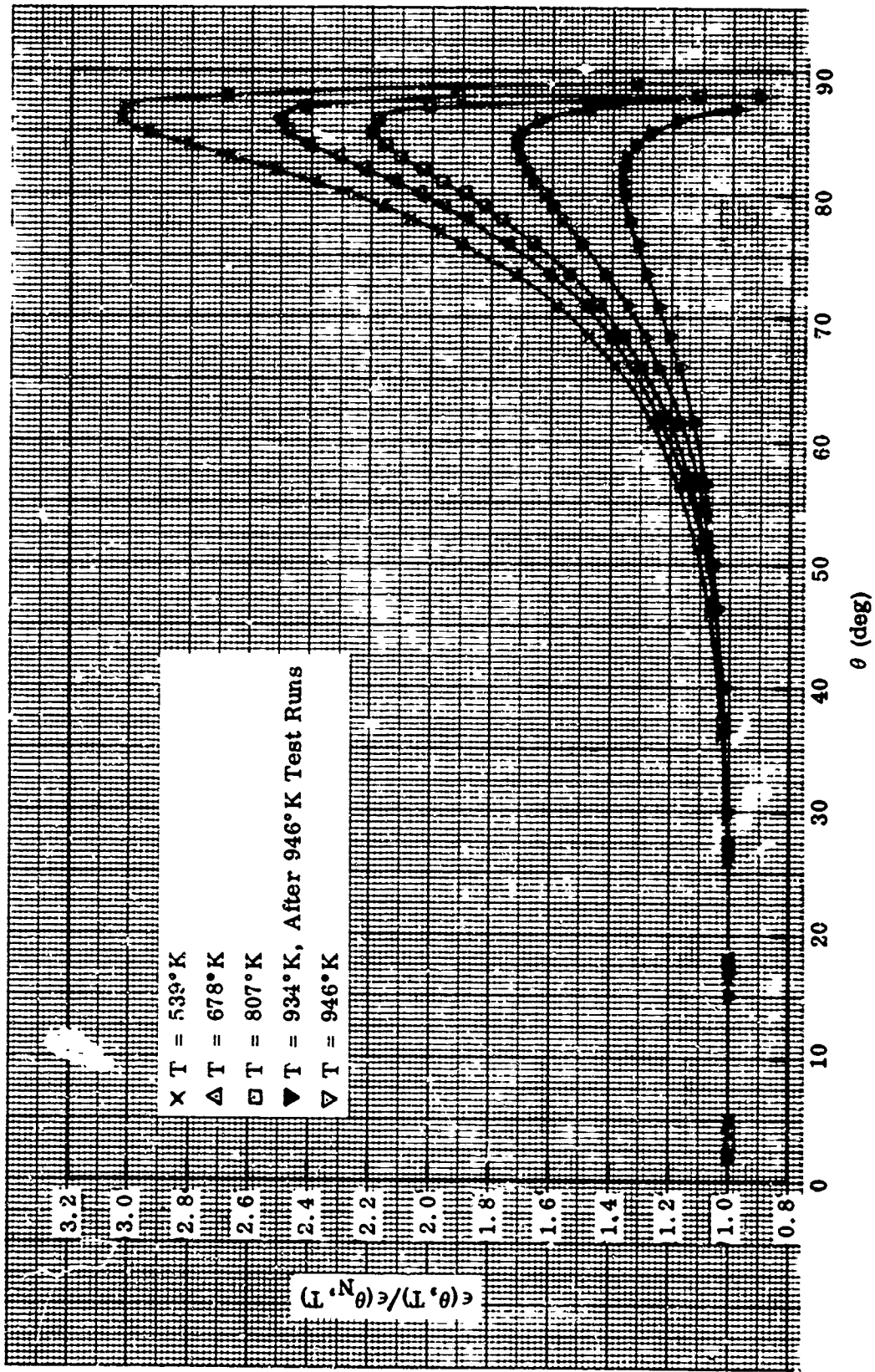
Figure 83 Relative Total Directional Emittance, Stainless Steel Sample No. 1S-2
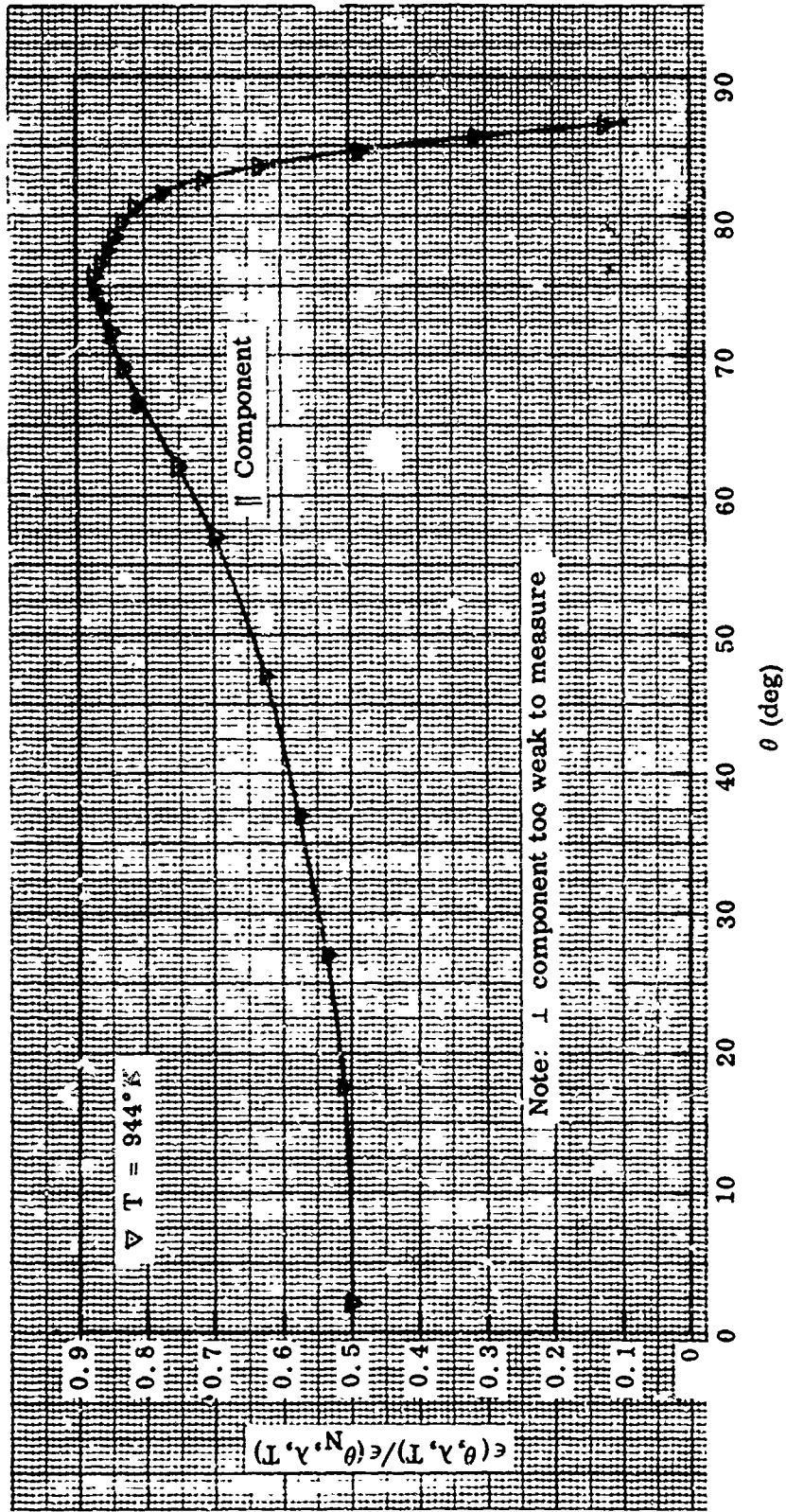
161

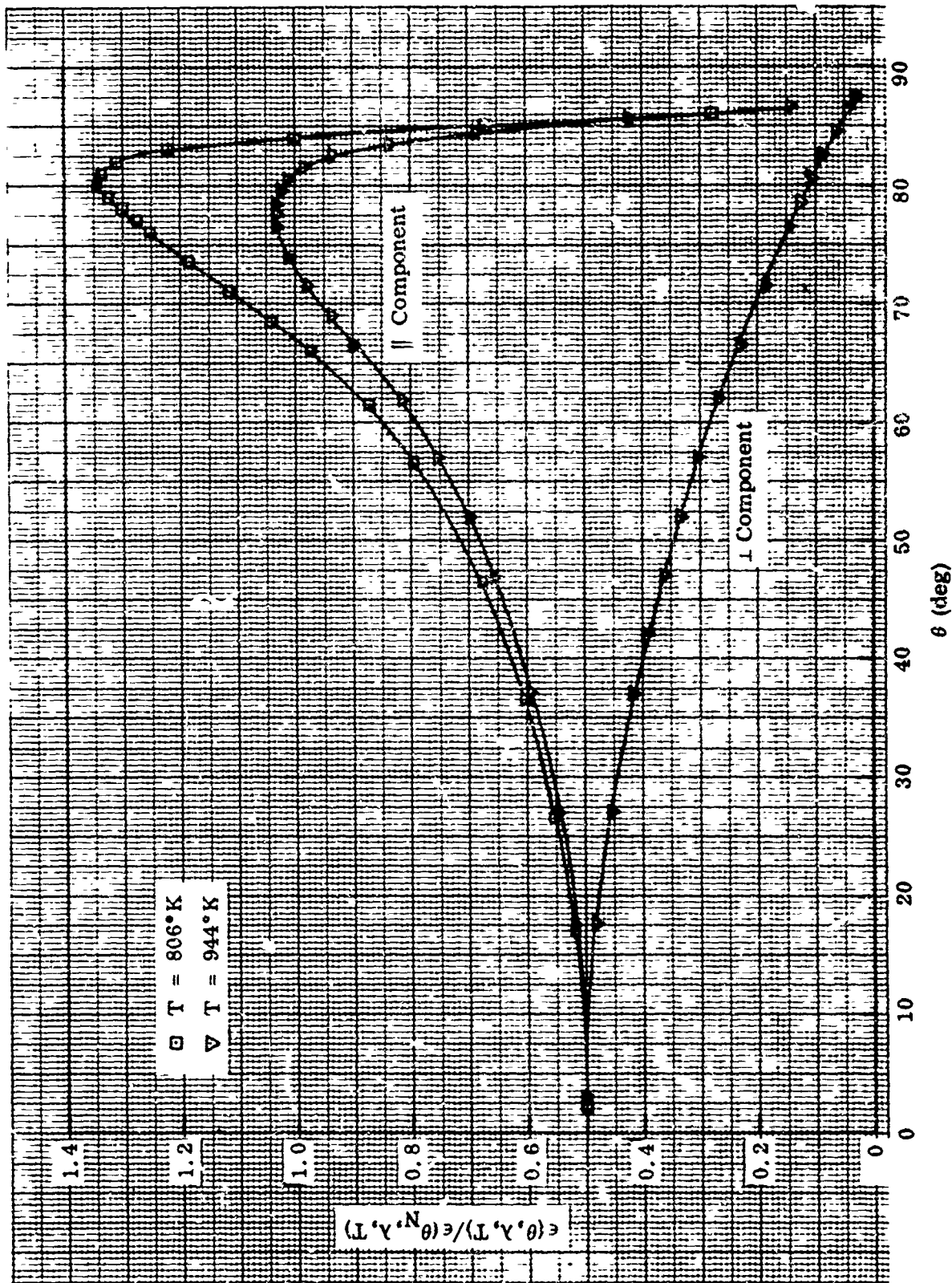Figure 84 Relative Spectral Directional Emittance at $\lambda = 1.5~\mu$, Stainless Steel Sample No. 1S-2

162

Figure 85 Relative Spectral Directional Emittance at $\lambda = 2\ \mu$, Stainless Steel Sample No. 1S-2
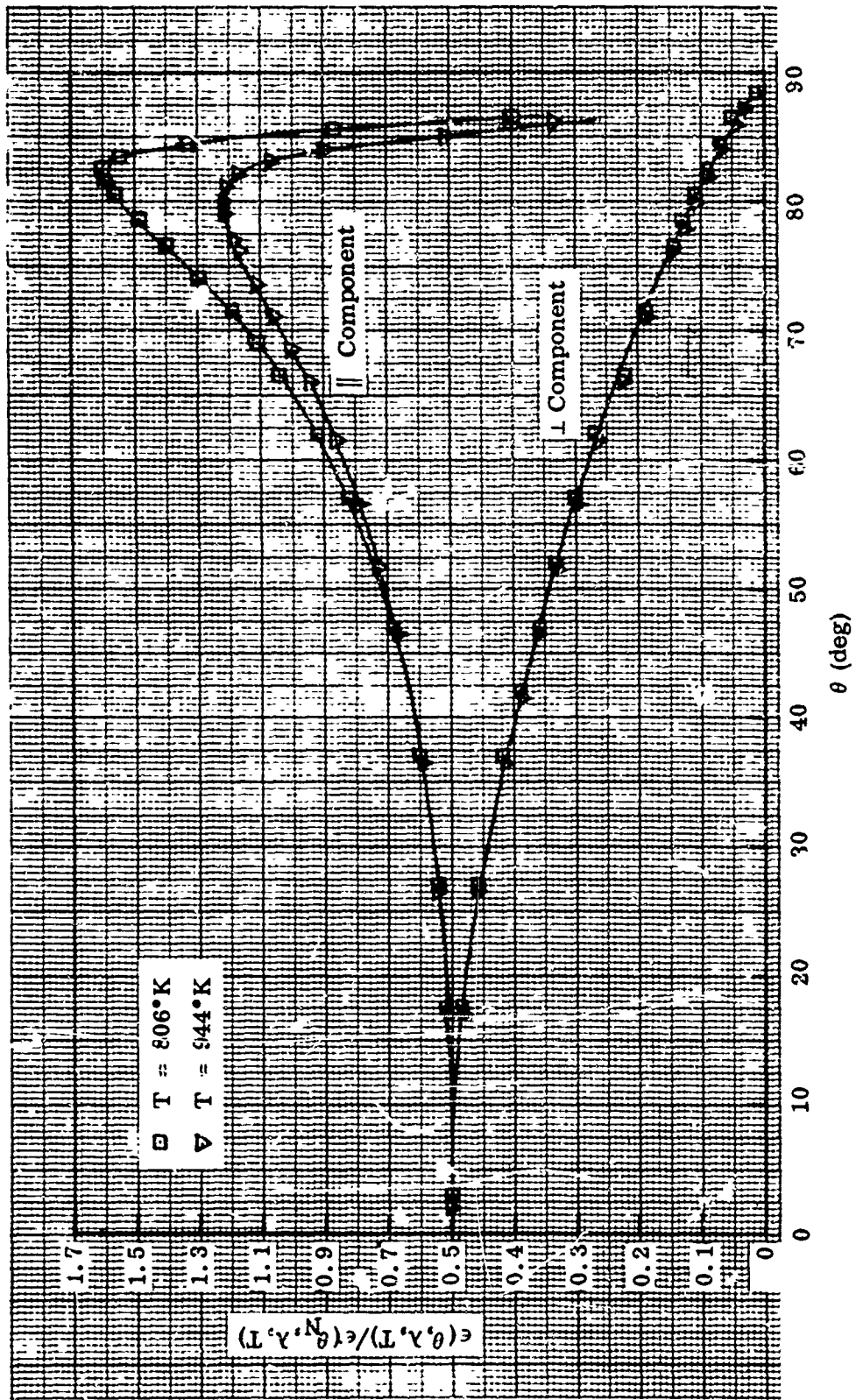
163

Figure N6 Relative Spectral Directional Emittance at $\lambda = 3\ \mu$, Stainless Steel Sample No. 1S-2
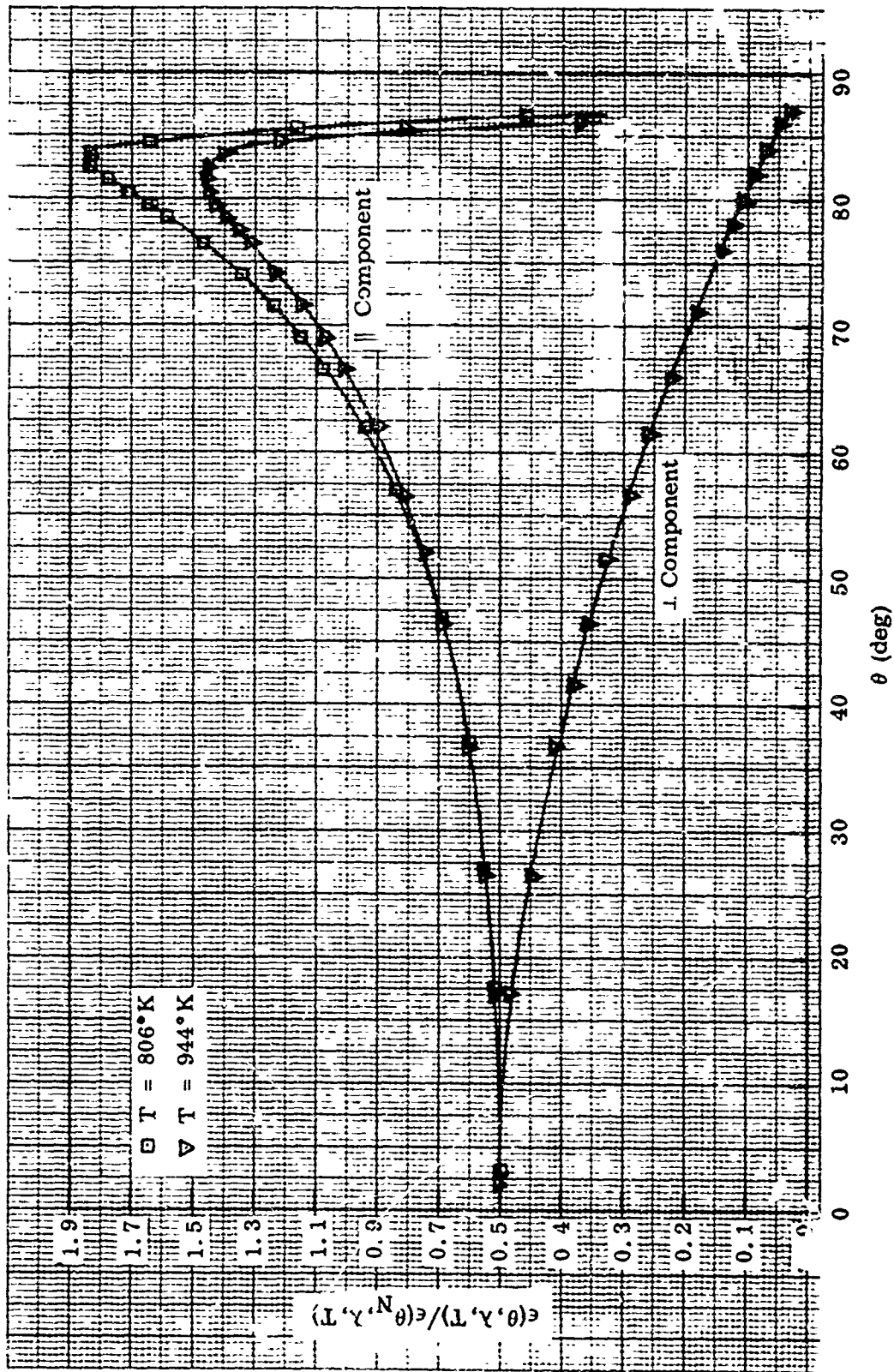
164

Figure 87 Relative Spectral Directional Emittance at $\lambda = 4 \mu$, Stainless Steel Sample No. 1S-2
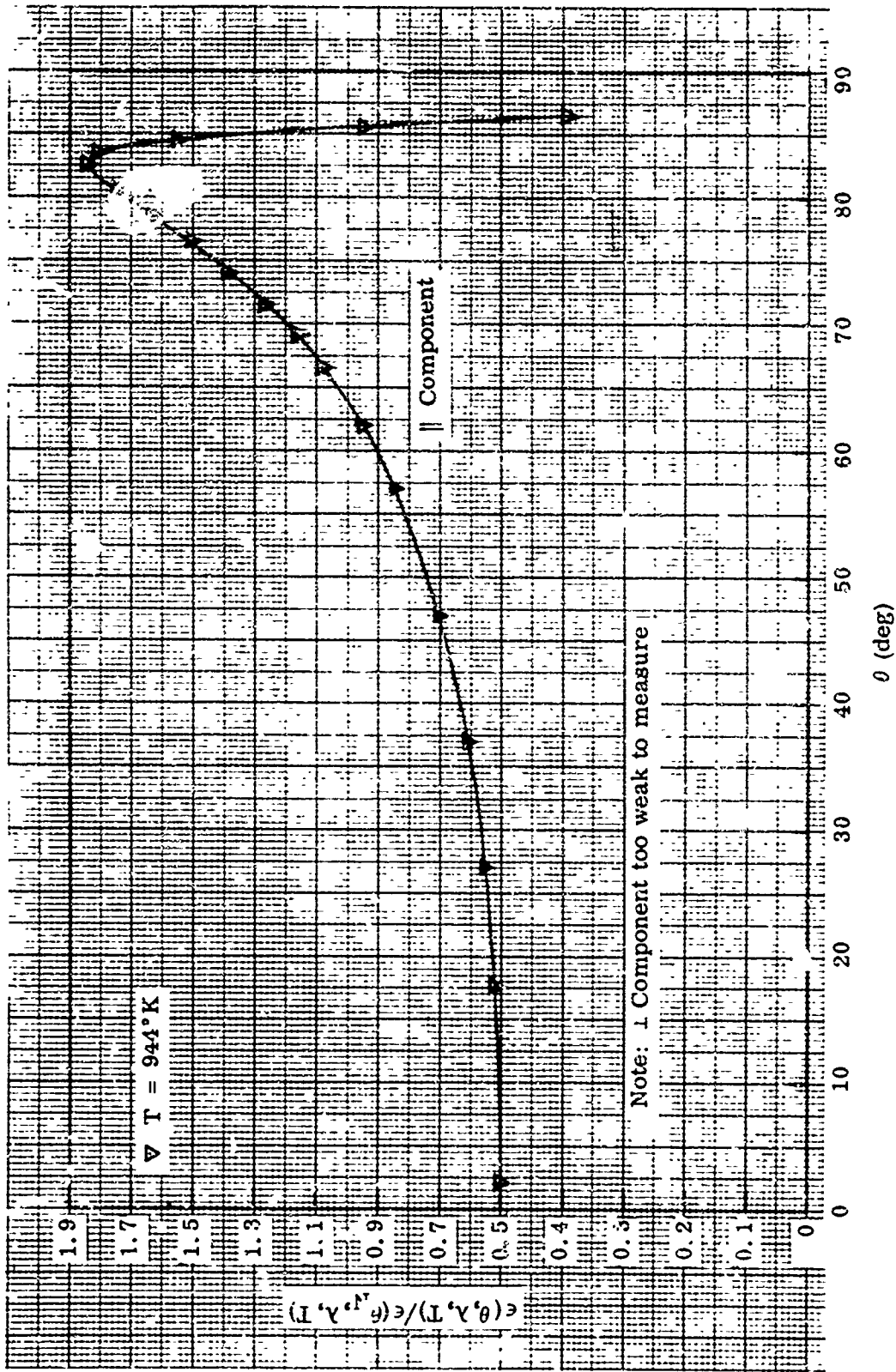
165

Figure 85 Relative Spectral Directional Emittance at $\lambda = 6 \mu$, Stainless Steel Sample No. 1S-2

166

7. STAINLESS STEEL SAMPLE NO. 2S

Preparation: Oxidized for 1/2 hr at 800°C in wet hydrogen furnace.

Initial Oxide Film Characteristics: Color: gold (interference film). Composition: primarily Fe_3O_4. Average thickness: 0.015 μ (based on weight gain data).

Test Procedure: Absolute and relative directional emittance data were obtained at 532, 673, 810, 952, and 1087°K (first temperature cycle), and the absolute emittance at 1081°K was rechecked at the conclusion of the directional emittance tests. An inspection of the sample showed the color of the oxide film had changed from gold to silvery gray. Absolute emittance values at 534, 668, 803, and 940°K were remeasured, and the relative total directional emittance at 534 and 811°K was rechecked (second temperature cycle) to determine the change in sample emittance characteristics due to the change in the oxide film. A test chamber pressure of 4×10^{-6} Torr was maintained throughout all tests.

Emittance Data: Absolute emittance values are shown in Table XX; relative total directional emittance data before and after the 1080°K tests in Figures 89 and 90, respectively; relative spectral directional emittance data at λ = 1.5, 2, 3, 4, 6, and 8 μ in Figures 91 through 96.

Remarks: The absolute and relative directional emittance data obtained during the first test temperature cycle are believed to be characteristic of the initial surface of the sample (i.e., the gold-colored oxide film) up to 952°K. During the 952°K tests additional oxidation began to occur, and it continued at an increased rate through the 1087°K tests. The effect of the increased oxide film thickness on the absolute total and spectral emittance properties of the sample is clearly shown by the data obtained at the end of the first test temperature cycle and in the second temperature cycle. All the directional emittance data show a high sensitivity to the change in oxide film thickness. The sensitivity is clearly wavelength dependent, causing quite drastic changes in the directional emittance characteristics at short wavelengths and only slight changes at long wavelengths. (See subsection V.2.b.)

Photomicrographs and electron micrographs of the sample surface are shown in Figures 30 and 31, respectively, and are discussed in subsection V.2.a. These micrographs show the initial gold-colored oxide film to be intermediate in appearance to the pre-test and post-test surfaces of sample 1S-2. The thickness of the silvery-gray oxide film on the post-test surface was not determined, but its relative total directional emittance characteristics (Figure 90) indicate a thickness about the same as that of the light-blue film that formed on sample 1S-2. The silvery-gray color seems to correspond with the "silvery hiatus" mentioned by Kubaschewski in (31).

An electron diffraction pattern of the initial gold-colored oxide film is shown in Figure 36. Most of the principal diffraction lines were identified with the pattern for Fe_3O_4; a few additional lines present were not identified. The diffraction pattern for the silvery-gray film on the post-test surface was essentially the same as that for the gold-colored film.

Table XX. Absolute Emittance Data for Stainless Steel Sample No. 2S

Temperature (°K)	Time at Temp. (hr, min)	ε(T)	ε(θ_N, T)	$\epsilon(\theta_N, \lambda, T)$							
				1.5 μ	2 μ	3 μ	4 μ	6 μ	8 μ	10 μ	12 μ
First Temperature Cycle											
532[a]	1, 15	0.152	0.130								
673[a]	1, 45	0.173	0.153								
810[a]	2, 0	0.194	0.175	0.322	0.269	0.221	0.187	0.153	0.129	0.110	0.088
952[a]	3, 20	0.222	0.216	0.381	0.303	0.243	0.204	0.167	0.141	0.119	0.101
1087[a]	6, 0	0.250	0.272	0.600	0.413	0.302	0.243	0.190	0.157	0.132	0.114
1081		0.366	0.319	0.606	0.458	0.344	0.265	0.206	0.173	0.142	0.121
Second Temperature Cycle [b]											
534[a]	0, 50	0.192	0.153								
669	,30	0.233	0.195								
803[a]	2, 10	0.281	0.237	0.553	0.442	0.338	0.260	0.195	0.163	0.130	0.107
940	0, 35	0.345	0.306	0.640	0.487	0.359	0 277	0.206	0.174	0.140	0.117

(a) Directional emittance data obtained at these temperatures.
(b) Additional sample oxidation during the preceding tests at 952 and 1087° K changed the color of the oxide film from gold to silver-gray.
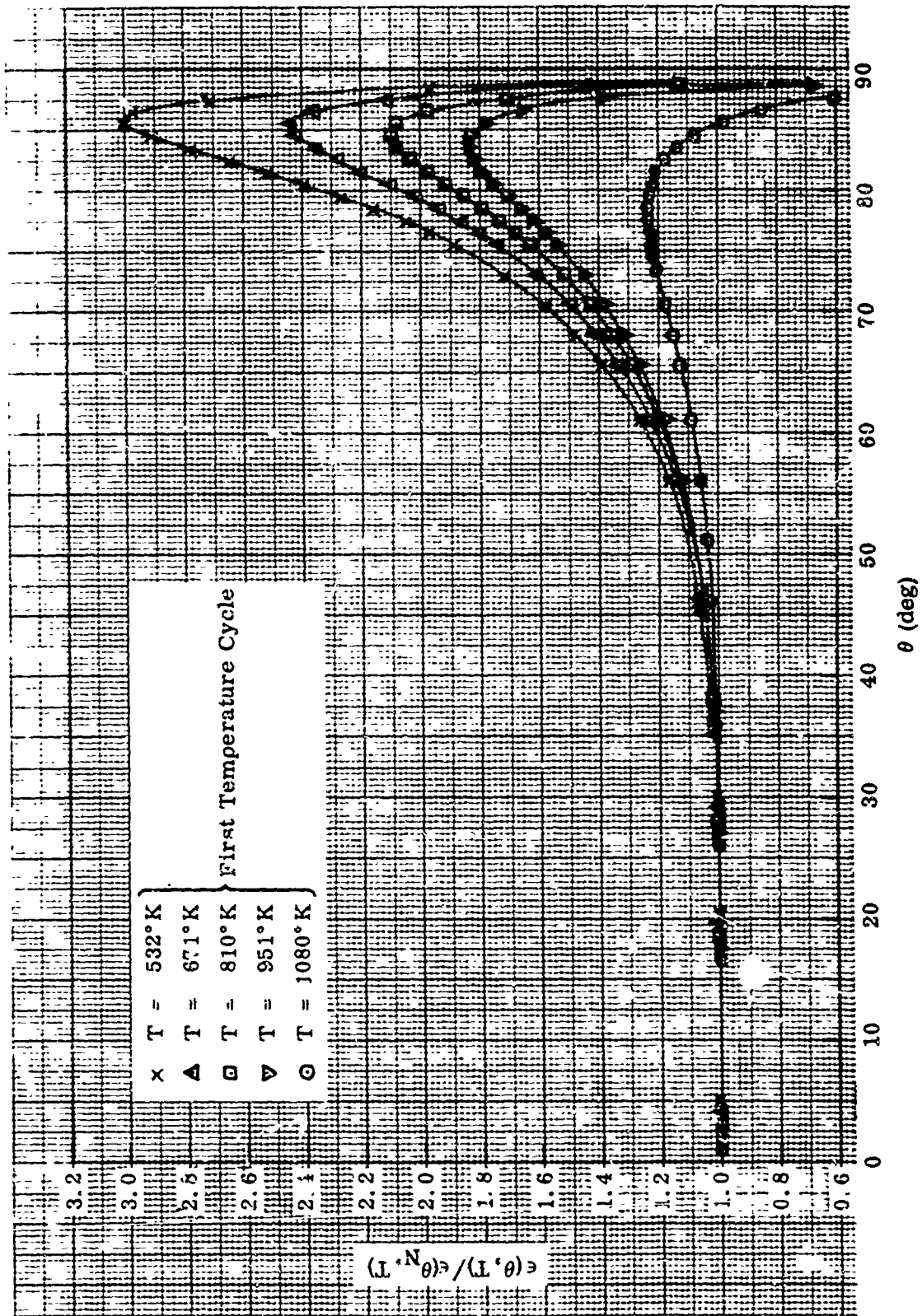
168

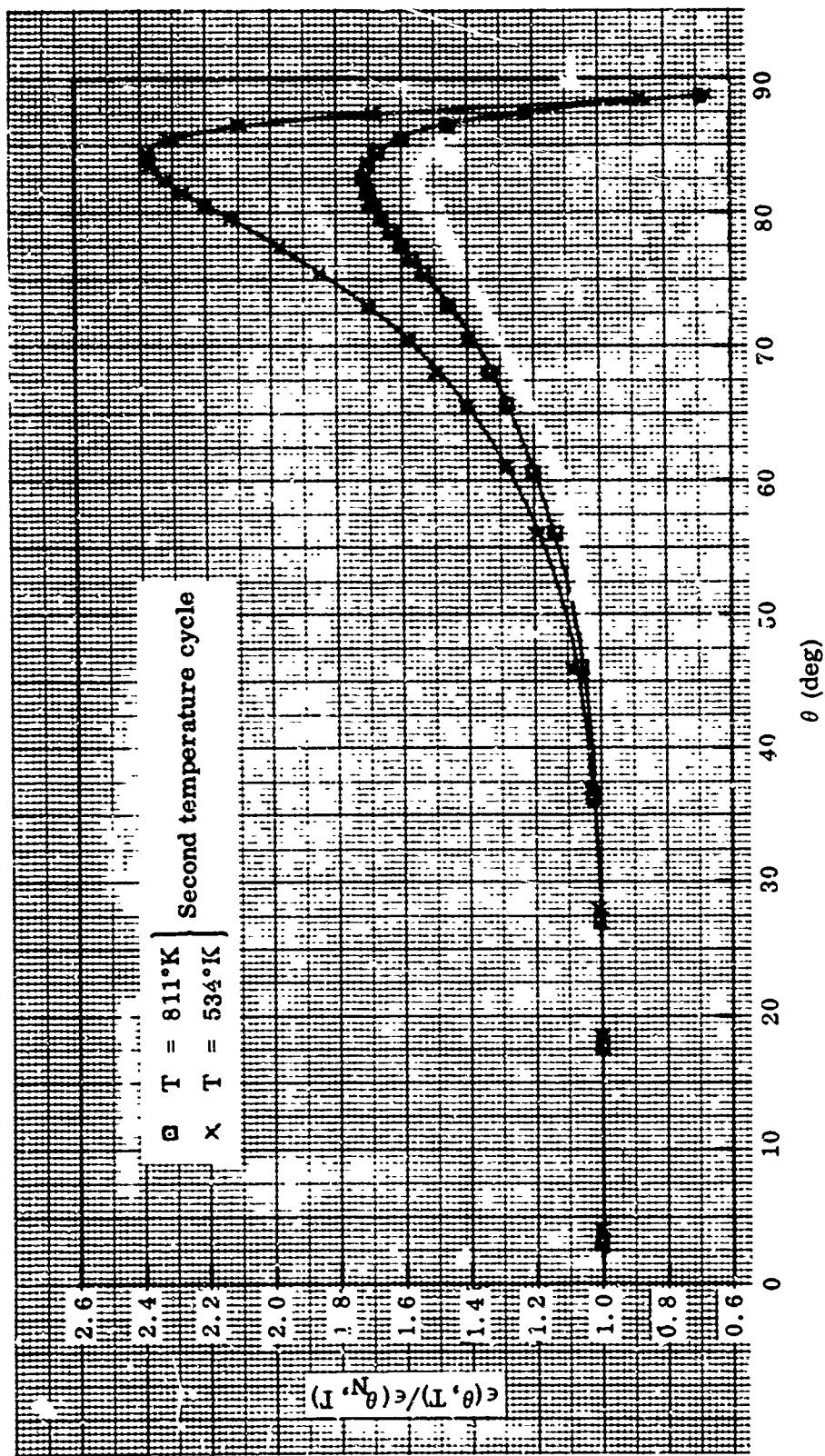Figure 89   Relative Total Directional Emittance Before 1080°K Tests, Stainless Steel Sample No. 2S

Figure 90 Relative Total Directional Emittance After 1080°K Tests, Stainless Steel Sample No. 2S
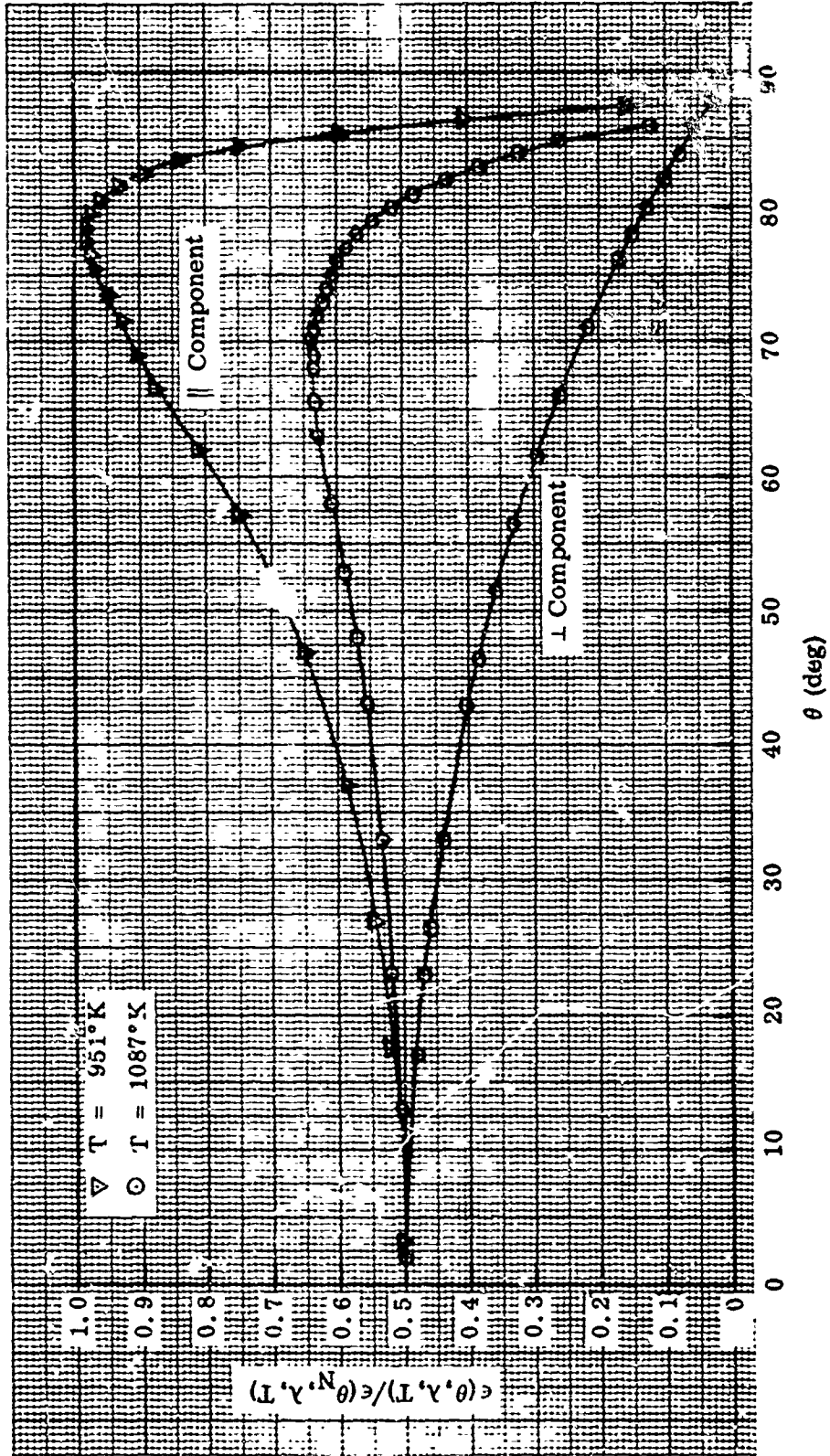
170

Figure 91 Relative Spectral Directional Emittance at $\lambda = 1.5\ \mu$, Stainless Steel Sample No. 2S
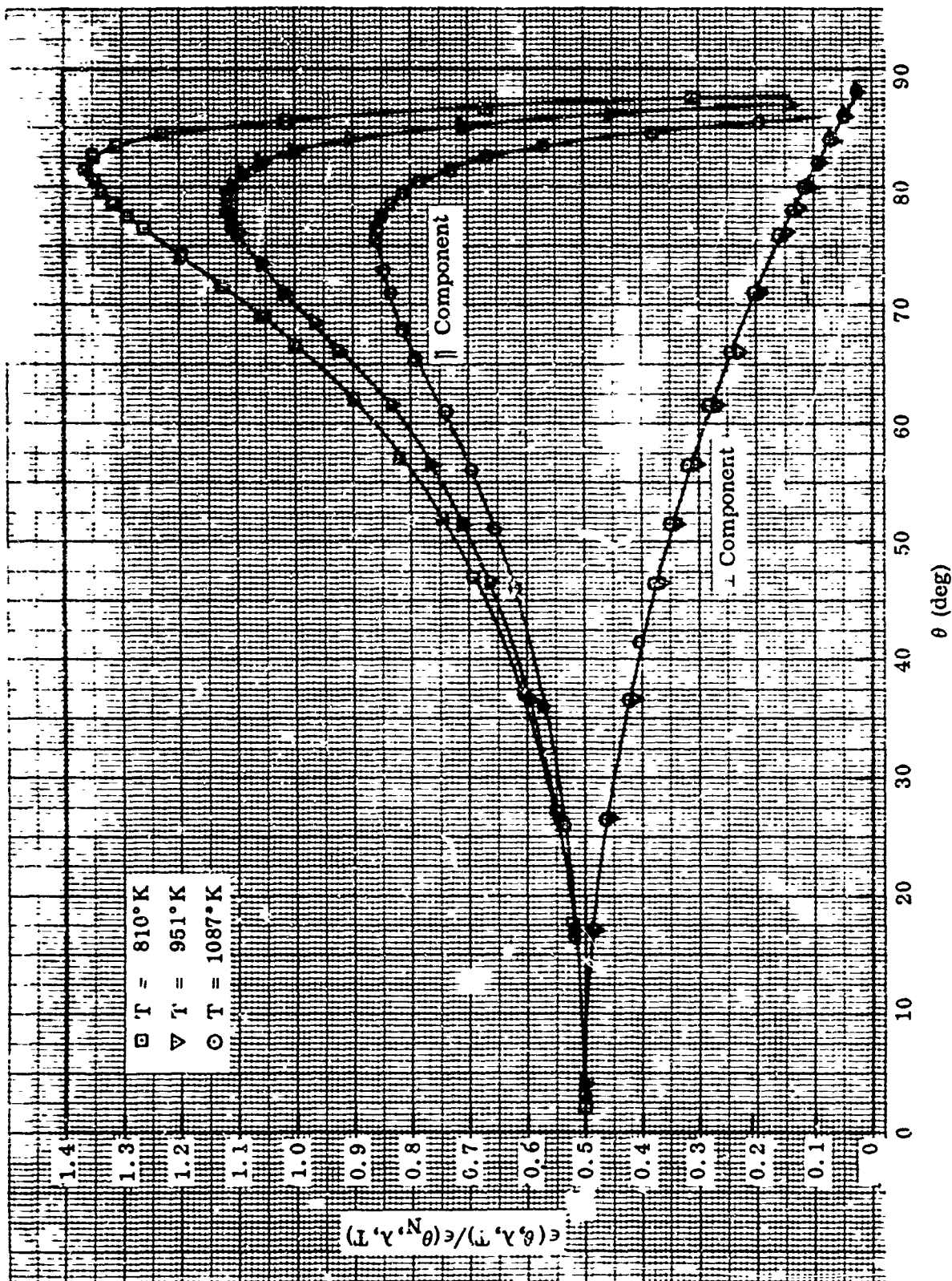
171

Figure 92 Relative Spectral Directional Emittance at $\lambda = 2\ \mu$, Stainless Steel Sample No. 2S

172

Figure 93 Relative Spectral Directional Emittance at $\lambda = 3\ \mu$, Stainless Steel Sample No. 2S

173

Figure 94 Relative Spectral Directional Emittance at $\lambda = 4\,\mu$, Stainless Steel Sample No. 2S

174

Figure 95   Relative Spectral Directional Emittance at $\lambda = 6\ \mu$, Stainless Steel Sample No. 2S

175

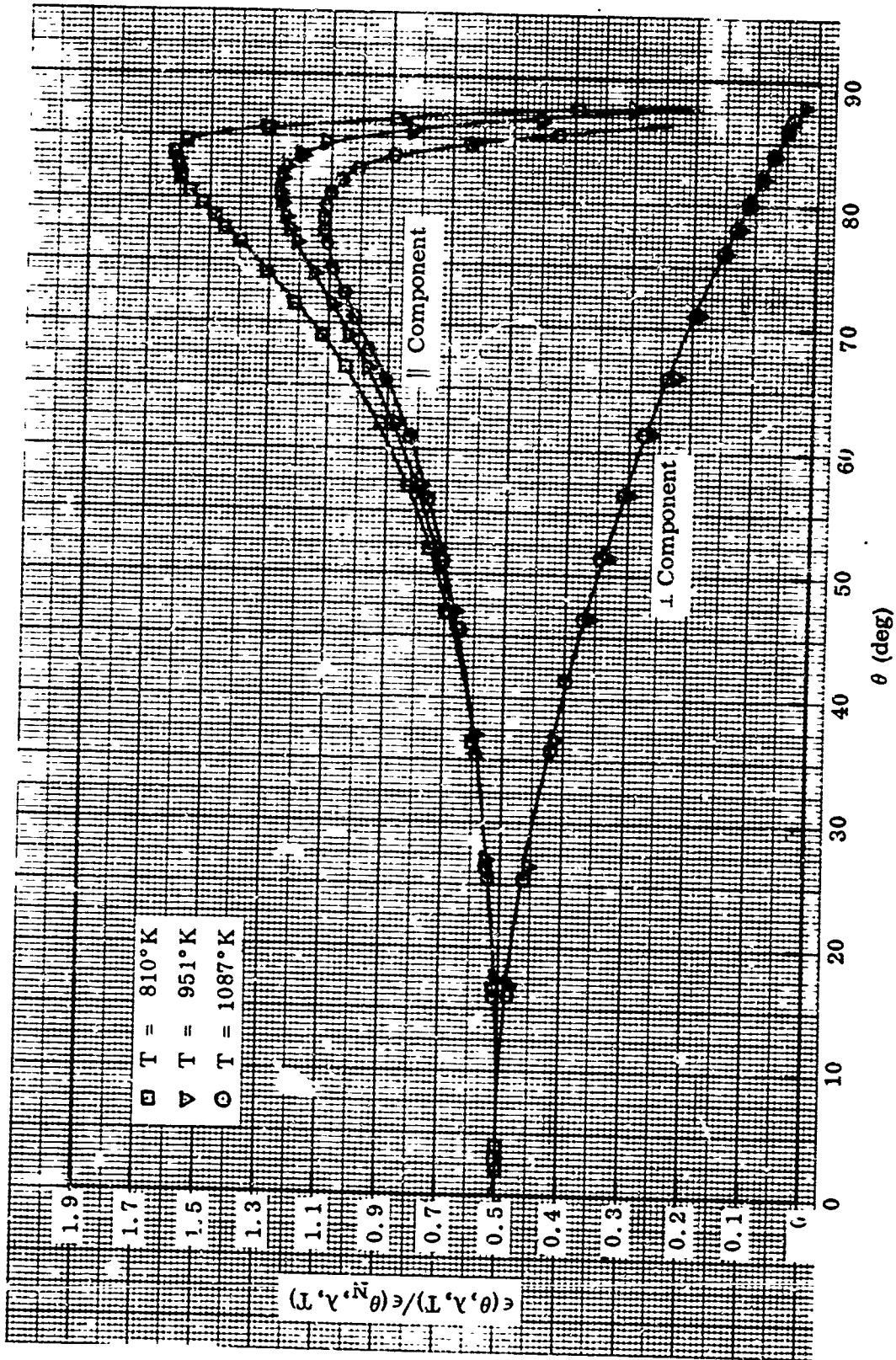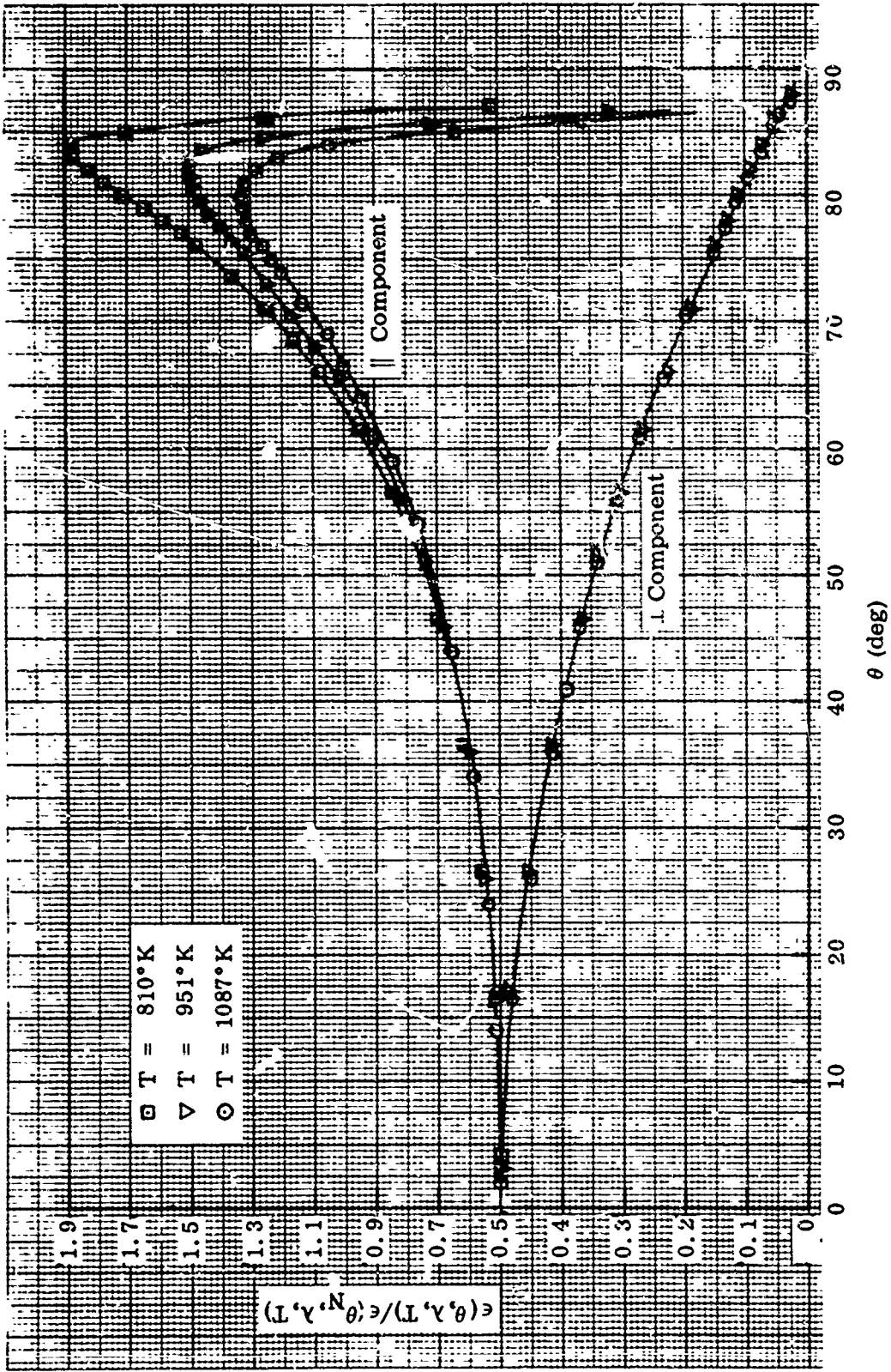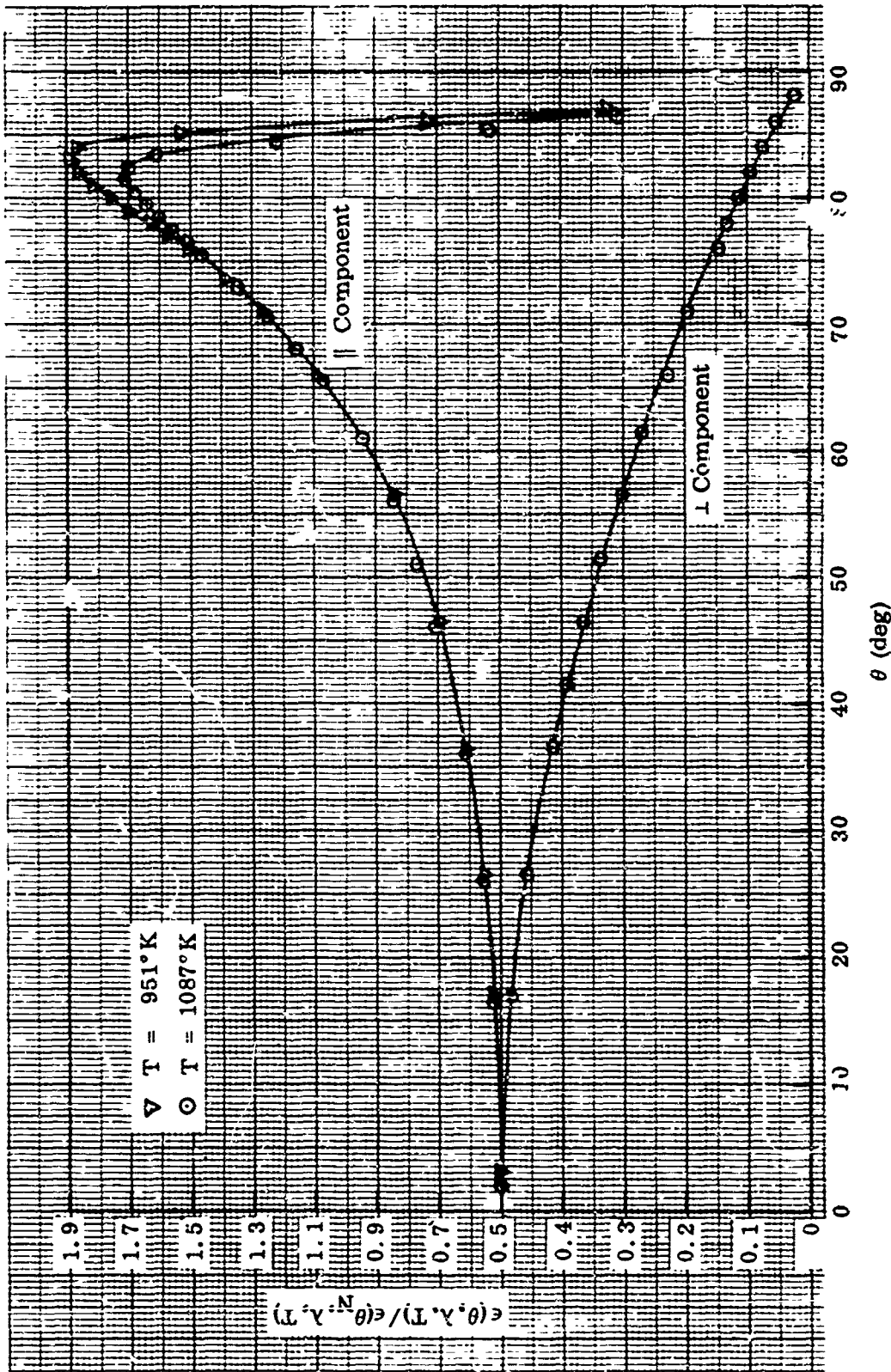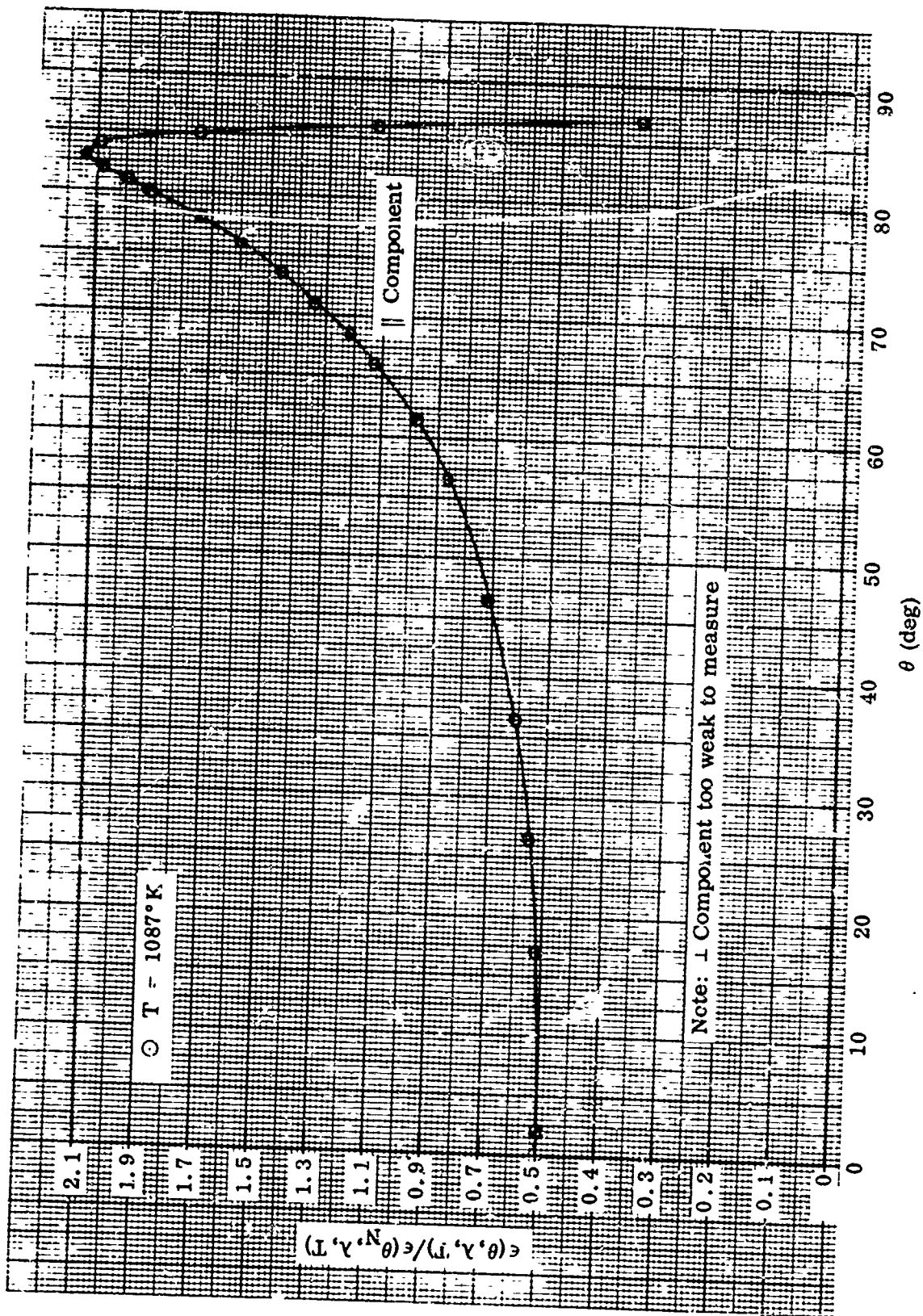Figure 96 Relative Spectral Directional Emittance at $\lambda = 8\ \mu$, Stainless Steel Sample No. 2S

176

8. STAINLESS STEEL SAMPLE NO. 3S

Preparation: Oxidized for 1/2 hr at 800 °C in wet hydrogen furnace.

Initial Oxide Film Characteristics: Color: Purple (interference film). Composition: primarily Fe_3O_4. Average thickness: 0.17 μ (based on weight gain data).

Test Procedure: Absolute and relative directional emittance data were obtained at 533, 668, 807, 953, and 1090°K. No additional tests were made because of the unstable nature of the oxide film and emittance at 1090°K. A test chamber pressure of 2.5×10^{-6} Torr was maintained until midway through the 1090°K tests, when the pressure rose to 6×10^{-6} Torr.

Emittance Data: Absolute emittance values are shown in Table XXI; relative total directional emittance data in Figure 97; relative spectral directional emittance data at λ = 1.5, 2, 3, 4, 6, and 8 μ in Figures 98 through 103.

Remarks: The absolute and relative directional emittance data obtained are believed to be characteristic of the initial surface of the sample (i.e., the purple oxide film) up to 950°K. During the 953°K tests, additional oxidation occurred, as evidenced by the higher spectral normal emittance values at this temperature and at 1090°K. Shortly after the absolute emittance data were obtained at 1090°K, the total emittance of the sample began to drop, and during the directional emittance tests at this temperature the electrical power to the sample had to be dropped several times to keep the temperature from exceeding 1100°K. At the conclusion of the tests, the relative total directional emittance characteristics were observed to be approaching those for unoxidized stainless steel and the oxide film had almost entirely disappeared, leaving the surface bright and clean; consequently no further emittance tests were made. The reason for the unstable condition of the oxide film is unknown, and it is contrary to the changes in oxide film thickness on the other stainless steel samples. To prevent a recurrence of this instability, the maximum test temperature for the remaining samples was lowered from 1090 to 950°K.

A photomicrograph and an electron micrograph of the initial purple-colored oxide film on this sample surface are shown in Figures 30 and 31, respectively, and are discussed in subsection V.2.a. No studies of the post-test surface were made. Electron shadowgraphs of the initial oxide film from this sample are shown in Figures 34 and 35 and are discussed in subsection V.2.a. The pictures show the film thickness to be highly variable and almost discontinuous in spots. Consequently, accurate measurement of the film thickness by this method was not possible. An electron diffraction pattern of the initial purple-colored oxide film is shown in Figure 36. The pattern is similar to that obtained for the gold-colored oxide film on sample 2S, which indicates the composition of the oxide to be primarily Fe_3O_4.

177

Table XXI. Absolute Emittance Data for Stainless Steel Sample No. 3S

Temperature (°K)	Time at Temp. (hr, min)	$\epsilon(T)$	$\epsilon(\theta_N, T)$	$\epsilon(\theta_N, \lambda, T)$							
				1.5 μ	2 μ	3 μ	4 μ	6 μ	8 μ	10 μ	12 μ
533[a]	0, 45	0.272	0.261								
668[a]	0, 45	0.358	0.352								
807[a]	2, 0	0.436	0.455	0.960	0.900	0.669	0.457	0.276	0.203	0.161	0.132
953[a]	3, 15	0.517	0.564	0.990	0.923	0.715	0.494	0.311	0.232	0.186	0.154
1090[a,b]	5, 30	0.579	0.634	1.00	0.956	0.714	0.488	0.317	0.245	0.198	0.168

(a) Directional emittance data obtained at these temperatures.
(b) Sample emittance was observed to drop significantly midway through the 1090° K directional emittance tests due to instability of the oxide film.
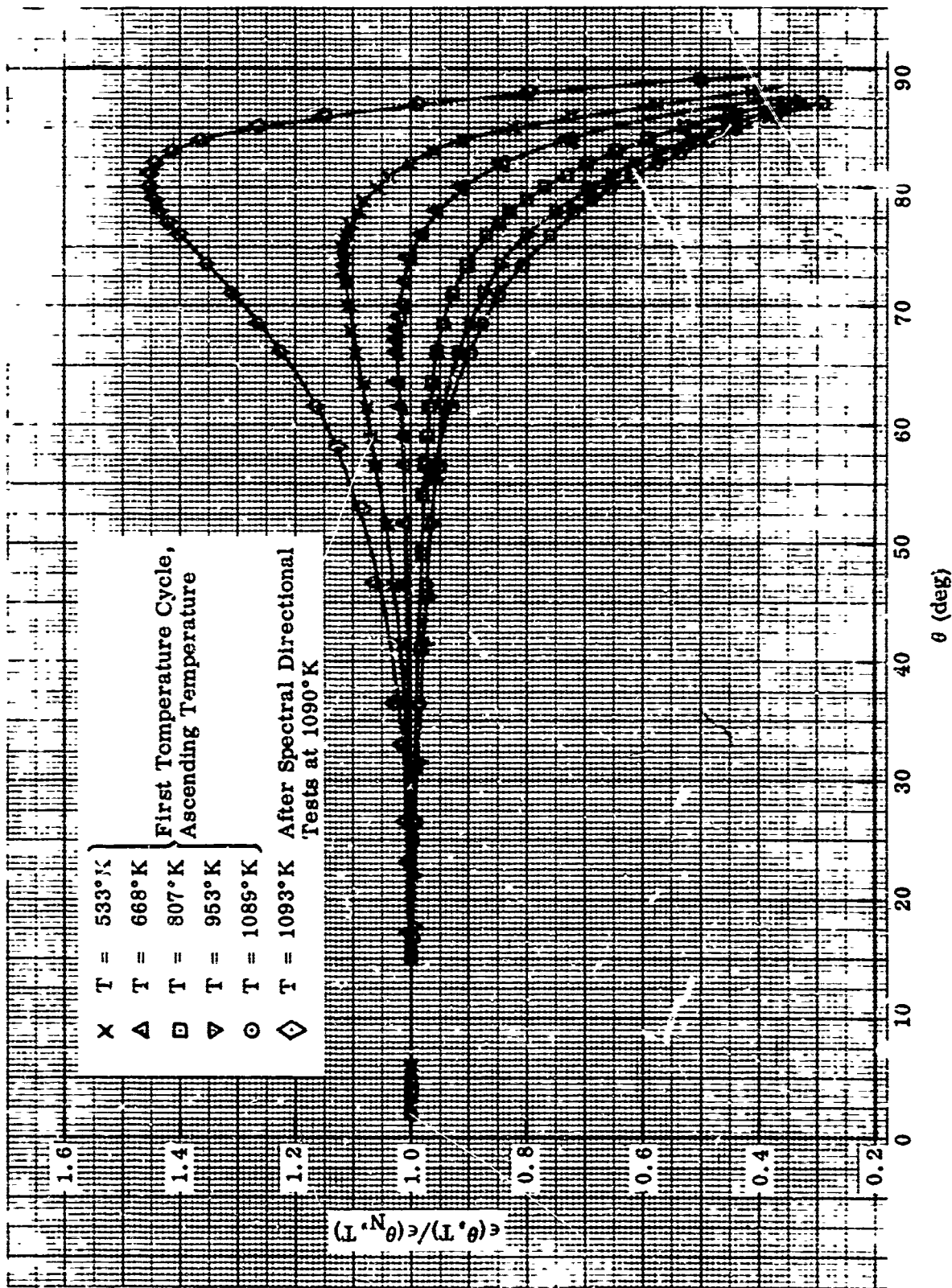
Figure 97 Relative Total Directional Emittance, Stainless Steel Sample No. 3S
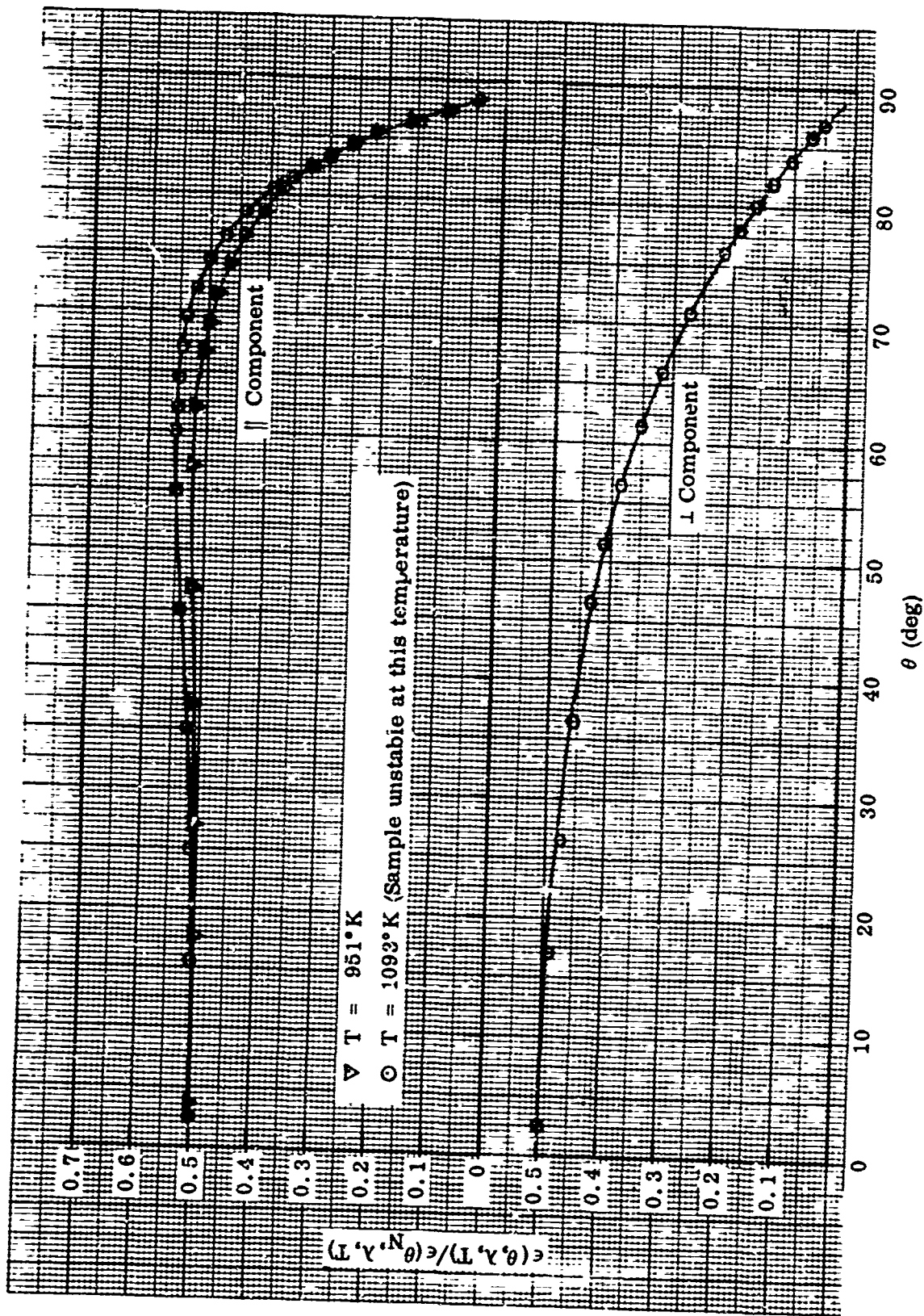
179

Figure 98 Relative Spectral Directional Emittance at $\lambda = 1.5\ \mu$, Stainless Steel Sample No. 3S

180

Figure 99 Relative Spectral Directional Emittance at $\lambda = 2\,\mu$, Stainless Steel Sample No. 3S

181

Figure 100 Relative Spectral Directional Emittance at $\lambda = 3\ \mu$, Stainless Steel Sample No. 3S

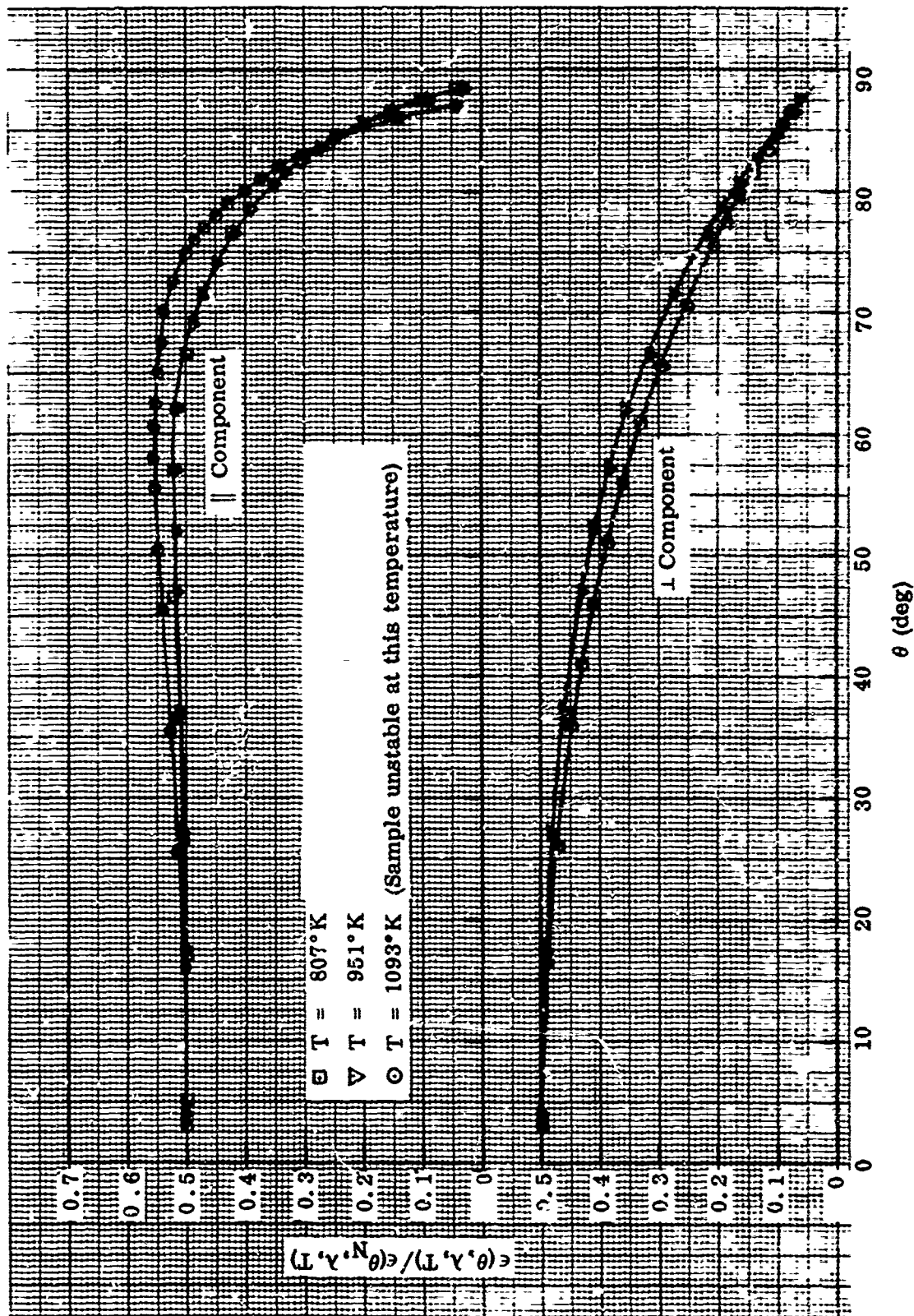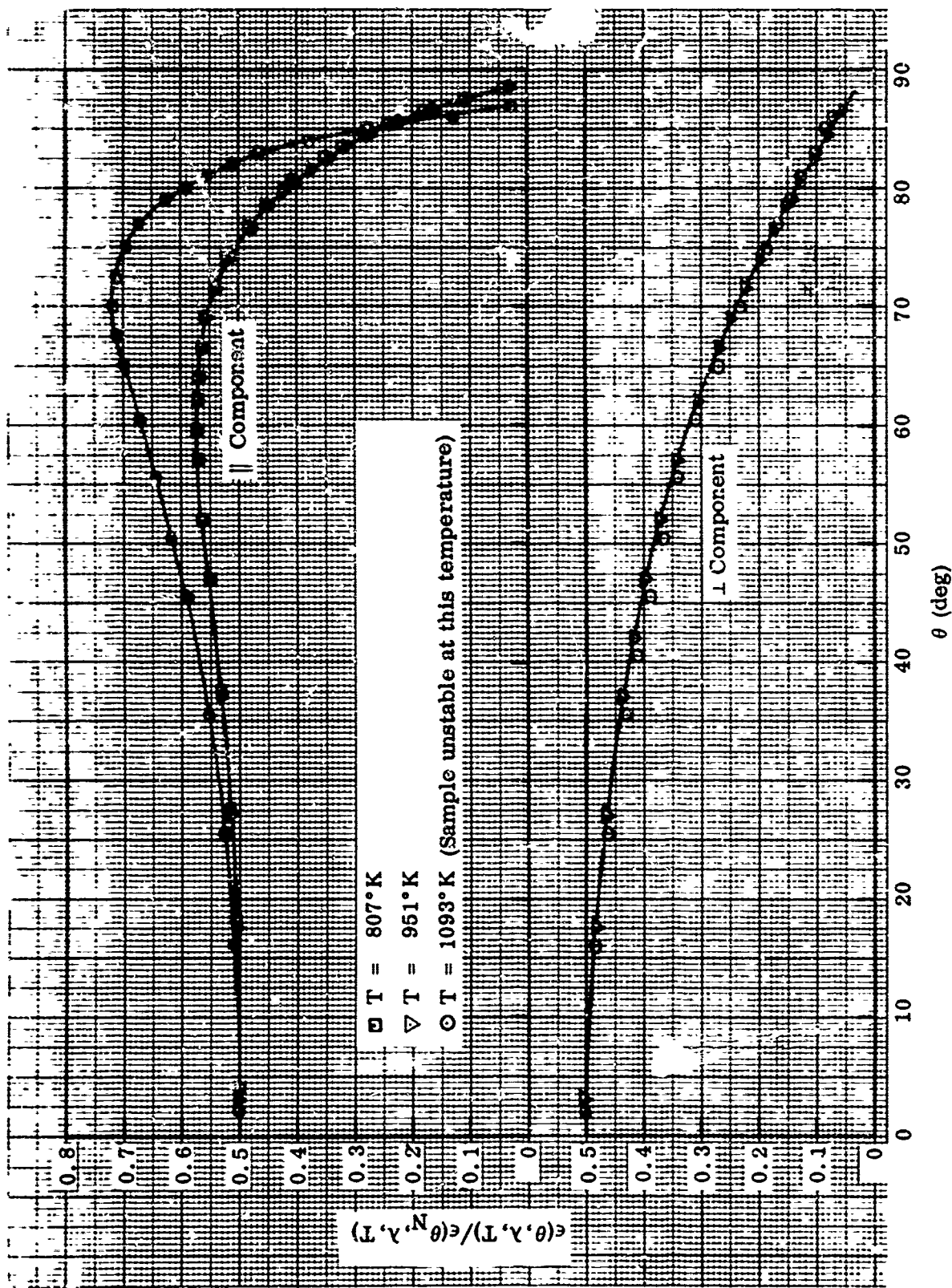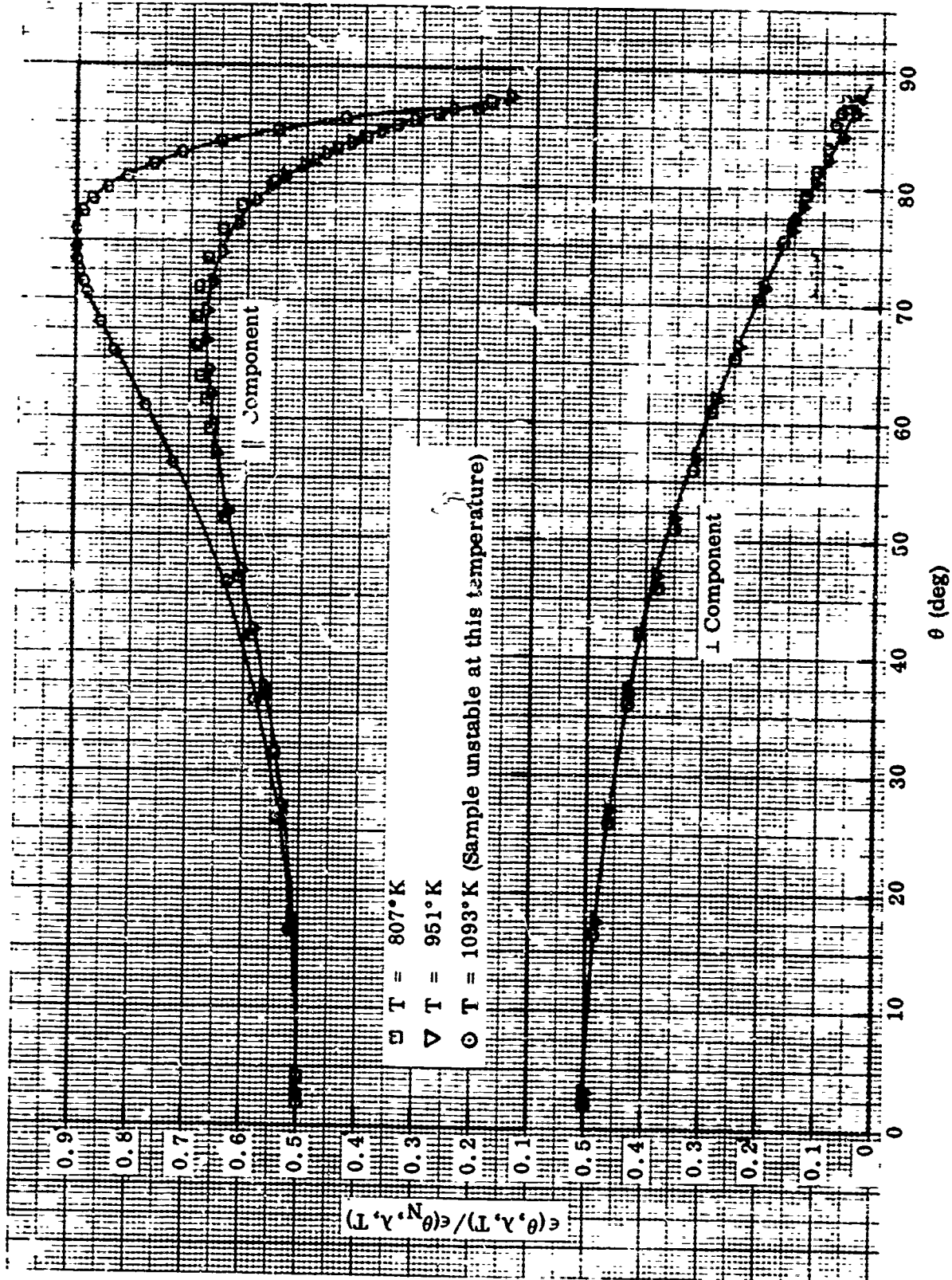Figure 101 Relative Spectral Directional Emittance at $\lambda = 4\ \mu$, Stainless Steel Sample No. 3S

183

Figure 102 Relative Spectral Directional Emittance at $\lambda \sim 6\ \mu$, Stainless Steel Sample No. 3S

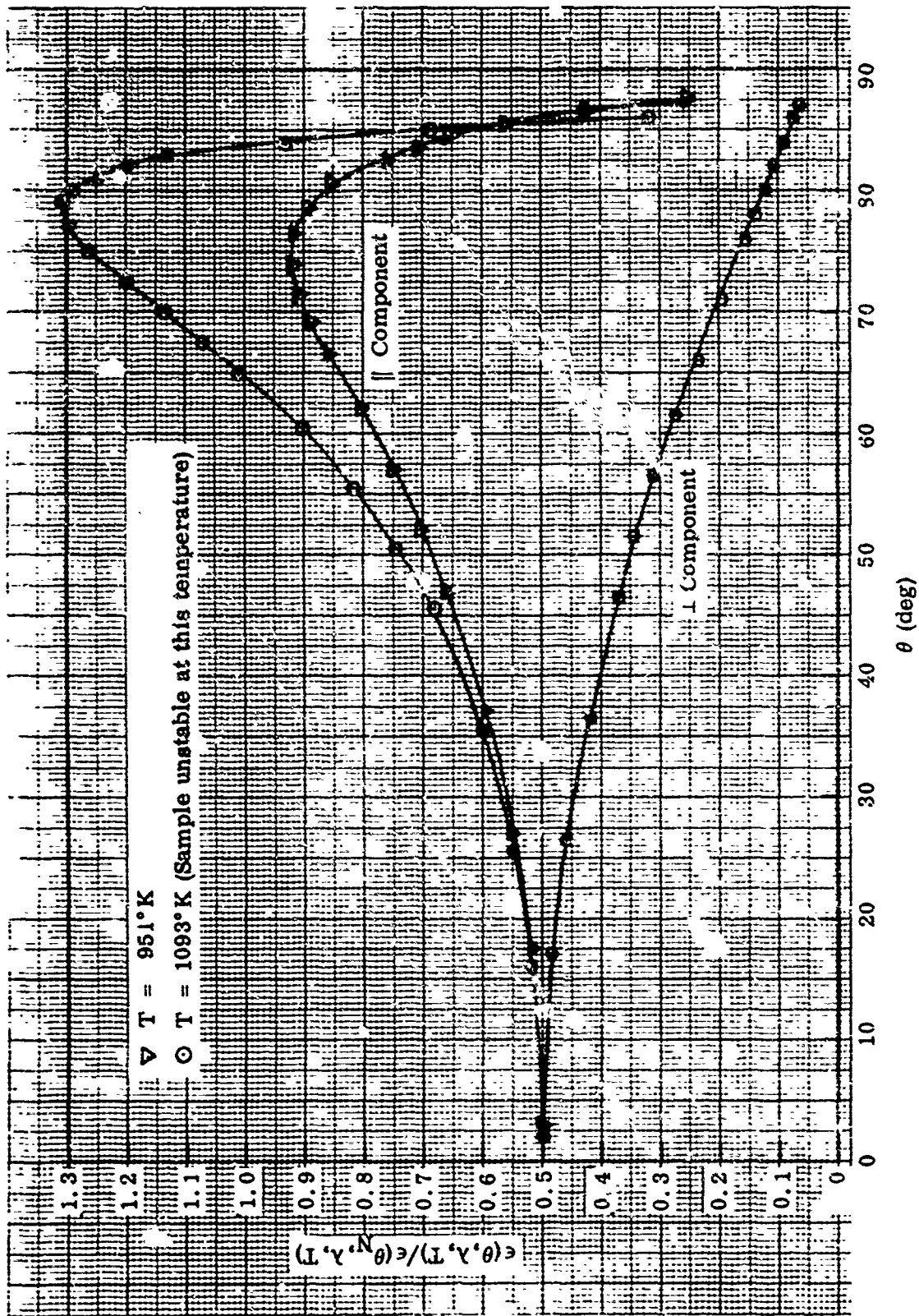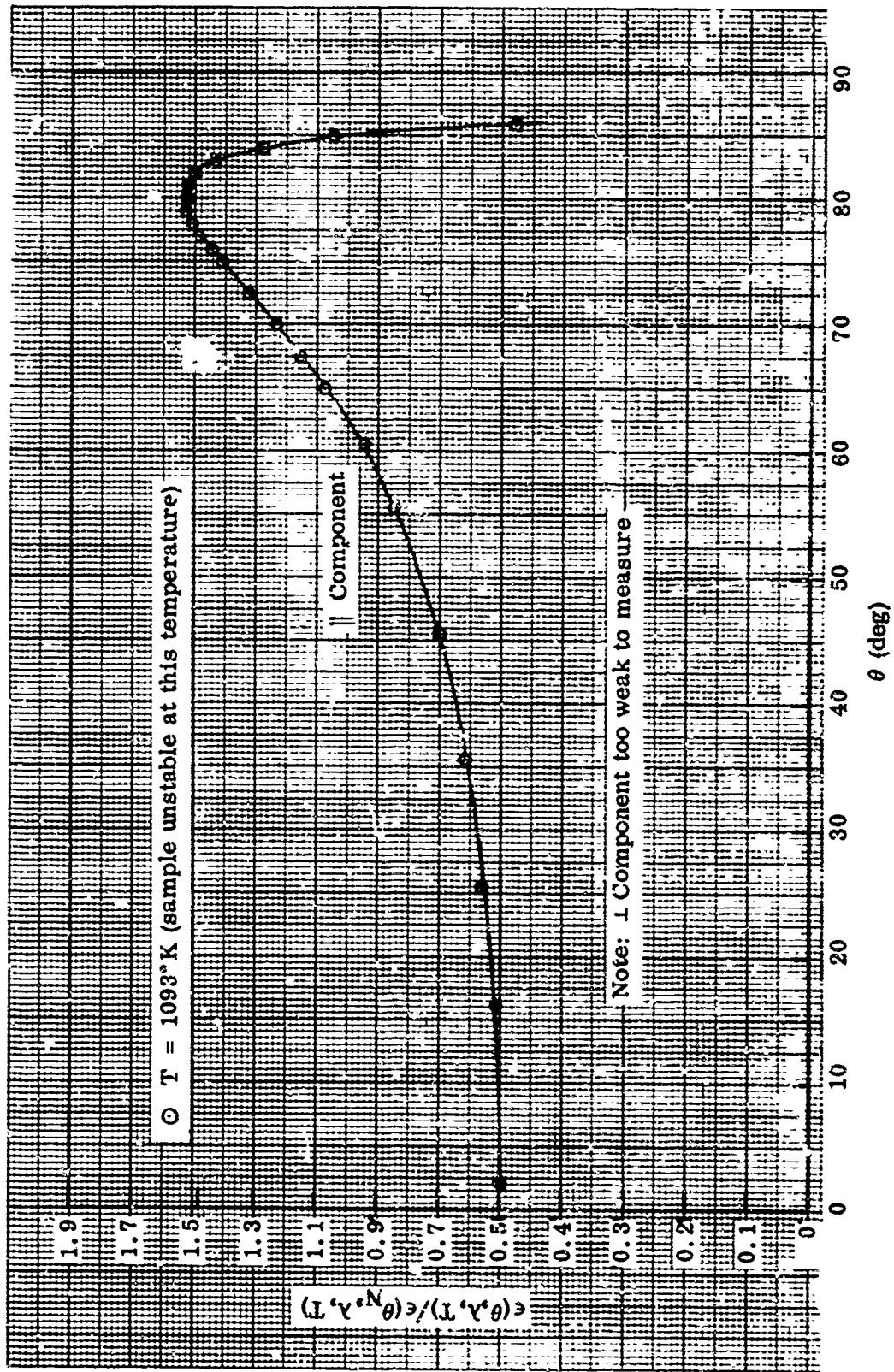Figure 103 Relative Spectral Directional Emittance at $\lambda = 8 \mu$, Stainless Steel Sample No. 3S

9. STAINLESS STEEL SAMPLE NO. 4S

Preparation: Oxidized for 1/2 hr at 1000°C in wet hydrogen furnace.

Initial Oxide Film Characteristics: Color: Dull gray. Composition: primarily Fe_3O_4. Average thickness: 0.95 μ, (based on weight gain measurements).

Test Procedure: Absolute and relative directional emittance data were obtained at 537, 676, 818, and 957°K (first temperature cycle). Absolute emittance values were re-checked at all four temperatures after the 957°K tests. A test chamber pressure of 4.5×10^{-6} Torr was maintained throughout all tests.

Emittance Data: Absolute emittance values are shown in Table XXII; relative total directional emittance data in Figure 104; relative spectral directional emittance data at λ = 1.5, 2, 3, 4, 6, and 8 μ in Figures 105 through 110.

Remarks: The absolute and relative directional emittance data obtained during the first test temperature cycle are believed to be characteristic of the initial surface of the sample (i.e., the dull gray oxide film). The absolute emittance data obtained during the second test temperature cycle were significantly higher at all temperatures and wavelengths, indicating that a significant change in the oxide film occurred while the directional emittance data at 979°F were obtained. The appearance of the sample after the emittance tests, however, was essentially the same as at the start of the tests, and no significant changes in the relative directional emittance characteristics were observed.

Photomicrographs and electron micrographs of the surface are shown in Figures 30 and 31, respectively, and are discussed in subsection V.2.a. The electron micrographs indicate the initial oxide film to be quite rough with large oxide nodules covering about 50% of the surface. After the 950°F tests, the appearance of the oxide was significantly different although its color and visual appearance remained the same. A photomicrograph and an electron micrograph of a cross-section, metallurgical mount of the sample, after the emittance tests, are shown in Figure 33 and are discussed in subsection V.2.a.

An electron diffraction pattern of the initial oxide on this sample is shown in Figure 36. Most of the principal diffraction lines were identified with the pattern for Fe_3O_4, but numerous additional lines were not identified. The pattern for the oxide after the emittance tests was essentially the same as that shown for the initial oxide.

186

Table XXII. Absolute Emittance Data for Stainless Steel Sample No. 4S

Temperature (°K)	Time at Temp. (hr, min)	$\epsilon(T)$	$\epsilon(\theta_N, T')$	$\epsilon(\theta_N, \lambda, T')$							
				1.5 μ	2 μ	3 μ	4 μ	6 μ	8 μ	10 μ	12 μ
First Temperature Cycle											
537[a]	0,45	0.554	0.580								
676[a]	0,40	0.586	0.637								
818[a]	1,40	0.615	0.689	0.979	0.936	0.869	0.665	0.620	0.615	0.591	0.536
957[a]	5,0	0.648	0.725	0.955	0.921	0.805	0.669	0.625	0.624	0.609	0.553
Second Temperature Cycle											
536	0,20	0.586	0.599								
670	0,20	0.619	0.661								
811	0,40	0.650	0.721	1.000	1.000	0.872	0.717	0.642	0.633	0.606	0.561
949	0,40	0.691	0.769	1.000	0.998	0.870	0.707	0.648	0.647	0.635	0.573

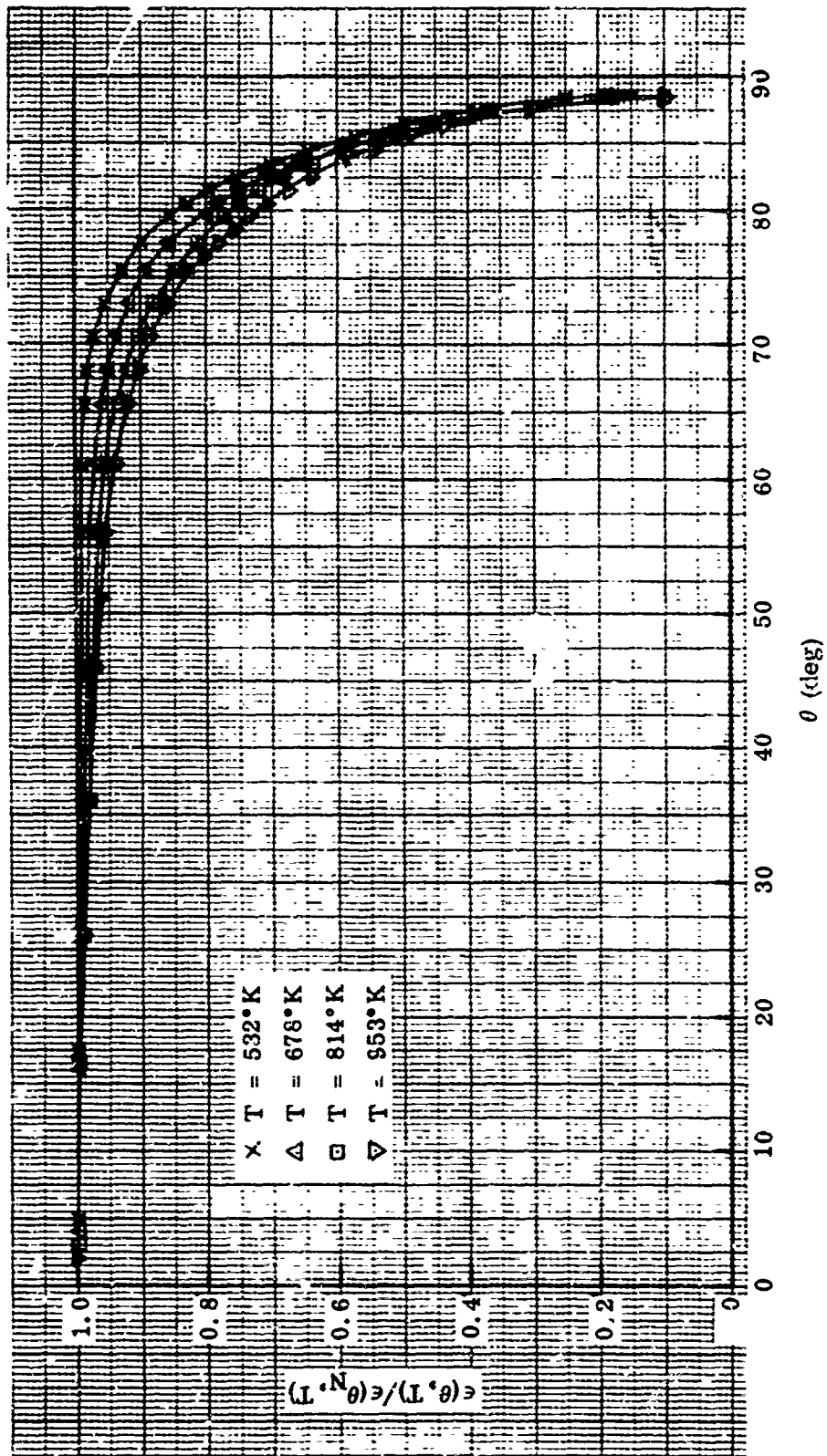(a) Directional emittance data obtained at these temperatures.

Figure 104 Relative Total Directional Emittance of Stainless Steel Sample No. 4S

Figure 105 Relative Spectral Directional Emittance at $\lambda = 1.5\ \mu$, Stainless Steel Sample No. 4S

189

Figure 106 Relative Spectral Directional Emittance at $\lambda = 2 \mu$, Stainless Steel Sample No. 4S

190

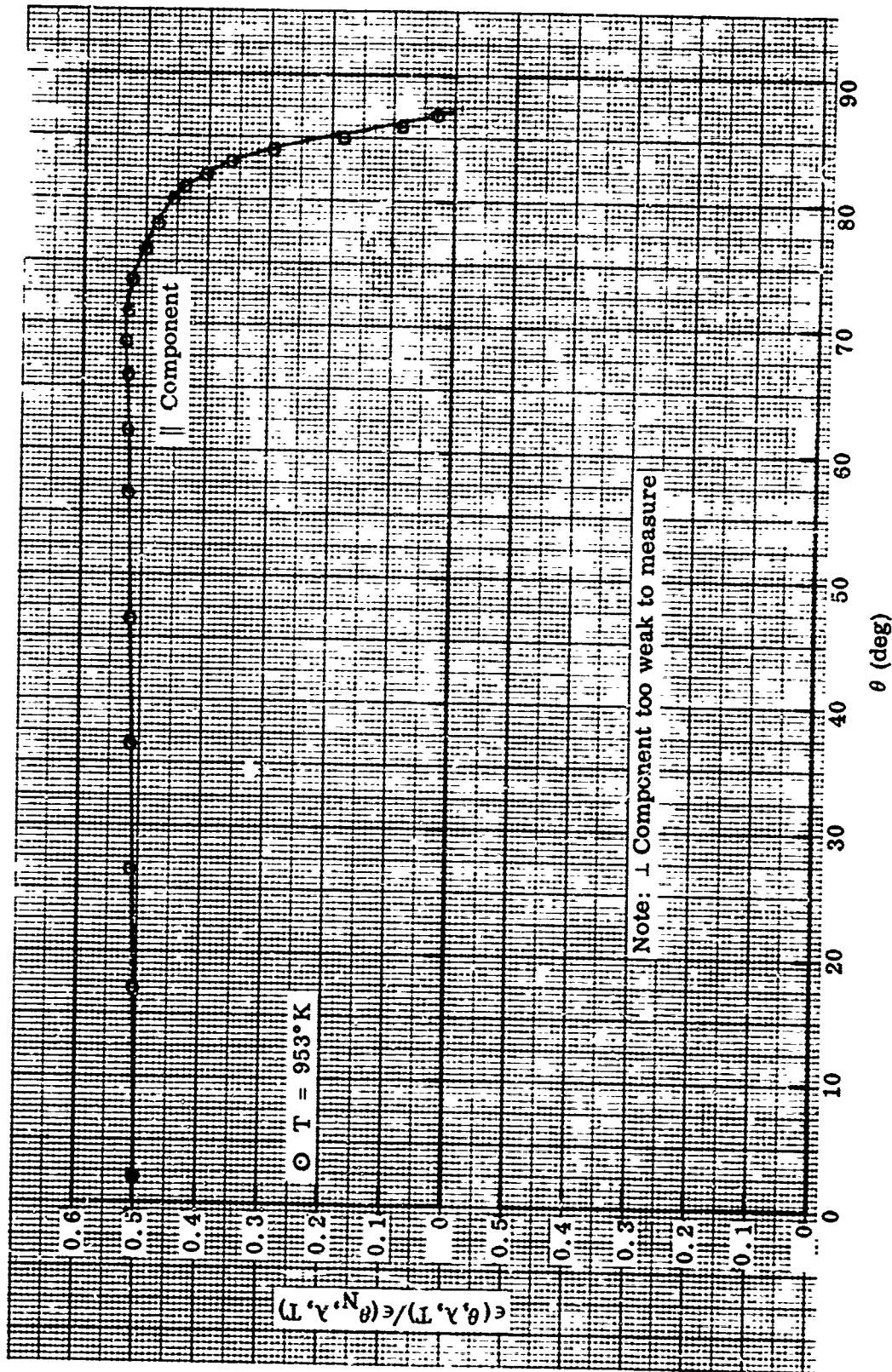Figure 107 Relative Spectral Directional Emittance at $\lambda = 3\,\mu$, Stainless Steel Sample No. 4S
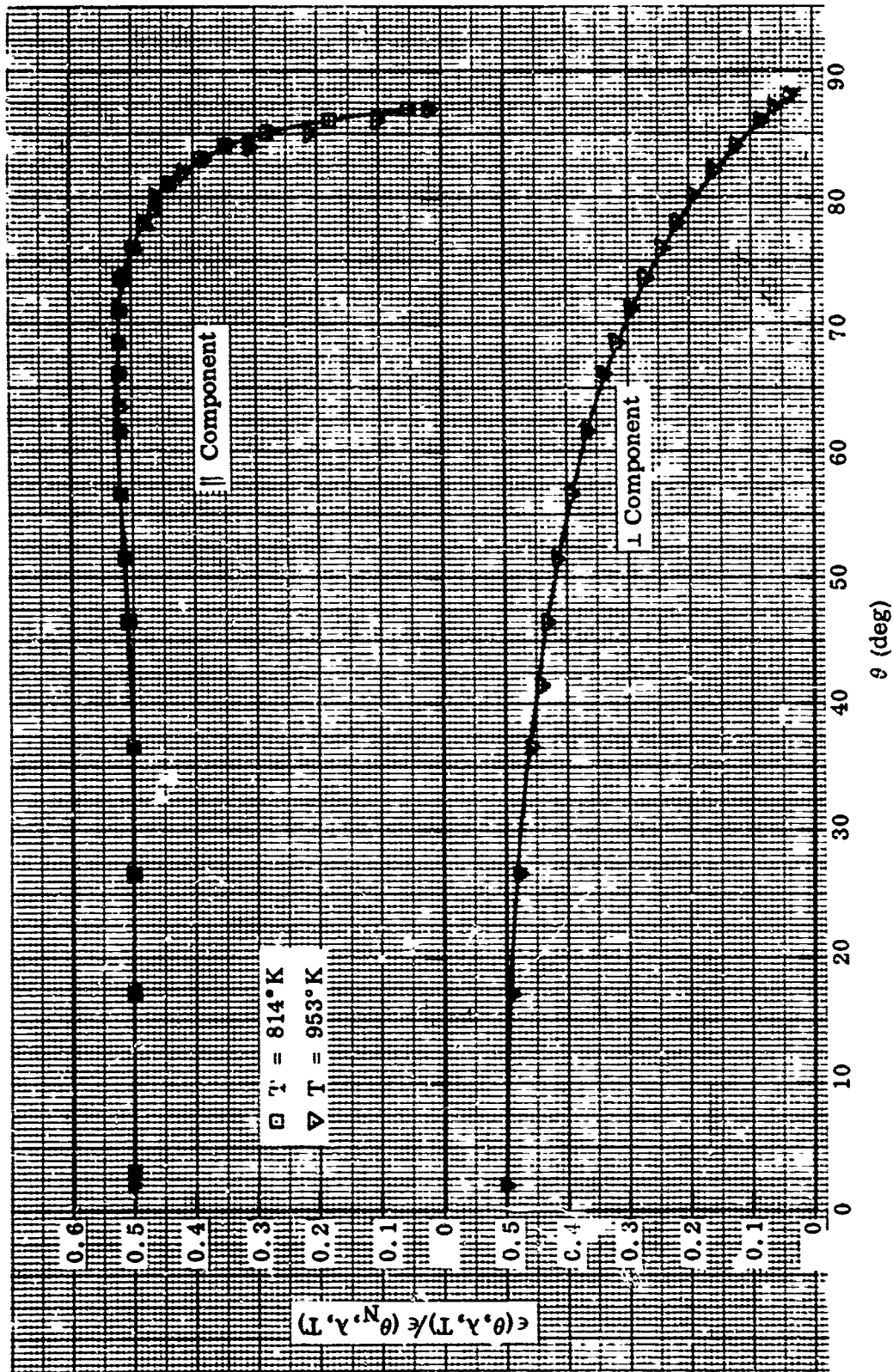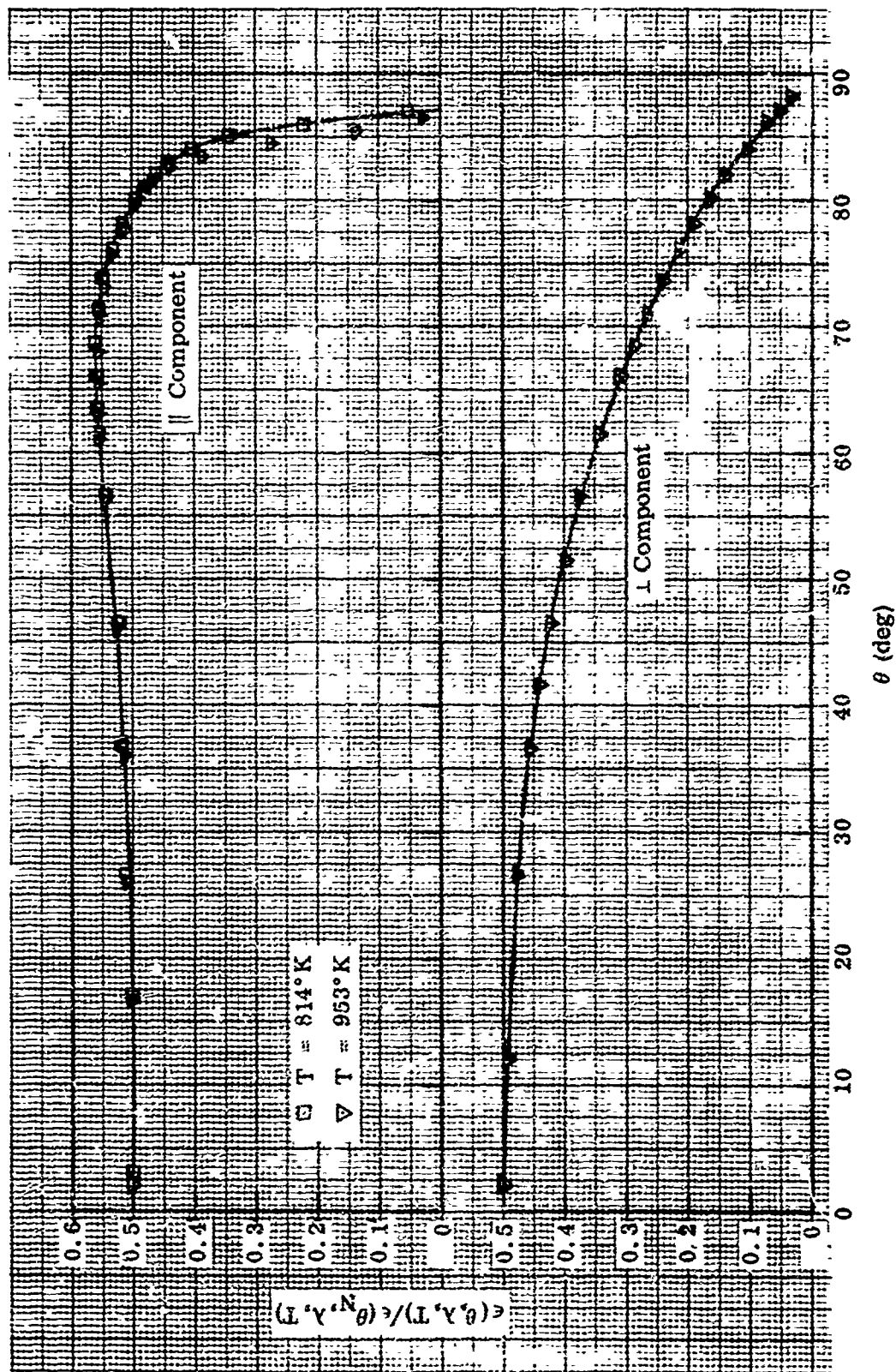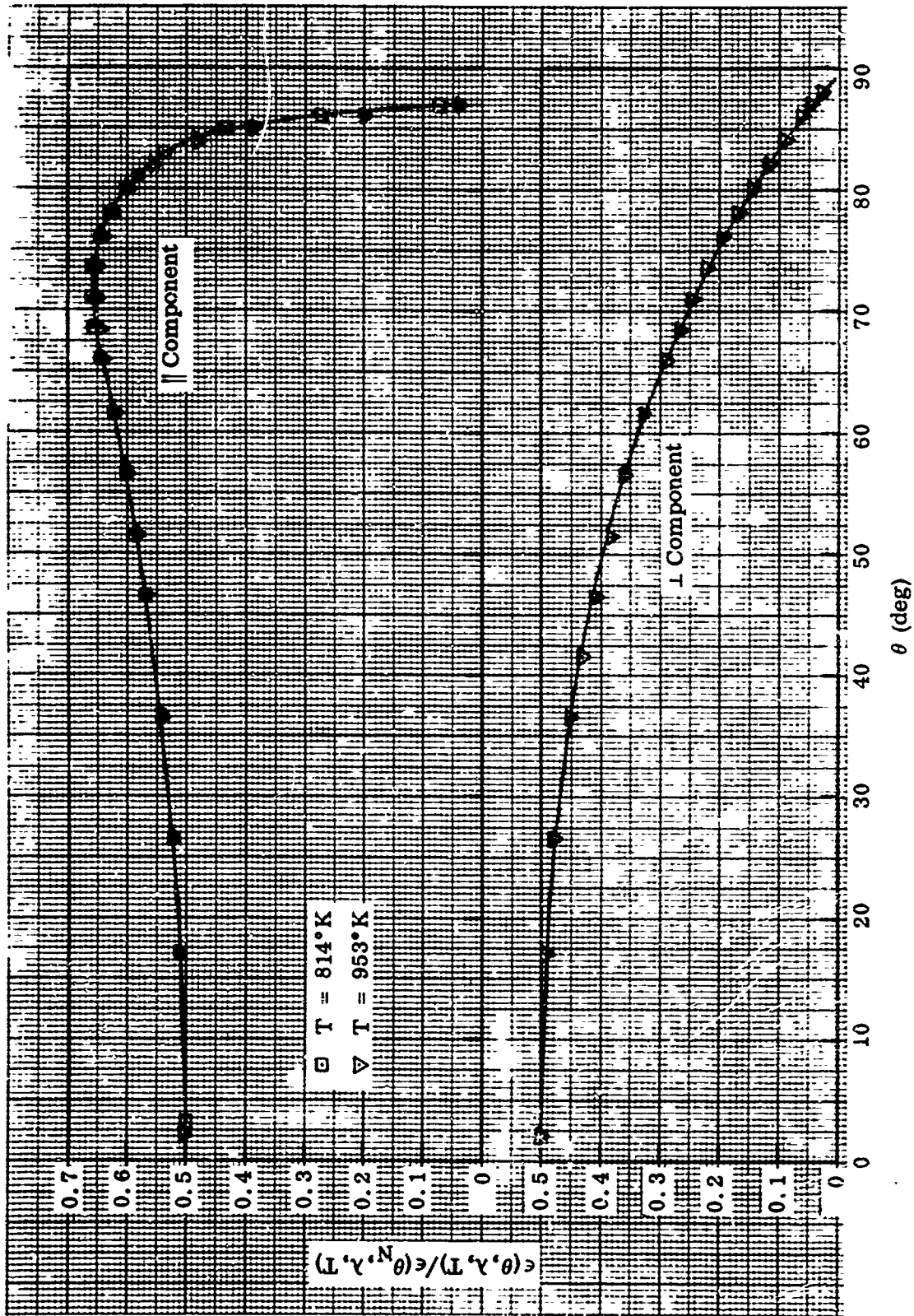
191

Figure 108 Relative Spectral Directional Emittance at $\lambda = 4\ \mu$, Stainless Steel Sample No. 4S
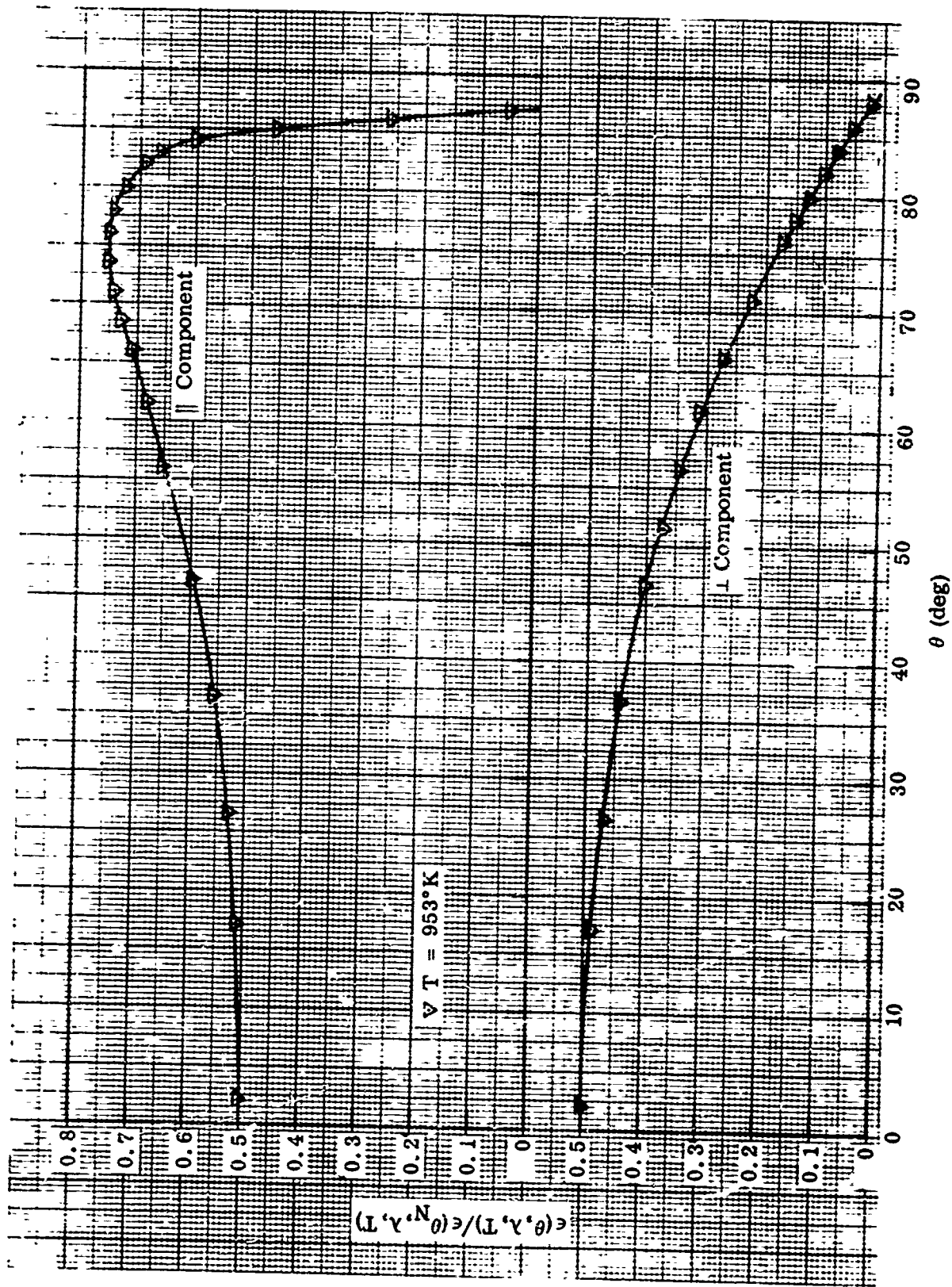
Figure 109 Relative Spectral Directional Emittance at $\lambda = 6\,\mu$, Stainless Steel Sample No. 4S
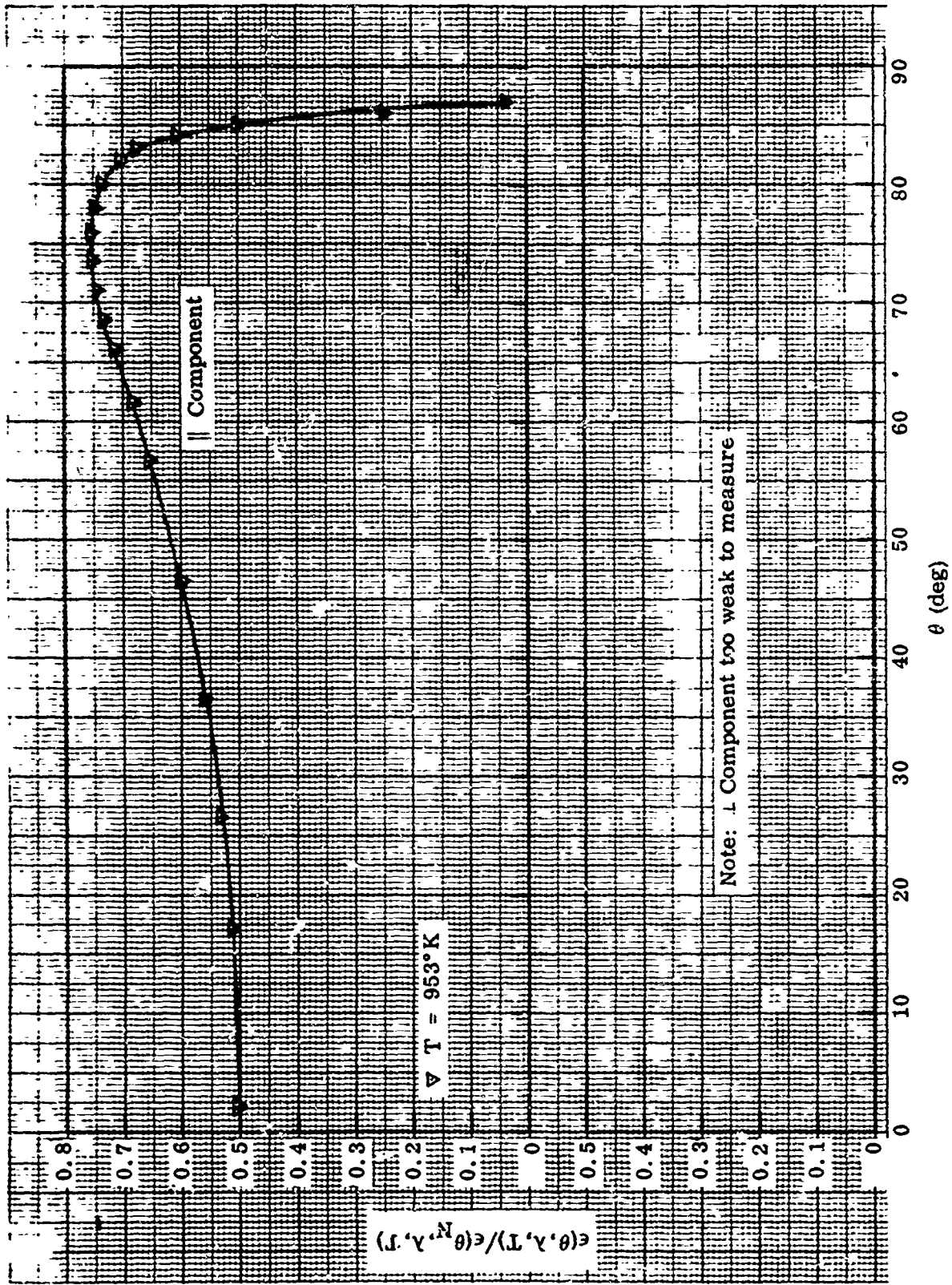
Figure 110 Relative Spectral Directional Emittance at $\lambda = 8\ \mu$, Stainless Steel Sample No. 4S

194

10. STAINLESS STEEL SAMPLE NO. 5S

Preparation: Oxidized for 1-1/2 hr at 1000°C in wet hydrogen furnace.

Initial Oxide Film Characteristics: Color: Dull brownish-gray. Composition: primarily Fe_3O_4. Average thickness: 1.4 μ (based on weight gain measurements).

Test Procedure: Absolute and relative directional emittance data were obtained at 535, 679, 809, and 950°K (first temperature cycle). Absolute emittance values were remeasured at all four temperatures after the 950°K tests (second temperature cycle) to check the stability of the sample. A test chamber pressure of 3.5 to 5 $\times$ 10^{-6} Torr was maintained throughout all tests.

Emittance Data: Absolute emittance values are shown in Table XXIII; relative total directional emittance data in Figure 111; relative spectral directional emittance data at λ = 1.5, 2, 3, 4, 6, and 8 μ in Figures 112 through 117.

Remarks: The absolute and relative directional emittance data obtained indicate that this sample remained fairly stable throughout the emittance tests. The lone exception is the absolute emittance values at 541°K (second temperature cycle), which are slightly higher than the initial values determined at this temperature. This suggests a possible change in the long-wavelength spectral emittance characteristics. No visual change in the appearance of the sample was observed.

Photomicrographs and electron micrographs of the sample surface are shown in Figures 30 and 31, respectively, and are discussed in subsection V.2.a. Although the electron micrographs indicate a considerable change in the appearance of the oxide during the emittance tests, the visual appearance and color of the oxide were unchanged. A photomicrograph and electron micrograph of a cross-section, metallurgical mount of the sample, after the emittance tests, are shown in Figure 33 and are discussed in subsection V.2.a.

An electron diffraction pattern of the initial oxide on this sample is shown in Figure 36. The pattern appears to be essentially the same as that for sample 4S, indicating the oxide composition to be primarily Fe_3O_4 plus an unknown (possibly spinel) phase. The pattern for the oxide after the emittance tests was essentially the same as that shown for the initial oxide.

Table XXIII. Absolute Emittance Data for Stainless Steel Sample No. 5S

Temperature (°K)	Time at Temp. (hr, min)	$\epsilon(T)$	$\epsilon(\theta_N, T)$	$\epsilon(\theta_N, \lambda, T)$							
				1.5 μ	2 μ	3 μ	4 μ	6 μ	8 μ	10 μ	12 μ
First Temperature Cycle											
535[a]	1,10	0.735	0.813								
679[a]	0,45	0.789	0.878								
809[a]	3,15	0.802	0.917	1.000	0.986	0.943	0.944	0.897	0.831	0.859	0.802
950[a]	3,30	0.826	0.928	1.000	1.000	0.960	0.961	0.910	0.845	0.874	0.823
Second Temperature Cycle											
541	0,40	0.764	0.841								
675	0,20	0.793	0.878								
814	0,30	0.817	0.911	1.000	0.992	0.947	0.955	0.901	0.830	0.853	0.810
952	0,45	0.828	0.938	1.000	1.000	0.955	0.955	0.908	0.835	0.864	0.810

(a) Directional emittance data obtained at these temperatures.

196
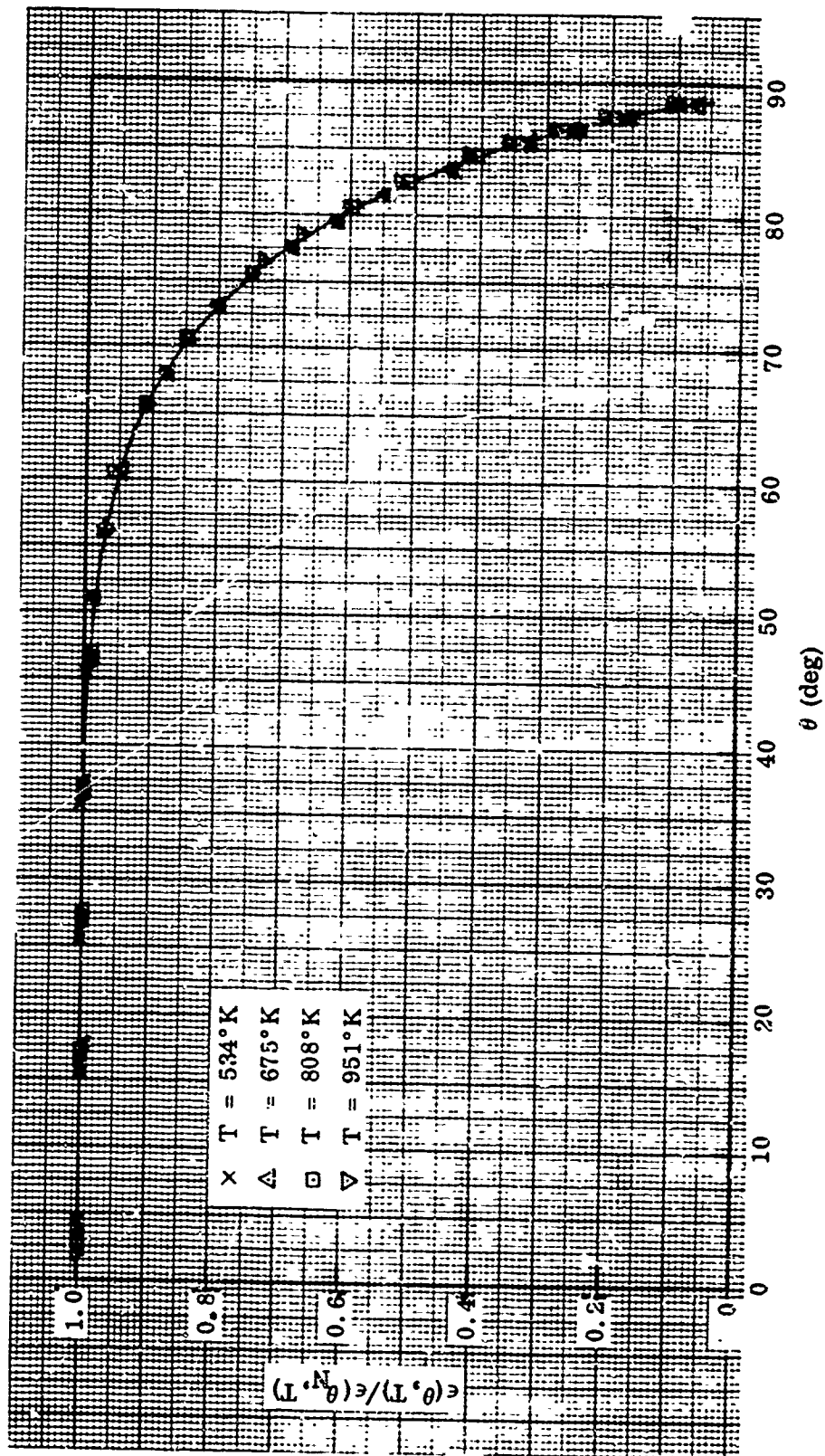
Figure 111 Relative Total Directional Emittance of Stainless Steel Sample No. 5S

Figure 112 Relative Spectral Directional Emittance at $\lambda = 1.5\ \mu$, Stainless Steel Sample No. 5S

198

Figure 113 Relative Spectral Directional Emittance at $\lambda = 2\ \mu$, Stainless Steel Sample No. 5S

199

Figure 114 Relative Spectral Directional Emittance at $\lambda = 3\ \mu$, Stainless Steel Sample No. 5S

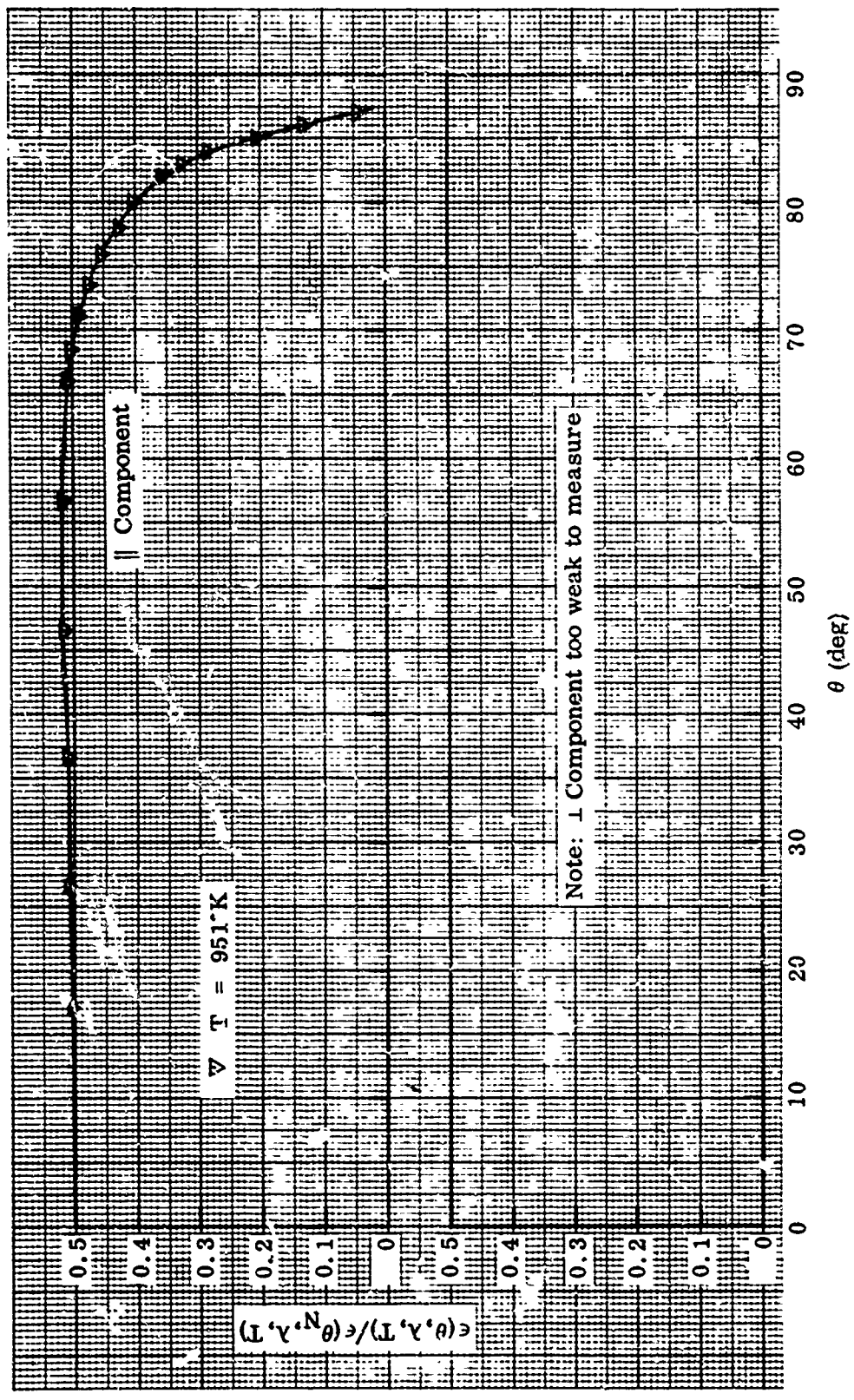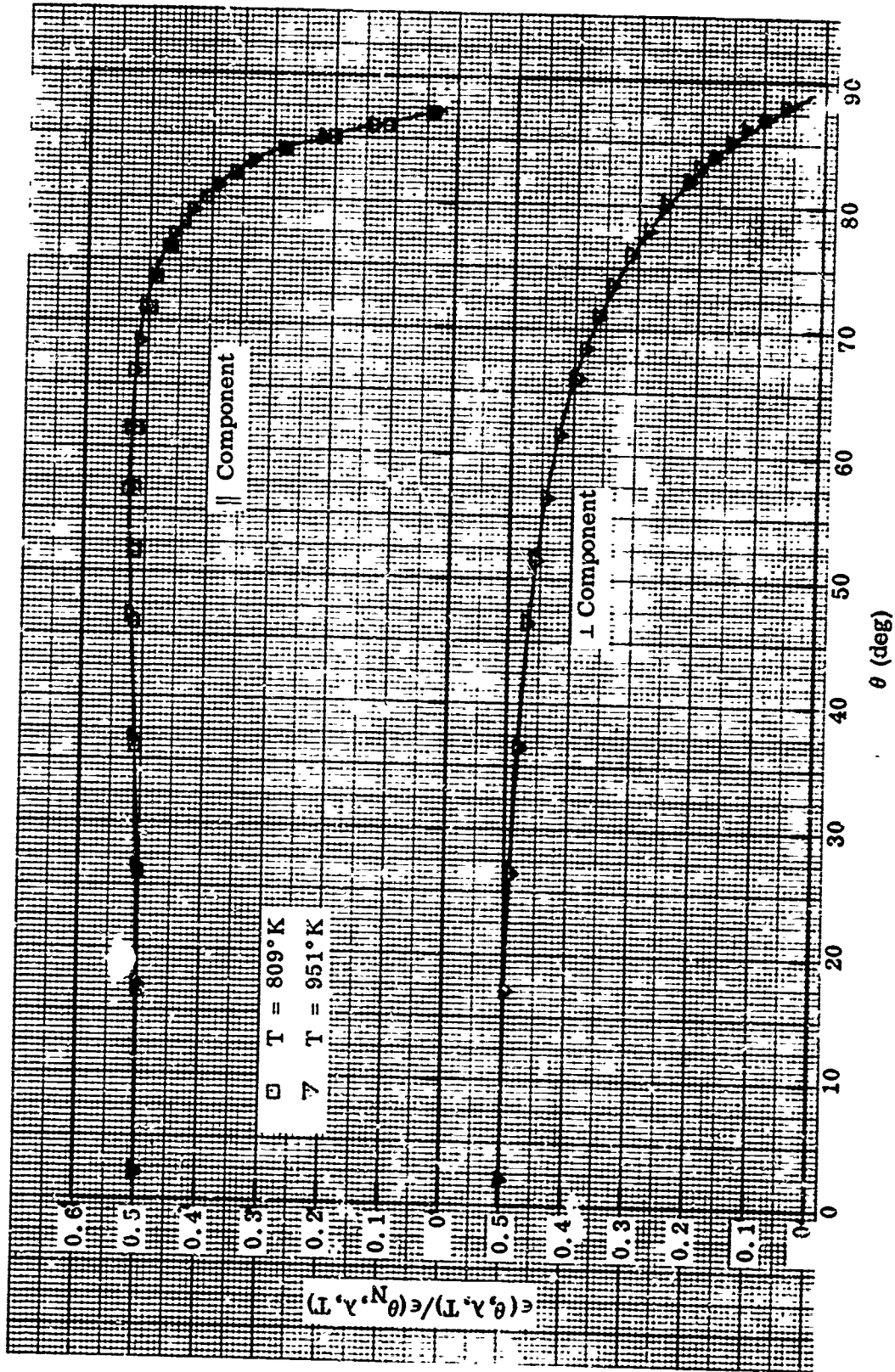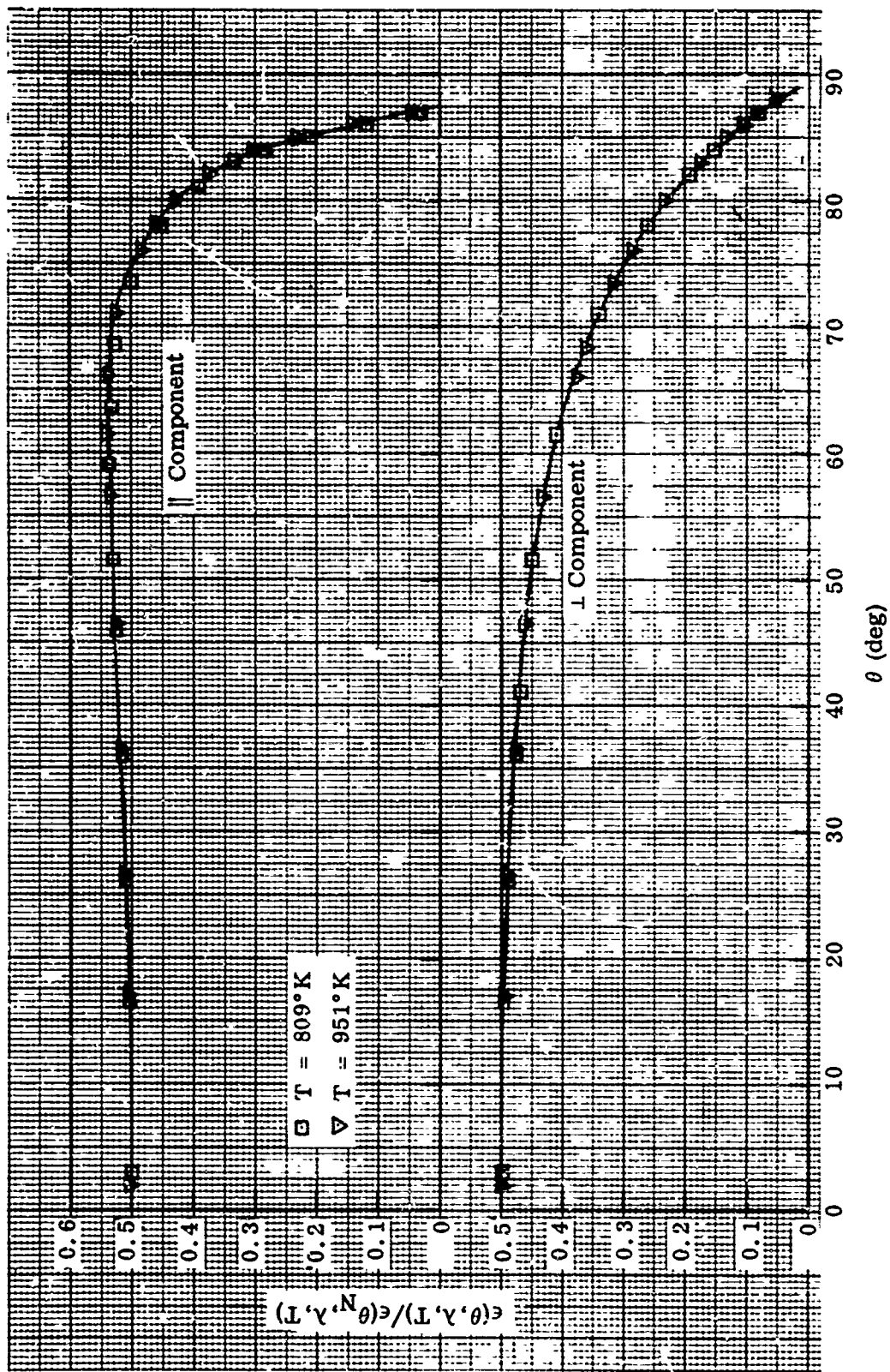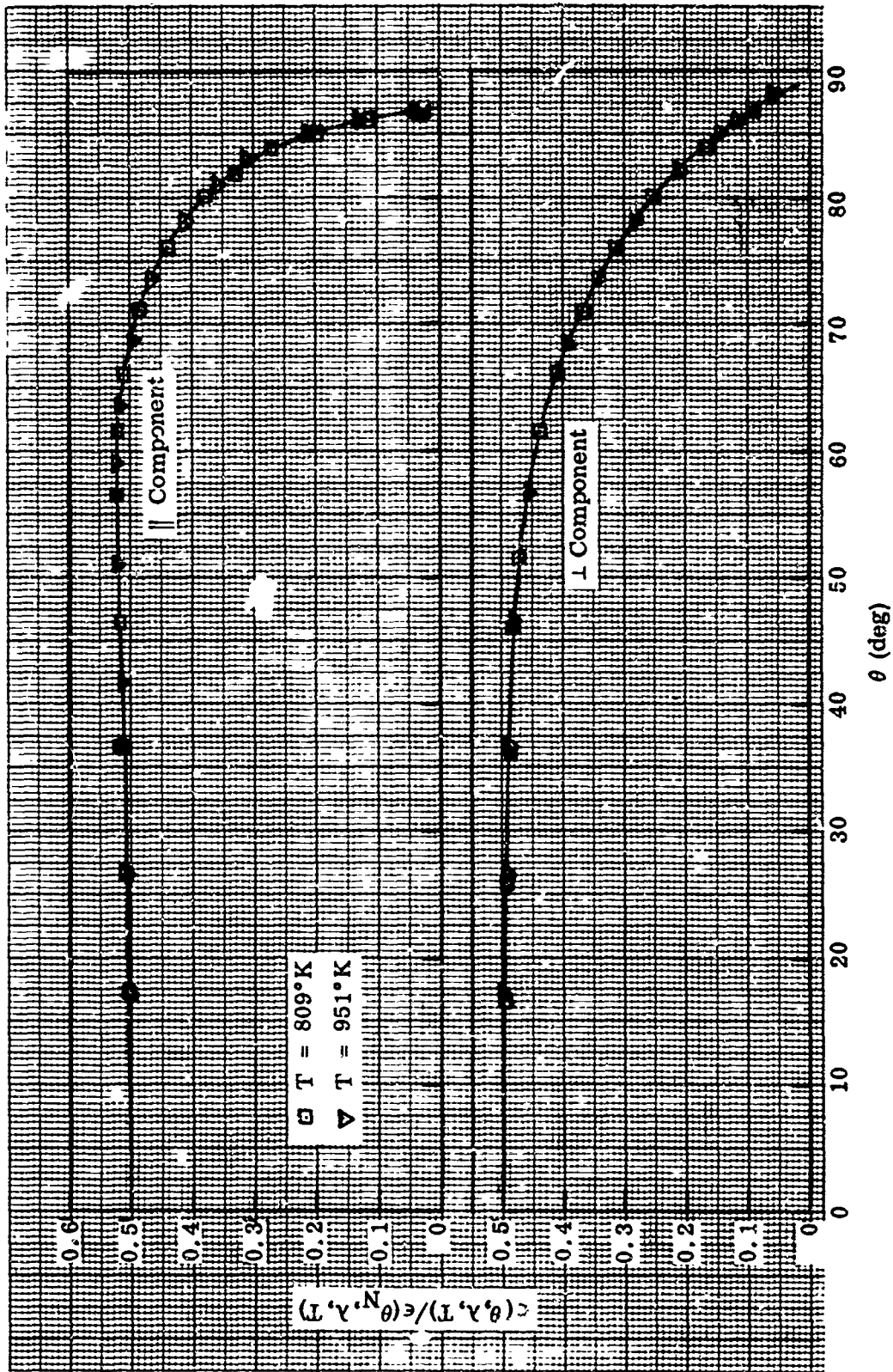Figure 115 Relative Spectral Directional Emittance at $\lambda = 4\ \mu$, Stainless Steel Sample No. 5S
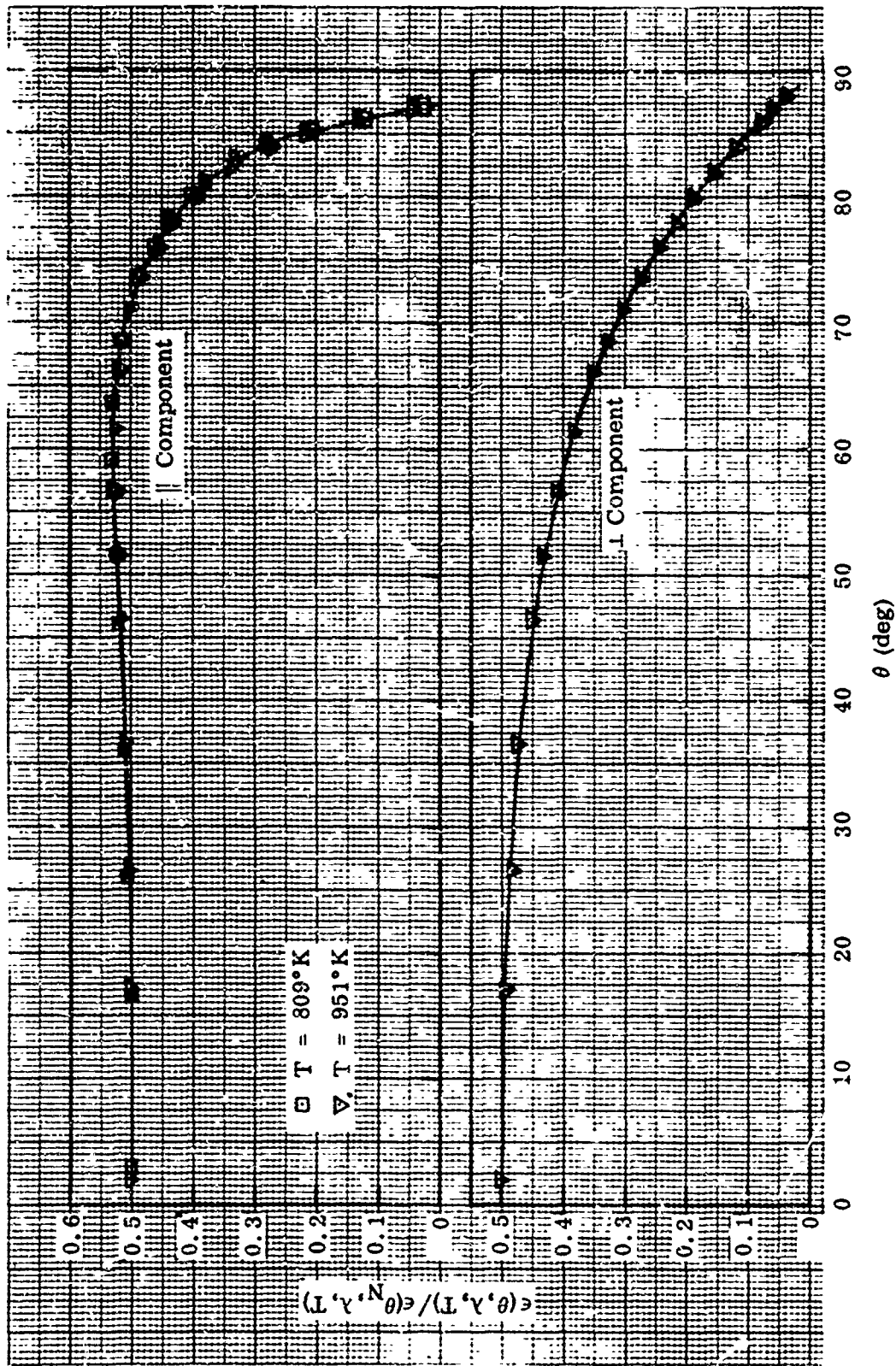
Figure 116   Relative Spectral Directional Emittance at $\lambda = 6\,\mu$, Stainless Steel Sample No. 5S
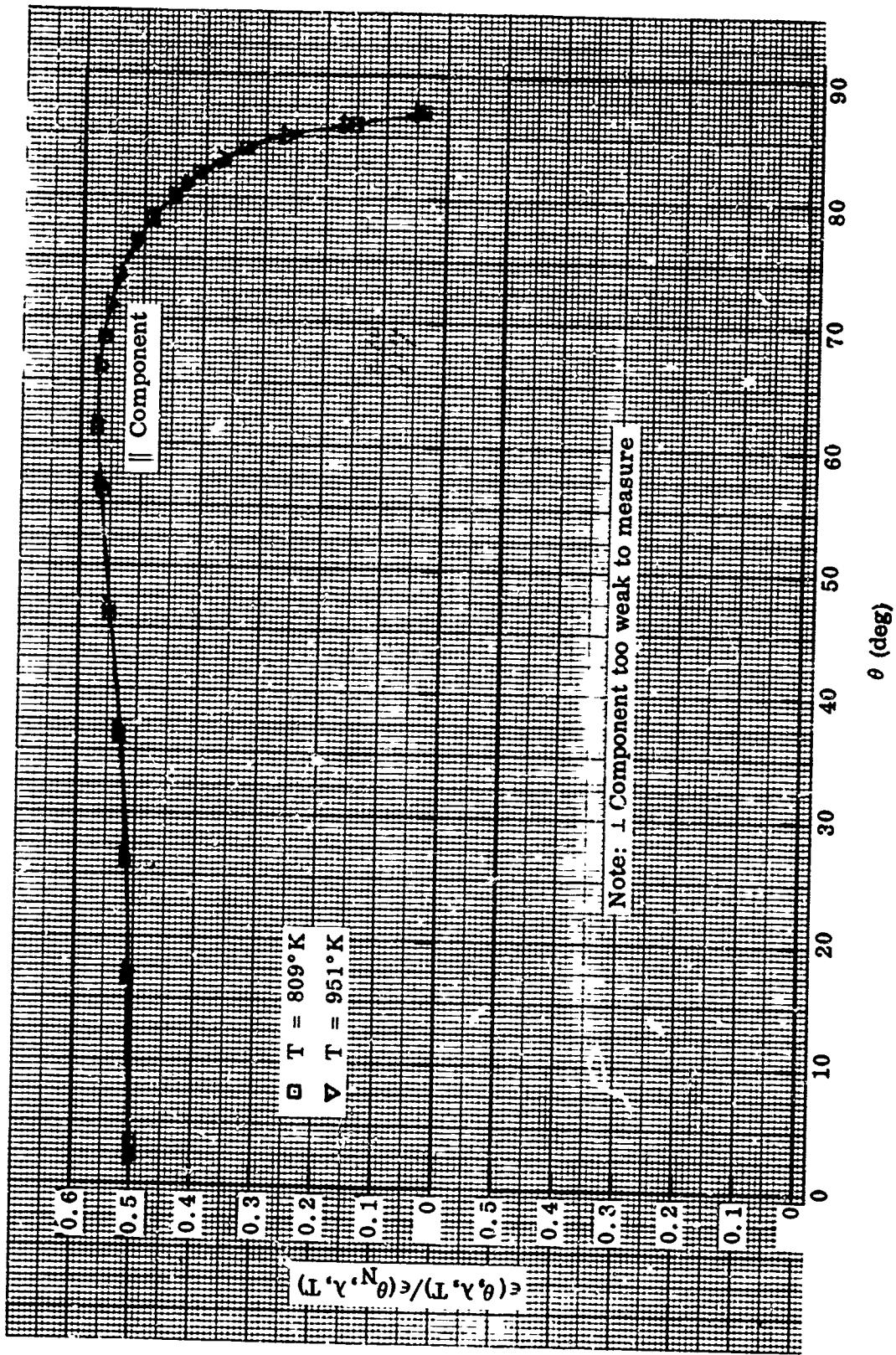
Figure 117 Relative Spectral Directional Emittance at $\lambda = 8\ \mu$, Stainless Steel Sample No. 5S

203

11. STAINLESS STEEL SAMPLE NO. 1R

Preparation: Unoxidized, electropolished by the method described in subsection III.2.a. Roughened by shot blasting with size XL "Glas-Shot", 30 psi at 4 in. Annealed for 10 min at 1045°C in dry hydrogen.

RMS Roughness: Before emittance tests, 20 μin.; after, not measured (oxidized).

Test Procedure: Absolute and relative directional emittance data were obtained at 539, 673, 810, and 947°K, and the absolute and relative total directional emittance values were remeasured after the 947°K tests, (first temperature cycle). Absolute emittance values at 539, 675, and 811°K were remeasured (second temperature cycle) to indicate the change in sample emittance characteristics due to oxidation. The test chamber pressure was maintained at 2.5×10^{-6} Torr throughout all tests.

Emittance Data: Absolute emittance values are shown in Table XXIV; relative total directional emittance data in Figure 118, relative spectral direction emittance data at λ = 1.5, 2, 3, 4, and 6 μ in Figures 119 through 123.

Remarks: The absolute and directional emittance data obtained up to 947°K in the first test temperature cycle are believed to be characteristic of the roughened, unoxidized stainless steel surface. During the 947°K directional emittance tests the sample oxidized to a uniform reddish-gold color. The emittance data obtained during the second temperature cycle show that the oxide film had very little effect on the total normal and total hemispherical emittance of the sample at temperatures lower than 675°K, and very little effect on the spectral normal emittance at wavelengths longer than 4 μ. The effect of the oxide film on the relative total directional emittance of the sample at 950°K is shown in Figure 118.

A comparison of the relative total directional emittance data with data obtained for the unroughened sample (1S-2) indicates that roughening had a significant effect [i.e., lower $\epsilon(\theta)_{max}$ values] on this property at the lower test temperatures, but the 950°K data were about the same for both samples. The effect was not as noticeable in the relative spectral directional emittance data.

Photomicrographs and electron micrographs of the sample are shown in Figures 30 and 31, respectively, and are discussed in subsection V.2.a. The electron micrograph of the reddish-gold oxide film shows the appearance to be intermediate to that of the initial gold-colored oxide film on sample 2S and the final blue-colored oxide film that formed on sample 1S-2. No attempt was made to determine the thickness of the oxide film.

An electron diffraction pattern of the oxide was obtained and was identical to that shown in Figure 36 for sample 1S-2, indicating the composition to be primarily Fe_3O_4.

Table XXIV. Absolute Emittance Data for Stainless Steel Sample No. 1R

Temperature (°K)	Time at Temp. (hr, min)	$\epsilon(T)$	$\epsilon(\theta_N, T)$	$\epsilon(\theta_N, \lambda, T)$							
				1.5 μ	2 μ	3 μ	4 μ	6 μ	8 μ	10 μ	12 μ
First Temperature Cycle											
539[a]	1,40	0.153	0.127								
673[a]	1,0	0.173	0.153								
810[a]	2,30	0.194	0.175	0.276	0.245	0.212	0.183	0.152	0.127	0.106	0.096
947[a]	6,0	0.212	0.193	0.290	0.255	0.219	0.192	0.161	0.134	0.114	0.095
946[a]		0.223	0.212	0.353	0.290	0.238	0.200	0.164	0.136	0.119	0.104
Second Temperature Cycle[b]											
539	0,30	0.15	0.130								
675	0,30	0.174	0.159								
811	0,45	0.202	0.187	0.337	0.283	0.231	0.192	0.153	0.127	0.107	0.087

(a) Directional emittance data obtained at these temperatures.
(b) A reddish-gold oxide film formed during the 947° K emittance tests at the end of the first temperature cycle.

Figure 118 Relative Total Directional Emittance, Stainless Steel Sample No. 1R

The chart legend shows:

▽	T = 953°K
⊟	T = 815°K
△	T = 674°K
×	T = 536°K
▶	T = 944°K (After 953°K directional emittance tests)

Y-axis: $\epsilon(\theta, T)/\epsilon(\theta_N, T)$ — values 0.8, 1.0, 1.2, 1.4, 1.6, 1.8, 2.0, 2.2, 2.4, 2.6, 2.8

X-axis: θ (deg) — values 0, 10, 20, 30, 40, 50, 60, 70, 80, 90

Figure 119 Relative Spectral Directional Emittance at $\lambda = 1.5\ \mu$, Stainless Steel Sample No. 1R

207

Figure 120 Relative Spectral Directional Emittance at $\lambda = 2\,\mu$, Stainless Steel Sample No. 1R

Figure 121 Relative Spectral Directional Emittance at $\lambda = 3\ \mu$, Stainless Steel Sample No. 1R
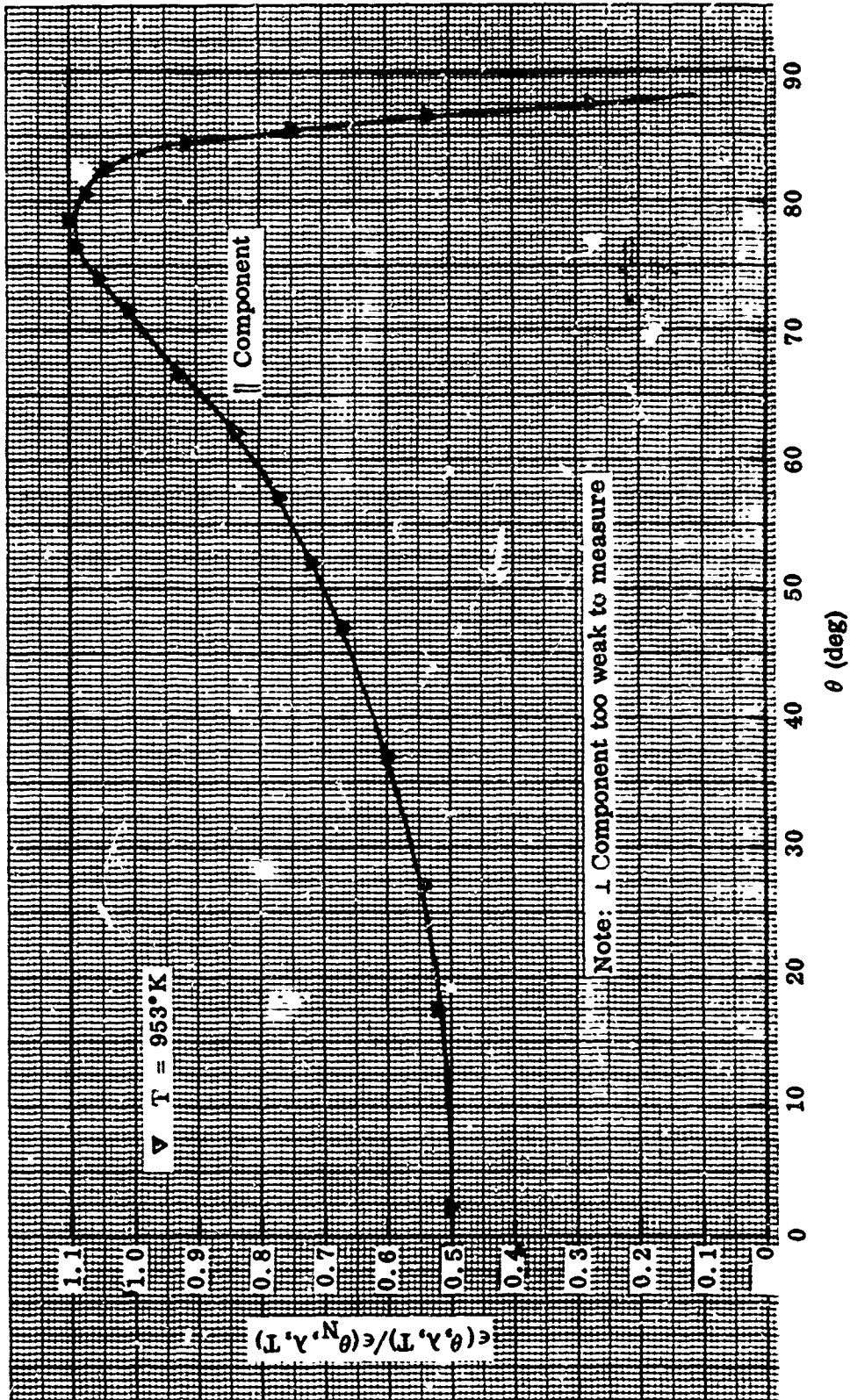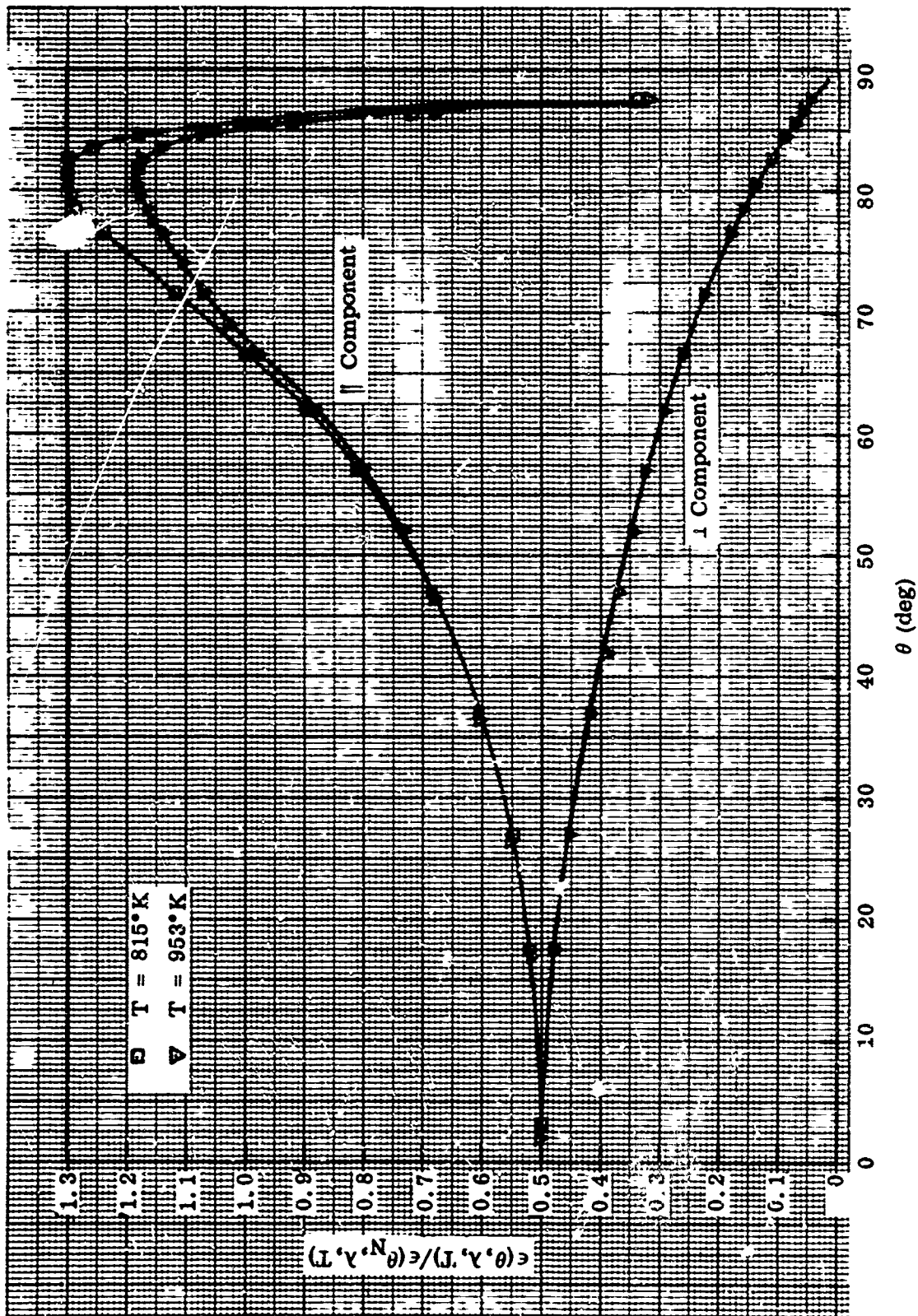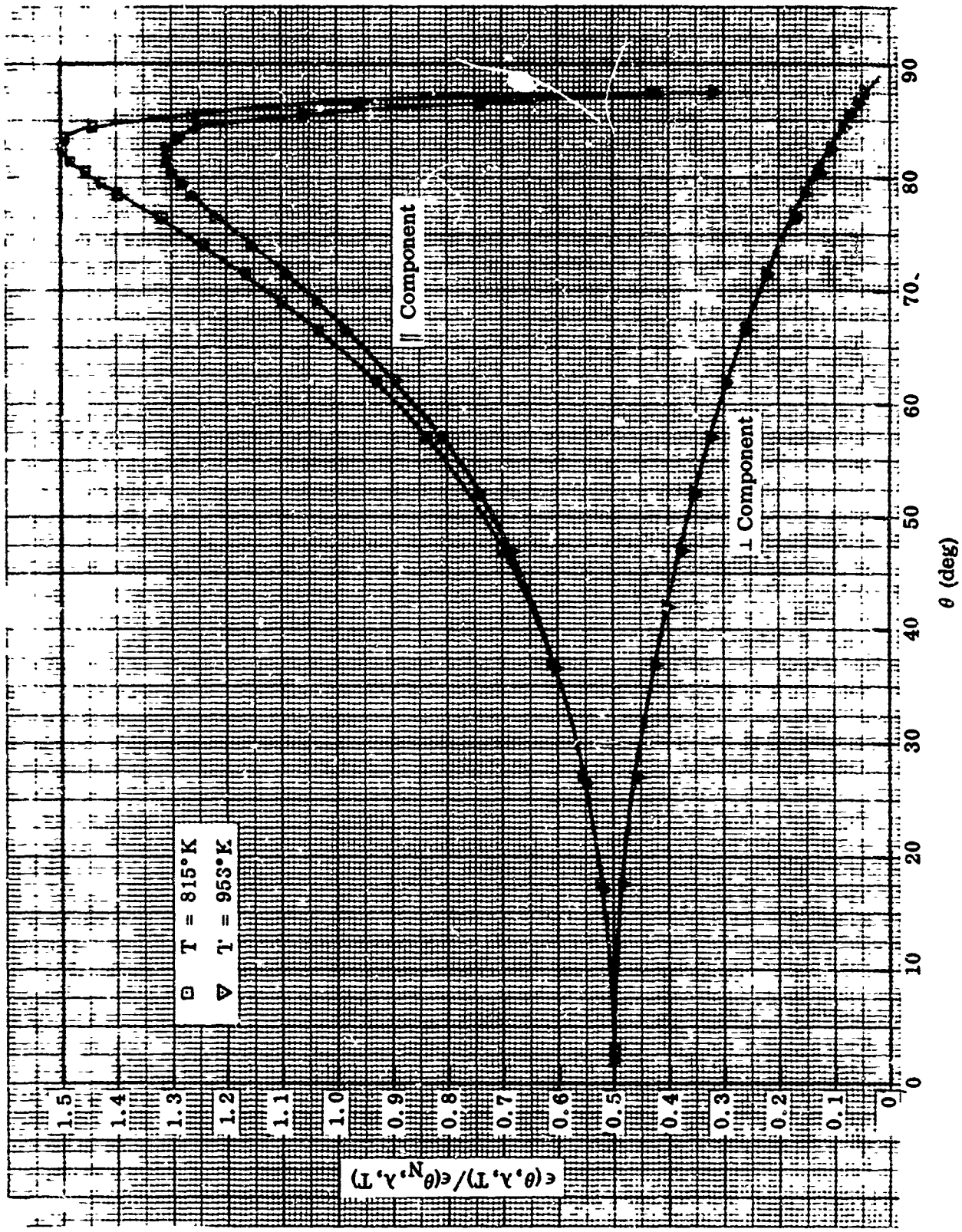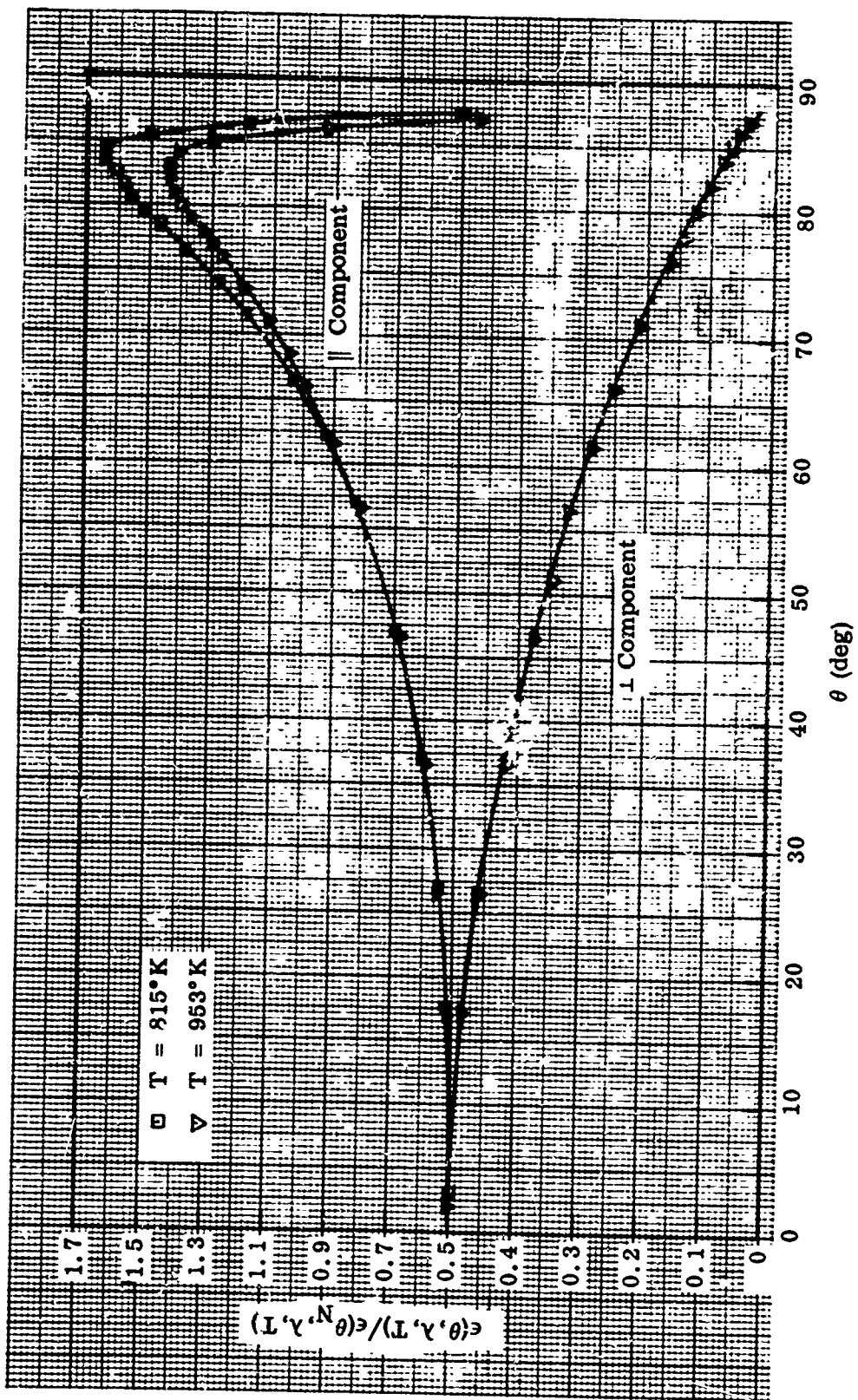
209

Figure 122 Relative Spectral Directional Emittance at $\lambda = 4 \, \mu$, Stainless Steel Sample No. 1R
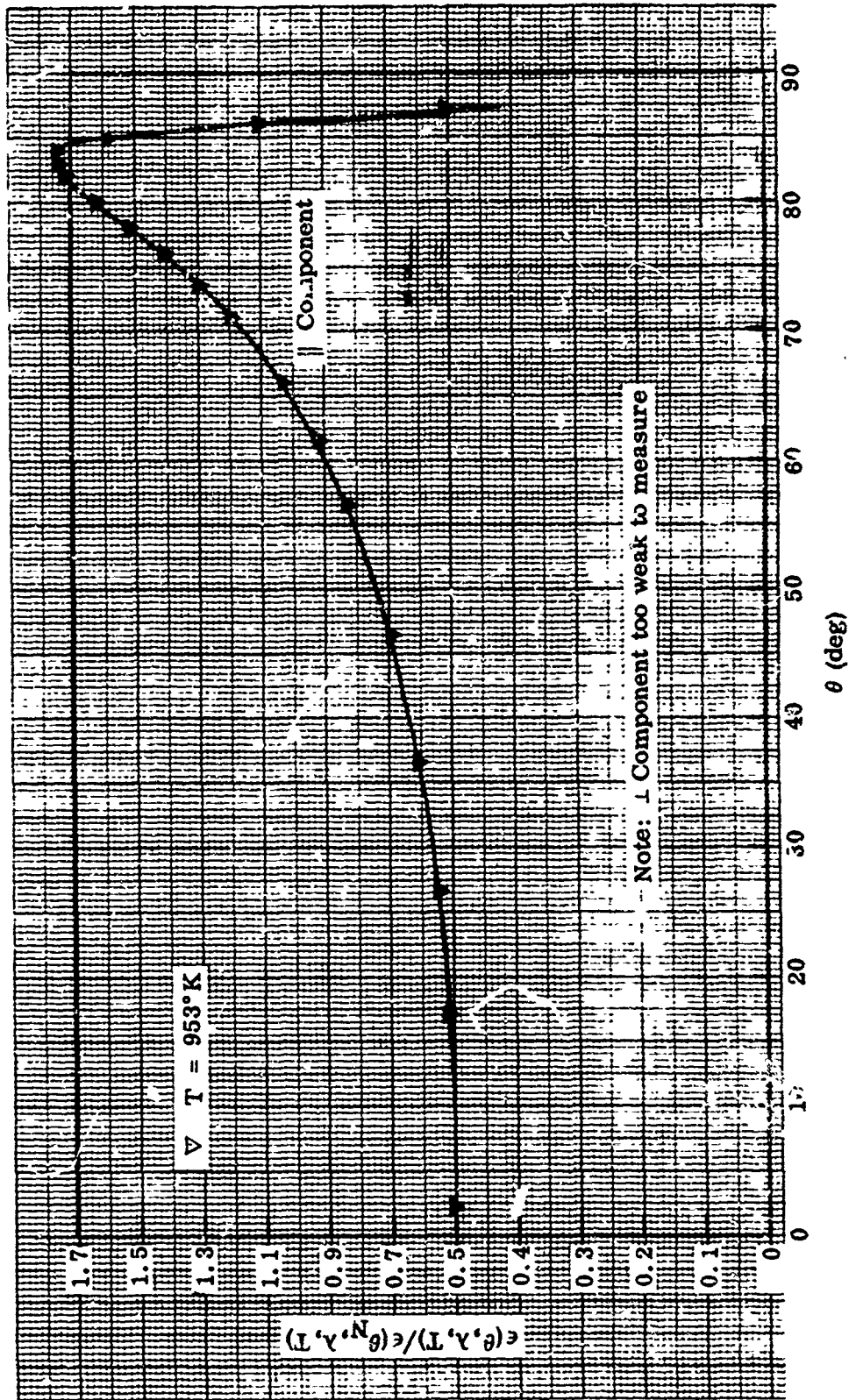
210

Figure 123 Relative Spectral Directional Emittance at $\lambda = 6\,\mu$, Stainless Steel Sample No. 1R

211

12. STAINLESS STEEL SAMPLE NO. 3R

Preparation: Electropolished, roughened, and annealed in the same manner as stainless steel sample no. 1R. Oxidized for 1/2 hr at 800° C in wet hydrogen furnace.

Initial Oxide Film Characteristics: Color: Purple (interference film). Composition: primarily Fe_3O_4. Average thickness: 0.165 μ (based on weight-gain measurements).

Test Procedure: Absolute and relative directional emittance data were obtained at 535, 677, 810, and 949° K, and the absolute and relative total directional emittance values were remeasured after the 949° K emittance tests (first temperature cycle). Absolute emittance data were remeasured at 540, 675, and 808° K (second temperature cycle) to determine the change in sample emittance characteristics due to the change in the oxide film. The test chamber pressure was maintained at 1.5×10^{-6} Torr throughout all tests.

Emittance Data: Absolute emittance values are shown in Table XXV; relative total directional emittance data in Figure 124; relative spectral directional emittance data at $\lambda = 1.5$, 2, 3, 4, 6, and 8 μ in Figures 125 through 130.

Remarks: The absolute and relative directional emittance data obtained during the first test temperature cycle up to 949° K are believed to be characteristic of the initial surface of this sample (i.e., the purple oxide film). The absolute emittance data obtained at the end of the 959° K tests and during the second test temperature cycle indicate that additional sample oxidation occurred during the 949° K directional emittance tests. Only slight changes in the total and spectral directional emittance data were observed, however. At the conclusion of the emittance tests, the color of the oxide film had changed from purple to blue-gray.

Photomicrographs and electron micrographs of the sample are shown in Figures 30 and 31, respectively, and are discussed in subsection V.2.a. No attempt was made to determine the thickness of the oxide film after the emittance tests.

An electron diffraction pattern of the initial oxide film was identical to that shown in Figure 36 for sample 3S, indicating the composition to be primarily Fe_3O_4.

Table XXV. Absolute Emittance Data for Stainless Steel Sample No. 3R

Temperature (°K)	Time at Temp. (hr, min)	$\epsilon(T)$	$\epsilon(\theta_N, T)$	$\epsilon(\theta_N, \lambda, T)$							
				1.5 μ	2 μ	3 μ	4 μ	6 μ	8 μ	10 μ	12 μ
First Temperature Cycle											
535[a]	1,55	0.259	0.249								
677[a]	0,45	0.319	0.334								
810[a]	2,30	0.382	0.413	0.824	0.800	0.629	0.442	0.280	0.205	0.168	0.139
949[a]	6,30	0.439	0.490	0.847	0.825	0.647	0.463	0.308	0.226	0.186	0.154
950[a]		0.477	0.543	0.847	0.867	0.735	0.538	0.337	0.243	0.195	0.162
Second Temperature Cycle[b]											
540	0,45	0.263	0.276								
675	0,30	0.346	0.376								
808	0,45	0.413	0.467	0.842	0.871	0.738	0.525	0.305	0.213	0.168	0.135

(a) Directional emittance data obtained at these temperatures.
(b) Appearance of oxide film changed from purple to bluish-gray during 950°K emittance tests at the end of the first temperature cycle.
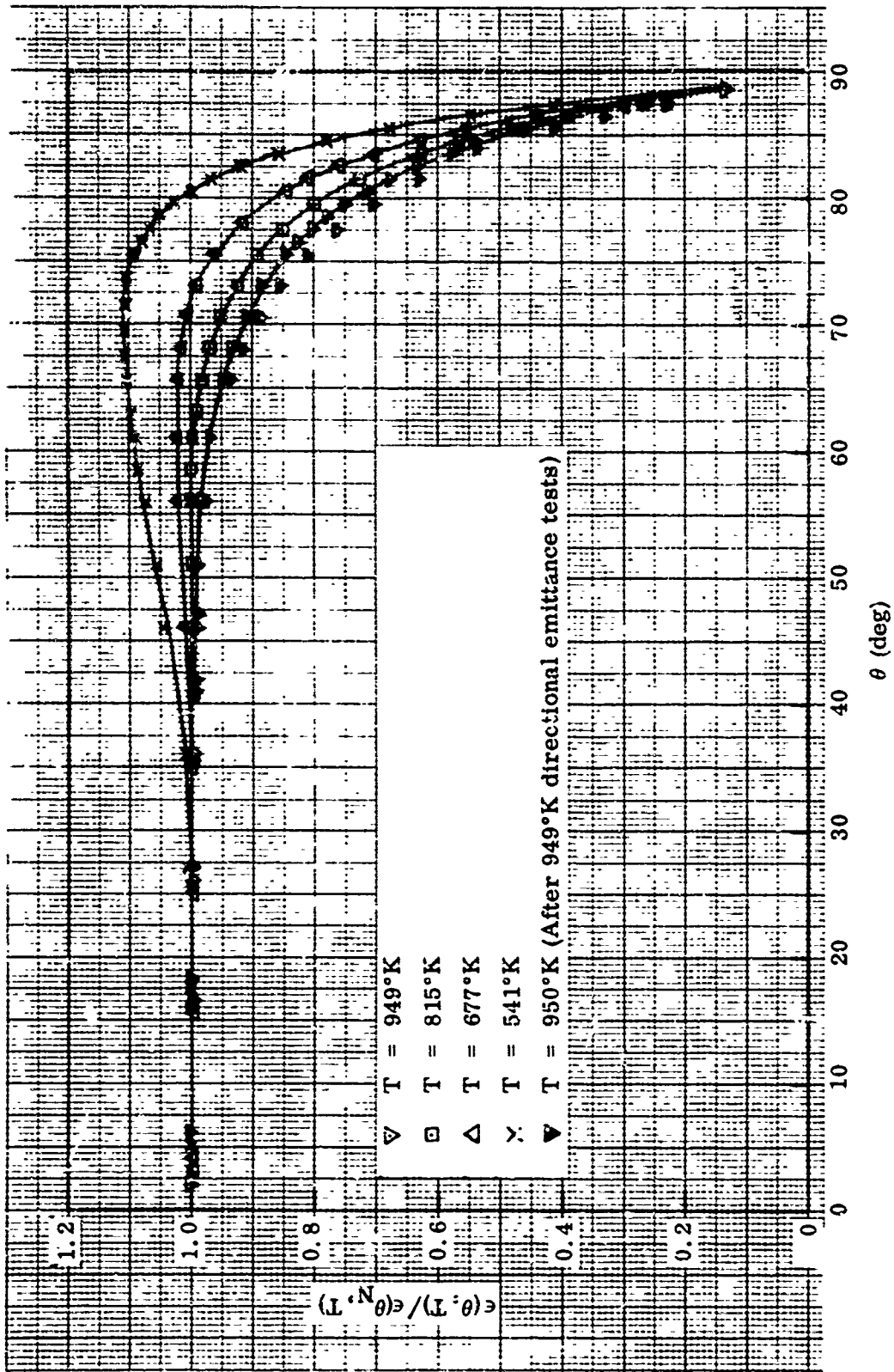
Figure 124 Relative Total Directional Emittance of Stainless Steel Sample No. 3R

214

Figure 125 Relative Spectral Directional Emittance at $\lambda = 1.5\ \mu$, Stainless Steel Sample No. 3R

215

Figure 126 Relative Spectral Directional Emittance at $\lambda = 2\,\mu$, Stainless Steel Sample No. 3R

216

Figure 127 Relative Spectral Directional Emittance at $\lambda = 3\ \mu$, Stainless Steel Sample No. 3R

Figure 128 Relative Spectral Directional Emittance at $\lambda = 4\ \mu$, Stainless Steel Sample No. 3R
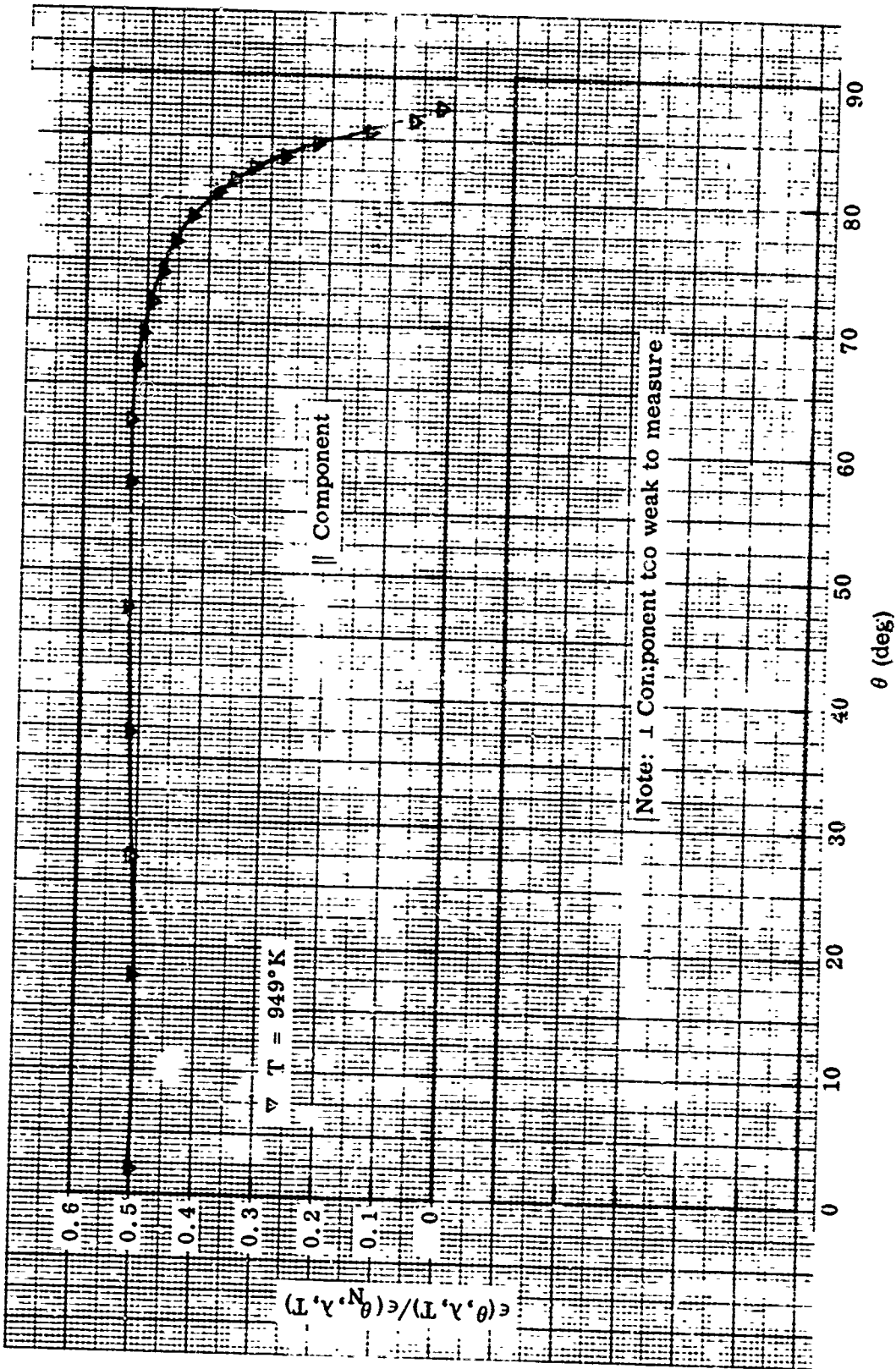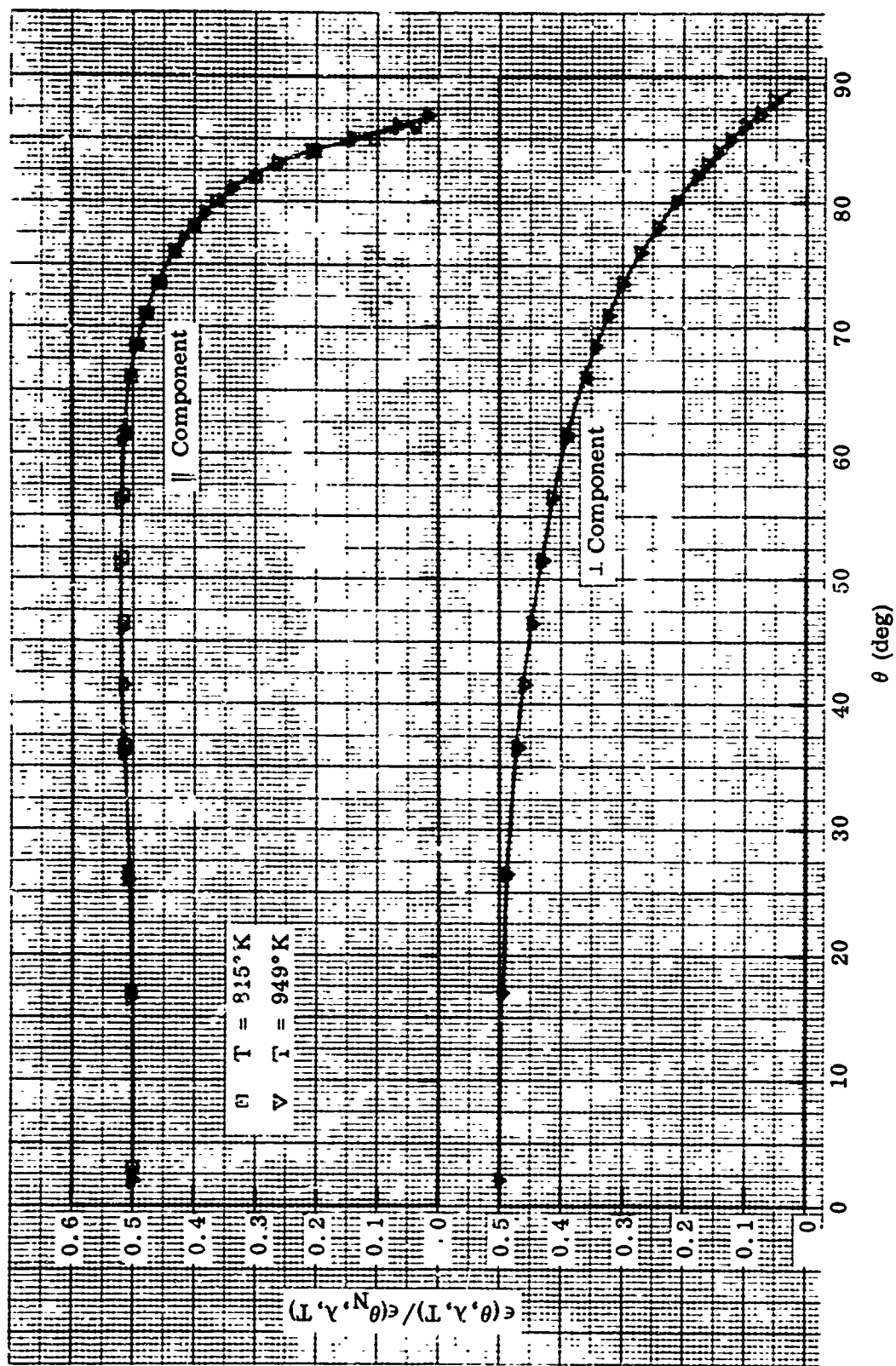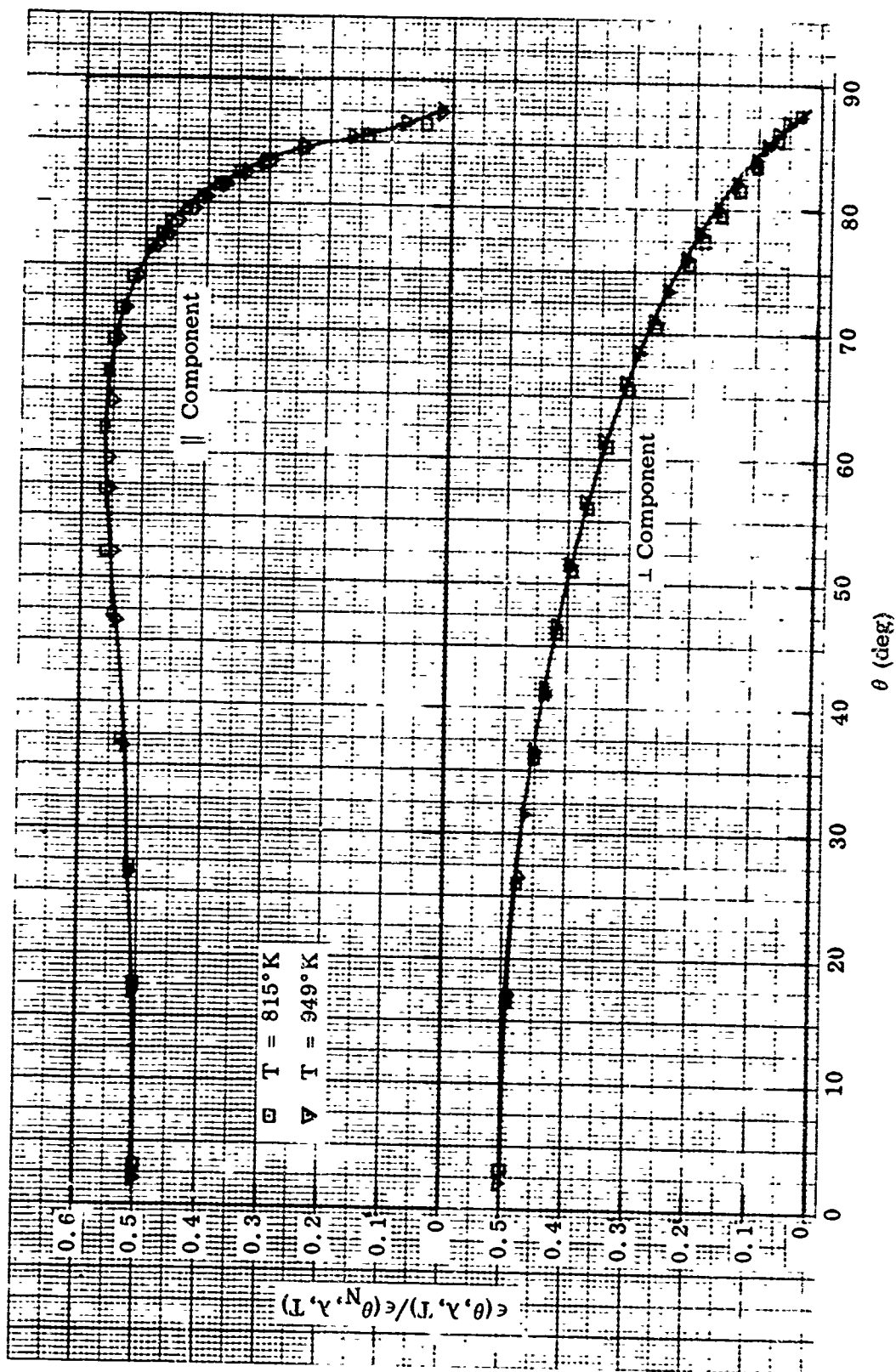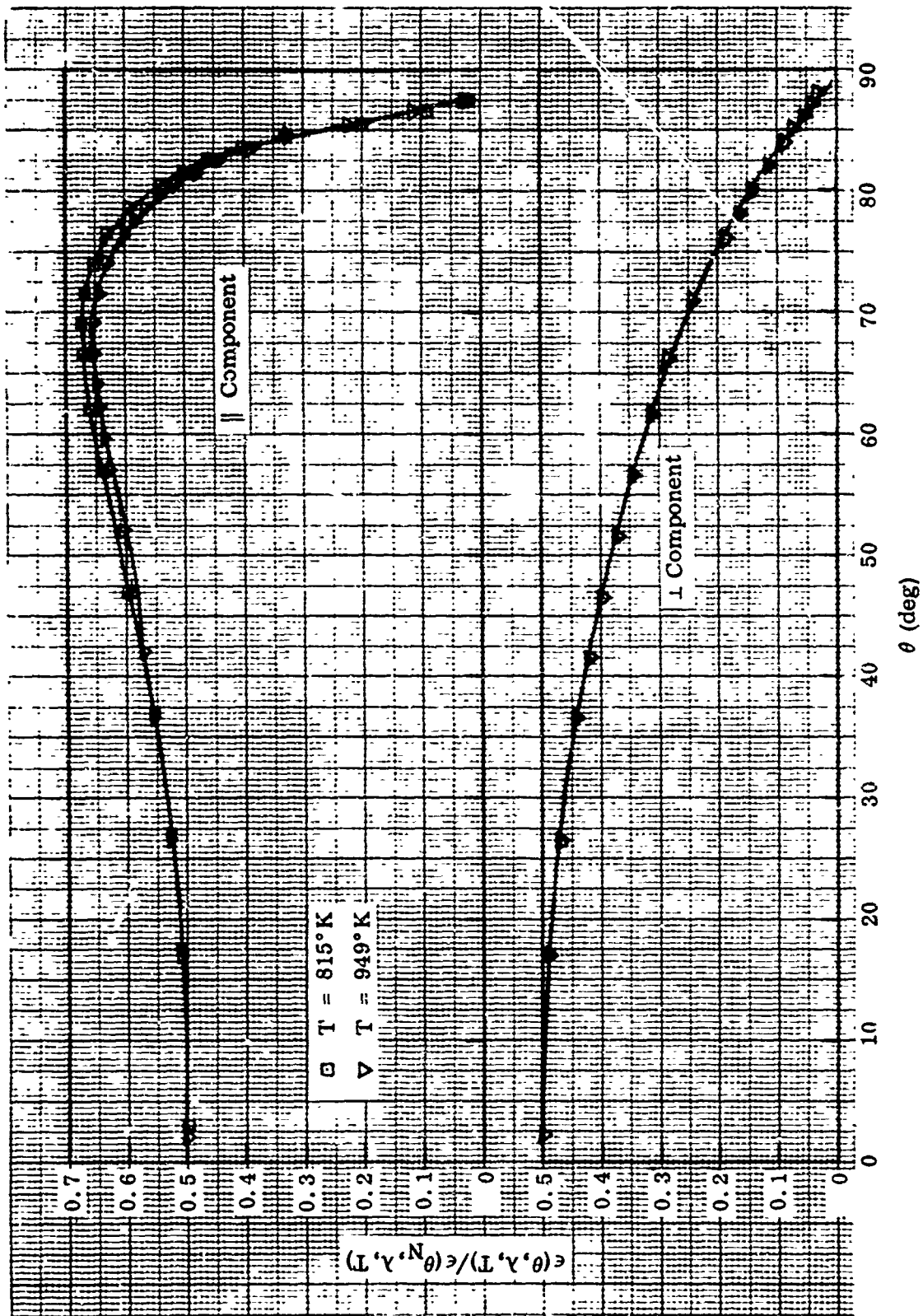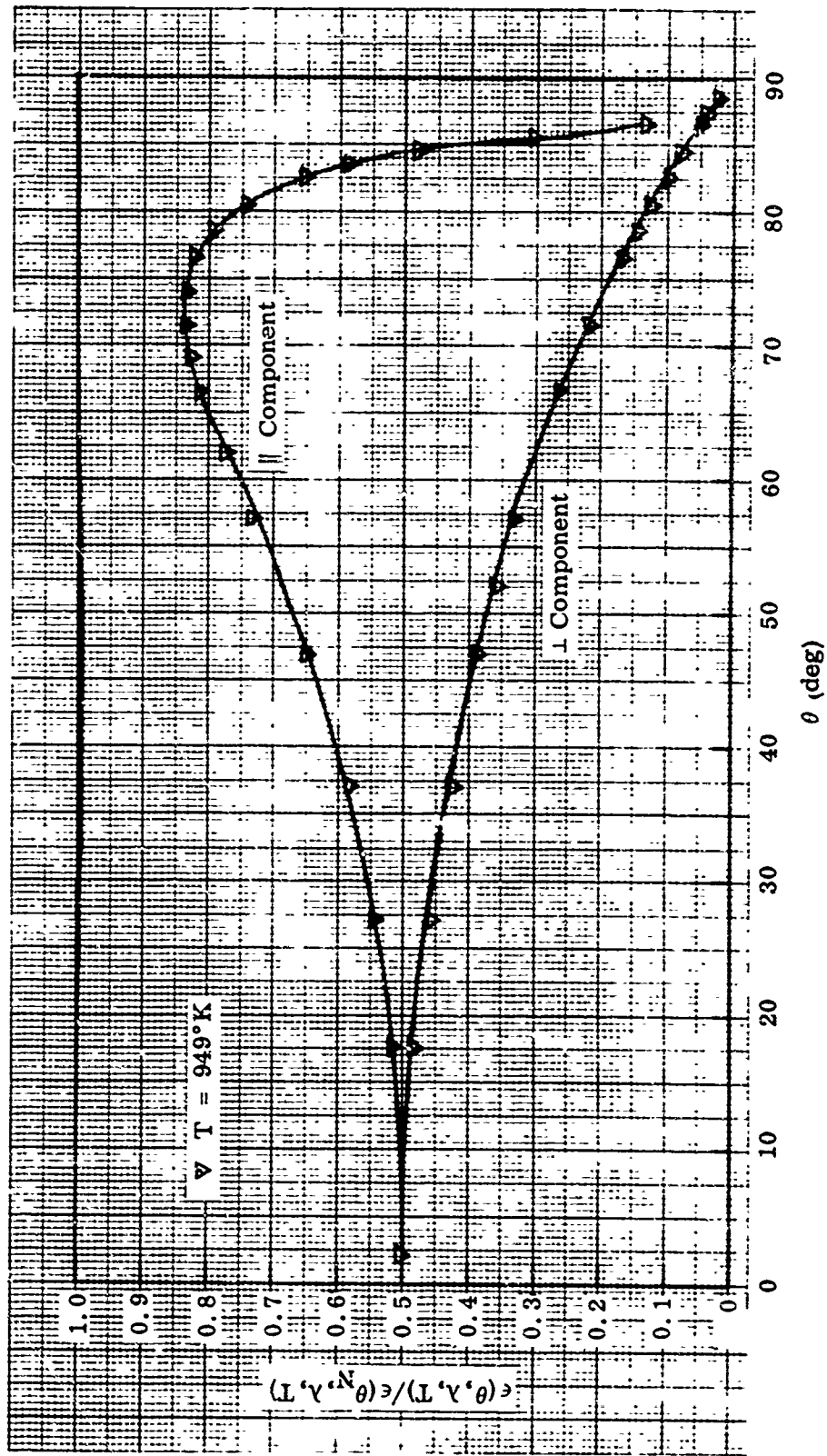
218

Figure 129 Relative Spectral Directional Emittance at $\lambda = 6 \mu$, Stainless Steel Sample No. 3R
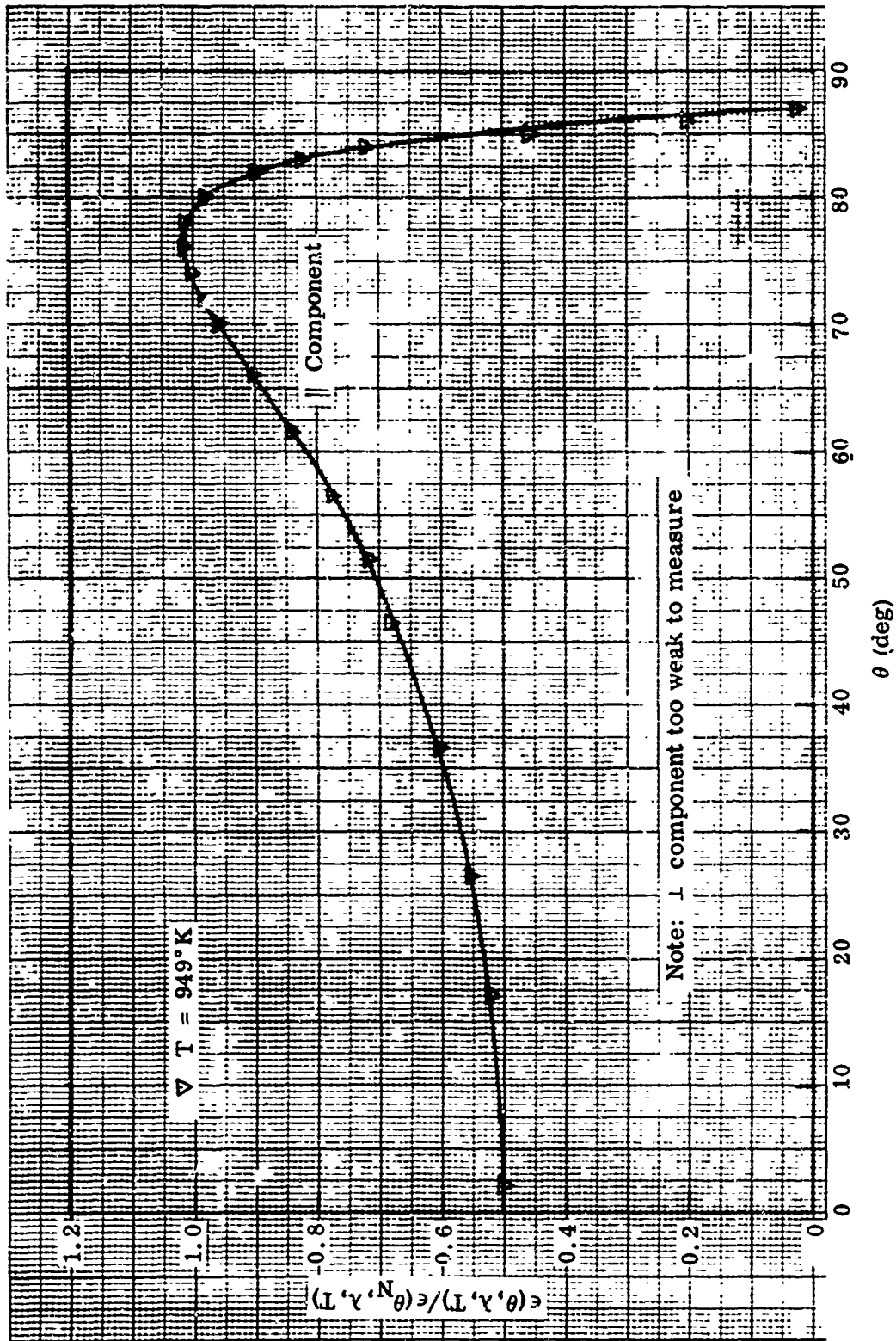
219

Figure 130 Relative Spectral Directional Emittance at $\lambda = 8 \mu$, Stainless Steel Sample No. 3R

13. STAINLESS STEEL SAMPLE NO. 5R

Preparation: Electropolished, roughened. and annealed in the same manner as stainless steel sample no. 1R. Oxidized for 1-1/2 hr at 1000° C in wet hydrogen furnace.

Initial Oxide Film Characteristics: Color: Dark gray. Composition: Primarily Fe_3O_4. Average thickness: 1.5 μ (based on weight gain measurements).

Test Procedure: Absolute and relative directional emittance data were obtained at 535, 675, 815, and 951° K, and the absolute and relative total directional emittance values were remeasured after the 951° K tests (first temperature cycle). Absolute emittance values were remeasured at 535, 678, and 813° K (second temperature cycle) to check the stability of the sample. The test chamber pressure was maintained at 1.5×10^{-6} Torr throughout all tests.

Emittance Data: Absolute emittance values are shown in Table XXVI; relative total directional emittance data in Figure 131; relative spectral directional emittance data at λ = 1.5, 2, 3, 4, 6, and 8 μ in Figures 132 through 137.

Remarks: The absolute and relative directional emittance data indicate that this sample remained stable throughout the emittance tests. Similarly, no change in the visual appearance of the sample was noticed. The absolute total and spectral normal emittance values were generally slightly higher than those determined for sample 5S, but the total hemispherical emittance values were about the same. These differences correlate with the slightly thicker oxide film indicated for this sample by the initial weight-gain data. The relative directional emittance characteristics of the two samples appeared to be about the same.

Photomicrographs and electron micrographs of the sample are shown in Figures 30 and 31, respectively, and are discussed in subsection V.2.a. No attempt was made to determine the oxide film thickness after the emittance tests.

An electron diffraction pattern of the initial oxide film was identical to that shown in Figure 36 for sample 5S, indicating the composition to be primarily Fe_3O_4.

Table XXVI. Absolute Emittance Data for Stainless Steel Sample No. 5R

Temperature (°K)	Time at Temp. (hr, min)	ε(T)	ε(θ_N, T)	$\epsilon(\theta_N, \lambda, T)$							
				1.5 μ	2 μ	3 μ	4 μ	6 μ	8 μ	10 μ	12 μ
First Temperature Cycle											
535[a]	1, 15	0.755	0.799								
675[a]	0, 45	0.790	0.853								
815[a]	3, 0	0.807	0.879	0.950	0.967	0.958	0.930	0.828	0.754	0.812	0.792
951[a]	5, 50	0.836	0.899	0.995	0.977	0.963	0.934	0.848	0.765	0.827	0.820
951[a]		0.838	0.901	0.997	0.997	0.973	0.950	0.842	0.763	0.827	0.816
Second Temperature Cycle											
535	0, 45	0.757	0.799								
678	0, 25	0.791	0.850								
813	0, 40	0.809	0.881	0.988	0.998	0.968	0.939	0.837	0.762	0.819	0.798

(a) Directional emittance data obtained at these temperatures.

222
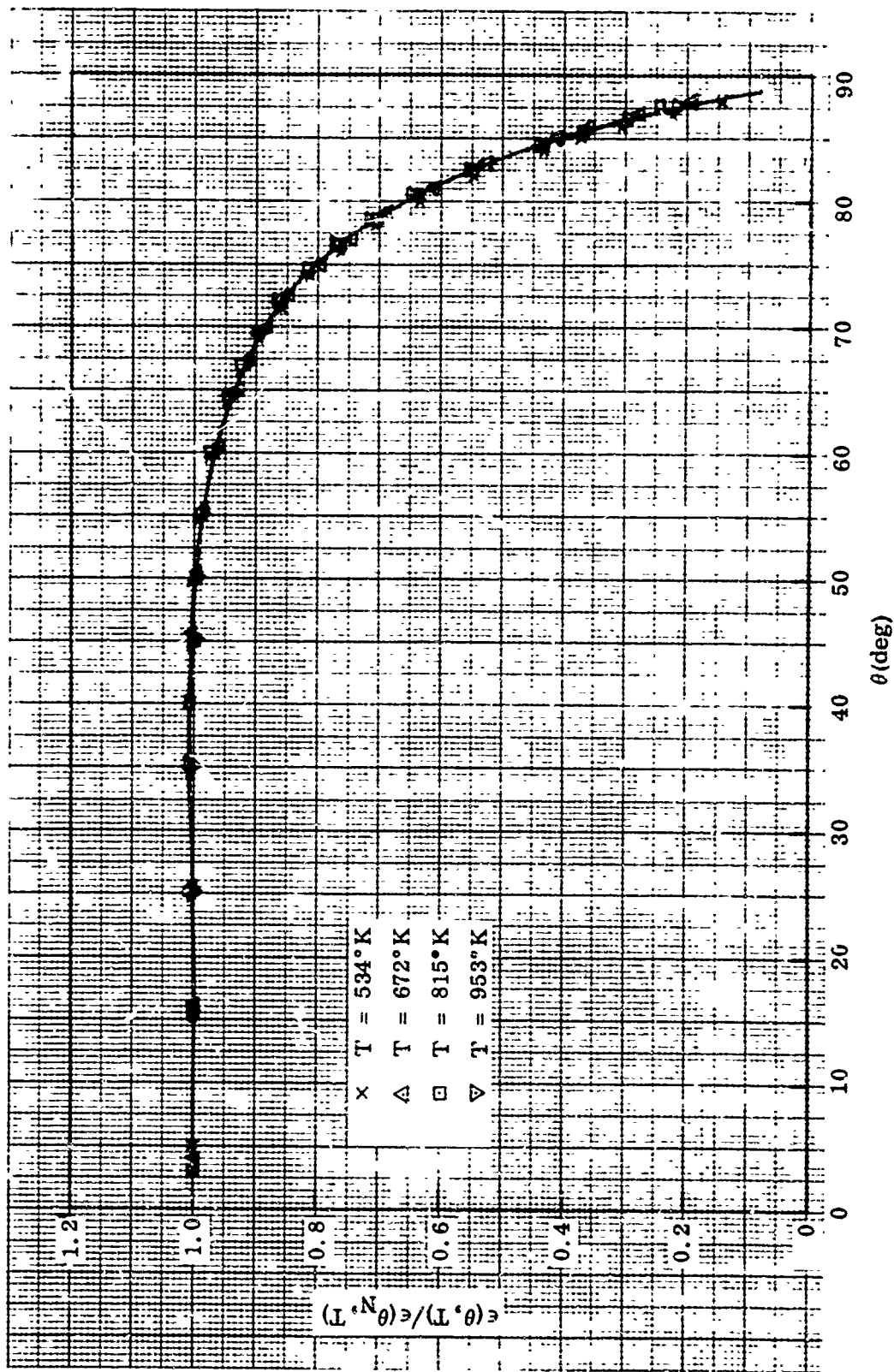
Figure 131 Relative Total Directional Emittance of Stainless Steel Sample No. 5R

223
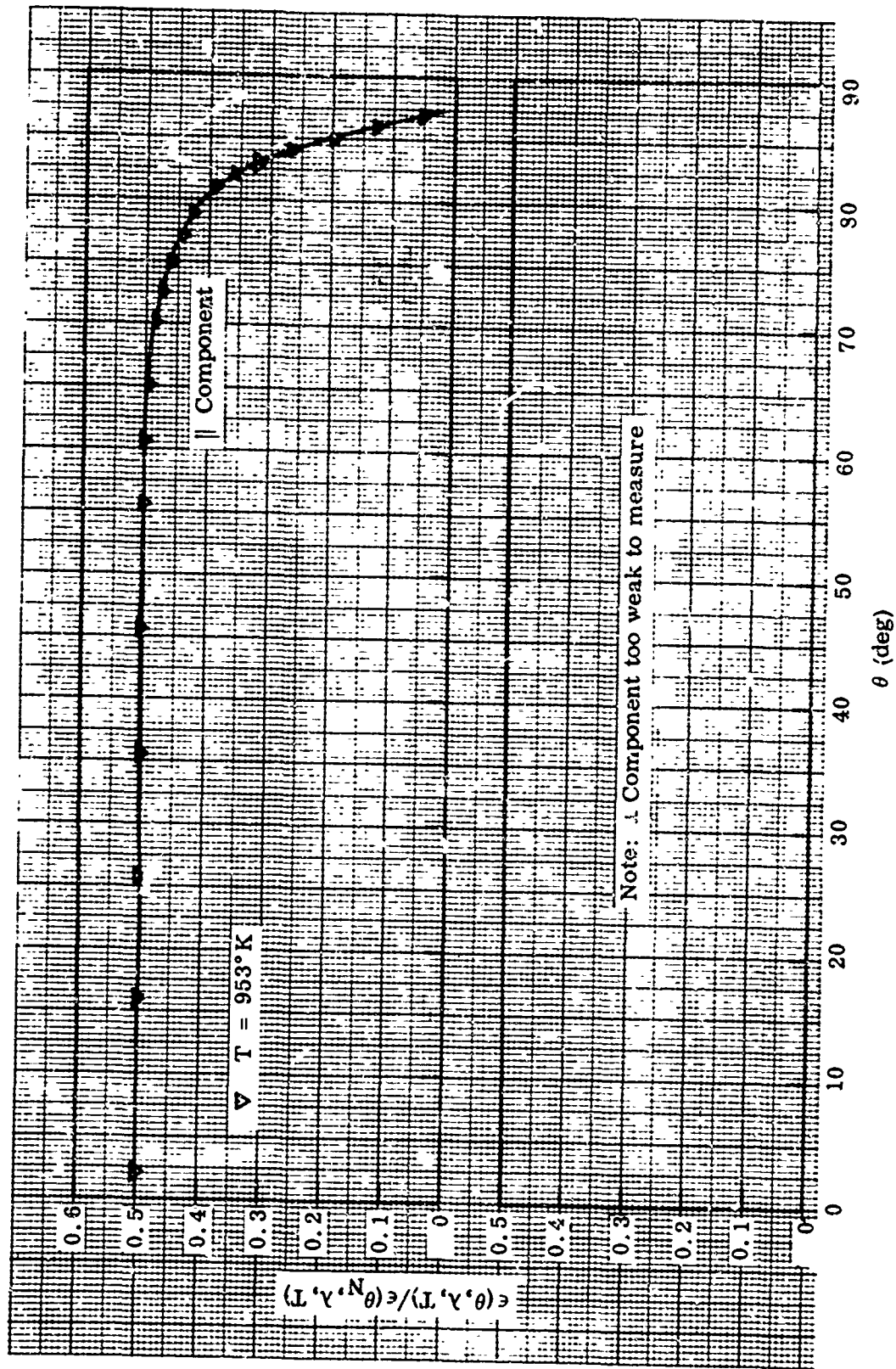
Figure 132 Relative Spectral Directional Emittance at $\lambda = 1.5\ \mu$, Stainless Steel Sample No. 5R
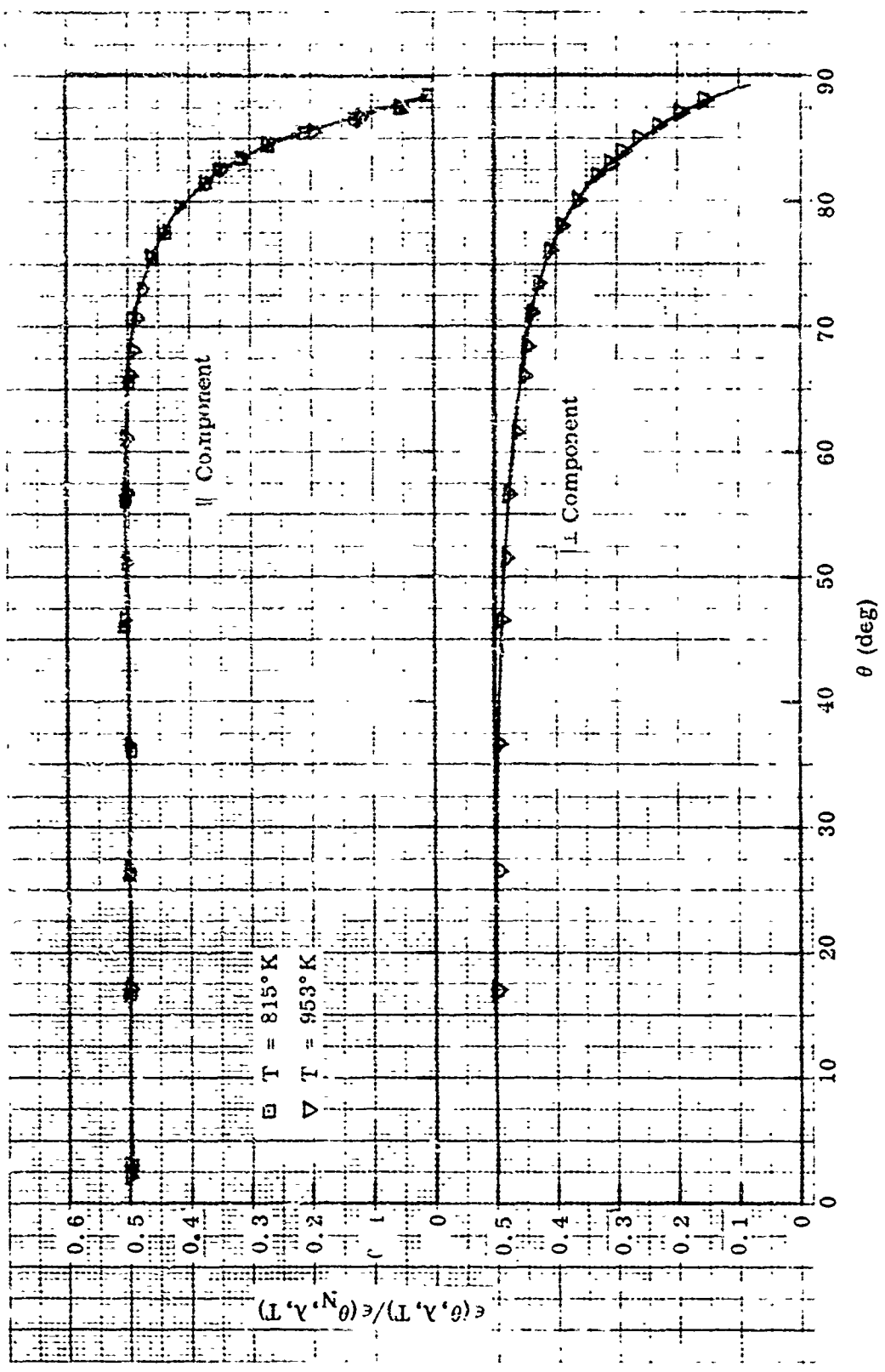
Figure 133   Relative Spectral Directional Emittance at $\lambda = 2 \mu$, Stainless Steel Sample No. 5R

225
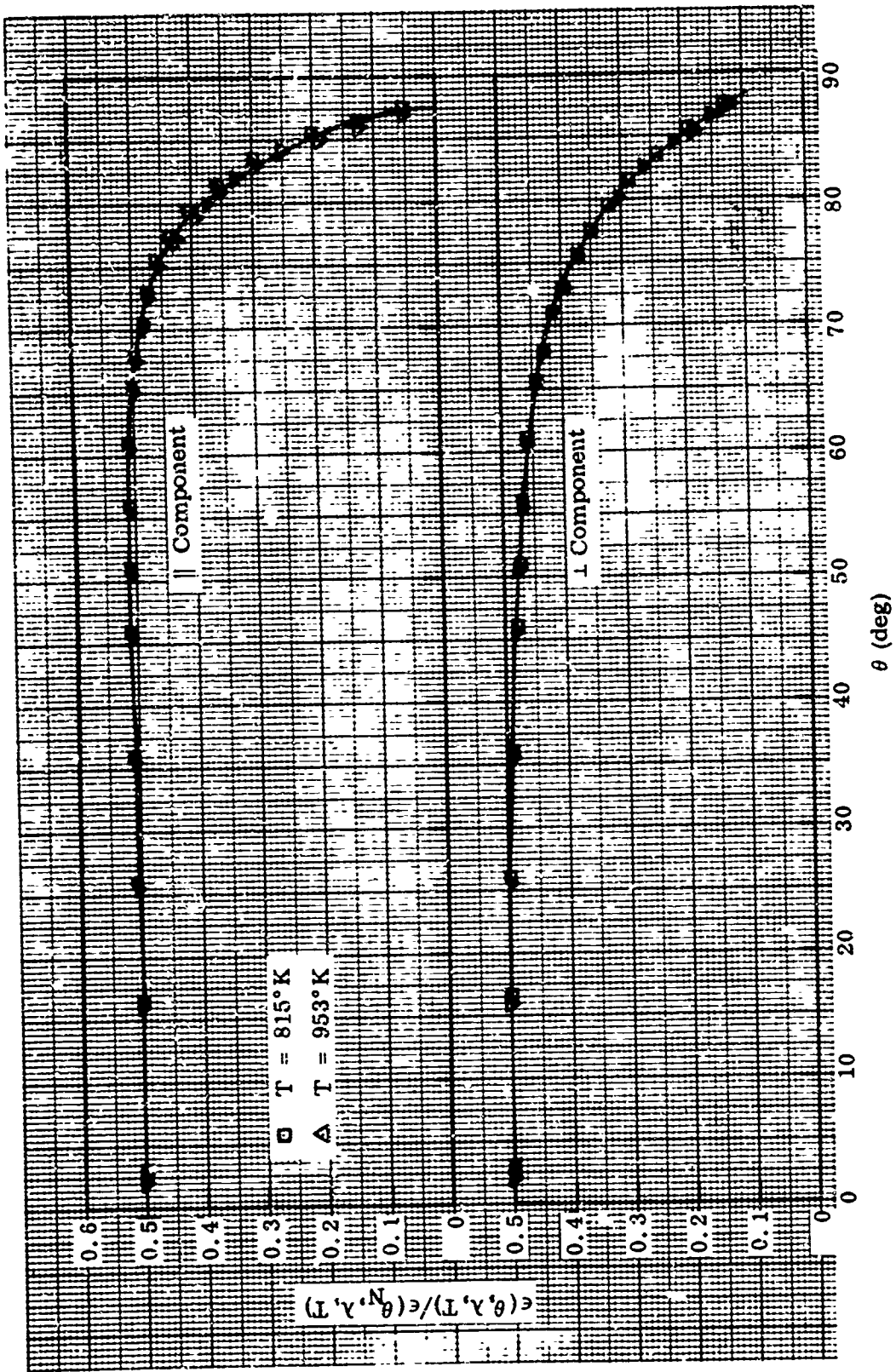
Figure 134   Relative Spectral Directional Emittance at $\lambda = 3 \mu$, Stainless Steel Sample No. 5R

226
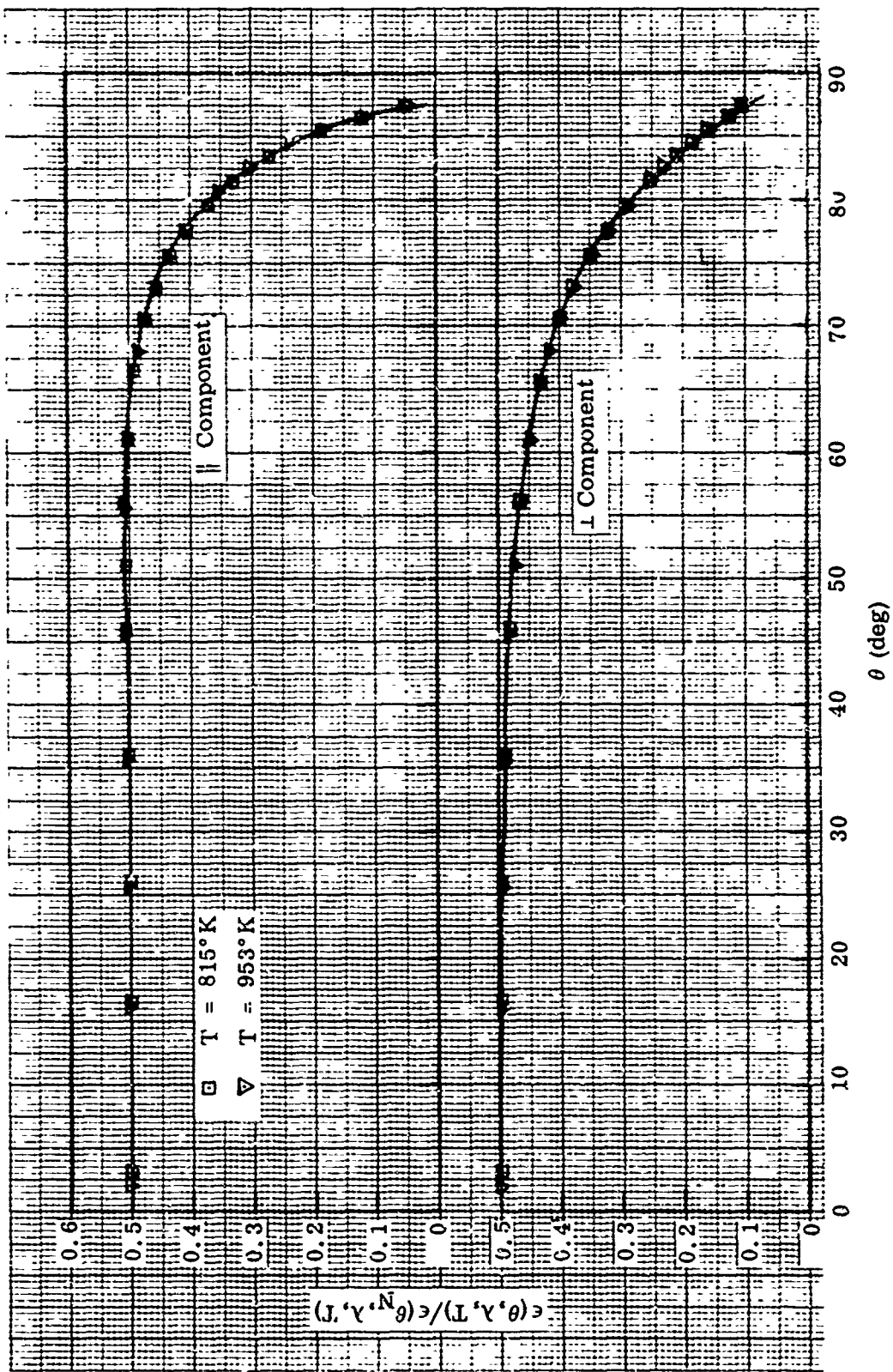
Figure 135   Relative Spectral Directional Emittance at $\lambda = 4\ \mu$, Stainless Steel Sample No. 5R

227
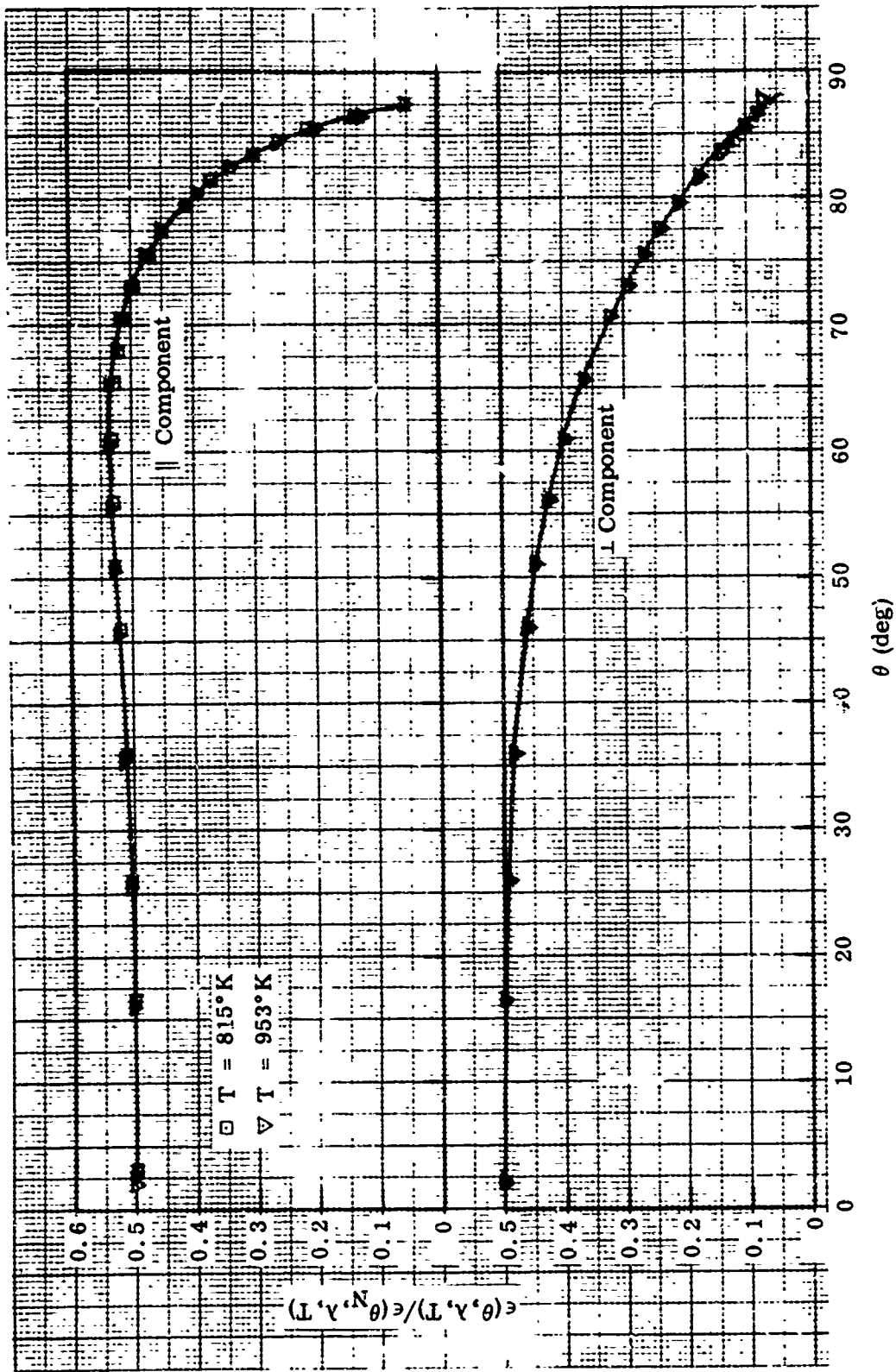
Figure 136 Relative Spectral Directional Emittance at $\lambda = 6\ \mu$, Stainless Steel Sample No. 5R

228
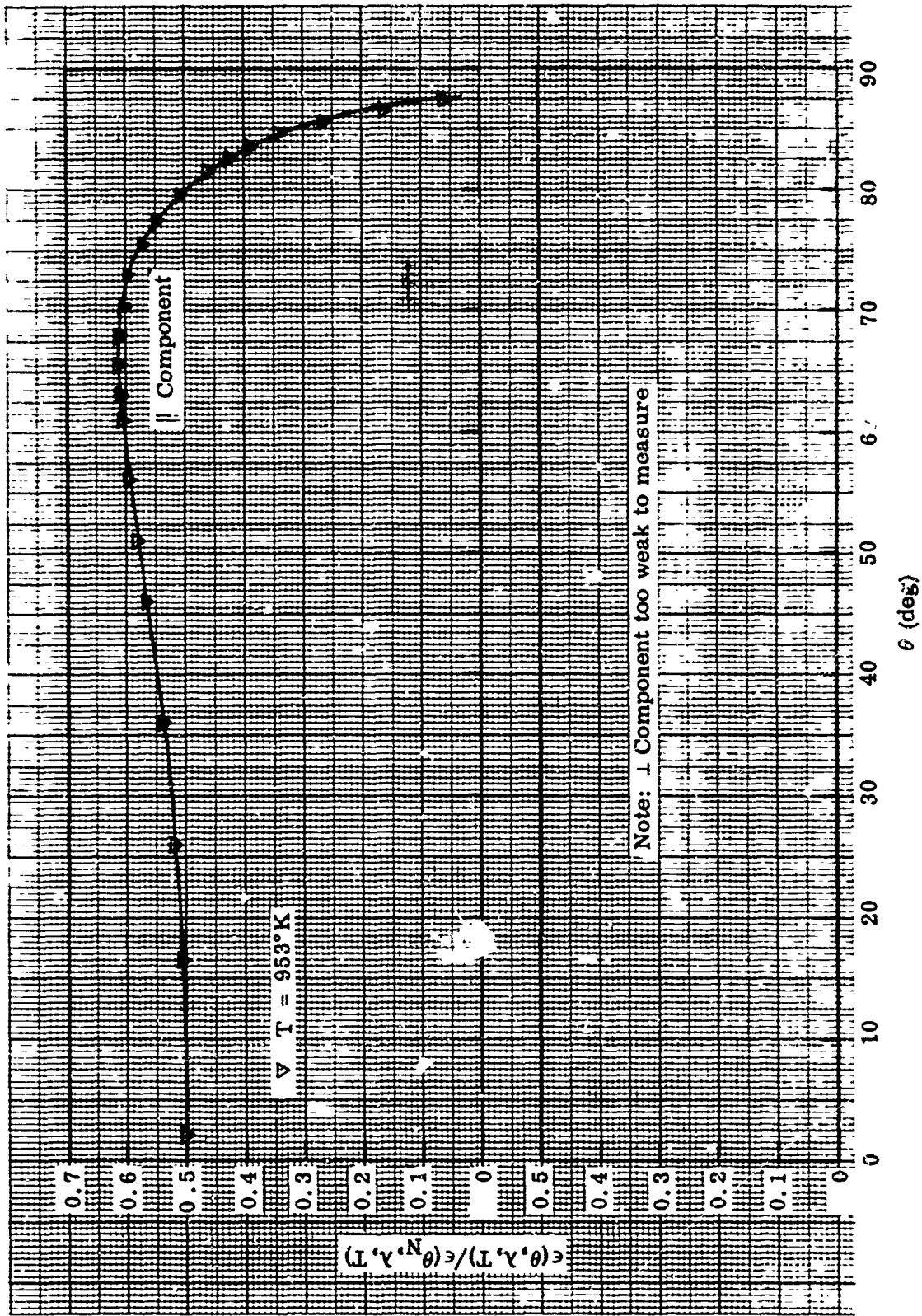
Figure 137 Relative Spectral Directional Emittance at $\lambda = 8\ \mu$, Stainless Steel Sample No. 5R

229

14. STAINLESS STEEL SAMPLE NO. 1S-3

Preparation: Unoxidized (same as sample no. 1S-2)

RMS Roughness: Not measured, but assumed to be the same as for stainless steel sample no. 1S-2.

Test Procedure. All emittance tests were made with the sample in a low-pressure atmosphere of high-purity hydrogen. Absolute and relative directional emittance data were obtained at 529 and 953°K (first temperature cycle). The sample surface was inspected and appeared bright and clean (i.e., unoxidized). Absolute and relative directional emittance data were then obtained at 531, 674, 814, 955, and 1086°K, and the absolute and relative total directional emittance values were remeasured at the end of the 1086°K tests (second temperature cycle) to check the stability of the sample.

Emittance Data: Absolute emittance values are shown in Table XXVII; relative total directional emittance data in Figure 138; relative spectral directional emittance data at $\lambda = 1.5, 2, 3, 4, 6,$ and 8μ in Figures 139 through 144.

Remarks: This sample was the third of three smooth, unoxidized stainless steel samples tested. (Data for the second sample are given in subsection VII.6.) The sample was tested in a low-pressure atmosphere of hydrogen gas in an attempt to eliminate the surface oxidization problem encountered with the two previous samples. The emittance data indicate that surface oxidation was inhibited at temperatures up to 1086°K, but that oxidation occurred during the 1086°K tests.

To make these tests, high-purity hydrogen gas was leaked into the test chamber at a continuous flow rate of 0.03 cfh. This flow rate changed the ionization pressure gage reading from 2×10^{-6} to 8×10^{-4} Torr, raised the foreline thermocouple gage reading from 5 to 150 μ, and produced an audible change in the sound of the fore pump, indicating a positive flow rate through the chamber. Except for this modification, the test procedure was the same as for the previous samples.

After the first test temperature cycle, the sample surface was observed to be bright and clean. Emittance data were then obtained at the remaining temperatures. At 1086°K, changes in the spectral directional emittance were noted which indicated that the surface was oxidizing. Absolute emittance values determined at the end of the 1086°K tests also indicated oxidization, and the tests were terminated. The surface of the sample was observed to be uniformly covered with a light, gold-colored oxide film at the conclusion of the emittance tests.

In general, the absolute emittance data for this sample are about the same as for sample 1S-2, although the low-temperature total hemispherical emittance values appear to be slightly high. This may be due to the conductive transfer of heat from the sample by the hydrogen gas. The relative total and spectral directional emittance data for this sample are believed to be representative for the unoxidized stainless steel up through the 950°K test. The change in directional emittance due to the oxide that formed at 1090°K is indicated in Figure 138.

A surface photomicrograph of the gold-colored oxide film that formed at 1090°K was identical in appearance to that shown in Figure 30 for sample no. 1S-2. No electron micrographs or diffraction patterns of the oxide were obtained, but the characteristics are assumed to be very similar to those for samples 1S-2 and 2S.

230

Table XXVII. Absolute Emittance Data for Stainless Steel Sample No. 1S-3

Temperature (°K)	Time at Temp. (hr, min)	ε(T) (a)	ε(θ_N, T)	$\epsilon(\theta_N, \lambda, T)$							
				1.5 μ	2 μ	3 μ	4 μ	6 μ	8 μ	10 μ	12 μ
First Temperature Cycle											
529[b]	0,45	0.166	0.117								
953[b]	4,0	0.210	0.192	0.300	0.258	0.219	0.187	0.154	0.129	0.113	0.095
Second Temperature Cycle											
531[b]	1,0	0.171	0.121								
674[b]	0,45	0.184	0.153								
814[b]	4,15	0.199	0.175	0.309	0.259	0.217	0.185	0.150	0.124	0.107	0.089
955[b]	0,30	0.215	0.196								
1086[b]	5,15	0.229	0.215	0.354	0.296	0.237	0.197	0.164	0.138	0.112	0.106
1089[b]		0.242	0.232								

(a) No correction made for the hydrogen atmosphere effect on the calorimetric determinations of ε(T). Values appear to be high due to this effect.

(b) Directional emittance data obtained at these temperatures.
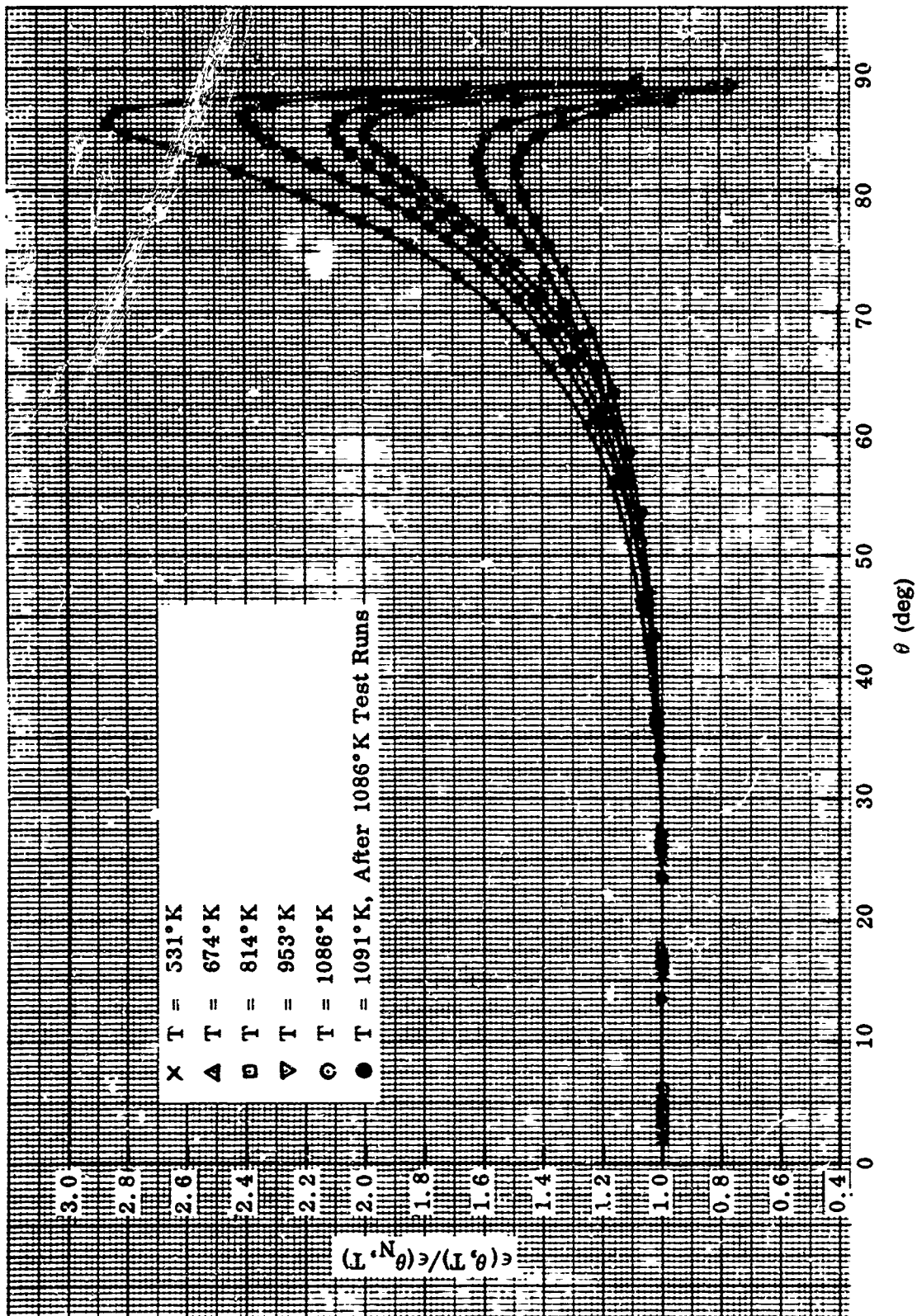
Figure 138 Relative Total Directional Emittance of Stainless Steel Sample No. 1S-3

Legend:
× T = 531°K
▲ T = 674°K
▣ T = 814°K
▽ T = 953°K
○ T = 1086°K
● T = 1091°K, After 1086°K Test Runs

Vertical axis: $\epsilon(\theta, T)/\epsilon(\theta_N, T)$

Horizontal axis: θ (deg)

Figure 139 Relative Spectral Directional Emittance at $\lambda = 1.5 \, \mu$, Stainless Steel Sample No. 1S-3

233

Figure 140 Relative Spectral Directional Emittance at $\lambda = 2\,\mu$, Stainless Steel Sample No. 1S-3

234

Figure 141 Relative Spectral Directional Emittance at $\lambda = 3\ \mu$, Stainless Steel Sample No. 1S-3
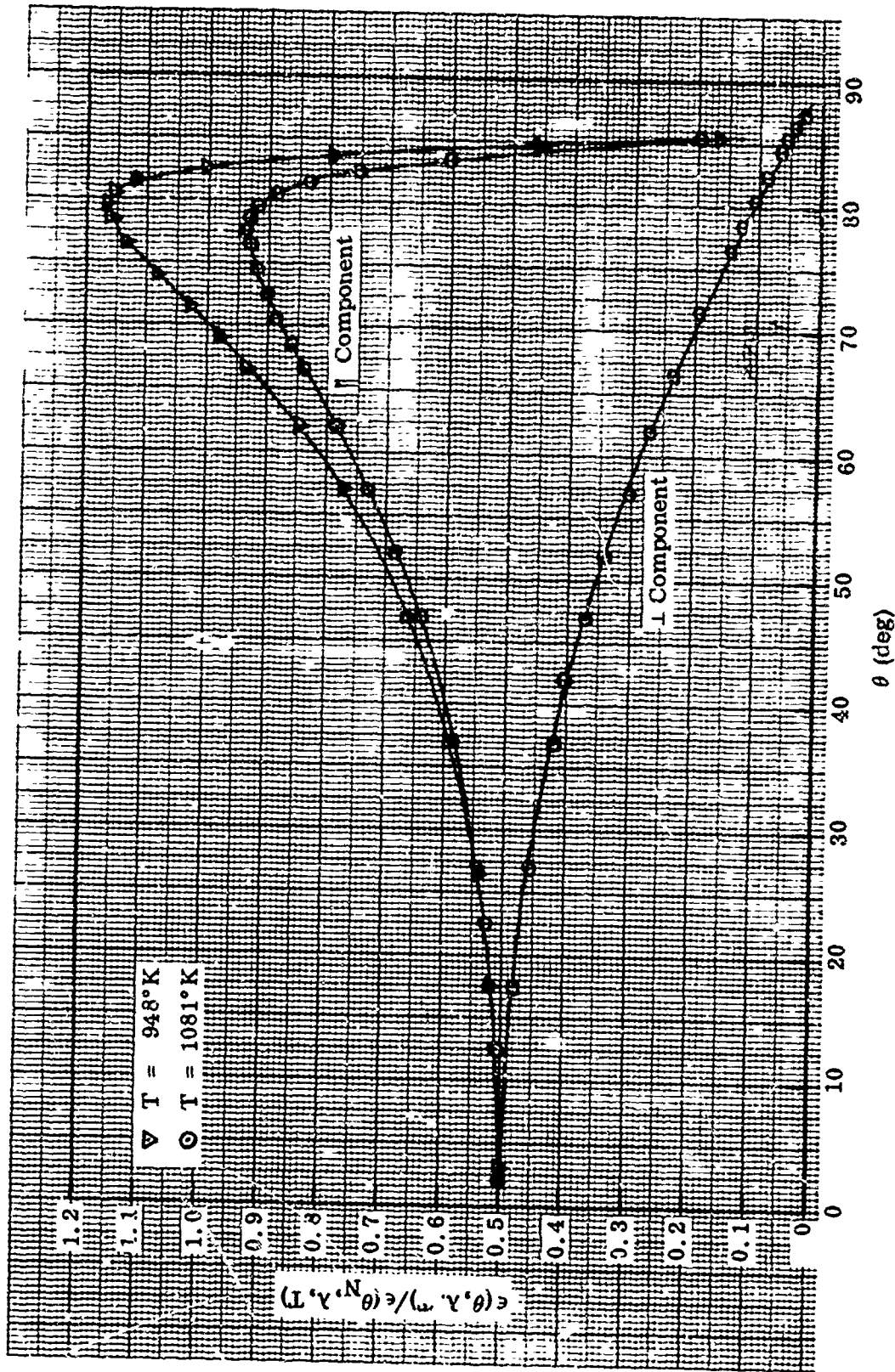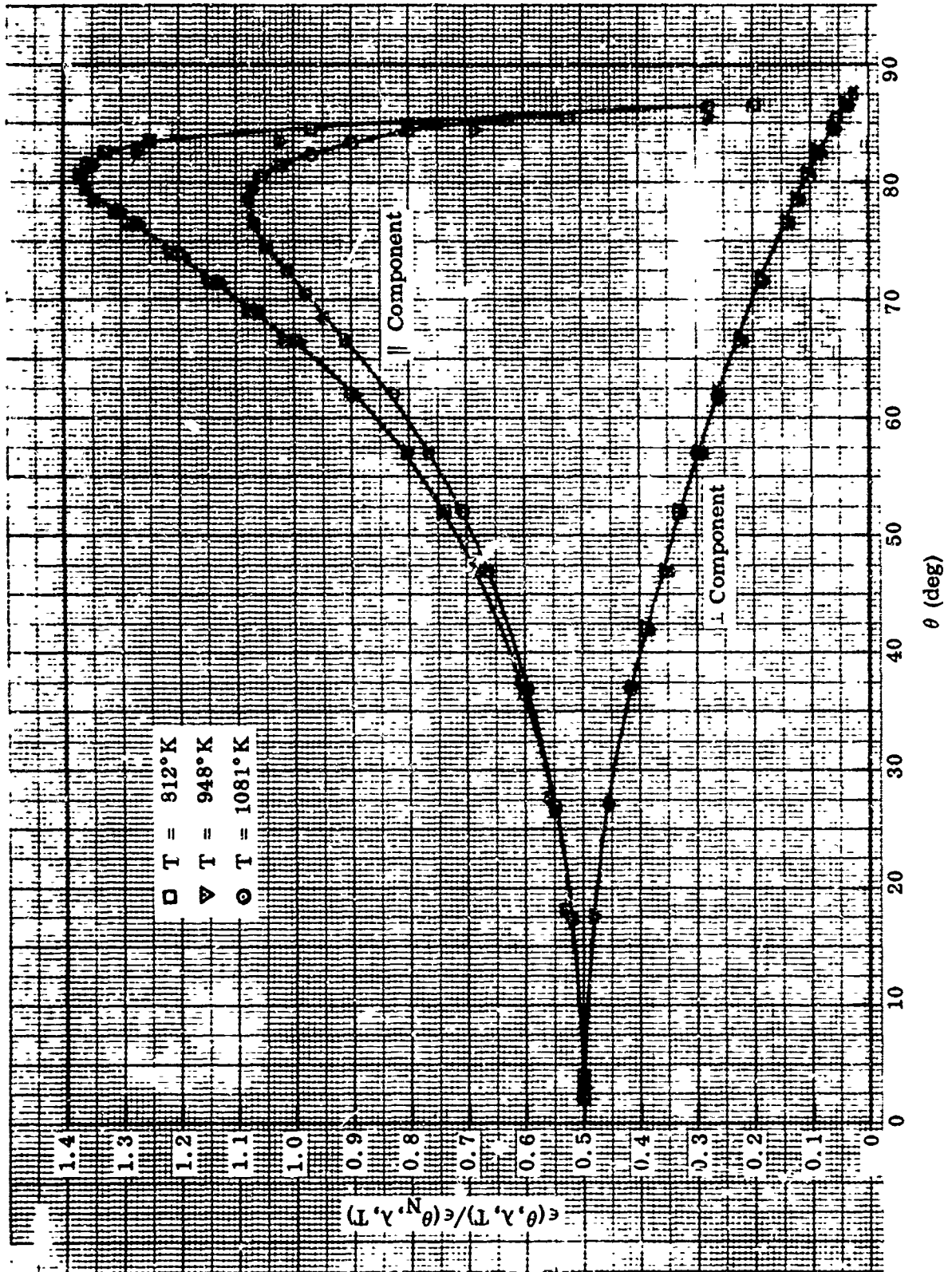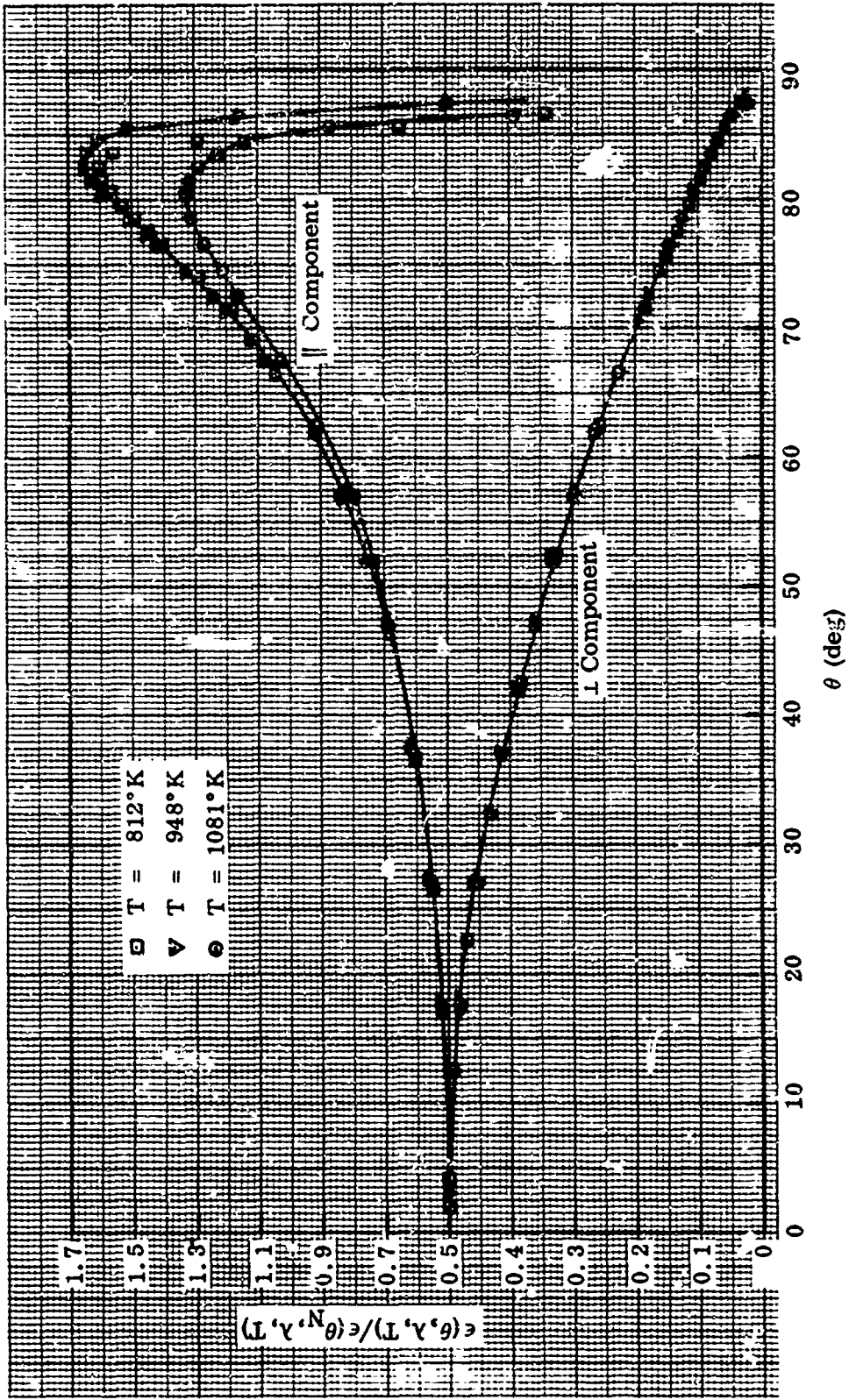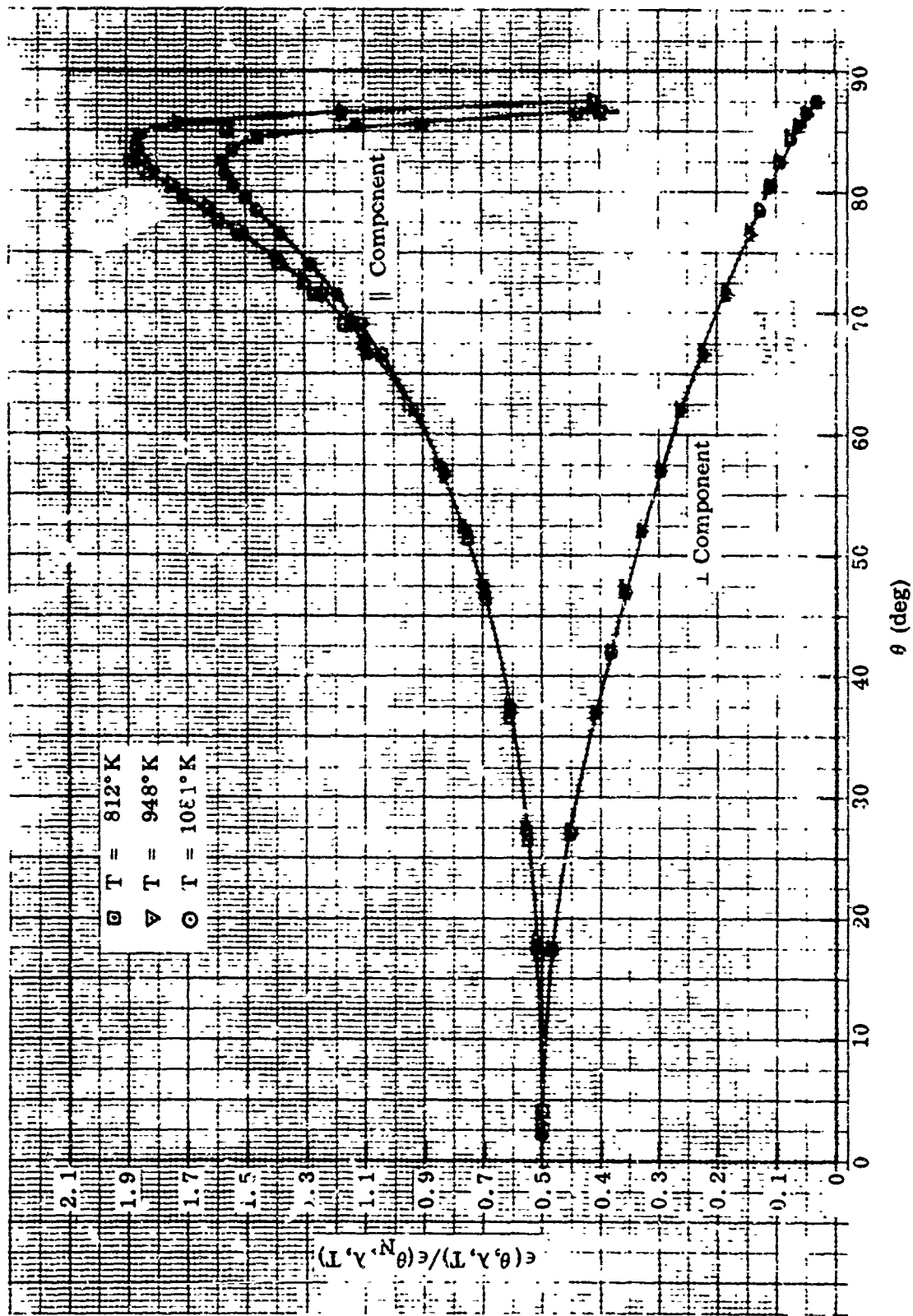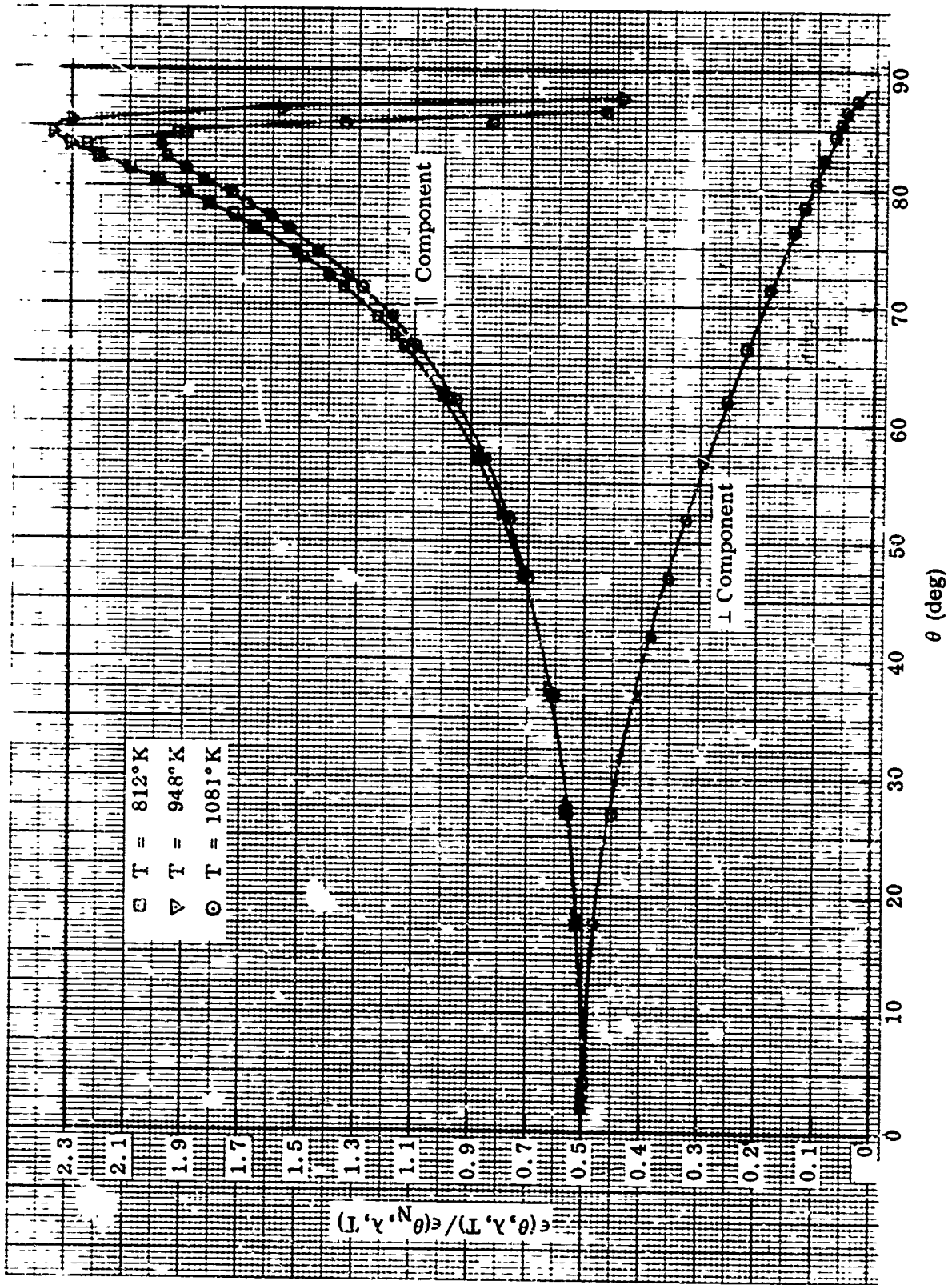
235

Figure 142 Relative Spectral Directional Emittance at $\lambda = 4\ \mu$, Stainless Steel Sample No. 1S-3

Figure 143 Relative Spectral Directional Emittance at $\lambda = 6 \mu$, Stainless Steel Sample No. 1S-3

237
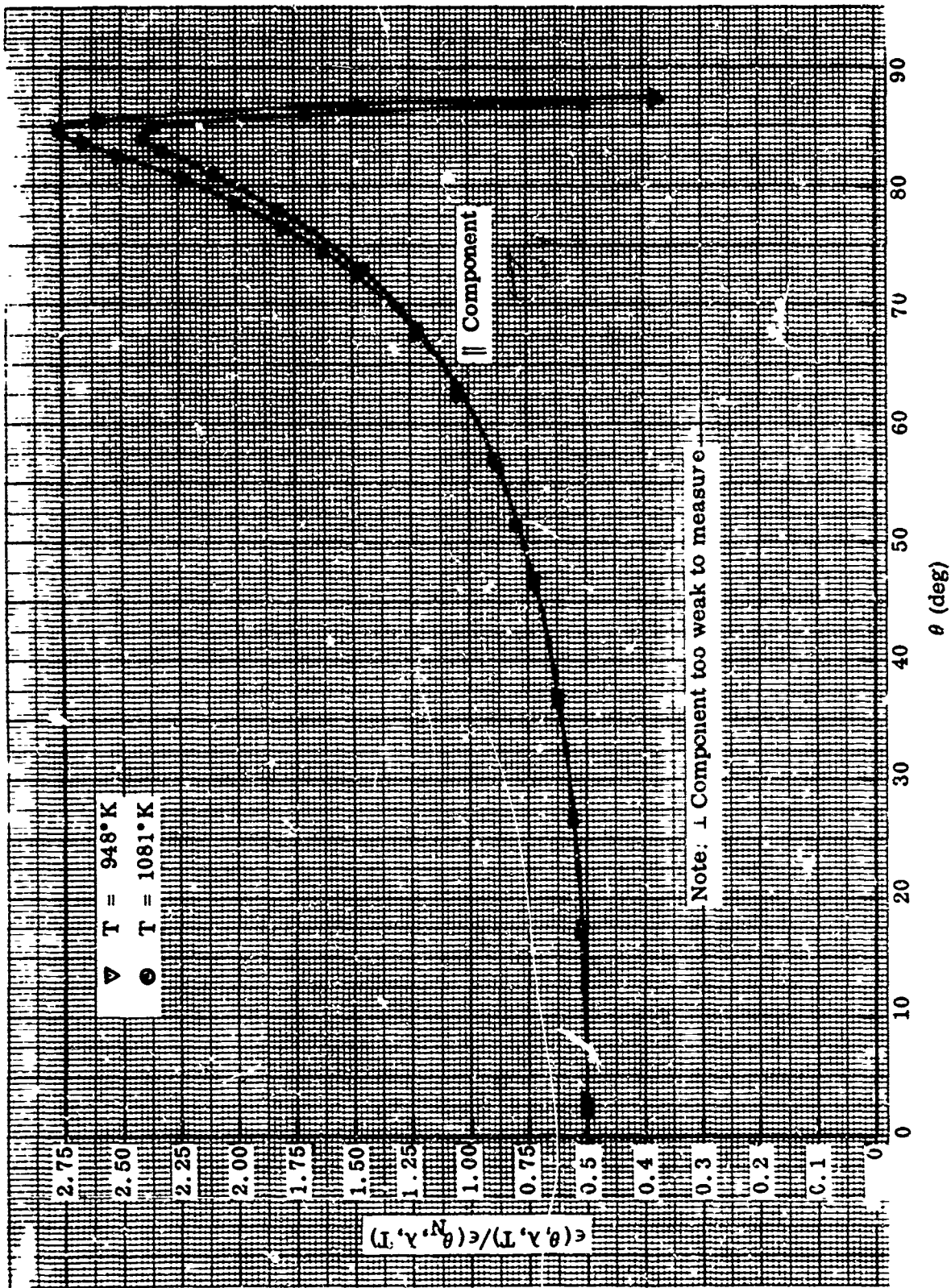
Figure 144 Relative Spectral Directional Emittance at $\lambda = 8 \mu$, Stainless Steel Sample No. 1S-3

238

Section VIII

REFERENCES

1. R. E. Rolling, A. I. Funai, and J. R. Grammer, <u>Investigation of the Effect of Surface Condition on the Radiant Properties of Metals</u>, AFML-TR-64-363, Nov 1964

2. M. P. Givens, "Optical Properties of Metals," in Solid State Physics, Vol. 6, New York, Academic Press, 1958, pp. 313 – 352

3. Born and Wolf, Principles of Optics, New York, Pergamon, 1959

4. A. I. Mahan, "Reflection and Refraction at Oblique Incidence on a Dielectric-Metallic Interface as a Boundary Value Problem in Electromagnetic Theory," J. Opt. Soc. Am., Vol. 46, 1956, pp. 913 – 926

5. F. Abelés, <u>Optical Properties and Electronic Structure of Metals and Alloys</u>, New York, John Wiley and Sons, 1966

6. H. C. Hottel, "Radiant-Heat Transmission," in <u>Heat Transmission</u>, by W. H. McAdams, New York, McGraw-Hill, 1954

7. J. R. Branstetter, "Radiant Heat Transfer Between Nongray Parallel Plates of Tungsten," NASA TN D-1088, 1961

8. J. R. Branstetter, "Formulas for Radiant Heat Transfer Between Nongray Parallel Plates of Polished Refractory Metals," NASA TN D-2902, 1965

9. R. E. Chupp and R. Viskanta, "Radiant Heat Transfer Between Concentric Spheres and Coaxial Cylinders," J. Heat Transfer, Vol. 88 1966, pp. 326 – 327

10. J. A. Wiebelt, <u>Engineering Radiation Heat Transfer</u>, New York, Holt, Rinehart and Winston, 1966

11. E. M. Sparrow and R. D. Cess, <u>Radiation Heat Transfer</u>, Belmont, Calif., Brooks/Cole, 1966

12. W. J. Parker and G. L. Abbott, "Total Emittance of Metals," <u>Symposium on Thermal Radiation of Solids</u>, NASA SP-55, 1965

13. D. K. Edwards and N. B. de Volo, "Useful Approximations for the Spectral and Total Emissivity of Smooth Bare Metals," <u>Advances in Thermophysical Properties at Extreme Temperatures and Pressures</u>, ed. by S. Gratch, N. Y., Am. Soc. Mech. Engrs., 1965

14. R. A. Seban, "The Emissivity of Transition Metals in the Infrared," <u>J. Heat Transfer</u>, Vol. 87, 1965, pp. 173 − 176

15. R. V. Dunkle, "Emissivity and Inter-Reflection Relationships for Infinite Parallel Specular Surfaces," <u>Symposium on Thermal Radiation of Solids</u>, NASA SP-55, 1965

16. R. E. Rolling and C. L. Tien, "Total Specular Reflectance of Rough Metallic Surfaces," <u>J. Spacecrafts and Rockets</u>, Vol. 3, 1966, pp. 1719 − 1722

17. D. K. C. MacDonald, "Electrical Conductivity of Metals and Alloys at Low Temperatures," <u>Handbuck Physik</u>, Vol. 14, 1956, p. 137

18. A. P. Lenham and D. M. Treherne, "Interpretation of the Infrared Optical Constants of Metals," <u>J. Opt. Soc. Am.</u>, Vol. 56, 1966, pp. 1076 − 1080

19. A. Vašíček, <u>Optics of Thin Films</u>, New York, Interscience Publications, 1960

20. O. S. Heavens, <u>Optical Properties of Thin Solid Films</u>, New York, Dover Publishers, 1965

21. A. F. Turner, "Reflectance Properties of Thin Films and Multilayers," in <u>Radiative Transfer From Solid Materials</u>, ed. by H. H. Blau, Jr., and H. Fischer, New York, Macmillan, 1962

22. P. H. Burning, G. Hass, and R. P. Madden, "Reflectance-Increasing Coatings for the Vacuum Ultraviolet and Their Applications," <u>J. Opt. Soc. Am.</u>, Vol. 50, No. 6, Jun 1960, pp. 586 − 597

23. H. E. Bennett, "Influence of Surface Roughness, Surface Damage, and Oxide Films on Emittance," <u>Symposium on Thermal Radiation of Solids</u>, NASA SP-55, 1965, pp. 145 − 152

24. D. K. Edwards and I. Catton, "Radiation Characteristics of Rough and Oxidized Metals," Part III of <u>Basic Heat Transfer Studies Related to the Use and Control of Solar Energy</u>, UCLA Report No. 64-14 (NSF Final Report G20246), Mar 1964

25. G. Hass, "Solar Absorptance and Thermal Emittance of Evaporated Metal Films With and Without Surface Coatings," <u>Symposium on Thermal Radiation of Solids</u>, NASA SP-55, 1965, pp. 189 − 195

26. J. C. Richmond, "Relation of Emittance to Other Optical Properties," NBS J. Res. Vol. 67C, No. 3, Jul – Sep 1963, pp. 217 – 226

27. J. C. Richmond, "Effect of Surface Roughness on Emittance of Nonmetals," J. Opt. Soc. Am., Vol. 56, Feb 1966, p. 253 – 254

28. H. J. Keegan, et al., "Effect of Surface Texture on Diffuse Spectral Reflectance," Symposium on Thermal Radiation of Solids, NASA SP-55, 1965, pp. 165 – 177

29. B. Piper and W. P. Callis, "Surface Finish Measurements on Non-Ferrous Materials," Am. Machinist, Special Report 476, 10 Aug 1959, pp. 105 – 120

30. R. M. Mahla and N. A. Nielsen, "An Oxide Replica Technique for the Electron Microscope Examination of Stainless Steel and High Nickel Alloys," J. Appl. Phys. Vol. 19, Apr 1948, pp. 378 – 382

31. O. Kubaschewski and B. E. Hopkins, Oxidation of Metals and Alloys, 2nd ed., New York, Academic Press, Inc., 1962

32. E. A. Gulbransen and K. F. Andrew, "Oxidation Studies on 304 Stainless Steel," J. Electrochem. Soc., Vol. 109, Jul 1962, pp. 560 – 564

33. National Bureau of Standards, "Standard X-Ray Diffraction Powder Patterns," NBS Circular 539

34. R. Newman and R. S. Halford, "An Efficient, Convenient Polarizer for Infrared Radiation," Rev. Sci. Inst., Vol. 19, Apr 1948, pp. 270 – 271

35. M. Pivovonsky and M. R. Nagel, Tables of Blackbody Radiation Function, New York, Macmillan, 1961

36. I. Simon, "Spectroscopy in Infrared by Reflection and Its Use for Highly Absorbing Substances," J. Opt. Sec. Am., Vol. 41. May 1951, pp. 336 – 345

37. J. C. Richmond and W. N. Harrison, "Equipment and Procedures for Evaluation of Total Hemispherical Emittance," Ceramic Bull., Vol. 39, 1960, pp. 668 – 673

38. G. L. Abbott, N. J. Alvares, and W. J. Parker, Total Normal and Total Hemispherical Emittance of Polished Metals, WADD-TR-61-94, Nov 1961

39. K. Giler, "Free Energy of Dissociation of Metal Oxides," Vacuum Symposium Transactions, 1957, p. 161

40. C. E. Wicks and F. E. Block, "Thermodynamic Properties of 65 Elements –
Their Oxides, Halides, Carbides, and Nitrides," Bureau of Mines Bulletin
605, 1963

41. J. C. Richmond, "Importance of Surface Films," Symposium on the Thermal
Radiation of Solids, NASA SP-55, 1965, pp. 157 – 158

42. J. W. Hickman and E. A. Gulbransen, "An Electron Diffraction Study of Oxide
Films Formed on High Temperature Oxidation Resistant Alloys," Trans.
Electrochem. Soc., Vol. 41, 1947, pp. 60 – 622

43. M. Deitch and J. Plunkett, "Time-Temperature Total Hemispherical Emittance
Study of Gold Plated Stainless Steel," Trans. ASM, Vol. 59, 1966, pp. 85 – 93

DOCUMENT CONTROL DATA - R&D

(Security classification of title, body of abstract and indexing annotation must be entered when the overall report is classified)

1 ORIGINATING ACTIVITY (Corporate author)	2a REPORT SECURITY CLASSIFICATION
Lockheed Palo Alto Research Laboratory	Unclassified
Lockheed Missiles & Space Company	**2b GROUP**
Palo Alto, California	N/A

3 REPORT TITLE

Investigation of the Effect of Surface Conditions on the Radiant Properties of Metals.
Part II, Measurements on Roughened Platinum and Oxidized Stainless Steel

4 DESCRIPTIVE NOTES *(Type of report and inclusive dates)*
Technical report, 1 Jan 1965 – 15 Sep 1966

5 AUTHOR(S) *(Last name, first name, initial)*
Rolling, R. E.
Funai, A. I.

6 REPORT DATE	7a TOTAL NO. OF PAGES	7b. NO. OF REFS
April 1967	242 text pages	43

8a CONTRACT OR GRANT NO.	9a ORIGINATOR'S REPORT NUMBER(S)
AF 33(657)-11281	
b PROJECT NO.	6-77-67-27
7360	
c	9b OTHER REPORT NO(S) *(Any other numbers that may be assigned this report)*
Task No. 736001	
d	AFML-TR-64-363, Part II

10 AVAILABILITY/LIMITATION NOTICES

Distribution of this document is unlimited.

11 SUPPLEMENTARY NOTES	12. SPONSORING MILITARY ACTIVITY
	Air Force Materials Laboratory
	Directorate of Laboratories
	Air Force Systems Command

13 ABSTRACT

Experimental results are presented to show the effect of surface roughness and of surface oxidation on the radiant properties of platinum and of 304 stainless steel. The radiant properties investigated include total and spectral normal, hemispherical, and directional emittance as a function of emission angle, polarization, temperature, and surface roughness or oxide film thickness.

Emittance data are presented for five platinum samples with surface roughness values between 0.20 and 2.50 μ, rms, at five temperatures between 865° and 1645°K, and at selected wavelengths between 1 and 12 μ. Similar data are presented for nine stainless steel samples with surface oxide film-thickness values between 0 and 1.5 μ, at five temperatures between 535° and 1090°K. Variations in the radiant properties of each material are explained in terms of the differences in surface characteristics of the samples, or of changes in their surface characteristics as the result of annealing, recrystallization, and oxidation during the high temperature emittance tests.

Methods used to evaluate the physical, chemical, and geometrical characteristics of the sample surface include: profilometry, optical and electron microscopy, x-ray and electron diffraction, and arc spectroscopy. The advantages and shortcomings of these methods are discussed and typical results are presented.

Distribution of this abstract is unlimited.

DD FORM 1 JAN 64 **1473**

14.	LINK A		LINK B		LINK C	
KEY WORDS	ROLE	WT	ROLE	WT	ROLE	WT
Surface roughness Oxide films Platinum Stainless steel Emittance of metal surfaces						

INSTRUCTIONS

1. ORIGINATING ACTIVITY: Enter the name and address of the contractor, subcontractor, grantee, Department of Defense activity or other organization (corporate author) issuing the report.

2a. REPORT SECURITY CLASSIFICATION: Enter the overall security classification of the report. Indicate whether "Restricted Data" is included. Marking is to be in accordance with appropriate security regulations.

2b. GROUP: Automatic downgrading is specified in DoD Directive 5200.10 and Armed Forces Industrial Manual. Enter the group number. Also, when applicable, show that optional markings have been used for Group 3 and Group 4 as authorized.

3. REPORT TITLE: Enter the complete report title in all capital letters. Titles in all cases should be unclassified. If a meaningful title cannot be selected without classification, show title classification in all capitals in parenthesis immediately following the title.

4. DESCRIPTIVE NOTES: If appropriate, enter the type of report, e.g., interim, progress, summary, annual, or final. Give the inclusive dates when a specific reporting period is covered.

5. AUTHOR(S): Enter the name(s) of author(s) as shown on or in the report. Enter last name, first name, middle initial. If military, show rank and branch of service. The name of the principal author is an absolute minimum requirement.

6. REPORT DATE: Enter the date of the report as day, month, year; or month, year. If more than one date appears on the report, use date of publication.

7a. TOTAL NUMBER OF PAGES: The total page count should follow normal pagination procedures, i.e., enter the number of pages containing information.

7b. NUMBER OF REFERENCES: Enter the total number of references cited in the report.

8a. CONTRACT OR GRANT NUMBER: If appropriate, enter the applicable number of the contract or grant under which the report was written.

8b, 8c, & 8d. PROJECT NUMBER: Enter the appropriate military department identification, such as project number, subproject number, system numbers, task number, etc.

9a. ORIGINATOR'S REPORT NUMBER(S): Enter the official report number by which the document will be identified and controlled by the originating activity. This number must be unique to this report.

9b. OTHER REPORT NUMBER(S): If the report has been assigned any other report numbers (either by the originator or by the sponsor), also enter this number(s).

10. AVAILABILITY/LIMITATION NOTICES: Enter any limitations on further dissemination of the report, other than those imposed by security classification, using standard statements such as:

  (1) "Qualified requesters may obtain copies of this report from DDC."

  (2) "Foreign announcement and dissemination of this report by DDC is not authorized."

  (3) "U. S. Government agencies may obtain copies of this report directly from DDC. Other qualified DDC users shall request through

                                                  ."

  (4) "U. S. military agencies may obtain copies of this report directly from DDC. Other qualified users shall request through

                                                  ."

  (5) "All distribution of this report is controlled. Qualified DDC users shall request through

                                                  ."

If the report has been furnished to the Office of Technical Services, Department of Commerce, for sale to the public, indicate this fact and enter the price, if known.

11. SUPPLEMENTARY NOTES: Use for additional explanatory notes.

12. SPONSORING MILITARY ACTIVITY: Enter the name of the departmental project office or laboratory sponsoring (paying for) the research and development. Include address.

13. ABSTRACT: Enter an abstract giving a brief and factual summary of the document indicative of the report, even though it may also appear elsewhere in the body of the technical report. If additional space is required, a continuation sheet shall be attached.

It is highly desirable that the abstract of classified reports be unclassified. Each paragraph of the abstract shall end with an indication of the military security classification of the information in the paragraph, represented as (TS), (S), (C), or (U).

There is no limitation on the length of the abstract. However, the suggested length is from 150 to 225 words.

14. KEY WORDS: Key words are technically meaningful terms or short phrases that characterize a report and may be used as index entries for cataloging the report. Key words must be selected so that no security classification is required. Identifiers, such as equipment model designation, trade name, military project code name, geographic location, may be used as key words but will be followed by an indication of technical context. The assignment of links, rules, and weights is optional.

GPO 886-551